



Design of a mobile post-treatment unit for the water used during fire extinguishment

Clément Baudequin

► To cite this version:

Clément Baudequin. Design of a mobile post-treatment unit for the water used during fire extinguishment. Chemical and Process Engineering. Ecole Centrale Paris, 2011. English. NNT : 2011ECAP0045 . tel-01543652

HAL Id: tel-01543652

<https://theses.hal.science/tel-01543652>

Submitted on 21 Jun 2017

HAL is a multi-disciplinary open access archive for the deposit and dissemination of scientific research documents, whether they are published or not. The documents may come from teaching and research institutions in France or abroad, or from public or private research centers.

L'archive ouverte pluridisciplinaire **HAL**, est destinée au dépôt et à la diffusion de documents scientifiques de niveau recherche, publiés ou non, émanant des établissements d'enseignement et de recherche français ou étrangers, des laboratoires publics ou privés.



**ÉCOLE CENTRALE DES ARTS
ET MANUFACTURES
« ÉCOLE CENTRALE PARIS »**

THÈSE
présentée par

Clément BAUDEQUIN

pour l'obtention du

GRADE DE DOCTEUR

Spécialité : Génie des Procédés

Laboratoire d'accueil : Laboratoire de Génie des Procédés et Matériaux

SUJET :

**Conception d'une unité mobile pour le post-traitement d'eau
utilisée pendant l'extinction d'incendie**

**Design of a mobile post-treatment unit for the water
used during fire extinguishment**

soutenue le : 28 octobre 2011

Confidentialité : 5 ANS

devant un jury composé de :

MOULIN Philippe,
LAPICQUE François
RAKIB Mohammed
COUALLIER Estelle
RABILLER-BAUDRY Murielle
SEVERAC Romain
PABON Martial
AVILA RODRIGUEZ Mario

Professeur, Université Paul Cézanne, Aix-Marseille III
Directeur de recherche CNRS, LRGP
Professeur, ECP
Maître de conférences, ECP
Professeur, Université Rennes 1
Docteur, Du Pont de Nemours
Docteur, Du Pont de Nemours
Professeur, Université de Guanajuato, Mexique

Rapporteur
Rapporteur
Directeur
Co-encadrante
Présidente
Examineur
Invité
Invité

2011ECAP0045

Remerciements

Ce travail a été effectué au Laboratoire de Génie des Procédés et Matériaux de l'École Centrale Paris, et financé par Du Pont de Nemours France SAS.

Je tiens à remercier les rapporteurs qui ont accepté de juger ce travail : Philippe MOULIN, professeur à l'université Aix-Marseille III et François LAPICQUE, directeur de recherche CNRS au Laboratoire Réactions et Génie de Procédés de Nancy ; ainsi que les membres du jury : Martial PABON et Romain SEVERAC, docteurs, Du Pont de Nemours, Mario AVILA RODRIGUEZ, professeur à l'université de Guanajuato, Mexique, Mohammed RAKIB, professeur et Estelle COUALLIER, maître de conférences, respectivement directeur et codirectrice de thèse à l'École Centrale Paris, ainsi que Murielle RABILLER-BAUDRY, professeur à l'université Rennes 1, qui a accepté de présider ce jury.

À Perrine, pour son soutien et la grande clémence qui parfois me fit défaut,
À ma famille pour être ma famille,
À Estelle, pour son empathie, son soutien et ses conseils,
À Zhaohuan pour son aide fort appréciée lors de l'urgence des derniers essais,
À Mohammed pour sa parole aussi rare que précieuse, et pour m'avoir accueilli au sein de son équipe,
À Romain et Martial, pour leur sens aigu mais néanmoins humain du management, et aussi pour avoir rendu ce travail possible,
À Hélène, pour son incroyable générosité et sa gentillesse (non moins incroyable),
À Barbara M. pour son indulgence à l'égard de mes maladresses,
À Charles et Philippe pour leurs personnalités hautes en couleur et l'ambiance vivifiante qui en a découlé,
À Barbara C.L. pour son hospitalité lors de mon exil temporaire,
À Isabelle, Fabienne, Sandra, Émilie, Cécile, Annie, Vincent, Thierry, Jean, Géraldine et Catherine pour la sérénité intellectuelle permise par tous les services qu'ils m'ont aimablement rendus,
À tous les autres que j'ai injustement oubliés...

Du fond du cœur, merci.

List of symbols

AB interactions: Lewis acid-base-type polar interactions ($mN\ m^{-1}$)

AFFF: aqueous film-forming foams

AR-FFFP: alcohol resistant film forming fluoroprotein foams

AR-AFFF: Alcohol resistant film forming foams class B fires: fires of flammable liquids

FFFP: Film forming fluoroprotein foams

C : concentration ($mol\ L^{-1}$ or $g\ L^{-1}$)

C_F : feed concentration ($g\ L^{-1}$)

CF : concentration factor

C_P : permeate concentration ($g\ L^{-1}$)

C_R : retentate concentration ($g\ L^{-1}$)

CMC: critical micelle concentration ($mol\ L^{-1}$ or $g\ L^{-1}$)

D : diffusion coefficient ($m^2\ s^{-1}$)

EF : extraction factor

IFW: industrial firefighting water

J : flux ($L\ h^{-1}\ m^{-2}$)

K : adsorption equilibrium constant ($L\ mg^{-1}$)

K_{ow} : oil water partition coefficient

L : permeability ($L\ h^{-1}\ m^{-2}\ bar^{-1}$)

LW interactions: apolar Lifshitz-Van der Waals interaction ($mN\ m^{-1}$)

MF: microfiltration

MWCO: molecular weight cut-off ($g\ mol^{-1}$)

n_{agg} : aggregation numbers in surfactant micelles

NF: nanofiltration

PFW: pilot firefighting water
 Q_F : feed flow ($L h^{-1}$)
 Q_P : permeate flow ($L h^{-1}$)
 Q_R : retentate flow ($L h^{-1}$)
 R: retention, or rejection rate (%)
 R_a : membrane resistance due to adsorption (m^{-1})
 R_m : membrane resistance (m^{-1})
 RO: reverse osmosis
 S : spreading coefficient ($mN m^{-1}$)
 UF: ultrafiltration
 VRR : volume reduction ratio
 W_a : work of adhesion (J)
 W_c : work of cohesion
 δ : thickness of the diffusion layer (m)
 $\Delta G_{inter(SL)}$: free energy of interaction (J)
 η : water viscosity ($Pa s$)
 η_{CE} : current efficiency
 γ_{ij} is the interfacial tension, or interfacial free energy between two immiscible phases i and j in contact, in Jm^{-2} or $N m^{-1}$
 Γ : surface excess ($mol m^{-2}$)
 μ : chemical potential ($J mol^{-1}$)

Contents

List of symbols	i
General introduction	1
1 Context of the study	3
1.1 Industrial context	3
1.1.1 Firefighting foams	3
1.1.2 Firefighting foam formulations and flammable hydrocarbons types . .	6
1.1.3 Real firefighting waters	9
1.1.4 Industrial purpose	11
1.2 Scientific and conceptual context	12
1.2.1 Interfaces and surfaces	12
1.2.1.1 Interfacial tension	12
1.2.1.2 Intermolecular forces and interfacial tension	16
1.2.1.3 Adsorption at interfaces	19
1.2.2 Surfactants and interfacial phenomena in aqueous solutions	23
1.2.2.1 General definition and surfactants description	23
1.2.2.2 Molecular interactions in surfactant solutions	25
1.2.2.3 Micellisation of surfactants	26
1.2.2.4 Adsorption of surfactants	28
1.2.2.5 Fluorinated surfactants	32
1.2.3 Mixed surfactant systems and potential interactions between foam components	35
1.2.3.1 Mixed surfactant systems	35

1.2.3.2	Interaction of surfactants with proteins and polymers . . .	38
1.2.3.3	Types of surfactants in pilot firefighting waters and their potential interactions	39
1.2.4	Scientific purpose of the work	41
	Conclusion	42
2	Bibliographic study and process screening	43
2.1	Research and design strategy	43
2.2	Bibliography	44
2.2.1	Pretreatments processes for the suspended matter in firefighting waters	46
2.2.1.1	Physical processes	46
2.2.1.2	Physicochemical processes	46
2.2.2	Treatment processes for fluorinated surfactants	48
2.2.2.1	Adsorption processes	48
2.2.2.2	Membrane processes	54
2.2.2.3	Destructive processes	57
2.2.2.4	Extraction-based and miscellaneous processes	58
2.2.3	Comparison and selection of processes for the screening	58
2.3	Screening and preliminary experiments	61
2.3.1	Analytical methods	62
2.3.1.1	Suspended matter analysis	62
2.3.1.2	Surfactants analysis	62
2.3.2	Pilot firefighting waters used in the screening	65
2.3.3	Screening of pretreatment processes	72
2.3.3.1	Filtration and microfiltration experiments	73
2.3.3.2	Ultrafiltration experiments	77
2.3.3.3	Coagulation flocculation	80
2.3.3.4	Electrocoagulation	82
	Conclusion on the screening of the pretreatment processes	85
2.3.4	Screening of treatment processes	86
2.3.4.1	Adsorption	86

2.3.4.2	Electrocoagulation	89
2.3.4.3	Reverse osmosis	91
	Conclusion on the screening of treatment processes	93
	Conclusion	94
3	Pretreatment of firefighting water by electrocoagulation	97
	Introduction	97
3.1	Electrocoagulation theory and bibliography	97
3.1.1	Electrocoagulation principles	98
3.1.1.1	Description of the process	98
3.1.1.2	Processes for removal of the floc	98
3.1.1.3	Electrocoagulation process applications	99
3.1.2	Electrocoagulation theory	99
3.1.2.1	Coagulation theory	99
3.1.2.2	Electrocoagulation theory	100
3.1.2.3	Active species in electrocoagulation	101
3.1.2.4	Parameters influencing the electrocoagulation process . . .	103
3.1.3	Electrocoagulation in the scope of firefighting water pretreatment . .	104
	Conclusion	105
3.2	Material and methods	106
3.2.1	Electrocoagulation and filtration	106
3.2.1.1	Turbidity measurements	106
3.2.1.2	HPLC analysis	107
3.2.1.3	Aluminium atomic absorption spectrometry	109
3.2.1.4	Firefighting water used during the study of the pretreat- ment by electrocoagulation	109
3.3	Optimization of the electrocoagulation process applied to firefighting water .	109
3.3.1	Electrocoagulation of the suspended matter and turbidity removal from pilot firefighting waters	110
3.3.1.1	Identification of an indicator for the end of suspended mat- ter electrocoagulation	110

3.3.1.2	Assessment of the minimum charge loading and aluminium dose	113
3.3.2	Pretreatment of firefighting waters by electrocoagulation and floc removal	116
3.3.2.1	Pilot firefighting water by electrocoagulation–press filtration in the laboratory	116
3.3.2.2	Pilot firefighting water electrocoagulation on an industrial pilot	117
3.3.2.3	The case of industrial firefighting waters	120
	Conclusion	122
3.4	Study of some phenomena occurring during electrocoagulation of firefighting water	122
3.4.1	Influence of electrocoagulation on surfactant concentrations	122
3.4.2	Influence of the current density and charge loading	124
3.4.2.1	Influence of the current density and charge loading on aluminium concentration	124
3.4.2.2	Influence of the aluminium dose and pH on fluorinated surfactant concentration	125
3.4.2.3	Influence of current density on fluorinated surfactant concentrations	127
3.4.3	Influence of the fluorinated surfactant concentration on the minimal charge loading	128
	Conclusion	132
	Conclusion	133
4	Treatment of pretreated firefighting water by reverse osmosis	134
	Introduction	134
4.1	Description and theory of membrane processes	134
4.1.1	Membrane processes properties	135
4.1.1.1	The different kinds of membrane processes	135
4.1.1.2	Description of filtration operations	136

4.1.2	Membrane properties	139
4.1.3	Separation mechanisms	142
4.1.4	Flux decline and membrane fouling	143
4.2	Description of the membrane–surfactant system	146
4.2.1	Membrane processes and surfactants	146
4.2.2	<i>A priori</i> description of the membrane/pretreated firefighting water system	149
4.3	Material and methods	151
4.3.1	Solutions used for membrane processes experiments and surfactants analysis	151
4.3.2	Devices used for reverse osmosis experiments	154
4.3.2.1	Osmonics Sepa CFII cell	154
4.3.2.2	Millipore ProScale pilot	155
4.3.2.3	Polymem pilot	156
4.4	Experimental part	158
4.4.1	Screening of flat reverse osmosis and nanofiltration membranes in the Osmonics cell	158
4.4.2	Reverse osmosis of model and pilot pretreated firefighting waters with a spiral-wound SG module	162
4.4.2.1	Reverse osmosis of pretreated pilot firefighting water . . .	162
4.4.2.2	Reverse osmosis of synthetic pretreated firefighting water .	163
4.4.3	Study of the reverse osmosis on longer periods in an industrial pilot .	165
4.5	Discussion	169
4.5.1	Study of the flux decline with the spiral-wound SG membrane	170
4.5.2	Adsorption of surfactants at the RE2540-FE membrane	174
4.5.3	Diffusion of surfactants in the membrane	175
	Conclusion	177
5	Answers to the scientific and industrial purposes	179
	Introduction	179
5.1	Scientific purpose	179

5.1.1	Experimental context	180
5.1.2	The case of adsorption	182
5.1.3	The case of electrocoagulation	183
5.1.4	The case of reverse osmosis	184
5.2	Industrial scale-up	185
5.2.1	Industrial purpose	185
5.2.2	Results	186
5.2.2.1	Electrocoagulation	187
5.2.2.2	Membrane processes	187
5.2.3	Discussion	188
	Conclusion	191
	General conclusion	192
	References	194
	List of publications	195
	Bibliography	210
	List of figures	218
	List of tables	222

General introduction

Large class B fires – i.e. polar or non polar burning liquids – can occur in places like refineries, airports or chemical plants. Such fires can be put out with the help of fire fighting foams prepared from specific aqueous formulations, called foam concentrates diluted in water to 1–6% and applied with a nozzle under the form of foam. The very low apparent foam density allows it to be deposited at the surface of burning liquids. The foam spreads at the surface generating an aqueous film which reduces the emission of flammable vapors. Foam concentrates usually contain hydrocarbon surfactants or protein hydrolysates (synthetic or proteinic concentrate), and one or several fluorinated surfactants in case of high performance foam concentrates.

During industrial solvent fires large amounts of water and foam are used: several cubic meters per minute during several days. Resulting water consists of either water from the foam and water used to protect equipment and persons from the heat of the fire. Therefore its composition is expected to be somehow close to diluted foaming solution. In the emergency of a large fire event, every available foam concentrates are used: synthetic or proteinic concentrates. If alcohol resistant foam was used, hydrocarbon and fluorinated water soluble polymers might also be present. Hence this water may contain protein hydrolysates, various hydrocarbon and fluorinated surfactants and polymers in addition to burned solvent, particles and soot, with volume up to 750 m^3 of foam concentrate. This leads to an estimation of 25.000 m^3 of water on the basis of a 3% dilution. The present work aims at identifying the most appropriate technique to purify the water used during fire extinguishment. The final unit has to be mobile to be used on many different sites to absorb the fix cost of the equipment. The resulting techniques are expected to be sustainable in terms of water recovery, energy and material consumption versus straight incineration. They also have to be able to extract

fluorinated surfactants from water at a rate of 4,000-10,000 m^3 in 3-6 months.

In the first chapter, the industrial context of firefighting foams and firefighting water will be introduced. Firefighting foams are aqueous mixtures of air, additives as well as hydrocarbon and fluorinated surfactants. Surfactants are amphiphilic molecules able to lower interfacial tension. These compounds have the particularity to self-aggregate when their concentration reaches the critical micelle concentration. Fluorinated surfactants are a particular class of surfactants which can dramatically lower the water surface tension. This ability plays a key role in the efficiency of firefighting waters. In addition, fluorinated surfactants are highly resistant to thermal and chemical attacks. The current treatment for firefighting waters is therefore incineration in halogen resistant incinerators, which is very expensive. The work on water treatment processes could not be done without a proper understanding of the behavior of surfactants at interfaces. Therefore, the notions of interfacial tension, intermolecular interactions and adsorption will be introduced. These considerations will be applied to describe surfactant solutions.

After introduction of the industrial context and conceptual framework in chapter 1, the relevant processes identified in a bibliographic study will be screened in chapter 2. Because of the expected mobility of the final unit, not only efficiency based on experimental results, but also compactness and material sobriety will be important parameters for the choice of processes. Firefighting waters contain suspended matter which could be harmful for the treatment step. A pretreatment step will be therefore required. The two treatment steps identified during the screening are electrocoagulation for the pretreatment step and reverse osmosis for the treatment step will be deepened in chapter 3 and 4.

The results obtained in chapter 3 and 4 will be used to propose a flow sheet for the mobile unit, and for the scale-up of both pretreatment and treatment steps. Experimental results obtained in chapter 2, 3 and 4 will be used with the help of the consideration introduced chapter 1 to describe the water–solid surface–surfactant system, as observed during adsorption, electrocoagulation and reverse osmosis experiments.

Chapter 1

Context of the study

Introduction

The design of a mobile post-treatment unit for the water used during fire extinguishment has to be done in consideration to the interplay between firefighting waters and water treatment processes. This chapter is intended to introduce the context of this work. As an industrial context, the handling of firefighting water and fluorinated surfactants will be described. Firefighting waters contain various types of surfactants, which are a particular class of chemicals. The behavior of these molecules in regard to water treatment processes is an essential notion to the understanding of the underlying phenomenon encountered in this work. Therefore conceptual consideration of surface science and surfactant chemistry and molecular interaction will be introduced.

1.1 Industrial context

1.1.1 Firefighting foams

Large fire events involving flammable liquid hydrocarbons, like the one that occurred in Buncefield in 2005 can require several days of firefighting [1]. These fires are called *class B fires*, and are usually put out with specific firefighting foams like aqueous film-forming foams (AFFF) or film-forming fluoroprotein foams (FFFP). The key of fire extinguishment is to break the fire triangle (figure 1.1) by removing at least one of its three components, namely the fuel which is the flammable substance, the oxidizer which enables the combustion of the

fuel, namely oxygen, and heat which is necessary to reach the ignition temperature.

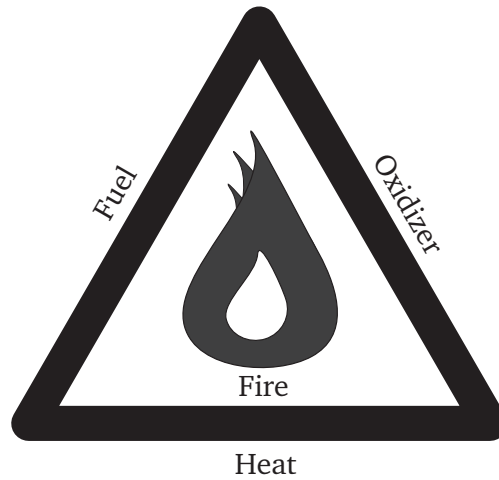


Figure 1.1: Fire triangle

In the case of class B fires at large scale, the fuel is not the liquid hydrocarbon itself but its vapors, and the oxidizer is generally the dioxygen of air (O_2). Basically, a firefighting foam is a mixture of water, air and foam concentrate. Foam concentrates are diluted in water to 0.5–6%v : v, then this foaming solution applied with firefighting device, like nozzles, under the form of foam [2] (figure 1.2). There are three categories of foams according to their expansion rate (equation 1.1), *i.e.* the volume of foam obtained with a given initial volume of foaming solution: low, medium and high expansion foams which have their own applications (table 1.1).

$$\text{Expansion rate} = \frac{\text{Volume of foam}}{\text{Volume of foaming solution}} \quad (1.1)$$

Table 1.1: Foam types according to their expansion rate

Foam type	Expansion rate	Application
Low expansion	1 : 1–20 : 1	Class B fires
Mid expansion	20 : 1–200 : 1	Vapor suppression
High expansion	> 200 : 1	Confined space firefighting

Therefore the foam, which consists of a mass of small air-filled bubbles, contains over 50% of air and has a lower apparent density than water or considered liquid hydrocarbons.

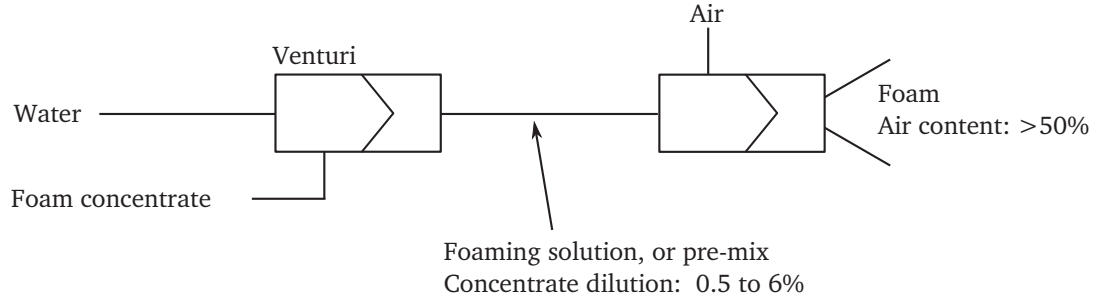


Figure 1.2: Typical system of foam generation, *i.e.* nozzle

Firefighting foams help to put out fires in several ways considering the fire triangle. Evaporation of the water brought provides effective cooling, but this effect is secondary. The main ways are related to the film-forming ability of these foams. The formation of this water film over the liquid hydrocarbon occurs when the spreading coefficient S is positive (figure 1.3 and 1.4):

$$S_{\text{Foaming solution/Hydrocarbon}} = \frac{\gamma_{\text{Hydrocarbon/Air}} - \gamma_{\text{Hydrocarbon/Foaming solution}}}{\gamma_{\text{Foaming solution/Air}}} \quad (1.2)$$

where γ_{ij} is the interfacial tension, or interfacial free energy between two immiscible phases i and j in contact, also referred to as surface tension of a liquid in case of a liquid/vapor interface. If one of the phases is a vapor phase or vacuum its index is often considered implicit, thus omitted. Further details about these interfacial phenomena will be covered in section 1.2.1. With a positive spreading coefficient, the foam and its aqueous film are able to spread naturally over the burning hydrocarbon, adequately covering it (figure 1.4). This separates the fuel from the oxidizer by stopping or at least highly reducing vapor emissions. A well-formulated foam correctly applied is stable, cohesive, resists to heat, suppresses vapors, puts out the fire quickly (fast knockdown characteristics) and prevents the risk of fire reignition (long burnback time). Surface tensions considered in spreading coefficients are static surface tensions. Dynamic surface tension play a key role which will not be covered here.

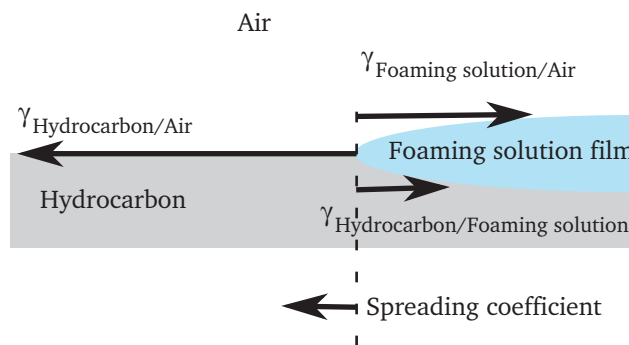


Figure 1.3: Film formation and spreading as a result of a positive spreading coefficient





	Hydrocarbon Surface tension		Aqueous solution Surface tension		Hydrocarbon/solution Interfacial tension		Spreading Coefficient
<div>water</div> <div>HC </div>	22	-	(72	+	44.5)	=	- 94.5
<div>Hydrocarbon surfactant</div> <div>HC </div>	22	-	(30	+	0)	=	- 8
<div>Fluorinated surfactant</div> <div>HC </div>	22	-	(16	+	6)	=	0
<div>AFFF solution</div> <div>HC </div>	22	-	(16	+	3)	=	3

Figure 1.4: Influence of the AFFF components on the spreading coefficient of a water drop on a hydrocarbon liquid.

1.1.2 Firefighting foam formulations and flammable hydrocarbons types

Firefighting foam formulation can be classified in two families: protein foams and synthetic foams (table 1.2) and there are different types of flammable liquid hydrocarbons that can be found in large amount in industrial environments (table 1.3). The two main solvent categories are polar and apolar hydrocarbons. The problem in case of fire with polar ones is their miscibility with water. They also can solubilise most of the foam components resulting in foam inefficiency.

Regular protein foams have good heat resistance, burnback and drainage characteristics

but slow knockdown ones. Hence special fluorinated surfactants were added to make fluoroprotein foams, which have better knockdown performances. Film forming fluoroprotein foams (FFFP) FFFP's are a combination of fluorinated surfactants with protein foam designed to combine the fuel tolerance and burnback resistance of a fluoroprotein foam with increased knockdown characteristics. FFFP foams release an aqueous film on the surface of the hydrocarbon fuel. However, these firefighting foams dissolve in polar or water miscible solvents like ethanol. For these fires, there are alcohol resistant film forming fluoroprotein foams (AR-FFFP), combinations of protein foam, fluorinated surfactant and polysaccharide polymer. When used on polar solvents, the polymer forms a gel which protects the foam from the solvent, preventing its destruction.

Synthetic foams foaming agents are synthetic surfactants instead of protein-based chemicals. Aqueous film forming foams (AFFF) contain a mixture of hydrocarbon and fluorinated surfactants to reach the fastest possible knockdown on fuel fire thanks to their fluidity. Like FFFP they form a film which naturally spreads at the surface of the hydrocarbon as a result of a positive spreading coefficient. Alcohol resistant film forming foams (AR-AFFF) are obtained with mixtures of hydrocarbon and fluorinated surfactants, soluble polymers and/or soluble fluoropolymers. Like with AR-FFFP, the polymers form a protective gel layer on polar or water miscible solvents.

Table 1.2: Firefighting foams

(a) Proteinic foams		(b) Synthetic foams	
Types of foam	Components	Types of foam	Components
Protein foams	Protein hydrolysates	Synthetic foam	Hydrocarbon surfactants, cosolvent
Fluoroprotein foams (FP)	Protein hydrolysates, anionic and zwitterionic hydrocarbon, surfactant, fluorinated polymer/telomer	Aqueous film forming foams (AFFF)	Hydrocarbon surfactants, fluorinated surfactants, cosolvent
Film forming fluoroprotein foams (FFFP)	Protein hydrolysates, anionic and zwitterionic hydrocarbon surfactant, fluorinated polymer/telomer, fluorinated surfactant	Alcohol resistant aqueous film forming foams (AFFF AR)	Hydrocarbon surfactants, fluorinated surfactants, polysaccharide, fluorinated polymer
Alcohol resistant film forming fluoroprotein foams (FFFP-AR)	FFFP, fluorinated polymer		

Protein hydrolysates and hydrocarbon surfactants mainly help to reduce $\gamma_{\text{Hydrocarbon Foaming solution}}$. To obtain the necessary positive spreading coefficient of film forming foams, crucial additives are employed: surfactants with partially fluorinated tails. Fluorinated surfactants have the ability to lower $\gamma_{\text{Foaming solution Air}}$ down to $15\text{--}20 \text{ mN m}^{-1}$ at 20°C versus $30\text{--}40 \text{ mN m}^{-1}$ for hydrocarbon surfactants [2]. In addition, fluorinated surfactants are highly resistant to thermal and chemical attacks and they hardly mix with long chain hydrocarbons like oils or fats.

Table 1.3: Some common flammable hydrocarbons in industrial environment

Apolar flammable hydrocarbons	Polar flammable hydrocarbons
Mineral spirit	Acetone
Kerosene	Ethanol
Gasoline	Isopropanol
Oil	Methyl tertibutyl ether (MTBE)
Heptane	Methyl isobutyl ether (MIBE)
Isopar H or G	Methy isobutyl ketone (MIBK)
Essence F	Methyl ether ketone (MEK)
Fuel	Propylene glycol

1.1.3 Real firefighting waters

During industrial solvent fires large amounts of water and foam may be applied: several cubic meters per minute during several days (figure 1.5). Resulting water consists of either water from the foam and water used to protect equipment and persons from the heat of the fire. Therefore its composition is expected to be somehow close to diluted foaming solution, with additional by-products of the fire (solid content, ashes, soot). In the emergency of a large fire event, every available foam concentrates are used: synthetic or proteinic concentrates. If alcohol resistant foams are used, hydrocarbon and fluorinated water soluble polymers might also be present. Hence this water may contain protein hydrolysates, various hydrocarbon and fluorinated surfactants and polymers in addition to burned solvent, particles and soot. With a volume up to 750 m^3 of foam concentrate [1], this may lead to estimations of 25.000 m^3 of firefighting water on the basis of a 3% dilution, without considering the random dilution due to extra water used for cooling.



Figure 1.5: Photographs from the Buncefield incident (credits: Chiltern Air Support)

Firefighting water recovery is generally not that problematic during large industrial fire events in places such as fuel depots, chemical plants and refineries. These infrastructures are designed to prevent the fuel (or any hydrocarbon contaminated liquid, such as firefighting water) from spreading and running off the site if it does escape from the tanks or pipework. The tanks are positioned within a walled area designed to prevent any escaping liquid from spreading into and outside the site [1]. These enclosures are called bundings, or ‘bunds’.

1.1.4 Industrial purpose

The current treatment for firefighting water containing fluorinated surfactants is straight incineration in halogen-resistant incinerators. This treatment process is very expensive and such incinerators may not be present on every continents. The industrial purpose of this work is to find the most appropriate alternative process, or combination of processes, to extract fluorinated surfactants from the firefighting water after a large scale fire event. The final unit is expected to be mobile to enable its shipment to the water and save the shipment of the water to the unit. The chosen processes will have to be as compact as possible, as autonomous as possible in raw materials and chemicals, and are expected to minimize the amount of matter to incinerate. The final unit is expected to treat the firefighting water of a large scale fire event, 4,000-10,000 m^3 , in 3–6 months, which leads to an estimated flow rate of 1,000 to 4,500 $L h^{-1}$, 24/7. The fluorinated surfactant concentration of the resulting water is expected to be less than 100 $\mu g L^{-1}$. To achieve this, not only the processes will have to be efficient, compact, autonomous and reliable, but also easily automatisable.

Given the variety and the complexity of the firefighting waters according to the initial foam concentrate and to the type of fire (table 1.4), numerous parameters may affect the properties of these waters. To cope with this complexity, target firefighting waters have been chosen as resulting from the extinguishment of apolar solvent fires with AFFF containing an hydrocarbon anionic surfactant, an hydrocarbon zwitterionic surfactant, an hydrocarbon non-ionic surfactant, a fluorinated zwitterionic surfactant and a cosolvent. Protein hydrolysates, polymers and seawater were voluntarily ignored at the beginning of the study and then some of them were progressively reintroduced to assess the robustness of the processes.

Table 1.4: Firefighting water complexity summary

	Protein foam	Synthetic foam
Apolar solvent	Protein hydrolysates, fluorinated surfactants, fresh or sea water	Hydrocarbon and fluorinated surfactants, fresh or sea water
Polar solvent	Protein hydrolysates, fluorinated surfactants, water soluble polymers, fresh or sea water	Hydrocarbon and fluorinated surfactants, hydrocarbon and fluorinated polymers, fresh or sea water

1.2 Scientific and conceptual context

The main components of firefighting foams are surfactants. Their role is to maximize the efficiency of the foam by modifying interfacial tensions. To understand the behavior of surfactants in foam, but also in water treatment processes, interfacial tension, intermolecular interactions and adsorption will be introduced. These notions will help the description of surfactant molecules and their behaviors at aqueous interfaces and in mixed surfactant systems.

1.2.1 Interfaces and surfaces

1.2.1.1 Interfacial tension

Interfacial phenomena were mentioned as playing a key role in the efficiency of firefighting foams without precision on the conceptual framework in which such phenomenon occur. *Interfaces* are boundaries between *immiscible phases*, which can be liquid/vapor (LV), liquid/solid (LS), solid/vapor (SV), liquid/liquid (LL) or solid/solid (SS). In a condensed phase, the molecules constituting the interface are less stable than the ones in the bulk because they lose a part of their stabilizing interactions with other bulk molecules [3, 4] (figure 1.6). This stability difference induces that bringing additional bulk molecules to the interface, *i.e.* extending the interfacial area, comes with an energy change. An interface carries interfacial free energy G_I , proportional to the number of molecules at the interface *i.e.* to its area a . At constant conditions of temperature, pressure and volume, to increase an interfacial area of Δa , one must provide a minimum ΔG_I which can be expressed by the following equation [5]:

$$\Delta G_I = \gamma \Delta a \quad (1.3)$$

with G_I in J , γ the interfacial tension in Jm^{-2} or Nm^{-1} , Δa in m^2 . Interfaces involving a vapor phase are usually called surfaces, thus interfacial tension in such cases is commonly called surface tension. γ can be seen either as the interfacial free energy ΔG_I per unit of area ($energy/(length)^2$) or as the surface tension ($force/length$). The interfacial tension reflects the contrast in terms of cohesion between the two phases constituting the interface, the force that tighten this interface, or the tendency of interfacial molecule to migrate back

to the bulk, which occurs in a dynamic equilibrium for fluid phases.

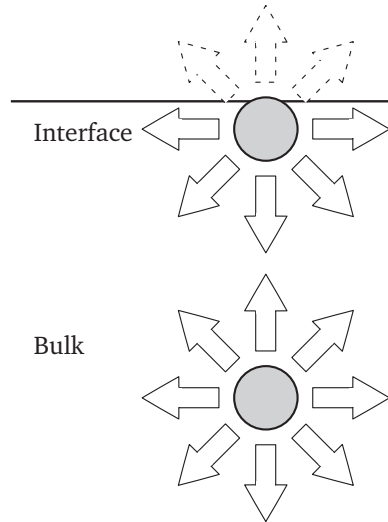
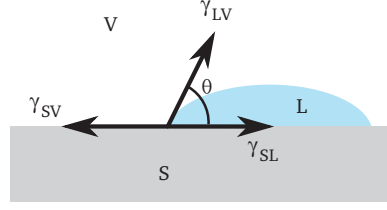


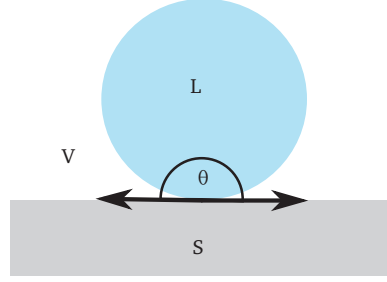
Figure 1.6: Stabilizing interaction differences of bulk and interface molecule in a pure liquid

Interfacial tensions are responsible for the contact angle formed by a drop of liquid L deposited on a solid surface S (figure 1.7a). The link between the contact angle θ and interfacial tensions is expressed in the Young equation (Young, 1805):

$$\gamma_{SV} = \gamma_{SL} + \gamma_{LV} \cos\theta \quad (1.4)$$



(a) Contact angle and interfacial tensions for a liquid drop L partially wetting a solid surface S



(b) Contact angle for a liquid drop L not wetting the solid surface S

Figure 1.7: Contact angles between a liquid L and a solid surface S in case of partial wetting and absence of wetting

For a solid surface, the vertical component of interfacial tensions is neglected and could be balanced by adhesion forces. This is a limit of the equation. Contact angles are the most experimentally accessible data accounting for affinities between interfaces: the higher the affinity, the lower the interfacial tension. Contact angles with water can be used to assess hydrophobicity or hydrophilicity of different surfaces, or more generally to study the wetting of a solid or liquid interface by another liquid. In its most general sense, wetting is the substitution on a substrate of a fluid by another immiscible fluid. In a more practical sense, wetting is the behavior of a liquid on a surface (a condensed phase–vapor interface): the liquid–surface interface can replace some surface–vapor interface. Wetting can be total or partial. Total wetting occurs if the liquid spontaneously spreads over the interface, *i.e.* if the surface free energy of the system decreases when the water replaces the air at the interface:

$$\Delta G_{SL} < 0 \iff \gamma_{LV}\Delta a + \gamma_{LS}\Delta a - \gamma_{SV}\Delta a < 0 \quad (1.5)$$

$$\iff \gamma_{SV} - (\gamma_{LV} + \gamma_{LS}) = S_{L/S} > 0 \quad (1.6)$$

In the hypothesis of the formation of a film, $S_{L/S}$ is the spreading coefficient of the liquid L on the surface S , as mentioned for firefighting foams in Section 1.1.1. If the spreading coefficient is positive then total wetting occurs. If it is negative, wetting remains partial and results in contact angles θ (equation 1.4). The liquid may also be unable to wet the surface, which would result in a contact angle of 180° (figure 1.7b). When a liquid L is brought to the contact of a surface S (Fig 1.8), the reversible work of adhesion W_a , or free energy of interaction $\Delta G_{inter(SL)}$ required to separate the surface S and a liquid L is expressed by the Dupré equation:

$$W_{aLS} = \Delta G_{interSL} = \gamma_{SV} + \gamma_{LV} - \gamma_{LS} \quad (1.7)$$

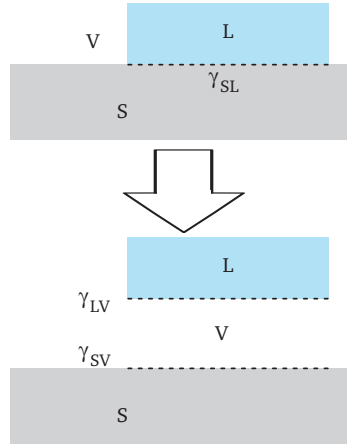


Figure 1.8: Work of adhesion, or free energy of interaction between a surface S and a liquid L

In a single liquid L , the work of cohesion corresponds to the free energy per unit area required to separate a volume of L by two distinct volumes (figure 1.9). The work of cohesion W_c for the liquid L can be expressed as:

$$W_{cLL} = 2\gamma_{LV} \quad (1.8)$$

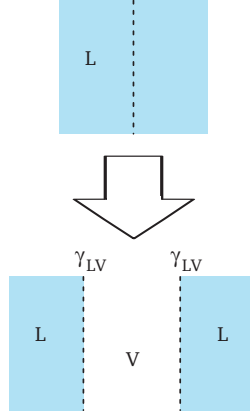


Figure 1.9: Work of cohesion for a liquid L

From equations 1.6, 1.7 and 1.8, we can see that the spreading coefficient is the balance between the cohesion of the liquid and its adhesion on the surface:

$$S_{SL} = W_{aLS} - W_{cLL} \quad (1.9)$$

Dupré's equation combined with Young's equation (equation 1.4) lead to the Young-Dupré equation:

$$-\Delta G_{inter SL} = \gamma_{LV}(1 + \cos\theta) \quad (1.10)$$

With contact angle measurements, one can assess the affinity of one liquid with different surfaces, or one surface to different liquids. The higher the wetting, the lower the contact angle, the lower the interfacial tension. Contact angles are especially useful to compare the hydrophilicity of different materials. However, when studying the interaction of a solid surface by a liquid, the most relevant thermodynamic parameter is γ_{SL} which, despite Young and Young Dupré equations, remains experimentally unreachable by conventional contact angle measurements [6]. Indeed, if γ_{LV} and the contact angle θ are known, one only obtain the resultant of γ_{SV} and γ_{SL} with the Young equation (equation 1.4), or the free energy of interaction $\Delta G_{inter SL}$ with the Young-Dupré equation (equation 1.10), which also contains γ_{SV} and γ_{SL} . Thus reaching the value of γ_{SL} requires a more sophisticated framework.

1.2.1.2 Intermolecular forces and interfacial tension

Intermolecular interactions can be expressed as the sum of the following terms [4]:

- Overlap repulsion: steric interaction occurring when molecules are close enough so their electron clouds overlap;
- Chemical interaction: covalent bonding (specific to certain systems);
- Electrostatic forces: Coulomb forces between opposite charges;
- Charge transfer: occurs when two molecules, one electron-donor and the other electron acceptor are close enough to exchange electrons, *i.e.* Lewis acid-base system (AB);
- Lifshitz-Van der Waals forces (LW):
 - Electrical multipole – electrical multipole: electrostatic forces between molecules having permanent multipoles (Keesom forces);
 - Electrical multipole – induced electrical multipole: occur between permanent multipoles and polarizable molecules (Debye forces);
 - Dispersion forces: arise between fluctuating dipoles and induced dipoles (London forces);

Though mentioned, steric and chemical interaction will not be detailed. Electrostatic and charge transfer (AB) forces are obviously polar forces. Lifshitz van der Waals (LW) forces, including the confusing Keesom and Debye forces, were shown to be apolar forces [6]. The predominant apolar forces are by far dispersion/London ones. These forces are responsible for the cohesion of non polar liquid alkanes for instance, and by extension to their interfacial tensions. Thus interfacial tensions of apolar compounds result essentially from one single Lifshitz Van der Waals (LW) term: γ^{LW} . Interfacial tension between an apolar entity S (which can be liquid or solid) with an apolar liquid L can be written as [6]:

$$\gamma_{SL}^{LW} = \left(\sqrt{\gamma_{SV}^{LW}} - \sqrt{\gamma_{LV}^{LW}} \right)^2 \quad (1.11)$$

Equation 1.11 implies that two identical apolar entities immersed in an apolar liquid cannot repel one another because neither γ_{SL}^{LW} nor ΔG_{SL}^{LW} can be negative. Hence the fact that similar *polar neutral entities* may repel to dissolve in polar solvents suggests that another component of surface tension is present in polar entities, and absent in non polar

ones: electron donor and electron acceptor interaction in Lewis acid-base system (AB). For a polar compound S , interfacial tension can be expressed as the sum of the Lifshits-Van der Waals and Lewis components [6]:

$$\gamma_{SV} = \gamma_{SV}^{LW} + \gamma_{SV}^{AB} \quad (1.12)$$

γ_S^{AB} , which represents the electron acceptor as well as the electron donor characters, is composed of two different interfacial tensions: γ_S^+ the electron acceptor and γ_S^- the electron donor components, such that:

$$\gamma_{SV}^{AB} = 2\sqrt{\gamma_{SV}^+ \gamma_{SV}^-} \quad (1.13)$$

This decomposition of interfacial tension reflects the multiple contributions to this phenomena, which is based on intermolecular interactions. Using this relation, one can express [6]:

- The interfacial tension between a polar liquid L and a condensed phase substance S :

$$\gamma_{SL} = \left(\sqrt{\gamma_{SV}^{LW}} - \sqrt{\gamma_{LV}^{LW}} \right)^2 + 2 \left(\sqrt{\gamma_{SV}^+ \gamma_{SV}^-} + \sqrt{\gamma_{LV}^+ \gamma_{LV}^-} - \sqrt{\gamma_{SV}^+ \gamma_{LV}^-} - \sqrt{\gamma_{LV}^+ \gamma_{SV}^-} \right) \quad (1.14)$$

- The free energy of interaction between S and L per unit area ($W_{aL/S}$):

$$\Delta G_{inter SL} = \gamma_{SL} - \gamma_{SV} - \gamma_{LV} = -2 \left(\sqrt{\gamma_{SV}^{LW} \gamma_{LV}^{LW}} + \sqrt{\gamma_{SV}^+ \gamma_{LV}^-} - \sqrt{\gamma_{SV}^- \gamma_{LV}^+} \right) \quad (1.15)$$

- The free energy of interaction between two identical molecules or particles S , dissolved or immersed in a polar liquid L :

$$\Delta G_{SLS} = -2\gamma_{SL} = -2 \left(\sqrt{\gamma_{SV}^{LW}} - \sqrt{\gamma_{LV}^{LW}} \right)^2 - 4 \left(\sqrt{\gamma_{SV}^+ \gamma_{SV}^-} + \sqrt{\gamma_{LV}^+ \gamma_{LV}^-} - \sqrt{\gamma_{SV}^+ \gamma_{LV}^-} - \sqrt{\gamma_{LV}^+ \gamma_{SV}^-} \right) \quad (1.16)$$

- The Young Dupré equation linking contact angles and interfacial tension components:

$$(1 + \cos\theta) \gamma_{LV} = -\Delta G_{inter SL} = -2 \left(\sqrt{\gamma_{SV}^{LW} \gamma_{LV}^{LW}} + \sqrt{\gamma_{SV}^+ \gamma_{LV}^-} - \sqrt{\gamma_{SV}^- \gamma_{LV}^+} \right) \quad (1.17)$$

Given the previous equations and contact angle measurements, it is possible to determine γ_{SV} . For this, contact angle measurements with the surface S and three liquids with known surface-thermodynamic properties are required. With the three resulting contact angles, one can solve the system of three equations (one equation 1.17 per liquid) to get the three unknown γ_{SV}^{LW} , γ_{SV}^+ and γ_{SV}^- constituting γ_{SV} (equations 1.12 and 1.13). Then γ_{SL} can be determined either by using the previously obtained γ_{SV} in the Young equation (equation 1.4), or by using the three components of γ_{SV} in equation 1.14. In the case of an interface between water and an immiscible apolar liquid, interfacial tension can be directly measured by appropriate tensiometers.

For solid surfaces one can distinguish two categories: high energy (HE) and low energy (LE) surfaces. Chemical bonds in HE surfaces can be ionic, covalent metallic and γ_{SAir} for such surfaces can range from 500 to 5000 $mN m^{-1}$. LE surfaces are molecular crystals, organic polymers or waxes and γ_{SAir} for such surfaces can range from 10 to 50 $mN m^{-1}$. The Zisman criterion states that for an apolar surface S , there exist a critical surface tension γ_C such as for a liquid L , if $\gamma_{LV} > \gamma_C$ L partially wets S whereas if $\gamma_{LV} < \gamma_C$ the wetting is total. γ_C is a property of the surface, and to wet it, a liquid must have a surface tension lower than its critical surface tension [3, 5].

Previously considered surfaces were assumed to be ideal surfaces, *i.e.* smooth and homogeneous surfaces. Regular surfaces often exhibit roughness and inhomogeneities. The structural nature of the surface plays a great role in wetting and contact angles: the roughness ratio r emphasizes the hydrophilicity and hydrophobicity of the surface. r is the ratio of the developed surface to the projection of the considered area. The Wenzel model relates the appearing contact angle θ^* on a rough surface to the Young angle θ_E :

$$\cos\theta^* = r \cos\theta_E \quad (1.18)$$

1.2.1.3 Adsorption at interfaces

Interfaces tend to minimize their interfacial free energy by decreasing their area by surface tension, or by covering themselves with any available component able to decrease the cohesion contrast between the two phases in presence. Hence high energy surfaces are subject to

pollution by adsorption [3]. Adsorption is a process in which some molecules, the adsorbate, migrate from the bulk to accumulate at a given interface, the adsorbent. The phenomenon is described by adsorption isotherms, which depict the relation between the adsorbent interface area, the number of molecule adsorbed and the equilibrium concentration.

Gibbs adsorption isotherm model treats the interface as a mathematical plane σ of area A , hosting n_i^σ molecules i . The surface excess is defined by $\Gamma_i = n_i^\sigma / A$. The interfacial plane is commonly located at the place where $\Gamma_{solvent} = 0$ to describe the surface excess of the solutes. The Gibbs adsorption equation is fundamental to all processes where monolayers are formed. At constant temperature its expression is:

$$-d\gamma_{LV} = \sum_i \frac{n_i^\sigma}{A} d\mu_i = \sum_i \Gamma_i d\mu_i \quad (1.19)$$

with the chemical potential $\mu_i^\alpha = \left(\frac{\partial G}{\partial n_i} \right)_{P, T, n_{j \neq i}}$ of the molecule i in the phase α .

For a binary solution of a solute s in a solvent at the interface, assuming constant temperature and expression of chemical potential in terms of concentration:

$$\Gamma_s = -\frac{1}{RT} \frac{d\gamma_{interface}}{d \ln c_s} \quad (1.20)$$

The Gibbs adsorption model only describes monolayer adsorption and its validity is often limited to adsorption at interfaces involving a “low energy medium” like air or low energy surfaces [4, 5], particularly in the absence of polar interactions.

Langmuir adsorption isotherm is the simplest model to depicts adsorption of molecules on solid surfaces. The expression of the Langmuir equation is:

$$\Theta = \frac{K_L c_s(b)}{K_L c_s(b) + 1} \quad (1.21)$$

for a solution of solute s , with Θ the fraction of available sites occupied by molecules, K_L the equilibrium constant of the solute between the bulk and the surface and $c_s(b)$ the bulk concentration of the solute [4]. The assumptions of the Langmuir equation are the following:

- The adsorbent is homogeneous
- Both solute and solvent have equal molar surface areas
- Both surface and bulk phases show ideal behavior (no solute-solute or solute-solvent interaction in either phases)
- The adsorption is monomolecular

Though its conditions are hardly ever met in practice, Langmuir equation accommodates many experimental situations where it should not apply [4]. There are more convenient expressions of the Langmuir equation for experiments:

$$\Gamma_s = \Gamma_m \frac{K c_s}{1 + K c_s} \quad (1.22)$$

$$q^* = q_{max}^* \frac{K c_s}{1 + K c_s} \quad (1.23)$$

with c_s the solute concentration at equilibrium in $mol L^{-1}$, Γ_s and Γ_m the surface concentration at equilibrium and at monolayer adsorption in $mol cm^{-2}$, q^* and q_{max}^* the equilibrium and monolayer mass concentrations of adsorbate per mass of adsorbent, and a a constant depending on the temperature and on the free energy of adsorption at infinite dilution. To check if adsorption follows the Langmuir equation, a plot of $\frac{1}{q^*}$ versus $\frac{1}{c_s}$ should be linear. If the surface concentration is not known, it can be replaced by the adsorbate mass per mass of substrate [5].

Freundlich adsorption isotherms are followed in practice by many components. It has found a wide application in describing experimental data. The Freundlich adsorption isotherm is obtained in the assumption of an exponential distribution of adsorption energy, rather than considering a homogeneous adsorbent with an ideal unique kind of adsorption site. It is assumed further that for each energy level, the coverage follows the Langmuir isotherm [7]. The expression of the Freundlich isotherm of a solute in a solvent is:

$$\Theta = K_F c_s^{1/n} \quad (1.24)$$

where K_F and n are constants under isothermal conditions, and $n > 1$. It can also be expressed in terms of weight of adsorbate per unit weight of adsorbent at equilibrium q^* :

$$q^* = K_F c_s^{1/n} \quad (1.25)$$

where $K_F = q_{max}^* A$.

1.2.2 Surfactants and interfacial phenomena in aqueous solutions

1.2.2.1 General definition and surfactants description

Surfactants, or surface active agents, are amphiphilic molecules that have the ability to lower interfacial tensions (section 1.2.1.1). Amphiphilic molecules either “like” polar and apolar phases, usually by means of one or several polar heads and one or several hydrophobic tails (see figure 1.10 for a simplified representation of a surfactant molecule). Hence, at an interface between a polar and an apolar phase, surfactants have the ability to lower interfacial free energies by presenting polar parts to the polar phase and apolar parts to the apolar phase. Surfactant molecules are of great variety resulting from the numerous combinations of polar heads (table 1.5) and apolar tails [5]. Hydrophobic parts can be straight-chain or branched-chain long alkyl groups (C_8 – C_{20}), long-chain alkylbenzene residue (C_8 – C_{15}), alkylnaphtalene residues, rosin or lignine derivatives, propylene oxide polymers, polysiloxane or fluorinated groups.

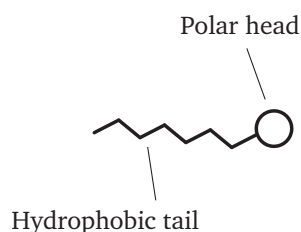


Figure 1.10: Simplified representation of a surfactant molecule

Table 1.5: Types of surfactants according to their polar heads [5]

(a) Anionic surfactants

Denomination	Formula
Carboxylic acid salts	$RCOO^{-}, M^{+}$
Acylated polypeptides	Partially hydrolyzed proteins
Sulfonic salts	$RSO_3^{-} M^{+}$
Sulfuric acid ester salts	$ROSO_3^{-} M^{+}$
Phosphoric and phosphoric acid esters	$RP(O)(O^{-} M^{+})_2$ and $R_2P(O)O^{-} M^{+}$

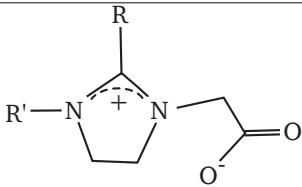
(b) Cationic surfactants

Denomination	Formula
Long chain amines and their salts	$RNH_3^{+} X^{-}$
	$RR'NH_2^{+} X^{-}$
	$RR'R''NH^{+} X^{-}$
	$RR'R''R'''N^{+} X^{-}$

(c) Nonionic surfactants

Denomination	Formula
Polyoxyethylenated (POE) alcohols, POE alkylphenols	$R(OCH_2CH_2)_xOH$
POE polyoxypropylene glycols	$R(CH_2CH_2O)_x(CH_2CH(CH_3)O)_yH$
POE mercaptans	$RS(CH_2CH_2O)_xH$
Long chain carboxylic acid esters	$RCOOR'$
Alcanolamine condensates, alcanolamides	$RCONHR'$
Alkylpolyglycosides	Long chain acetals of polysaccharides

(d) Zwitterionic surfactants

Denomination	Formula
β -N-Alkylaminopropionic acids	$RN^{+}H_2CH_2CH_2COO^{-}$
N-Alkyl- β -iminodipropionic acids	$RN^{+}H(CH_2COO^{-})(CH_2COOH)$
Imidazoline carboxylates	
N-Alkylbetaines	$R^{+}(CH_3)_2CH_2COO^{-}$
Amidoamines and amidobetaines	$RCONHCH_2CH_2N^{+}H(CH_2CH_2OH)CH_2COO^{-}$, $RCONHCH_2CH_2N^{+}H(CH_2CH_2OH)CH_2CH_2COO^{-}$, $RCINHCH_2CH_2CH_2N^{+}(CH_3)_2COO^{-}$
Amine oxides	$RN^{+}(CH_3)_2O^{-}$
Sulfobetaines	$RN^{+}(CH_3)_2(CH_2)_xSO_3^{-}$
Sulfamidobetaines	$RSO_2NH(CH_2)_xN^{+}(CH_3)_2(CH_2)_yCOO^{-}$

X^{-} : Cl^{-} , Br^{-} ; M^{+} : Na^{+} , K^{+} ; R: straight-chain or branched-chain alkyl groups (C_8 – C_{20}), alkylbenzen groups (C_8 – C_{15}), alkyl-2-naphthalene residue, rosin or lignin derivatives, fluorinated or polysiloxane groups.

1.2.2.2 Molecular interactions in surfactant solutions

According to Van Oss [6], differences between apolar/polar liquid interfaces and polar/polar liquid interfaces is well illustrated by the interfacial tensions of n-octane and n-octanol with water (table 1.6). Microscopic scale refers to molecular interfacial tension (which is related to miscibility) and macroscopic interfacial tension refers to the interface between the two phases. The only difference between those molecules is the presence of a polar OH group in n-octanol, which has an apolar tail and a rather polar head. This higher polarity explains the 20 mN m^{-1} lower interfacial tension of n-octanol at microscopic scale. However, whereas microscopic and macroscopic scale interfacial tension for n-octane and water remain unchanged, the macroscopic scale interfacial tension of n-octanol is dramatically (28 times) lower than for microscopic scale. In the latter case, macroscopic interfaces are far more stable and chemically alike because of local orientation of n-octanol OH polar groups toward the water.

Table 1.6: Differences in interfacial tension in mN m^{-1} of n-octane and n-octanol with water, on microscopic and macroscopic scales.

Interfacial tension	n-octane	n-octanol
Microscopic scale	50.8	30.8
Macroscopic scale	50.8	1.8

n-Octanol, though of little solubility in water, approaches surfactant features. According to the chemical natures of surfactant and solvent molecules, some interactions may take place. In surfactant solutions, intermolecular forces are basically of the same kind of those mentioned in section 1.2.1.2: electrostatic, charge transfer/Lewis acid-base system (AB) and Lifshitz-Van der Waals (LW) forces. However, in a binary surfactant–solvent mixture, there are basically three types of interactions: solvent–solvent, solvent–surfactant and surfactant–surfactant interactions.

Therefore the interaction between the solvent and the surfactant depends not only on the forces between these two molecules, but also on the magnitude of their self-interaction. Surfactant–surfactant interactions in case of an uncharged surfactant with a polar solvent such as water can be described by the free energy of surfactant self-interaction in water ΔG_{SWs} (per unit area) from equation 1.16 introduced in the previous section:

$$\Delta G_{sws} = -2\gamma_{sw} = -2 \left(\underbrace{\sqrt{\gamma_{SV}^{LW}} - \sqrt{\gamma_{WV}^{LW}}}_A \right)^2 - 4 \underbrace{\sqrt{\gamma_{SV}^+ \gamma_{SV}^-}}_B - 4 \underbrace{\sqrt{\gamma_{WV}^+ \gamma_{WV}^-}}_C + 4 \underbrace{\sqrt{\gamma_{SV}^+ \gamma_{WV}^-}}_D + 4 \underbrace{\sqrt{\gamma_{WV}^+ \gamma_{SV}^-}}_E \quad (1.26)$$

Only the negative terms of equation 1.26 can result in attractive surfactant interactions, whereas positive ones result in surfactants' mutual repelling, *i.e.* their dissolution. Hence, surfactants dissolve as a result of LW and AB interactions with water (*D* and *E*), whereas self-LW and self-AB interaction (*A* and *B*) as well as water self-AB interactions (*C*) act against surfactants dissolution (Fig 1.11). The hydrophobic effect, which tends to reject hydrophobic parts out of the water bulk, comes from the inability of the apolar tail to participate to the solvent's hydrogen bonding network rather than from LW forces. For charged surfactants, electrostatic repulsion between polar head of the same charge takes place. Overcoming of water–surfactant interactions by other interactions (surfactant–surfactant, surfactant–interface) results in aggregative behaviors such as micellisation of the surfactants and their adsorption at interfaces.

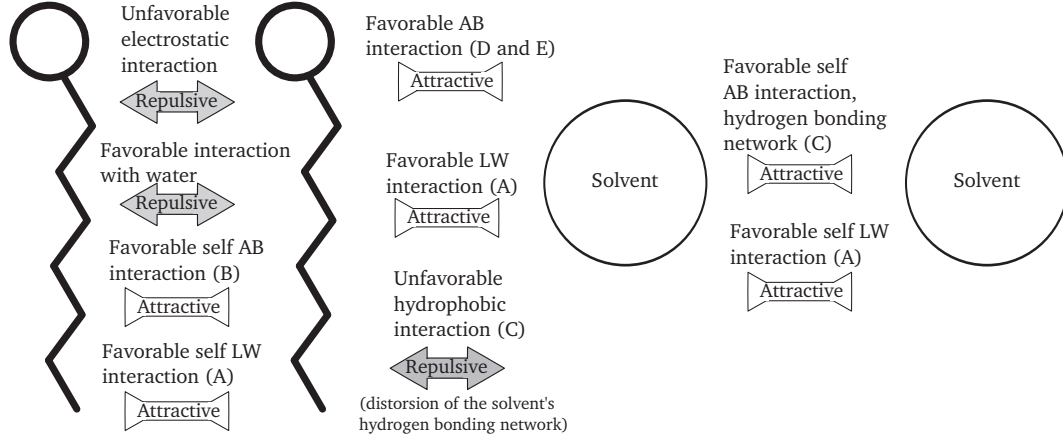


Figure 1.11: Summary of molecular interactions between a polar solvent and surfactant molecules. *A*, *B*, *C*, *D* and *E* refer to equation 1.26.

1.2.2.3 Micellisation of surfactants

In water, the limited solubility of hydrophobic chains make surfactants self-aggregate to form micelles when passing a threshold monomer concentration (figure 1.12). This concentration is called the critical micelle concentration (CMC). Above the CMC, any further increase of surfactant monomers concentration results in the formation of more micelles. The activity

and several other surfactant properties show a sharp break at the CMC. Micelles can be of various aggregation number and of various shape (table 1.7) according to the packing parameter [8]. The volume occupied by the hydrophobic parts in the core of the micelle V_H , the length of the hydrophobic chain in the core l_c and the cross sectional area a_0 of the hydrophilic head at the micelle–solution interface are used to calculate the packing parameter $\frac{V_H}{l_c a_0}$ (figure 1.13).

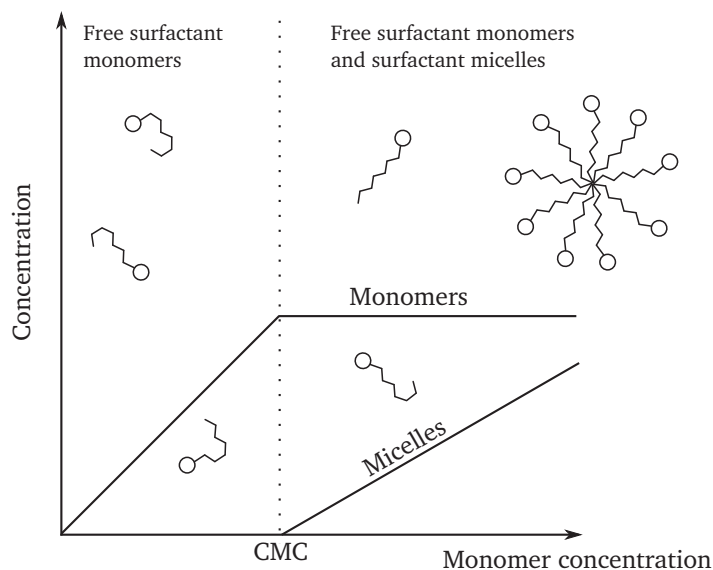


Figure 1.12: Surfactant monomers and micelle formation in water

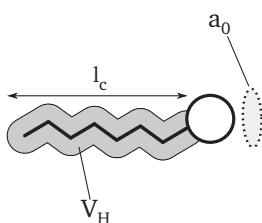


Figure 1.13: Packing parameter illustration

Table 1.7: Micellar structure according to the packing parameter

Value of the packing parameter $\frac{V_H}{l_c a_0}$	Structure of the micelle
0 – 1/3	Spheroidal
1/3 – 1/2	Cylindrical
1/2 – 1	Lamellar
> 1	Reversed micelles in non polar media

The surfactant solution can be considered as a multi-component system consisting of water, singly dispersed surfactant molecules, and aggregates of all possible shapes and aggregation numbers n_{agg} . At equilibrium, the chemical potential of free monomers must equal the chemical potential of surfactants involved in each aggregate μ_{agg_i} :

$$\mu_{agg_i}^\circ + kT \ln X_{agg_i} = n_{agg} [\mu_1^\circ + kT \ln X_1] \quad (1.27)$$

with μ_1° , $\mu_{agg_i}^\circ$ the standard state chemical potentials and X_1 , X_{agg_i} the molar fraction of the surfactant monomer in water and of the considered aggregate respectively [9]. Every addition of a surfactant molecule to the solution comes with an increase of free energy by the interplay of molecular interactions with water (figure 1.11). The CMC is the threshold concentration at which the chemical potential of the free monomer becomes equal to that of monomers involved in micelles. When present in sufficient amounts, micelles may organize in liquid crystals which have the ordered arrangement of solid crystals at liquid state. These arrangements generally increase the viscosity of the solution. In addition to micelle formation, surfactants may minimize free energy by adsorbing on interfaces or forming surface aggregates.

1.2.2.4 Adsorption of surfactants

The molecular interactions governing surfactant adsorption are the same as in surfactant solution and micellisation, but with an additional component: the interface on which adsorption takes place. This interface which can be liquid, vapor or solid phase. The main driving forces of surfactant adsorption on surfaces are electrostatic, charge transfer/Lewis acid-base system (AB) and Lifshitz-Van der Waals (LW) forces, with particular cases resulting from surface, surfactant and solvent chemical natures:

- Polar interactions:
 - Electrostatic interactions:
 - Lewis acid-base interactions, hydrogen bonding (AB);
 - Polarization of π electrons by strongly positive sites;
- Apolar interactions (LW):

- Hydrophobic interactions between hydrocarbon chains and hydrophobic sites;
- Hydrophobic lateral interaction between surfactant chains;
- $\pi - \pi$ interactions between aromatic nuclei;
- Solvation/desolvation forces in polar liquids:
 - Removal of the hydrocarbon chain and/or hydrophobic site from the water (favorable for adsorption);
 - Removal of the polar head and/or hydrophilic site from water (unfavorable for adsorption);
 - Replacement of solvent by surfactant molecules at the interface;

Table 1.8: Interactions driving the adsorption of surfactants in aqueous phase, according to the nature of the interface

	Hydrophobic interface	Hydrophilic interface	Charged interface
Favorable interactions for adsorption	LW interactions; Hydrophobic tail desolvation; Hydrophobic interface desolvation;	LW interactions; Hydrophobic tail desolvation; AB interactions and hydrogen bonding;	Electrostatic interaction (opposite charge); LW interactions; Hydrophobic tail desolvation; AB interactions and hydrogen bonding;
Unfavorable interactions for adsorption		Hydrophilic surface desolvation; Hydrophilic head desolvation;	Hydrophilic surface desolvation; Hydrophilic head desolvation; Electrostatic interaction (same charge);

These driving forces are encountered according to the nature of the interface (table 1.8). The most obvious case of interfacial surfactant adsorption is probably the adsorption of surfactants at the air water interface. The water surface tension decreases from 72.8 mN m^{-1} with the increasing surfactant concentration to a minimum value which is reached at the surfactant's CMC. The surfactants molecule orient their hydrophobic tail outside water toward the vapor phase and the hydrophilic heads toward the aqueous phase. As a result, the water

is shielded from the air by the hydrophobic tails and $\gamma_{water/air}$ decreases as the contrast between the two phases of the interface is weakened by this surfactant adsorption. This phenomenon can be described by the Gibbs adsorption model [5, 4].

Adsorption on hydrophobic surfaces The adsorption of surfactants on hydrophobic surface (liquid or solid) is generally driven by Liftshitz-Van der Waals interactions as well as by desolvation of hydrophobic parts of the surfactant and of the interface. This can also be described by the Gibbs adsorption model [5, 4]. At low concentration, adsorption of surfactants on hydrophobic surface is generally adsorption of isolated molecules parallel to the surface, forming a low density monolayer. At higher concentration, lateral interaction make the molecules erect with the head group towards the solution, forming various surface aggregates such as hemispheres, hemicylinders or dense monolayers [10, 11]. These surface aggregates, which are analogous to bulk-phase micelles, generally form at a critical aggregation concentration (CAC), much lower than the CMC. Adsorption isotherms of surfactants on hydrophobic interface generally show two steps: 1–Adsorption of isolated monomers, 2–Adsorption as surface aggregates (figure 1.14).

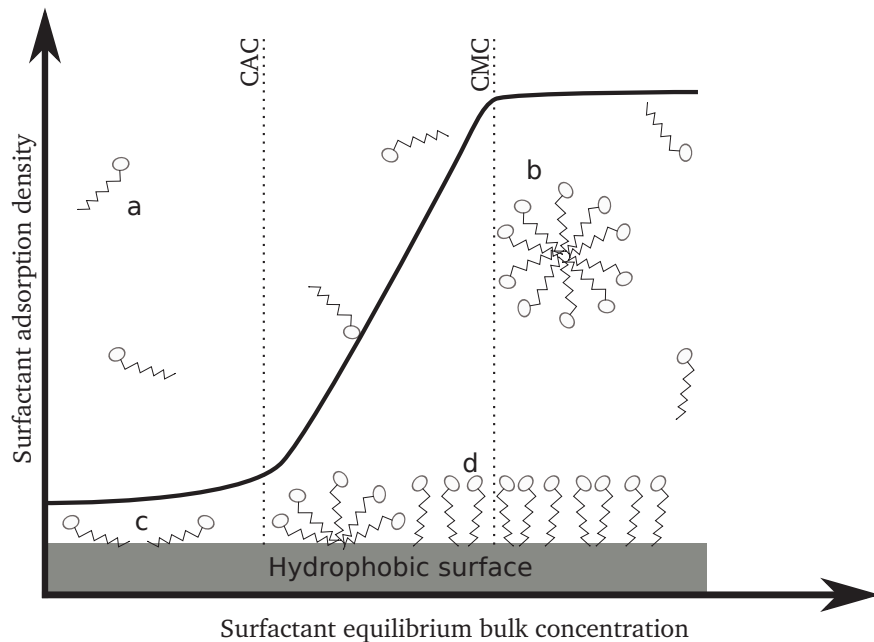


Figure 1.14: Adsorption of surfactants on hydrophobic surface. a: surfactant monomers, b: surfactant micelle, c: isolated adsorbed surfactant monomer, d: surface aggregates

Adsorption on hydrophilic surfaces On the contrary to hydrophobic surfaces, polar interaction may occur between a hydrophilic surface and the hydrophilic heads of the surfactants (Lewis AB interactions, hydrogen bonding). Therefore, if polar interactions overcome apolar ones, surfactants will adsorb at low concentration with their head towards the surface and their tail towards the bulk (Fig. 1.15). At higher concentrations surfactants also form surface aggregates on hydrophilic surface via lateral chain interaction. But as the orientation of monomers is reverted, so is the orientation of surface aggregates. Further increase in surfactant concentration leads to hydrophobic interactions between monomers and aggregates until saturation at the CMC. This case is well illustrated by the adsorption of ionic surfactants on oppositely charged surface, which leads to a so-called IV-region isotherms comprising the previous steps [11]. The adsorption of surfactants on a hydrophilic surface make this surface at first become more hydrophobic and then hydrophilic again with the coverage of surface aggregates. Several shapes of the surface aggregates of surfactants on hydrophilic surface have been proposed:

- Quasi two-dimensional analogues of the aggregate structures observed in bulk solution, i.e. spherical or cylindrical surface micelles, bilayer-type structures [12];
- “Half-micelles”, i.e. hemispheres, hemicylinders or dense monolayers, on top of a dense adsorbed monolayer with heads towards the surface [10];

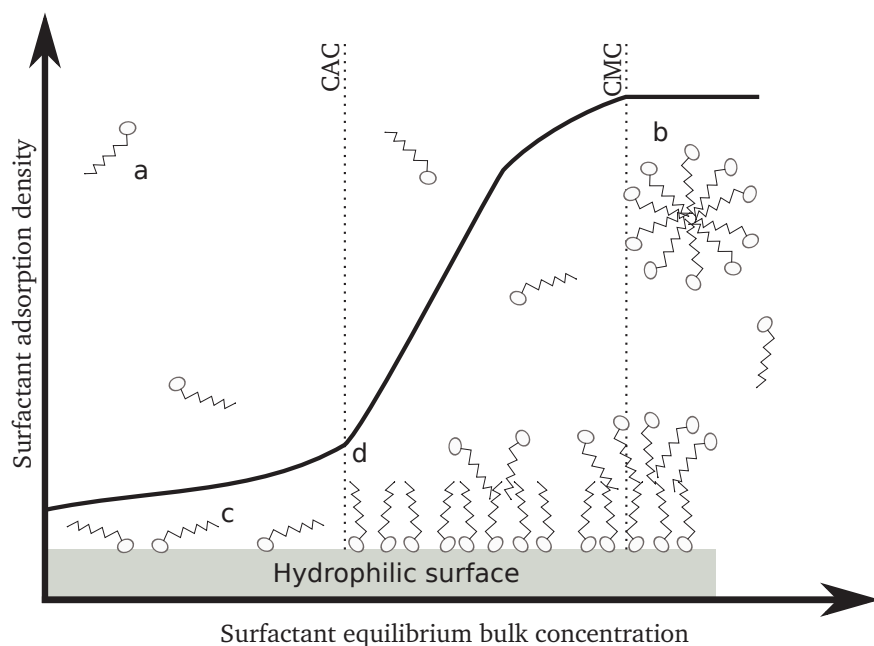


Figure 1.15: Adsorption of surfactants on hydrophilic surface. a: surfactant monomers, b: surfactant micelle, c: isolated adsorbed surfactant monomer, d: surface aggregates

1.2.2.5 Fluorinated surfactants

Fluorinated surfactants are a particular class of surfactants regarding their (saturated) hydrophobic chain. In comparison to classical hydrocarbon surfactant, some or all hydrogen in their hydrophobic chain have been substituted by fluorine atoms. Fluorinated surfactants can be perfluorinated in case of substitution of every hydrogen, or partially fluorinated otherwise [13]. Fluorotelomers are an important class of partially fluorinated surfactants in which $-CH_2-CH_2-$ groups have been inserted between the hydrophobic chain (figure 1.16) and the polar head. For instance, in a 6:2 fluorotelomer, the hydrophobic chain contains 6 perfluorinated carbons and 2 hydrogenated carbons, independently to its polar head (table 1.5).

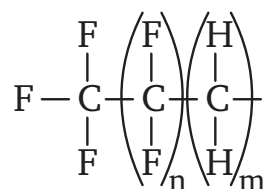


Figure 1.16: (n+1):m fluorotelomer hydrophobic tail

Regarding the polar head of perfluorinated surfactants, the three main chemical families are perfluorinated sulfonates, perfluoroalkyl carboxylate and perfluoroalkyl sulfonamide

(figure 1.17) [14]. Sulfonamide-based fluorinated surfactants (figure 1.17c) can be of great variety considering that R_1 may be a hydrogen or an alkyl group and R_2 an even more sophisticated organic group. The synthesis of perfluorinated and partially fluorinated surfactant and fluorotelomers will not be detailed here, but the interested reader can find a comprehensive review in [15].

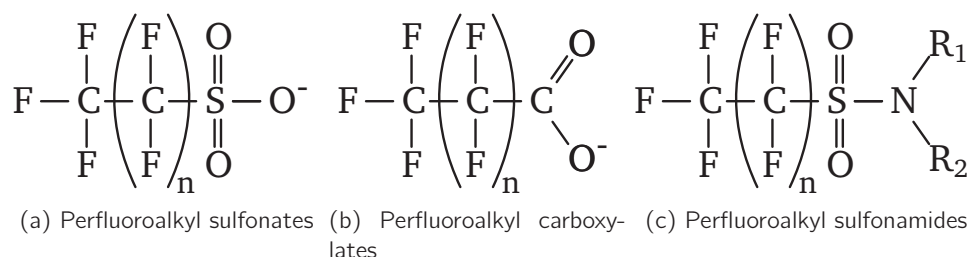


Figure 1.17: The three main families of perfluorinated surfactants regarding their polar heads, after [14]

Fluorinated surfactants are most commonly used as photolithographic chemicals in semiconductor industry, as emulsifiers in polymerization of fluoropolymers and as additive in high performance fire-fighting foams and electroplating baths [16]. The reason motivating the use of fluorinated surfactants are the very specific physical and chemical properties of this class of compounds.

Fluorine is the most electronegative element according to the Pauling electronegativity. The $\text{C}-\text{F}$ bond is the strongest known organic bond (table 1.9) and its ionization energy is high (figure 1.18). Hence fluorinated surfactants have outstanding chemical and thermal (figure 1.19) resistance compared to hydrocarbon surfactants [2].

Table 1.9: Bond energies in kcal mol^{-1} for various heteroatoms with hydrogen and methyl group [17]

Atoms (X)	Energy of $\text{H}-\text{X}$ bond	Energy of CH_3-X bond
<i>I</i>	71	56
<i>Si</i>	75	76
<i>Br</i>	87	70
<i>Cl</i>	103	84
<i>H</i>	104	105
<i>F</i>	135	109

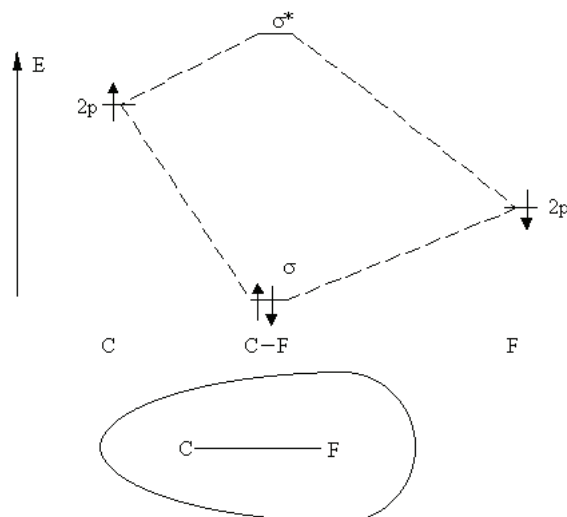


Figure 1.18: Molecular orbitals and polarity of the $C-F$ bond. Source: <http://www.math.jussieu.fr>

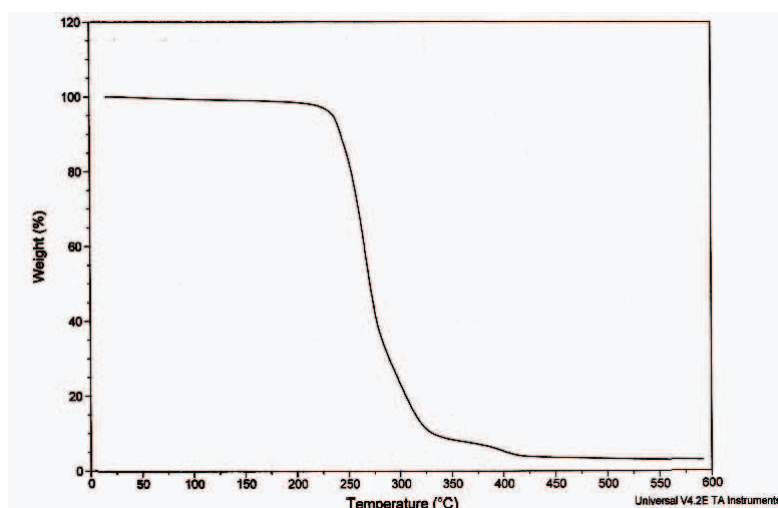


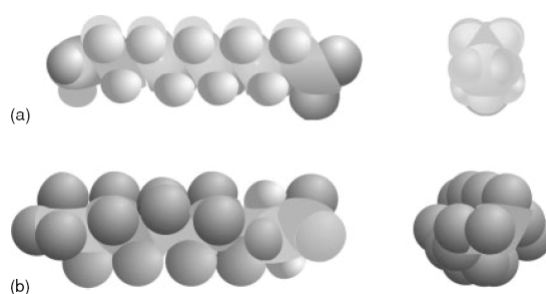
Figure 1.19: Thermogravimetric analysis of a fluorinated surfactant (with courtesy of DuPont)

The polarity of the $C-F$ bond is reversed compared to $C-H$ bond (figure 1.18). This leads to very low solid-vapor surface energies for fluorinated surfaces (table 1.10), leading to oil and water repellancy for fluorinated solid surface, and hydrophobicity as well as oleophobicity for fluorinated surfactants [2]. Finally, steric constraints in fluoroalkanes make the perfluorinated parts more rigid than hydrogenated chains (figure 1.20), protecting the carbone backbone from chemical attacks and increasing the ability of perfluorinated parts to self-organize.

Table 1.10: Surface tensions for ideal solid surfaces [18]

Surface end group	Surface tension ($mN m^{-1}$)
$-CF_3$	6
$-CF_2H$	15
$-CF_2-$	18
$-CH_3$	20.5
$-CH_2-$	31

Figure 1.20: Volume of (a): perhydrogenated and (b):perfluorinated homologous molecules



Not only are fluorinated surfactants more hydrophobic than hydrocarbon surfactants, they are also oleophobic and hardly mix with hydrocarbons. In addition, fluorinated surfactants can reduce the surface tension of the water to about $15\text{--}20\text{ mN m}^{-1}$ versus $30\text{--}40\text{ mN m}^{-1}$ for hydrocarbon surfactants, they have lower CMC and fluorinated compounds exhibit outstanding chemical and thermal stabilities [2].

1.2.3 Mixed surfactant systems and potential interactions between foam components

1.2.3.1 Mixed surfactant systems

Mixed surfactant systems, binary or multicomponent, are of great interest and have been widely studied in the passed three decades since surfactants are rarely used pure. In case of aqueous binary surfactant mixtures, properties of the solution like surface tension and CMC can, in case of ideal mixing, fall between the properties of the two single-surfactant solutions. In case of synergy, one or several properties of the mixture can fall outside the values for single components.

Clint has given a relationship between CMC of the mixture and molar fraction and CMC of single components in case of ideal mixing in micelles [19]. Then Rubingh adapted this

work to non ideal mixtures on the basis of regular solution theory [20], and Holland and Rubingh proposed a Nonideal Multicomponent Mixed Micelle Model based on binary interaction parameters between single surfactants [21]. Many mixed surfactant systems have been experimentally investigated: ionic–ionic, ionic–non ionic, ionic–zwitterionic, hydrocarbon–fluorinated for instance. A number of these combinations deviate from ideal mixing, showing synergies and sometimes presenting better performances than single surfactant solutions, but only those which might occur in the context of this work will be presented.

Binary anionic–non ionic surfactant mixtures On the basis of data from surface tension measurements, one can notice that in solutions of sodium dodecyl sulfate (SDS) and n-decanoyl-N-methyl glucamide and homologues (MEGA 8, 9, 10), every mixture shows a great synergism in terms of CMC and surface tension. SDS and MEGA showed positive synergy, resulting in attraction of the two surfactants, hence mixed micellization, decrease of the cmc of the mixture in regard to ideal mixing, and increase of surface tension reduction. Mixed micellization seems to be due to insertion of non ionic surfactant molecules in inter charged polar head spaces of anionic micelles, thus lowering electrostatic repulsion [22].

Mixture of SDS and polyoxyethylene lauryl ether (Brij 35) exhibits large negative deviation from ideality, indicating a strong attraction between the two surfactants. Adding an electrolyte to the mixture generally produces a decrease of this synergy, suggesting at least partly electrostatic interactions between SDS and Brij 35. This can be due to the formation of a complex between Na^+ , counter ion of SDS, and ether oxygens of the polyoxyethylene chain of Brij 35, interacting with negatively charged SDS [23]. But chelate-type cation binding to polyoxyethylene has not been well established and attraction between ethylene oxide and sulfate heads could also result from ion–dipole interaction [24].

Binary anionic–zwitterionic and nonionic–zwitterionic surfactant mixtures Surface tension measurements at the CMC in dodecyl dimethylamine oxide (DDAO) / SDS system exhibits strong synergistic effect, as surface tension of the mixture is far inferior to those of single components. The synergy was even larger than in the case of SDS / hexa ethylene glycol n-monododecyl ether ($C_{12}E_6$). This stronger interaction between anionic and zwitterionic surfactants could be due to ion pairing of the positive part of the zwitterionic surfactant

to the negative charge of the anionic one, electrostatic attraction between unlike charges and reduction of electrostatic repulsion between like ones. In addition, protonation of DDAO in mixed micelles should occur at higher pH than expected [24].

In SDS and cocoamidopropyl or dodecyl betaine mixtures, the solution can show strong synergistic effects on CMC and/or surface tension. These systems also exhibit the formation of large rod-like mixed micelles at low concentration, and cocamidopropyl betaine seem to dominate surfactant adsorption at air–water interface apparently due to a greater surface activity than SDS [25].

Goloub et al. showed an interesting behavior of mixed DDAO / $C_{12}E_6$ systems: when DDAO is neutral (pH 8) mixing is near to ideality, and when it is charged (pH 2) there is a positive synergy [24], highlighting the importance of electrostatic interactions in mixed micellization.

Hydrocarbon–fluorinated surfactant mixtures Most of studies on mixed surfactant systems containing an anionic hydrocarbon surfactant and a fluorinated surfactant deal with sodium perfluoroacetate (SPFO) [26, 27, 28, 29]. Mukerjee and Yang showed that the CMC for an aqueous mixture of SPFO and sodium decyl sulfate (SDeS) was higher than the CMCs of the individual components in water due to a negative synergy, suggesting the existence of two kinds of micelles, one rich in fluorosurfactants and one rich in hydrogenated surfactants [26]. Then followed the main and recurring question in this domain, whether SPFO and SDeS form mixed micelles, with detractors on both sides [27], and recently, 1H and ^{19}F NMR spectroscopy seemed to indicate that mixed micellization of SPFO and SDeS occurs according to a *patchwork model*, with a single type of micelles within which fluorinated surfactants are preferentially coordinated by fluorinated ones and hydrogenated surfactants by hydrogenated ones [29, 27]. Adsorption of surfactants on alumina in such systems seems to take place in mixed molecular aggregates, in which, after having reached saturation, a further increase of surfactant concentration in the mixed system leads to decyl sulfate desorption and increased perfluorooctanoate adsorption [28].

Binary mixtures of fluorocarbon and hydrocarbon non-ionic surfactants derived from the tris(hydroxymethyl)acrylamidomethane (THAM) have also been examined. For particular compositions, these systems presented two critical micelle concentrations. Above the sec-

and CMC, Barhelemy et al. proposed that two kinds of micelles (fluorocarbon-rich and hydrocarbon-rich) should coexist as a result of the incompatibility between the two types of surfactants [30]. In case of binary mixtures containing a fluorinated amphiphile surfactant, no synergism in surface tension was noticed with sodium dodecylbenzenesulfonate or 3-oxaheptanol, and the adsorption layers were mainly occupied by fluorinated surfactants [31]. Interaction between surfactants seems to depend not only on the nature of the hydrophobic part, hydrocarbon or fluorinated, but also on the nature of respective polar heads.

Viscoelasticity and worm-like micelles Small micellar aggregates of some surfactants exhibit enormous growth in one dimension and form very long and flexible worm-like micelles. These giant micelles are entangled to form a transient network, and exhibit viscoelastic behavior analogous to a flexible polymer solution. However, unlike polymers in solutions, worm-like micelles undergo breaking and recombination, and, therefore, exhibit complex rheological behavior. Incorporation of a various non-ionic amphiphiles as cosurfactant in the palisade layer of micellar aggregates has been shown to enable the formation of viscoelastic micellar solutions in dilute solution of different classes of surfactants. Worm-like micelles one-dimensional growth is enabled by the lowering of the average area of surfactant head group, resulting in an increase of the packing parameter and a decrease of the interfacial curvature in the aggregates [32]. Worm-like micelles have also been reported in mixed systems containing amino-acid based surfactants [33, 34]. Pilot firefighting water — in addition to cosolvent — may contain protein hydrolysates that could be constituted of such surfactants and may confer viscoelasticity and worm-like micelles formation in our solutions.

1.2.3.2 Interaction of surfactants with proteins and polymers

Protein–surfactant interaction Binding of anionic surfactant onto protein has been shown to result from hydrophobic interactions [35]. The more hydrophobic the surfactant is, the more it aggregates to the protein [36]. In case of a mixture of anionic surfactant and sodium caseinate, the more the concentration of surfactant increases, the more the size of the aggregates decreases, because of the increasing electrostatic repulsion between polar heads of the surfactants adsorbed on the proteins [37]. For surfactants having the same chain length, fluorinated surfactants binding to proteins has been shown to be stronger than

hydrocarbon surfactants [35].

Polymer–surfactant interaction In a surfactant–polymer mixture, when concentration of surfactant reaches the critical aggregation concentration, which is far much lower than CMC, surfactants form micellar-like aggregates with polymer in solution. If the polymer is charged, electrostatically-stabilized complexes form between polymer and unlike charged surfactant. There is also a contribution of surfactant–polymer hydrophobic interaction. With like charged surfactants, interaction is weaker and can only occur if the polymer has a very pronounced hydrophobic nature [38].

1.2.3.3 Types of surfactants in pilot firefighting waters and their potential interactions

The pilot firefighting water used in this work is a formulation containing several surfactants of different kind which might be subject to interaction and/or synergy. Regarding the properties of polar heads (figure 1.21, table 1.11) and the bibliography in the present section, some interactions may occur between components of this surfactant mixture. Non ionic surfactant and zwitterionic surfactants present in foam components might indeed show positive synergy with anionic sulfate surfactants, in terms of surface tension and mixed micellization. Because of the cosolvent, worm-like micelles might be present in firefighting water. However, before predicting surfactant mixture properties, one has to take care of the presence of impurities like fractions of homologue surfactants or alcohols in technical grade surfactants, and their influence on the properties of the solution [25].

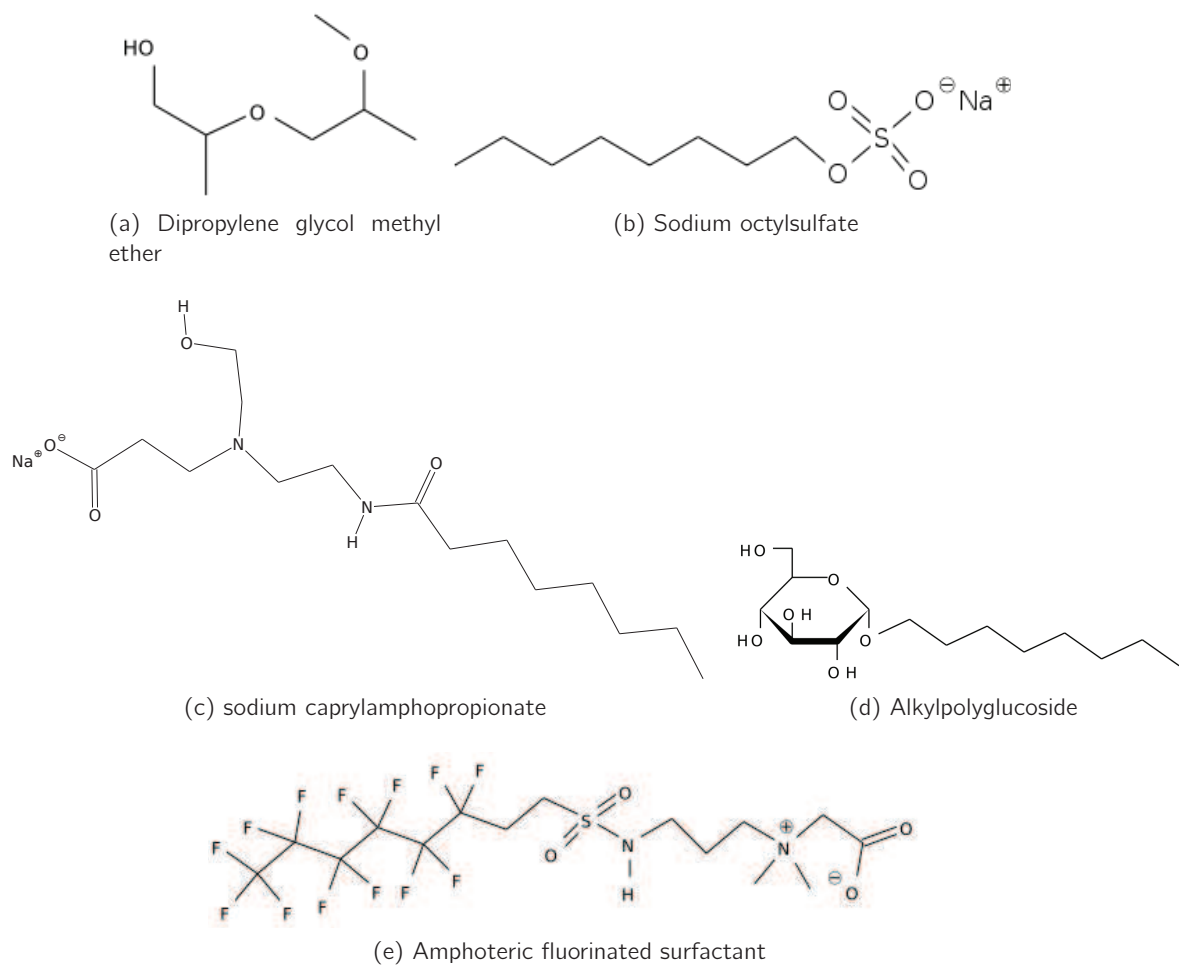


Figure 1.21: Formula of the compounds contained in the pilot firefighting waters

Table 1.11: Properties of pilot firefighting water components polar heads and their potential polar interactions

Compound	Name of commercial product	Type of surfactant	Polar parts properties	Potential polar interactions
Dipropylene glycol methyl ether (Fig 1.21a)	Dowanol [®] DPM	Cosolvent	Electron donor, electron acceptor	Electron acceptor, electron donor
Sodium octylsulfate (Fig 1.21b)	Disponil [®] SOS 842*	Anionic	Negatively charged, electron donor	Positive sites, dipoles, electron acceptor
sodium caprylamphopropionate (Fig 1.21c)	Tegotens [®] AM VSF*	Zwitterionic	Negatively and positively charged (dipole), electron donor	Charged sites, electron acceptor
D-Glucopyranose oligomers (C8-C10 alkyl polyglucosides, Fig 1.21d)	Simulsol [®] SL8*	Nonionic	Electron donor, electron acceptor	Electron acceptor, electron donor
Amphoteric fluorinated surfactant fraction (Fig 1.21e)	Forafac [®] 1157N*	Amphoteric	Negatively and positively charged (dipole), electron donor	Charged sites, electron acceptor

1.2.4 Scientific purpose of the work

In addition to the industrial purpose of providing a mobile viable alternative process to firefighting water incineration, the present work aims at studying the particular behavior of surfactants at interfaces in the context of water treatment processes such as electrocoagulation and membrane processes.

Conclusion

The context of the present work has been introduced. Extinguishment of large solvent fire leads to the production of firefighting waters, which are collected thanks to the design of industrial infrastructures. Depending on the nature of the firefighting foam used, the resulting water may require the removal of fluorinated surfactants potentially present. After decantation of the organic phase, firefighting waters essentially contain surfactants. Surfactants are amphiphilic chemicals having the ability to lower interfacial tension by adsorbing in an oriented fashion at interface. Surfactants can form aggregates in solution and on interfaces under certain conditions, and have a dramatic influence on interfacial phenomena. Hence, before considering any water treatment process, interfacial science and surfactant were introduced.

The work developed in the following chapters has a dual purpose. The industrial purpose is to provide an economically viable alternative to water incineration. The foreseen unit will have to be mobile and able to extract fluorinated surfactants from water at a rate of 1–4.5 m^3h^{-1} (20000 m^3 in 4–6 months). The scientific purpose of this work is the study of the behavior of surfactants in the context of water treatment processes, and particularly in membrane processes. The state of the art of relevant water treatment processes is covered in the following chapter.

Chapter 2

Bibliographic study and process screening

Introduction

The design of the mobile unit started with the bibliographic study of the processes used for the water containing fluorinated surfactants. The literature was very dense about the treatment of water containing perfluorinated surfactants, but these compounds were different from the fluorinated surfactant used in this work. Nevertheless, the processes identified and chosen from the bibliography were assessed in a screening. As most of the considered processes required a particle-free feed, the mobile unit was expected to comprise at least two steps: a pretreatment and a treatment step. The assessments of the processes were done on the basis of experiments with pilot firefighting waters of chosen composition and model solutions, turbidity measurements for the pretreatment, and fluorinated surfactant concentration measurements for treatment step. The most promising processes were chosen on the basis of the screening results and of the constraints of mobility for the unit, as stated in the following research and design strategy.

2.1 Research and design strategy

The industrial objective of this work is to design a mobile unit able to separate the fluorinated surfactants contained in firefighting water. Hence, the efficiency will not be the only

assessment parameter for the processes. The unit is expected to be mobile for two main reasons: the minimization of the transportation cost by sending the unit across continents to the water, and not the water to the unit, and the absorption of the fixed cost of the unit by reusing it on different sites.

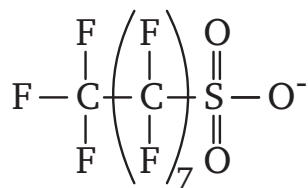
Therefore, the mobility has to be kept optimum by using preferably compact processes, as the unit has to fit in a container. In addition, the processes have to be as materially autonomous as possible. Raw materials such as chemicals, liquids or solids should be minimized, or avoided if possible, for supply and logistics considerations. For the same reasons, the output of the unit that may be liquid or solid waste, also has to be minimum and highly concentrated. Manual handling will be preferably avoided by the choice of processes as continuous and automatizable as possible.

The scientific purpose of this work is the study of the behavior of surfactants at the solid/liquid interface in water treatment processes. Real firefighting waters are complex solutions containing suspended matter and a variety of surfactants, not only of different polar heads, but also of different hydrophobic tails. Though the aim of this work is to apply the unit to real firefighting waters, the understanding and the optimization of several steps required the use of model and pilot solutions, which gradually approached the complexity of actual firefighting waters. After a bibliographic study, the most relevant processes were assessed during the screening. The selected processes were deepened in chapter 3 and 4 and finally, a possible design of the mobile unit was proposed in chapter 5.

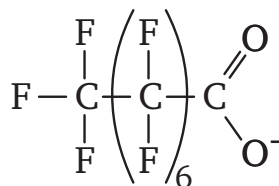
2.2 Bibliography

As the carbon-fluorine bond is highly resistant to biochemical degradation [39], fluorinated compounds such as a 6:2 fluorotelomer sulfonate and perfluorooctanoate [40] as well as others perfluorinated compounds [41] were found to resist conventional biological wastewater treatment processes. Therefore this kind of chemicals require specific water treatment processes. The most represented fluorinated surfactants in the literature of water treatment processes are perfluorooctane sulfonate (PFOS, figure 2.1a) and perfluorooctanoate (PFOA, figure 2.1b). The rest of studied fluorinated surfactants in this context are mainly various perfluoroalkyl sulfonates (figure 2.1c), carboxylate (figure 2.1d) [42] and in a lesser extent

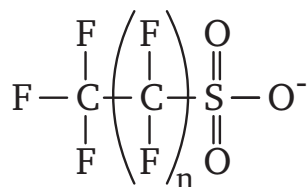
perfluoroalkyl sulfonamides (figure 2.1e).



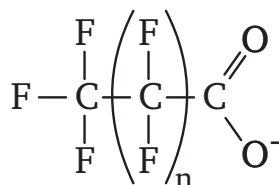
(a) Perfluorooctane sulfonate (PFOS)



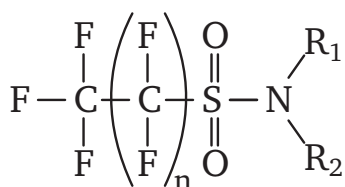
(b) Perfluorooctanoate (PFOA)



(c) Perfluoroalkyl sulfonates



(d) Perfluoroalkyl carboxylates



(e) Perfluoroalkyl sulfonamides

Figure 2.1: Fluorinated surfactants mostly found in the water treatment literature

This work focused on a particular fluorinated surfactant used in AFFF which will be designated as fluorinated surfactant in the rest of this work (figure 2.2). This compound markedly differs from the previous cited fluorinated surfactants: it is a 6:2 fluorotelomer with a carboxy betaine as apolar head and a sulfamide group as linker. The following bibliographic study will review the water treatment processes applied to fluorinated surfactants, and did

not intend to be an exhaustive list of water treatment processes. As firefighting water was found to contain suspended matter and most the treatment processes require particle free input, the bibliography will start by pretreatment processes.

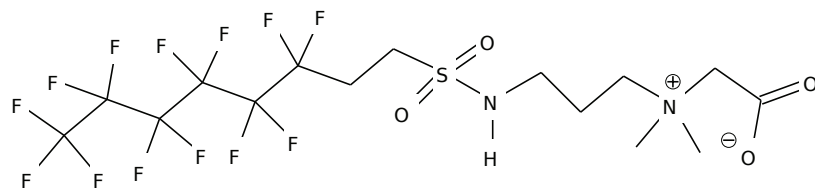


Figure 2.2: Chemical structure of the fluorinated surfactant considered in this work

2.2.1 Pretreatments processes for the suspended matter in firefighting waters

2.2.1.1 Physical processes

Suspended matter removal in water treatment processes can be achieved with physical processes such as filtration or decantation. Particles may be retained by various filtering media and filter designs according to the respective size distributions of pores and particles. With conventional filtration, the filter may be fouled by various mechanisms, giving various flux decrease profiles. These mechanisms and the corresponding equations will not be detailed here but can be found in the literature [43].

If the sedimentation speed is sufficient thanks to favorable interplay between gravity and buoyancy of the particles in water, suspended matter can be removed by natural decantation. Otherwise decantation can be enhanced with decanters of various design, or by centrifugation and hydrocycloning [44]. However, in case of stable colloidal suspension, decantation may be impossible and require a physicochemical treatment.

2.2.1.2 Physicochemical processes

Coagulation-flocculation is widely used in water treatment for the removal of dissolved and colloidal mater. The principle is to use *Al* salts, *Fe* salts or synthetic coagulants to neutralize electrostatic repulsion of negatively charged particles. Once their charges neutralized, particles can coagulate and form aggregates. However, the size of these aggregates is still too small to permit fast decantation or easy filtration, thus polymeric flocculants are used.

Their role is to gather the aggregates to form a floc that is easy to handle. Most of the commonly employed coagulating agents are listed below [45, 46, 47]

- Ferric salts: $FeCl_3$, $Fe_2(SO_4)_3$, polyferric chloride, polyferric sulphate;
- Aluminium salts: $AlCl_3$, $Al_2(SO_4)_3$, polyaluminum chloride (PAC);
- Cationic polymeric coagulating agents: cationic polyamines, linear polyacrylamide methacrylate copolymers, chitosan (chitosan is an expensive biopolymer of limited availability);
- Anionic polymeric coagulating agents: linear polyacrylamide acrylate copolymers;

The action of coagulating agents can be driven by electrostatic and/or hydrophobic interactions, and with aluminium and iron-based compounds, the Lewis acidic character has to be considered. Thus, as a result of surfactant–polymer interactions [38], coagulating agents may be stabilized in surfactant solutions, lowering their efficiency. For instance, the coagulation of solutions containing 5 g L^{-1} of soil and 5 g L^{-1} of anionic or non ionic surfactant using chitosan, polyacrylamide and polyaluminium chloride as coagulating agents was studied [48]. Chitosan was found to have the best efficiency on soil removal. The presence of nonionic surfactant increased the chitosan efficiency whereas the anionic surfactant made it strongly decrease. This could be explained in terms of favorable electrostatic interaction between the cationic chitosan and the anionic surfactant, resulting in the complexation of the coagulant.

Aluminium and ferric salts can be added under the form of conventional chemicals, but also by electrocoagulation. Electrocoagulation is a coagulation process in which the coagulant is generated in situ by electrochemical dissolution of a metallic anode, generally made of iron or aluminium. The metal hydroxide active species are able to remove various dissolved and suspended pollutants by means of several mechanisms which will be developed in Chapter 3. Electrocoagulation has been found able to efficiently treat laundry wastewater containing surfactants [49], and to remove an anionic hydrocarbon surfactant from various wastewaters [50, 51]. Though there seemed to be at our knowledge no literature directly involving fluorinated surfactants and electrocoagulation, this process remains interesting because of its underlying removal mechanisms.

2.2.2 Treatment processes for fluorinated surfactants

Processes will be presented from the most conventional to the most sophisticated. The most obvious processes for chemicals having the tendency to adsorb at interface is adsorption or surface-related processes, with various substrates “trapping” fluorinated surfactants. These compounds may also be removed from water by membrane processes, which let the water permeate through their membranes, and have the ability to retain chemicals according to various factors such as charge, molecular weight or molecule chemistry according to the membrane nature. Destructive processes such as oxidation and advanced oxidation processes are another class of processes used to remove organic matter from water. Their application to solution of fluorinated surfactants will be considered, as well as that of extraction processes.

2.2.2.1 Adsorption processes

To maximize the adsorption of fluorinated surfactants, one can take advantage of hydrophobic interaction between the adsorbent and the hydrophobic tail, but also of eventual polar and electrostatic interactions between the polar head and the adsorbent. Hence the main adsorbents found in literature for fluorinated surfactants are granular and powder activated carbon and ion exchange resins (table 2.1). As the most cited fluorinated surfactants are anionic, cationic adsorbents have also been reported to take advantage of electrostatic interaction between electric charges, even at high concentrations [52]. The adsorption of three fluorinated telomers: a cationic 8:2 pyridinium fluorotelomer, an anionic 6:2 fluorotelomer sulfonate and a non ionic 6:2 polyethoxylated fluorotelomer; has been studied on gold electrodes [53]. The adsorption of the cationic pyridinium fluorotelomer was driven by interaction between π electrons and the electrode, independently to the surface charge. Molecules showed flat adsorption until surface saturation with increasing equilibrium concentration, but no self-organization at the surface. The anionic surfactant only adsorbed when the electrode was positively charged, and showed a IV-region isotherm with self interaction at high concentrations (see Chapter 1, section 1.2.2.4). The non ionic fluorotelomer showed an intermediary behavior, between the anionic fluorotelomer on positive surface, and the cationic on negative surface, but in both cases with weaker interactions.

Activated carbon and resins were found suitable for the adsorption of perfluorinated

surfactants. The adsorption capacity was shown to be higher for longer perfluorinated chains [54, 55], and even higher in case of favorable electrostatic interaction [56, 52]. The possibility of self-organization of fluorinated surfactants at the adsorbent surface can increase the sorption capacity [2, 57, 52], showing the importance of pore dimensions in the adsorbent. However, adsorption was reported inadequate for very high concentrations [58] and some perfluorooctanoate showed adsorption plateau on activated carbon for equilibrium concentrations superior to $40\text{--}50\text{ mg L}^{-1}$. Some adsorbents showed selectivity for PFOS among other chemicals [56]. At the moment of this work, only one study involving the adsorption of a fluorotelomer potentially present in AFFF on activated carbon was found [2]. The adsorption of the fluorinated surfactant was studied alone and in mixture with a cosolvent and an anionic surfactant. Though showing interesting results in terms of adsorption performance, the other chemicals of the mixture were also shown to adsorb strongly on the activated carbon. In this kind of context, no additional information was found on competitive adsorption of hydrogenated and fluorinated surfactants, and the behavior of the adsorbent near saturation remains unknown. Moreover, the majority of these studies involved model solution, and the action of firefighting foam additives such as protein hydrolysates or polymers would require proper study. Removal by means of interaction with different coagulants, which can involve the same kind of interaction as in adsorption were treated in section 2.2.1.2.

Table 2.1: Adsorption processes applied to fluorinated surfactants

Surfactants	Substrates	Main results	Reference
Perfluoro octanoate (PFOA, 10–40 $mg\ L^{-1}$)	Powder activated carbon	99% removal, Langmuir isotherm.	[59]
Perfluoro octane sulfonate (PFOS, 10 $\mu g\ L^{-1}$)	Ion exchange polymer and granular activated carbon	Best performances with a crosslinked aromatic polymer: 99.99% removal after 23,000 bed volumes	[60]
PFOS (10–5,000 $\mu g\ L^{-1}$)	Ionic and non ionic exchange polymer, granular activated carbon	Best performances with polymers: ionic polymer for concentration $>1\ \mu g\ L^{-1}$, non ionic polymer below.	[61]
PFOS, PFOA (20–250 $mg\ L^{-1}$)	Powder and granular activated carbon and anion exchange resin (polystyrene divinylbenzene)	Adsorption velocity (powder activated carbon $>$ granular activated carbon and resin) depends on adsorbent's dimension. High sorption capacity for both surfactants on powder activated carbon and resin. Adsorption governed by electrostatic and hydrophobic interactions. Possible hemimicelle formation in intraparticle pores.	[57]

Surfactants	Substrates	Main results	Reference
PFOA ($\sim 1,000 \text{ mg L}^{-1}$), PFOS ($\sim 3,000 \text{ mg L}^{-1}$)	Granular activated carbon Calcium fluoride solid Anion exchange resins	Activated carbon: PFOS and PFOA resulting concentration $>1 \text{ mg L}^{-1}$ with solutions diluted 50 times, but both found moderately adsorbable compared to other chemicals. Calcium fluoride: partial removal. Ion exchange resins: loadings of $686 \text{ mg PFOA g}^{-1}$ and $151 \text{ mg PFOS g}^{-1}$ of resin for the most efficient one, but slow kinetics.	[58]
Amphoteric fluorinated surfactant; Amphoteric fluorinated surfactant (54 mg L^{-1}), anionic surfactant (564 mg L^{-1}), cosolvent (400 mg L^{-1})	Activated carbon	Best performances with higher pore dimension, $>99.69\%$ removal for the fluorinated surfactant, adsorption of every compound of the mixture (no selectivity).	[2]

Surfactants	Substrates	Main results	Reference
PFOS, perfluoro butane sulfonate (PFBS), PFOA	Granular activated carbon, zeolites and anaerobic and activated sludges	The longer the perfluorinated chain, the higher the sorption on activated carbon. PFOA and PFBS: adsorption plateau on activated carbon for equilibrium concentrations exceeding $40\text{--}50\text{ mg L}^{-1}$. PFOS affinity with the substrates: granular activated carbon > hydrophobic zeolite > anaerobic granular sludge > activated sludge. Moderate activated carbon capacity for high PFOS concentrations ($>80\text{ mg L}^{-1}$).	[54]
PFOS, PFOA and shorter perfluorocarboxylates ($0.5\text{--}3\text{ mg L}^{-1}$)	Suspended matter from surface water, powder activated carbon and polyaluminium chloride (coagulant)	Adsorption of perfluorinated surfactants on suspended matter, electrostatic interaction between the positively charged polyaluminium chloride and dissolved surfactants. Competitive adsorption in mixtures: the longer the perfluorinated chain, the lesser the resulting concentration.	[55]
PFOS ($50\text{--}400\text{ mg L}^{-1}$)	Crosslinked chitosan beads	Higher sorption capacity than some reported adsorbents. Electrostatic interaction with positively charged surface groups on chitosan, Hydrophobic self-interaction and multilayer adsorption of PFOS at high concentration.	[52]

Surfactants	Substrates	Main results	Reference
PFOS, PFOA, and 2,4-dichlorophenoxyacetic acid, sodium dodecyl benzene sulfonate, sodium pentachlorophenate and phenol. (50 mg L ⁻¹)	Chitosan-based imprinted polymer adsorbent	High adsorption capacity and selectivity for PFOS when in mixture with one of the other chemicals, due to electrostatic interaction.	[56]

2.2.2.2 Membrane processes

Membrane processes are a class of processes involving a selective membrane and a driving force to perform separation operations. In membrane processes, the feed stream is divided in two streams: the concentrate or retentate stream, and the permeate stream (Fig. 2.3). Depending on the nature of the operation performed, the stream of interest will generally be either the permeate in case of purification, or the retentate in case of concentration.

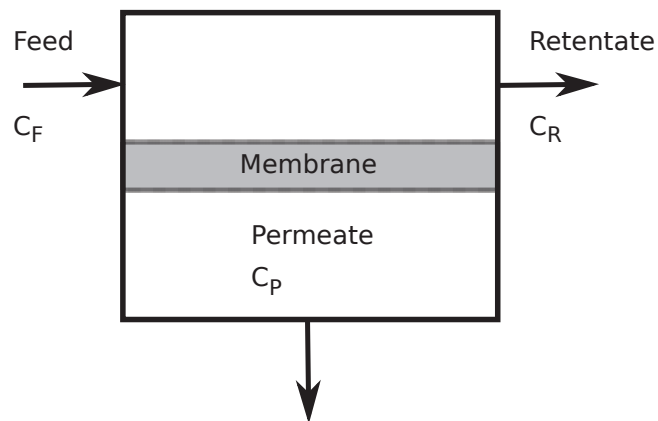


Figure 2.3: Membrane process

The performance of membrane processes is determined by two parameters: the selectivity and the flow. Selectivity can be expressed by the retention rate R (Eq. 2.1). The retention rate is expressed as follows:

$$R = 1 - \frac{C_P}{C_R} \quad (2.1)$$

with C_P and C_R the concentration of the solute in the permeate and in the retentate respectively. R can vary between 100% in case of complete retention of the solute (*ideal* semipermeable membrane) to 0% if the solute and the solvent can pass the membrane freely without modification of the feed composition. The flow passing through the membrane is generally expressed in terms of flux density J which is the ratio between the permeate flow Q_P and the membrane area A :

$$J = \frac{Q_P}{A} \quad (2.2)$$

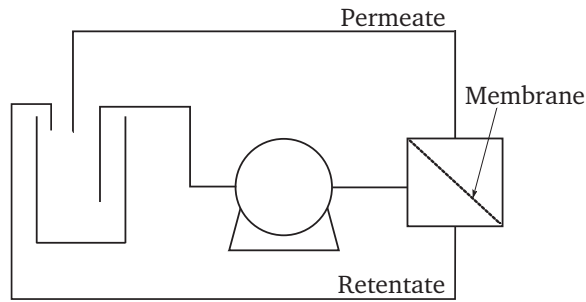
In SI units, flux density is expressed in $m^3 m^{-2} s^{-1}$ but in practice it is generally expressed in $L h^{-1} m^{-2}$. The permeability L of the membrane, in $L h^{-1} m^{-2} bar^{-1}$ is given by:

$$L = \frac{J}{\Delta P} \quad (2.3)$$

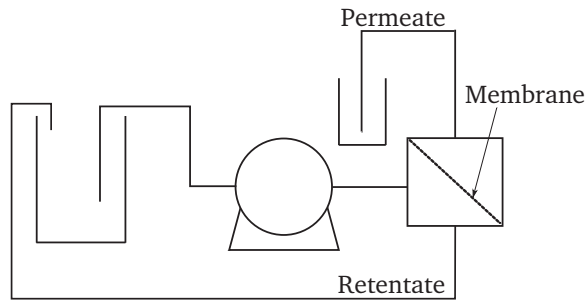
The Volume Reduction Ratio, VRR , represents ratio of treated retentate and is expressed as follows in terms of volume:

$$VRR = \frac{V_0}{V_f} \quad (2.4)$$

with V_0 the initial feed volume and V_f the final retentate volume. With membrane pilots, experiments in batch mode can be done according to two main setups (figure 2.4). In full recycling mode, the permeate is returned to the feed, whereas in concentration it is extracted.



(a) Full recycling mode. $V_0 = V_f$, $VRR = 1$.



(b) Concentration mode. $V_0 > V_f$, $VRR > 1$.

Figure 2.4: The two main setups for membrane pilots

The differences between filtration membrane processes, namely microfiltration, ultrafiltration, nanofiltration and reverse osmosis, result from the kind of semipermeable membrane used and their corresponding properties (table 2.3). The fluorinated surfactant has a length of 1.8 nm [2], which should lead to a micellar diameter near 4 nm at least assuming spherical micelles, and even bigger micelles for cylindrical or lamellar micelles. Considering surfactant solutions, the processes of interest may be ultrafiltration, nanofiltration and reverse osmosis.

Table 2.3: Membrane processes and relative order of magnitude of membrane properties [62]

Membrane processes	Pore size	Applied pressure (<i>bar</i>)	Water permeability ($L\text{ h}^{-1}\text{ m}^{-2}\text{ bar}^{-1}$, at 20°C)
Microfiltration	$0.1\text{--}10\text{ }\mu\text{m}$	0.1–5	500–10000
Ultrafiltration	$50\text{--}100\text{ nm}$	1–5	50–100
Nanofiltration	1 nm	10–40	10–100
Reverse osmosis	$< 1\text{ nm}$ (dense)	30–80	3–20

Ultrafiltration can be used to treat sufficiently concentrated surfactant solutions, retaining micelles and letting surfactant monomers permeate (figure 2.5) [63, 64]. This permeate containing surfactants at concentration near to the CMC can then be treated by nanofiltration or reverse osmosis to remove the remaining traces [65]. The main issues in membrane processes dealing with surfactants are membrane fouling, surfactant rejection and adsorption, which depend on surfactant–membrane interactions.

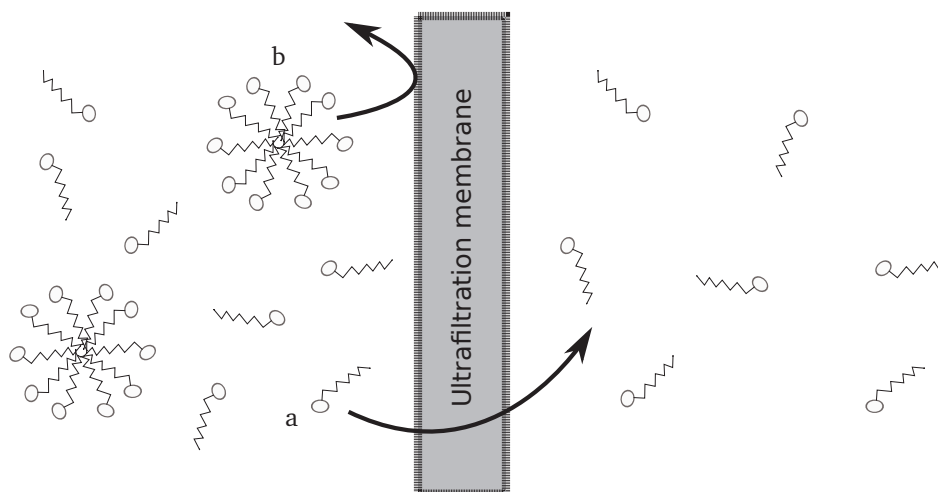


Figure 2.5: Ultrafiltration of a micellar surfactant solution. a: surfactant monomer, b: surfactant micelle. Dynamic equilibrium between surfactant monomers and micelles, as well as surfactant adsorption not pictured.

Kaya et al. studied filtration of two anionic surfactants — linear alkyl benzene sulfonate (LABS) and sodium lauryl ether sulfate (MLABS) — and one non-ionic surfactant — nonyl phenol ethoxylate (NPE) — in single and mixed solutions, with membranes of different pore size and hydrophilicity [65]. With single surfactant, results show that the more hydrophilic the membrane was, the more it was fouled by anionic surfactants; and the more hydrophobic it was, the more it was fouled by the non-ionic surfactant. Anionic and non-ionic surfactant mixtures behave like single anionic surfactant solution with every membrane, showing higher fouling on hydrophilic ones. The synergy between anionic and non-ionic surfactants seemed to result in “hiding” the non-ionic surfactant to the membrane.

In literature, most of fluorinated surfactants nanofiltration works deal with perfluoroalkyl sulfate or carboxylate [66, 67, 68]. PFOS Rejection efficiencies for NF membranes can reach 90–99% [67] and for feed concentrations from 0.5 to 1500 $mg\ L^{-1}$, reverse osmosis membranes could reject 99% or more [66, 67]. According to Steinle and Darling [68], anionic perfluorinated surfactants adsorb only at the surface of the reverse osmosis membranes whereas uncharged perfluorinated surfactant perfluorooctane sulfonamide (FOSA) could adsorb far much in the membrane matrix. The difference of retention rates showed that the behavior of the surfactant regarding the membrane was closely related to the chemistry of its polar head.

2.2.2.3 Destructive processes

Fluorinated surfactants can be incinerated at high temperature in halogen resistant incinerators, but water incineration is not economically acceptable. Due to its particular nature, carbon-fluorine bond is highly resistant to biochemical degradation [39] and advanced oxidation processes like ozonation. Ozone with either UV or hydrogen peroxide, and Fenton's reagent were found to be inefficient on the perfluorinated part of several anionic and non ionic fluorinated surfactants [69].

Photocatalysis, a light induced oxidation with help of an heterogeneous catalyst, has been used to successfully degrade fluorinated surfactants in F^- and CO_2 [70, 71, 72]. Sonolysis, a degradation by high frequency ultrasound from a probe, has also been reported to degrade perfluorinated compounds [73, 74], however with the drawback of low molecular weight

fluoroalkane emanations. Photocatalysis was also coupled to sonolysis to degrade fluorinated compounds but the trifluoroacetic acid, the ultimate product of the reaction, seemed to be resistant to the process [75]. In addition, classic photocatalysis showed low photonic efficiencies [76].

2.2.2.4 Extraction-based and miscellaneous processes

Liquid–liquid extraction of PFOS with n-hexane was studied and showed little removal efficiency. PFOS had a partition coefficient of 17 in n-octanol, but the authors discarded this technology because of its cost, due to solvent supply and purification, in addition to the necessity of further solvent removal from treated water [58]. Fluorinated surfactants, as well as fluorinated tellomers are known to be soluble in supercritical CO_2 ($scCO_2$) [77, 78, 79]. Fluorinated surfactants can form reverse micelles in $scCO_2$, and can be used to facilitate the extraction of hydrophilic high molecular weight molecules such as proteins or amino acids from water [78, 79]. $scCO_2$ extraction, though used for the extraction of compounds from solid materials, can also be used to extract liquid phases. This technique could be a good candidate as a selective extraction of fluorinated surfactants from firefighting water but, because of the required apparatus and technical expertise, this process will not be covered in the present work.

As perfluorinated surfactants are (believed) non volatile, evaporation of water containing PFOS and PFOA was studied. The foaming behavior of the solution was problematic and antifoaming agent had to be used, and these additives increased the viscosity of the solution. PFOA was found slightly volatile under its acidic form. At neutral pH, both PFOS and PFOA concentrations were $<1\text{ mg L}^{-1}$ but after discussion of the authors based on process flow diagrams, evaporation was considered more complicated and more expensive than ion exchange [58].

2.2.3 Comparison and selection of processes for the screening

The review of candidate processes for the treatment of firefighting water indicates that the final process will comport at least two steps: a pretreatment step and a treatment step, and maybe a final treatment to remove eventual remaining traces of fluorinated surfactant and

confer a safety margin in case of failure of previous steps. The selection of the processes to screen was done according to the bibliographic study, and to the constraints of the mobile unit. The comparison between identified processes is summarized in table 2.4.

Table 2.4: Comparison of the processes identified in the bibliographic study

(a) Pretreatment processes for the suspended matter of the firefighting waters

Processes	Expected efficiency	Sobriety in raw material	Sobriety in waste production	Cheapness	Compactness	Feasibility in the laboratory	Specific remarks
Filtration	?	+	+	+	+	+	Filter fouling and replacement
Decantation	?	+	+	+	+	+	Might not be efficient on fine and colloidal particles
Centrifugation	?	+	+	+	+	+	Might not be efficient on fine and colloidal particles
Coagulation–floculation	?	--	--	-	-	+	Floc removal required
Electrocoagulation?	+	+/-	-	-	+	+	Floc removal required

(b) Treatment processes for the fluorinated surfactants of the firefighting waters

Processes	Expected efficiency	Sobriety in raw material	Sobriety in waste production	Cheapness	Compactness	Feasibility in the laboratory	Specific remarks
Adsorption	++	--	--	+	-	++	The adsorbent may be recycled with organic solvents.
Membrane processes	++	++	+	-	+	++	Membrane may be subject to fouling. Important initial cost.
Advanced oxidation processes	-	?	+	-	+	--	Efficiency hindered by the stability of the carbon–fluorine bond.
Liquid–liquid extraction	--	-	?	+	+	+	Not efficient.
scCO ₂ extraction	++	?	+	-	?	--	Interesting process, but lack of capacity and expertise in the laboratory.

Filtration or decantation compared to coagulation processes have the advantage of not requiring *a priori* any loading of chemicals. However filtration may presents drawbacks of eventual fouling and decantation may not be efficient on colloidal suspensions. Therefore the use of coagulants may be required. Electrocoagulation has the advantage compared to conventional coagulation of not requiring large tanks of salts and sepcific steps for the solubilization and dilution of the coagulating agent. Coagulating techniques produce sludges which may require a filtration step.

Processes like scCO₂ extraction or advanced oxidation processes were excluded of the experimental screening due to lack of capability and expertise in the laboratory, and resulting by-products. Adsorption has been shown to be efficient for fluorinated surfactant removal, but significant amount of adsorbents may be needed. This amount may be reduced by regeneration but at the cost of an additional step involving polar organic solvents. Membrane processes like nanofiltration or reverse osmosis have the advantage of not requiring chemical input, but this kind of process has a high initial cost and membranes may be subject to fouling.

On the basis of the present consideration, the selected processes for the screening were for the pretreatment: filtration on various media, ultrafiltration, coagulation flocculation and electrocoagulation; and for treatment processes: adsorption on resin and activated carbon, electrocoagulation and membrane processes.

2.3 Screening and preliminary experiments

In the previous bibliographic section, several processes were identified and some of them were chosen for the screening. The mobile unit for the treatment of firefighting water seemed to require at least two steps: a pretreatment step to remove the suspended matter, and a treatment step to remove fluorinated surfactants. The aim of the process screening was to compare the efficiency of the different processes in order to identify the most appropriate processes or combination of processes. Hence, reliable comparison basis were needed. Before presenting the results of the screening, the following section will introduce the analytical methods for suspended matter and fluorinated surfactant concentration measurements. To be able to compare the processes, their feed compositions had to be stable. Therefore,

this screening was done with standardized approximation of real firefighting waters: pilot firefighting waters. The preparation and the properties of these water will be described in section 2.3.2.

2.3.1 Analytical methods

To compare the efficiency of the processes, the selected analytical methods were of two kinds. Analytical methods for suspended matter were used to compare pretreatment processes, whereas surfactant analysis was intended to compare treatment efficiencies.

2.3.1.1 Suspended matter analysis

Suspended matter contained in firefighting water could be estimated by solid content determination, though this measurement also includes non-volatile compounds such as surfactants in addition to suspended solids. Granulometry measurements with an appropriate granulometer can provide the size distribution of particles in firefighting water. Though not measuring directly the amount of suspended solids, turbidity measurements are also of interest. Turbidity is due to suspended matter that scatters light. It represents the amount of fine matter responsible for the cloudiness of the sample [80].

Suspended matter was estimated on the basis of turbidity measurements, in nephelometric turbidity units (*NTU*), which were achieved with a HACH 2100AN turbidimeter. Granulometry measurements were performed with a Malvern Mastersize X (Malvern Instruments) coupled to the Malvern Sizer software. The focus was 100 *mm*, enabling the granulometry of 0.1 to 80 μm particle size to be determined. Solid content measurements were done with a Sartorius MA45 moisture analyzer. 5 *mL* of sample were put in an aluminum cup and heated until mass stabilization. Mass variation of the cup was measured with a precision weighing machine to deduce the amount of the solid content remaining after water and volatile compounds evaporation.

2.3.1.2 Surfactants analysis

Usual methods for surfactant analysis are titration, spectrometry or chromatography [81]. Chromatography, liquid chromatography particularly, is of great interest because of its ability

to characterize and quantify individual surfactants in complex mixtures. High performance liquid chromatography (HPLC) in appropriate conditions can separate various surfactants from complex mixtures [81, 82, 83]. Several detectors can be used but the most relevant depends mainly on the surfactant's nature and on analytical conditions. UV detectors are sensitive to surfactants with chromophores only, conductivity detectors detect charged surfactants and refractive index detectors are incompatible with gradient elution which is often a necessity in case of complex mixtures. The most universal detector is mass spectrometry (MS), but though very sensitive, this method is rather expensive.

A more appropriated method is evaporative light scattering detector (ELSD), which enables the detection of non-volatile compounds. ELSD is compatible with gradient techniques, and very inexpensive compared to MS. It has been used coupled to HPLC to successfully determine individual surfactants concentrations in mixtures [81, 82, 83]. The output of the HPLC column first comes in the heated nebulizer. It is mixed with a support gas and turned into mist. Too big droplets are evacuated *via* the siphon and the rest of the mist is evaporated in the evaporation chamber. At this step, volatile compounds are in vapor phase whereas non volatile compounds form an aerosol able to scatter light. In the detection chamber, a light source illuminates eventual aerosols and the resulting scattered light is measured (figure 2.6). This complex mechanism leads to a non-linear empirical quantitative law described by the relation:

$$A = aC^b \quad (2.5)$$

with A the area of the peak, C the concentration of the analyte, a the response factor and b the response index measured from the slope of the curve $\log A = f(\log C)$ for the considered analytes [84]. To analyze complex surfactant mixtures by ELSD, they have to be previously separated by proper chromatography conditions including appropriate fixed and mobile phases. Surfactant analysis by HPLC generally involves reverse phase silica columns with an apolar C_8 or C_{18} fixed phase, and mobile phases are generally mixtures of water and a polar solvent such as methanol, acetonitrile or tetrahydrofuran [81, 82, 83]. For better detector response and peak resolution, according to the supplier, additives such as trifluoroacetic acid or ammonium acetate may be used. The composition of the mobile

phase might require fine gradient tuning to separate complex surfactant solutions.

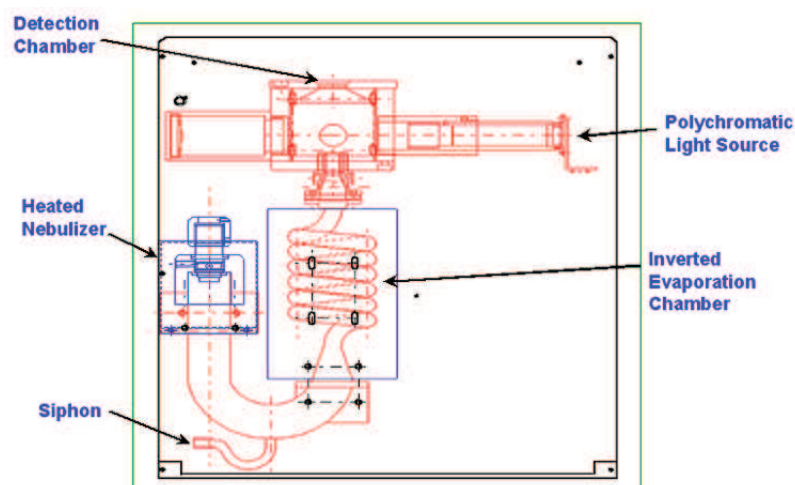


Figure 2.6: Evaporative light scattering detector schematics.

Source: <http://www.spectrotech.com>

The fluorinated surfactant used was Forafac[®] 1157N (DuPont) which main compound is the fluorinated surfactant considered in this work. Forafac[®] 1157N is a fluorinated amphoteric surfactant fraction of homologues with different chain lengths. Pilot firefighting waters contained Forafac[®] 1157N and some of the model solutions used in the present screening only contained the major compound of the fraction.

Sample homogenization was achieved in 60 mL glass vials, using a Heidolph Topmix 94323 vortex. High performance liquid chromatography (HPLC) measurements were performed with an analytical system composed of a Knauer K-501 HPLC pump (Eurosep Instruments), a Rheodyne valve with a 40 μ L injection loop, an Eclipse Zorbax XDB-C8 analytical column (Agilent Technologies, 4.6 mm diameter, 150 mm length, 5 μ m particle size), a column oven at 35°C and the mobile phase was methanol:water 70 : 30 v:v at a 0.5 mL min⁻¹ isocratic flow rate. The detector was an ESA Evaporative Light-Scattering Detector (ELSD, Chromachem, Eurosep Instrument), attenuation was 2, nitrogen pressure was 1.5 bar, nebulization and evaporation temperatures were 50 and 70°C respectively, data acquisition and processing was done with Azur[®] software. Simultaneous resolution of the anionic, non ionic, amphoteric hydrocarbon surfactants and fluorinated surfactant could not be achieved with the aforementioned mobile phase, which was intended to resolve the fluorinated surfactant only, with a limit of detection of 1.4 mg L⁻¹. The calibration curve was established from 4

to 1000 mg L^{-1} , the error was below 5%, every analysis was done twice and out of range concentrated samples were diluted. Samples with a turbidity superior to 2 NTU were filtered on Roth $0.45 \mu\text{m}$ PVDF-made syringe. After PVDF filtration the recovery rate of fluorinated surfactant was 90%.

2.3.2 Pilot firefighting waters used in the screening

As seen in chapter 1, real firefighting waters are expected to be mixtures of solvents, firefighting foam ingredients, in addition to by-products formed during the combustion, more or less randomly diluted in either tap or sea water. These waters may contain various hydrocarbon surfactants, various fluorinated surfactants, some cosolvents, protein hydrolysates and soluble polysaccharide polymers, polar and/or apolar solvents, and additives according to formulation of the firefighting foam used. Real firefighting waters can be of a great variety, and obtaining samples in sufficient amounts to run experiments is difficult.

The assessment of the processes identified and chosen during the previous bibliographic study required controlled conditions. The firefighting water used had to be readily available in sufficient amounts, and its composition had to be stable to compare the processes on a reliable basis. Hence it was decided to produce Pilot Firefighting Waters (PFW) by the extinguishment of artificial solvent fires with a specific firefighting foam.

Pilot firefighting waters were produced by the extinction of 0.25 m^2 (2 L) heptane fires by a 3% AFFF (figure 2.7), which components are listed in table 2.5. Developed formulas of concerned molecules are given in figure 2.8. After dilution in water, the composition of the foaming solution was expected to be close to the concentrations given in table 2.6. An additional more or less random dilution was due to both cooling and clean-up operations with tap water. The n-heptane and the eventual emulsion at the n-heptane/water interface were discarded by decantation. The pilot firefighting waters used in the following screening consisted of the aqueous phase of the mixture collected after the fire extinguishment.



Figure 2.7: n-heptane fire for pilot firefighting water production (0.25 m^2).

Table 2.5: Components of the 3% foaming base used to generate pilot firefighting waters. Deionized water represented 72.6% wt, diethanolamine was added to reach $pH 7.5$.

Chemical name	Name of commercial product	Active content	CAS	Supplier
Dipropylene glycol methyl ether	Dowanol [®] DPM	100%wt	34590-94-8	Dow Chemicals
Sodium octylsulfate	Disponil [®] SOS 842*	40%wt	142-31-4	Cognis
sodium caprylamphopropionate	Tegotens [®] AM VSF*	50%wt	64265-45-8	Evonik GmbH
D-Glucopyranose oligomers (C8-C10 alkyl polyglucosides)	Simulsol [®] SL8*	60%wt	68515-73-1	Seppic
Amphoteric fluorinated surfactant fraction	Forafac [®] 1157N*	27%wt		DuPont

*: Commercial products.

Table 2.6: Foaming solution composition after dilution of the foaming base to 3% v:v in tap water

Chemical name	Active compound concentration ($mg\ L^{-1}$)
Dipropylene glycol methyl ether (Dowanol [®] DPM)	3000
Sodium octyl sulfate (Disponil [®] 842)	960
sodium caprylamphopropionate (Tegotens [®] AM VSF)	360
Octyl glucoside (Simulsol [®] SL8)	360
Fluorinated surfactant from the fraction	270

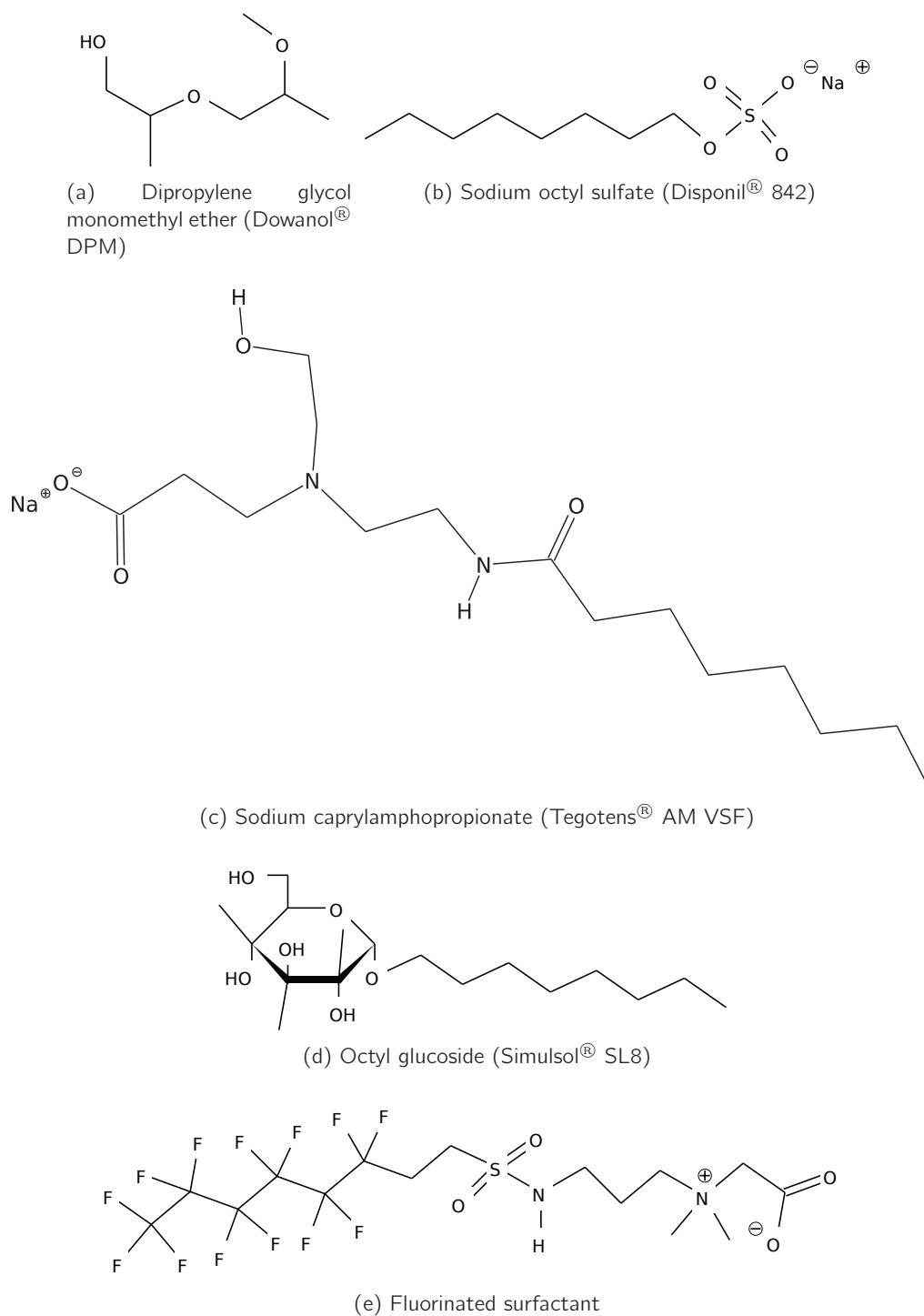


Figure 2.8: Molecules contained in the pilot firefighting waters

Pilot firefighting water represented a simplification in several points regarding real firefighting waters:

- Relatively small scale fire: short combustion and extinguishment time, “moderate” heating;

- Synthetic foam only: no protein hydrolysates;
- AFFF, not AR-AFFF foaming base: no soluble polymers;
- Apolar solvent fire: though n-heptane is a standard apolar solvent for AFFF assessment, it is not miscible with water on the contrary to polar solvent, and can be removed by decantation;
- Tap water only: in some cases the foaming base may be diluted in sea water;

Although simplified, the resulting pilot firefighting waters (PFW) presented marked differences with simple foaming solutions, especially regarding the pretreatment step. Several firefighting waters were tested in addition to the PFW. As these waters could be more or less complex and very different, their closeness to the sophistication of actual firefighting water was represented according to several relevant scaled factors (figure 2.9).

Pilot firefighting water used in the screening of pretreatment processes came from two different batches. The resulting pilot firefighting waters were labeled “Pilot firefighting water 1” (PFW1) and “Pilot firefighting water 2” (PFW2) in the following sections. The foaming base compositions were both those of AFFF (table 2.6). Both solutions showed close properties (table 2.7). The fluorinated surfactant concentration was more than three times less than expected and was initially assumed to be due to water dilution, as rinsing water was recovered during PFW production. Later, these concentration differences would also seem to be due to adsorption of the fluorinated surfactant on the fine particles contained in the firefighting waters.

Foaming solutions of both PFW showed turbidities near 2 *NTU* and contained 1300–1400 *mg L⁻¹* of solid content. Considering the solid content of PFW2 (table 2.7), the effective turbidity could be due to 200–300 *mg L⁻¹* only of dry matter, the remaining due to initial foam active ingredients. Thus a turbidity of 2 *NTU* or less appeared to be a reliable aim for the pretreatment process, corresponding to firefighting waters containing no additional suspended matter.

Pilot firefighting water had limited availability and some experiment in the screening required solutions of different concentration ranges. Hence part of the following screening experiments were done with model firefighting waters. These model waters were prepared

by direct dilution of the chemicals from the pilot firefighting water foaming base in deionized water. The composition of these solutions will be given in the sections of the corresponding experiments.

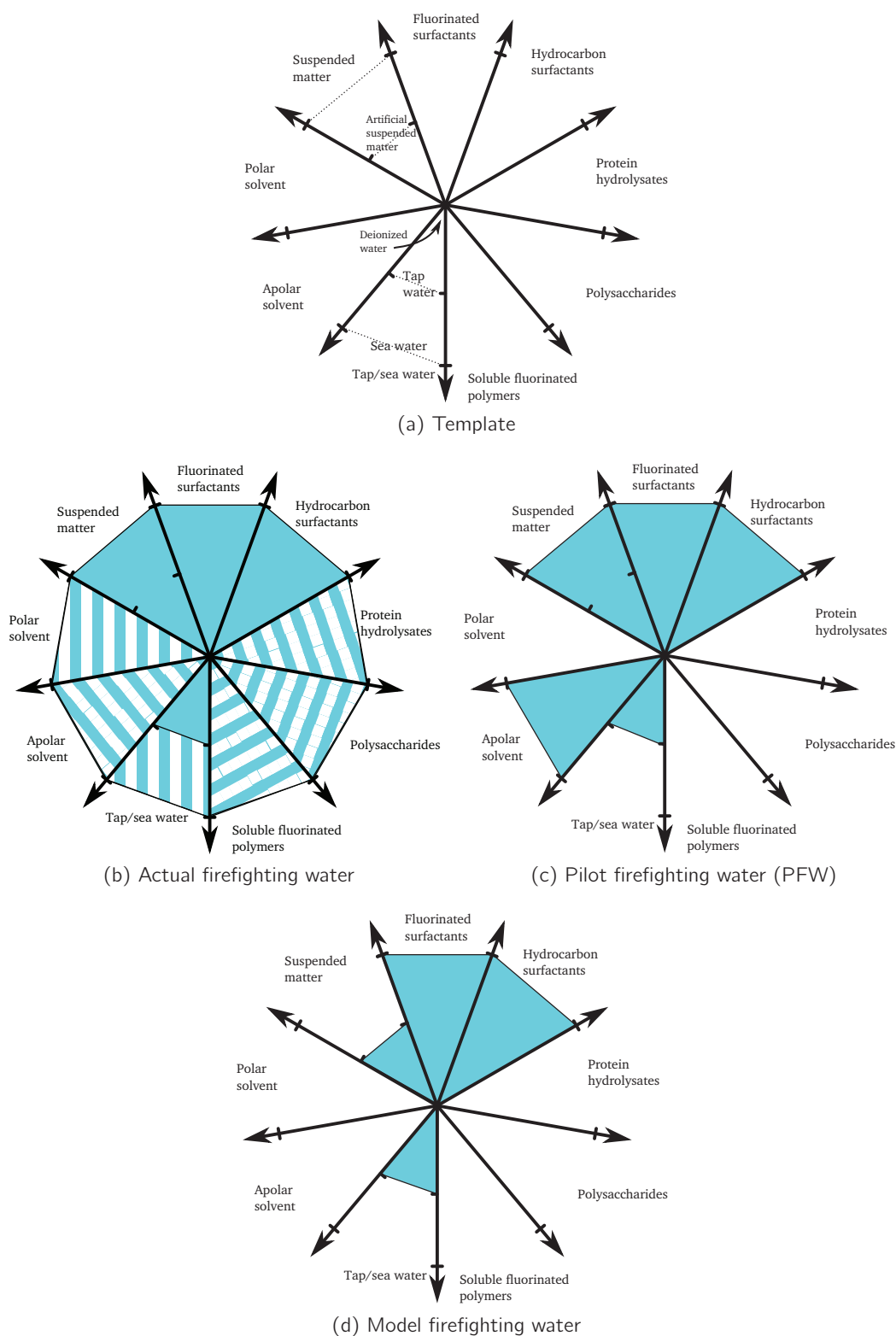


Figure 2.9: Assessment chart for the representativity firefighting waters relative to actual firefighting waters. Dashed area: possible, yet unknown presence of the considered compound.

Table 2.7: Pilot firefighting waters properties

Denomination	Pilot firefighting water 1 (PFW1)	Pilot firefighting water 2 (PFW2)
Volume (L)	20	17
Turbidity (NTU)	30	27
Minimal particle size (μm)	0.2	0.2
Turbidity after 0.45 μm filtration* (NTU)	7.7	4.2
Solid content ($mg L^{-1}$)	Not measured	1620
Fluorinated surfactant ($mg L^{-1}$)	82	94

*: samples filtered with 0.45 μm PVDF syringe filters.

2.3.3 Screening of pretreatment processes

The screening of pretreatment processes was done on the basis of experiments with pilot firefighting water 1 and 2, which sophistication is represented in figure 2.10. The aim of the pretreatment was to get rid of the suspended matter contained in pilot firefighting waters, and decrease their turbidity down to the turbidity of foaming solutions: 2 NTU or lower. The turbidity of PFW2 (27 NTU, table 2.7) were 17 NTU after 24 h decantation and 4.3 NTU after 15 min (10, 000 rpm) centrifugation, thus these processes were not considered as efficient pretreatment processes. Therefore a pretreatment step with physical and/or physicochemical processes was required.

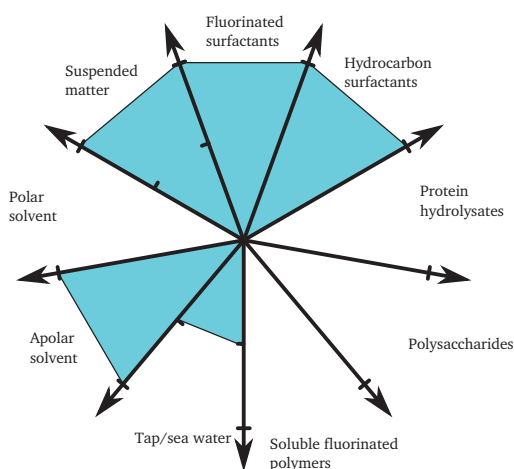


Figure 2.10: Sophistication of pilot firefighting waters 1 and 2

2.3.3.1 Filtration and microfiltration experiments

Clarification of PFW2 was tried with Durieux filters. The filter was put in a funnel and the pilot firefighting water permeated by gravitation (figure 2.11). Gravitational permeation was very slow and the filters had to be replaced several times because the flow stopped. 6 L of clarified PFW2 could finally be obtained in 24 h. The turbidity of this solution was decreased from 30 to 11 NTU, but it was still too high. Filtration on Durieux filters was not an efficient pretreatment process.

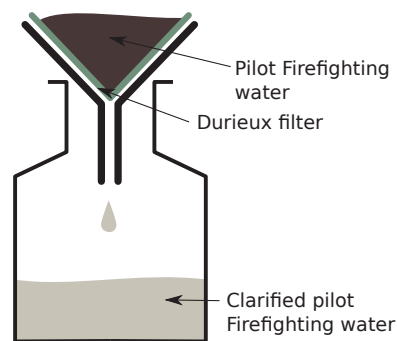


Figure 2.11: Pilot firefighting water Durieux filter clarification

Filtration with 0.7 μm filter paper experiments were done with a model solution: MFW1 (table 2.8) and with the PFW1. The MFW1 represented a foaming solution diluted twice, to model the random dilution due to rinsing water. Filtration with 0.7 μm filter paper was done under vacuum with a glass frit as support (figure 2.12). Filtration of PFW1 and MFW1 with 0.7 μm filter papers both showed high fouling (figure 2.13). The filtration flow dropped by 80–90% after 600 mL of permeate, and filter paper replacement did not increase significantly the flow. The fouling seemed to occur on the glass frit, not on the filter papers.

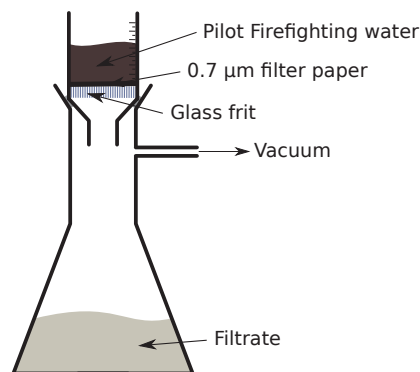


Figure 2.12: Pilot firefighting water 0.7 μm paper filter microfiltration

Table 2.8: MFW1 composition

Compound	Concentration ($mg L^{-1}$)
Dipropylene glycol methyl ether (Dowanol [®] DPM)	1508
Sodium octyl sulfate (Disponil [®] 842)	482
Alkyl propionate (Tegotens [®] AM VSF)	110
Octyl glucoside (Simulsol [®] SL8)	122
Fluorinated surfactant from the fraction	138

Filtration profiles were studied. The ratio t/V , with t the time of filtration and V the permeate volume during filtration of MFW1, was plotted against V (figure 2.14a). t/V was found to be function of V , indicating a cake filtration profile [43]. This kind of profile is expected when the particles contained in the filtered solution form a cake at the surface of the filter. For the filtration of PFW1, the ratio t/V was found to be function of t the time of filtration (figure 2.14b). This corresponded to a standard blocking profile, which occurs when the pores are partially or completely blocked at the surface of the filtering media [43].

These results were quite unexpected, as MFW1 contained no particles, and PFW1 that contained particles did not foul with a cake formation profile. The turbidity of the PFW1 permeate decreased from 30 to 20 NTU , which showed that $0.7 \mu m$ filter paper filtration was not efficient enough, without even considering the high and unusual fouling.

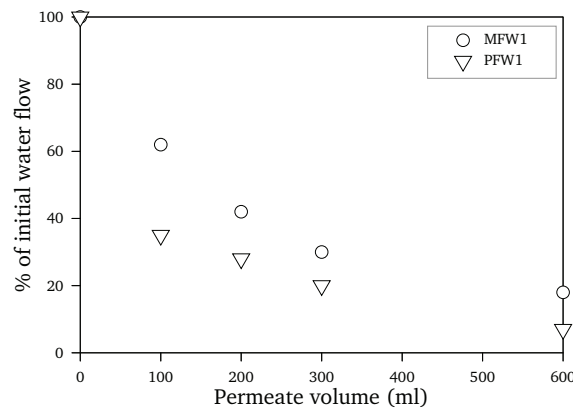
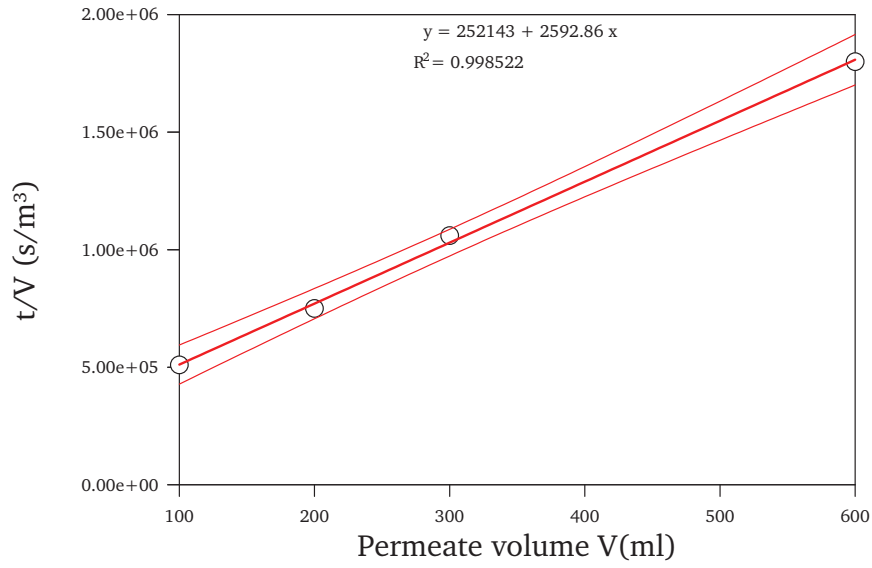
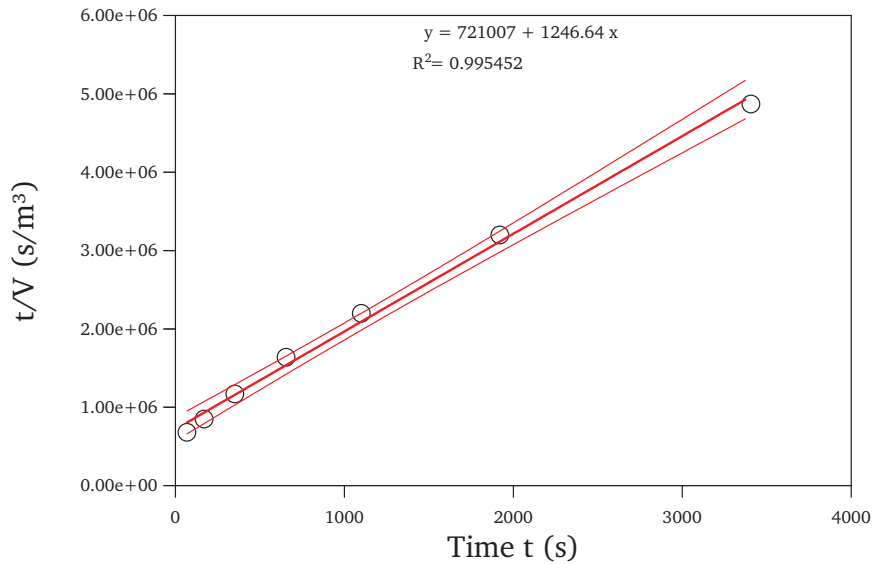


Figure 2.13: Flow evolution during model firefighting water 1 (MFW1) and pilot firefighting water 1 (PFW1) filtrations on $0.7 \mu m$ paper filter, under vacuum, with a glass frit support.



(a) Fouling profile during MFW1 filtration on $0.7 \mu\text{m}$ paper filter



(b) Fouling profile during PFW1 filtration on $0.7 \mu\text{m}$ paper filter

Figure 2.14: Fouling profiles during model firefighting water 1 (MFW1) and pilot firefighting water 1 (PFW1) filtrations on $0.7 \mu\text{m}$ paper filter, under vacuum, with a glass frit support.

After these filtration trials, microfiltration with an Osmonics JX1812C-34D PVDF $0.3 \mu\text{m}$ pore size, 0.32 m^2 area microfiltration membrane was done with a Millipore ProScale pilot, in full recycling mode (figure 2.4a) at 1 bar. The solutions used for microfiltration experiment were MFW1 and PFW2 after clarification with Durieux filter. The turbidity of this solution was 11 NTU , which was near to the 8 NTU of $0.45 \mu\text{m}$ syringe filtered PFW1. Though still not reaching the pretreatment aim, this turbidity was assumed sufficient to run Millipore pilot microfiltration experiments on Durieux filter clarified firefighting water.

Microfiltration of particle-free MFW1 was done to assess eventual membrane fouling due to surfactants. Permeability rapidly decreased at the beginning of the experiment (figure 2.15) to reach a plateau at $180 \text{ L h}^{-1} \text{ m}^{-2} \text{ bar}^{-1}$, which represented 48% of initial water permeability (Tab 2.9a). After the experiment the membrane was rinsed successively with water, ethanol then water and initial water permeability was recovered. Initial fluorinated surfactant concentration was 121 mg L^{-1} in the retentate, and then rapidly decreased to a plateau of 86 mg L^{-1} probably by means of adsorption on the membrane.

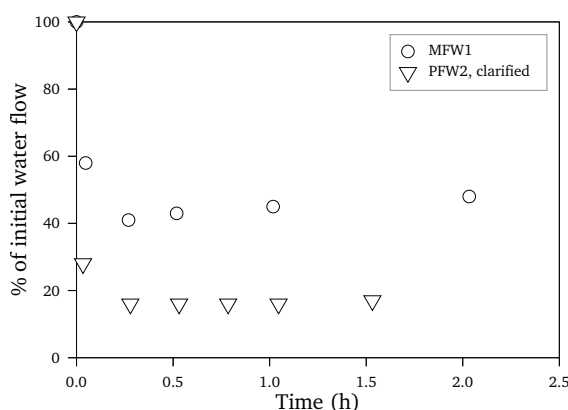


Figure 2.15: Evolution of permeabilities during model firefighting water 1 (MFW1) and clarified pilot firefighting water 2 (PFW2, after Durieux filter clarification) filtrations on $0.3 \mu\text{m}$ PVDF Osmonics microfiltration membrane

Clarified PFW2 microfiltration showed a stronger permeability decrease (figure 2.15) to reach $54 \text{ L h}^{-1} \text{ m}^{-2} \text{ bar}^{-1}$, which was 17% of initial water permeability. Turbidity in the permeate was 0.7 NTU . In the retentate, turbidity decreased (table 2.9b), indicating that particles present in the PFW2 seemed to adsorb at the membrane surface or inside it.

Table 2.9: Evolution of the fluorinated surfactant concentrations during microfiltration experiments with a 0.3 μm PVDF Osmonics membrane

(a) Fluorinated surfactant concentrations during model firefighting water 1 (MFW1) microfiltration

	Permeate concentration ($mg L^{-1}$)	Retentate concentration ($mg L^{-1}$)	% of initial water permeability
0 min	-	121	-
15 min	85	86	41%
2 h	78	86	48%

(b) Turbidity and fluorinated surfactant concentrations during clarified pilot firefighting water 2 (PFW2) microfiltration

	Fluorinated surfactant ($mg L^{-1}$)		Turbidity (NTU)		% of initial water permeability
	Permeate	Retentate (PVDF filtered)	Permeate	Retentate	
0 min	-	59	-	11	-
15 min	24	45	0.7	6	16%
90 min	28	31	0.7	3	17%

Fluorinated surfactant concentrations varied from 59 $mg L^{-1}$ to 45 and 28 $mg L^{-1}$ (PVDF filtered samples), whereas they remained stable during MFW1 microfiltration. Water-ethanol-water cleaning was not sufficient to recover initial water permeability: fouling was irreversible, final water permeability was 33% of the initial one. The filtration of a clarified PFW2, with a turbidity of only 11 NTU (near to 0.45 μm PVDF syringe filtration turbidity) was efficient to remove turbidity, but could cause dramatic irreversible fouling in the membrane. This suggested that small particles were very harmful for the microfiltration membrane, which was not surprising considering the size of the smallest particles (0.2 μm) and the membrane cutoff (0.3 μm). Hence ultrafiltration membranes, filtering media with smaller pores, were tested.

2.3.3.2 Ultrafiltration experiments

Ultrafiltration experiments were done on a Rayflow X100 ultrafiltration pilot with a Watson Marlow 624U peristaltic pump, a LAUDA RM6 thermocryostat, and 200 cm^2 polyethersulfone membranes from Novasep. Transmembrane pressure was set to 1 bar and feed temperature was maintained at 25°C. Different membrane cutoffs were tested: 10, 30 and 100

kDa. Ultrafiltration tests took place in two parts: a full recycling phase (figure 2.4a) until flux equilibrium was reached; and a concentration phase (figure 2.4b) until a target volume reduction ratio (*VRR*, equation 2.4) of 2 was reached.

During the ultrafiltration of the PFW1 full recycle phase, the membrane permeabilities decreased and reached a plateau. During concentration phase, fluxes slightly decreased again, except for the 10 *kDa* which flux remained stable and even slightly increased (figure 2.16). At the end of full recycle phase permeabilities were $9 \text{ L h}^{-1} \text{ m}^{-2} \text{ bar}^{-1}$, $6 \text{ L h}^{-1} \text{ m}^{-2} \text{ bar}^{-1}$ and $11.5 \text{ L h}^{-1} \text{ m}^{-2} \text{ bar}^{-1}$ for 10 *kDa*, 30 *kDa* and 100 *kDa* cutoffs respectively. The lower flux was for 30 *kDa*, which was confirmed at the end of concentration phase: permeabilities were 8.3, 5.5 and 8.6 $\text{L h}^{-1} \text{ m}^{-2} \text{ bar}^{-1}$ for 10, 30 and 100 *kDa* cutoffs respectively (table 2.10). For the 30 *kDa* membrane, permeability was so low that a *VRR* of only 1.33 could be reached. The decrease of 100 *kDa* permeability with increasing *VRR* could be due to progressive fouling of the larger pores of this membrane with increasing surfactant concentration and micelles.

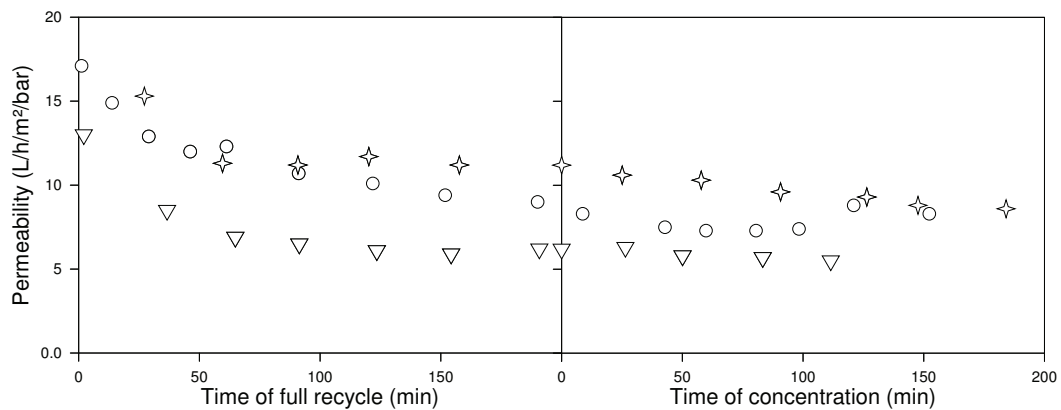


Figure 2.16: Membrane permeabilities during ultrafiltration with polyethersulfone membranes of the pilot firefighting water 1 (PFW1). Membrane cutoffs: ○: 10 *kDa*; ▽: 30 *kDa*; ☆: 100 *kDa*.

Table 2.10: Summary of permeability properties of the different membranes used for ultra-filtration of firefighting water 1

Membrane cutoff	End of the full recycle phase		End of the concentration phase		Final volume reduction rate
	Permeability	% of initial water permeability	Permeability	% of initial water permeability	
10 <i>kDa</i>	9	26%	8.3	24%	2
30 <i>kDa</i>	6	11%	5.5	10%	1.33
100 <i>kDa</i>	11.5	8%	8.6	6%	2

Permeabilities given in $L\ h^{-1}\ m^{-2}\ bar^{-1}$

Fluorinated surfactant concentrations in retentate decreased during full recycle phases from $76\ mg\ L^{-1}$ to 62, 61 and $68\ mg\ L^{-1}$ for the 10, 30 and 100 *kDa* membranes respectively. In permeates, fluorinated surfactant concentrations were near to $54\ mg\ L^{-1}$, the fluorinated surfactant cmc (table 2.12). Some fluorinated surfactant seemed to adsorb on the membranes which seemed to be able to retain micelles of fluorinated surfactant.

Table 2.11: Turbidity in permeate and retentate during ultrafiltration of MFW1 with different membranes

Membrane cutoff	10 <i>kDa</i>		30 <i>kDa</i>		100 <i>kDa</i>	
	Retentate	Permeate	Retentate	Permeate	Retentate	Permeate
Beginning of recycle	34.3	0.4	31	0.1	34.3	0.17
Beginning of concentration	37	0.326	34.3	0.17	32	0.15
End of concentration	73	0.17	43.6	0.18	64	0.14

Turbidity values are given in *NTU*.

Table 2.12: Fluorinated surfactant concentrations in permeate and retentate during ultrafiltration of MFW1 with different membranes

Membrane cutoff	10 <i>kDa</i>		30 <i>kDa</i>		100 <i>kDa</i>	
	Retentate	Permeate	Retentate	Permeate	Retentate	Permeate
Beginning of recycle	76	54	76	44	76	55
Beginning of concentration	62	57	61	53	68	58
End of concentration	75	56	68	52	86	56

Concentrations given in $mg\ L^{-1}$

Fluorinated surfactant retention rates at the beginning of concentration phase were between 8% and 15%, whereas at the end of this phase they were between 24% and 35% (table 2.13) and every membrane showed a very high fouling (table 2.10). At the end of experiments black particles had deposited on the membrane surface and were easily removed by a high speed flushing without applied transmembrane pressure. Initial permeabilities were recovered for the three membranes after water washing.

Table 2.13: Retention rates of the fluorinated surfactant during ultrafiltration of pilot fire-fighting water 1 with polyethersulfone membranes

Membrane cutoff	10 <i>kDa</i>	30 <i>kDa</i>	100 <i>kDa</i>
Beginning of recycle	29%	42%	28%
Beginning of concentration	8%	13%	15%
End of concentration	25%	24%	35%

Ultrafiltration provided low turbidity permeates and was not irreversibly fouled by PFW1. Ultrafiltration seemed more appropriate to particle removal than microfiltration, but at the cost of serious fouling. Ultrafiltration showed only partial retention of the fluorinated surfactant, with permeate concentrations near to its cmc. This was conform to the retention of micelles as seen in the bibliography (figure 2.5). Neither filtration, nor microfiltration were found to be adequate pretreatments for the removal of firefighting water suspended matter removal: physical processes were not sufficient thus physicochemical ones were required.

2.3.3.3 Coagulation flocculation

As filtration processes alone were not sufficient for the treatment of pilot firefighting water, coagulation–flocculation and electrocoagulation were tested. Coagulation with aluminium or ferric salt was not tested directly but via electrocoagulation in the next section. This process presents the advantage of not requiring chemicals other than a metallic soluble anode, thus limiting chemical supply and handling. In the present section, polymeric coagulants and flocculants obtained from Floerger were used:

- polymeric cationic coagulants: FL 4440, FL 2650, FL 42, DEC 53
- mixed inorganic and polymeric cationic coagulants: FLB 1725, FLB 4525
- polymeric anionic flocculants : AN 910 SH, AN 934 SH

- polymeric cationic flocculants : FO 4650 SH, FO 4800 SH

Usual concentrations for these products are 1–5 mg L^{-1} in water, and 1 : 1 coagulant:flocculant concentration ratio. To be efficient, flocculant has to be oppositely charged to the coagulant. Coagulants and flocculants were diluted to 100 mg L^{-1} in deionized water, so that adding 1 mL of these solutions to 100 mL increased coagulant or flocculant concentration of 1 mg L^{-1} in pilot firefighting water.

Preliminary experiments were done for each cationic coagulant and both anionic flocculant with 100 mL of PFW1 whereas the two cationic flocculants were tested alone. With cationic coagulants and anionic flocculants, no coagulation nor flocculation was observed in usual concentrations: particles remained in suspension. Floc formation was only obtained with 5 mg L^{-1} of cationic flocculants. After a few seconds a black floc appeared in solution, collecting particles. The cationic flocculants FO 4650 SH and FO 4800 SH were then tested on firefighting water volumes of 500 mL to collect samples for granulometry, turbidity and chromatographic analysis.

Without flocculant, 74% of the initial turbidity in the PFW1 was removed by filtration on an 0.45 μm PVDF syringe filter, and initial minimal particle size was 0.2 μm (table 2.14). With cationic flocculants, the turbidity was measured after decantation and was 3 and 13 NTU for 5 mg L^{-1} for FO 4650 SH and FO 4800 SH in PFW1 respectively. The floc settled spontaneously. With 5 mg L^{-1} of FO 4650 SH and FO 4800 SH, minimal particle size grew to 1.1 and 0.9 μm respectively. Turbidity removal also increases to 97% and 93% to reach values of 0.8 and 2 NTU after filtration with FO 4650 SH and FO 4800 SH respectively. These turbidities were compatible with the targeted turbidity of < 2 NTU for the pretreatment. FO 4650 SH seemed to have a better efficiency due to a higher minimal particle size. Cationic flocculants also remove some surfactants: 28% of fluorinated surfactant for FO 4650 SH and FO 4800 SH.

Table 2.14: Cationic flocculants preliminary experiments results

	Turbidity (<i>NTU</i>)	Minimal particle size (μm)	Turbidity after $0.45 \mu m$ filtration (<i>NTU</i>)	Fluorinated surfac- tant ($mg L^{-1}$)
PFW1	30	0.2	7.7 / –74%	82
PFW1, FO 4650 SH 5 $mg L^{-1}$	25	1.1	0.8 / –97%	67 / –18%
PFW1, FO 4800 SH 5 $mg L^{-1}$	37	0.9	2.0 / –95%	61/ –26%

Conventional coagulation–flocculation with polymeric cationic coagulants and anionic flocculants was inefficient. This low efficiency was probably due to interactions of the coagulants with the surfactants contained in firefighting water, which stabilize coagulants *via* electrostatic and hydrophobic interactions. Polymeric cationic flocculants, though interacting with the fluorinated surfactant, were able to make the suspended matter flocculate.

The particles in firefighting water were most likely stabilized by the surfactant mixture, which contained anionic surfactants. The efficiency of long chain cationic polymeric flocculants was probably due to electrostatic interaction with particles interacting with surfactants. However, flocculants had to be used at several times the usual concentration, and the resulting floc was very sticky thus difficult to handle and an additional filtration was required.

2.3.3.4 Electrocoagulation

Electrocoagulation is a specific case of coagulation. Cationic coagulants Al^{3+} or Fe^{3+} are introduced electrochemically by aluminium or iron anode oxidation, while H_2 bubbles are produced at the cathode, taking the floc to the surface by electroflotation [49, 85]. It could also be described as *in situ* generation of the coagulant, avoiding the continuous addition of chemicals. For this work, the electrocoagulation device was composed of a Plexiglas cell of 5.7 L, 4 aluminum electrodes with a total surface of $815 cm^2$ as the anode and 5 stainless steel electrodes as a cathode (figure 2.17). The removal of the floc, which will be investigated later, was done by syringe filtration on $.45 \mu m$ PVDF-made syringe filters. The experiment was done with 3 L of PFW2. A current of 2 A was applied during 60 min. The

current density was 24.5 A m^{-2} .

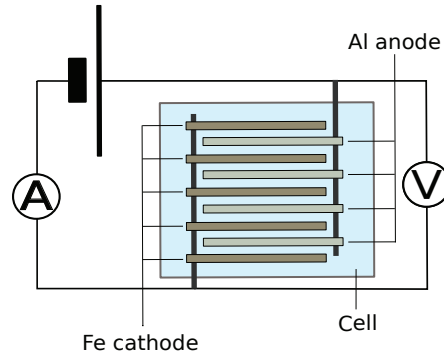


Figure 2.17: Schema of the electrocoagulation cell

The mean voltage was 15 V during 1 h of PFW2 electrocoagulation and pH slightly increased from 8 to 9.6 for reasons that will be covered in Chapter 3 (figure 2.18). Aluminum electrocoagulation was reported to have the better efficiency in a pH range from 5 to 9 [49]. However, pH was relatively stable, floc formation and flotation did not seem to be affected.

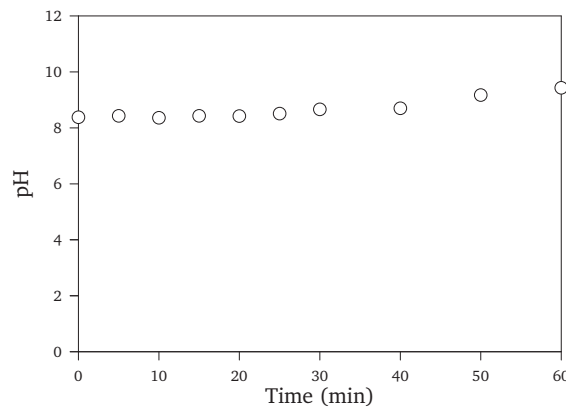


Figure 2.18: pH during electrocoagulation of pilot firefighting water 2 (PFW2, 3 L), 60 min , at 2 A (current density of 24.5 A m^{-2})

During the first 5 min nothing happened on the visual point of view, except the beginning of floc formation. At 5 min the turbidity was higher than at the beginning, and after 15 min the solution seemed clearer. At 30 min the floc at the surface presented 3 layers of different colors: the upper one was thin, white and foamy, the middle one was dark gray and the last one was white (figure 2.19). It seemed that particles had been electrocoagulated and electroflottated to the surface between 5 and 15 min , when the solution was the most turbid. After 15 min , the turbidities were near 1 NTU or less after $0.45 \mu\text{m}$ PVDF syringe filtration (figure 2.20) and the floc looked like a conventional non-sticky sludge.

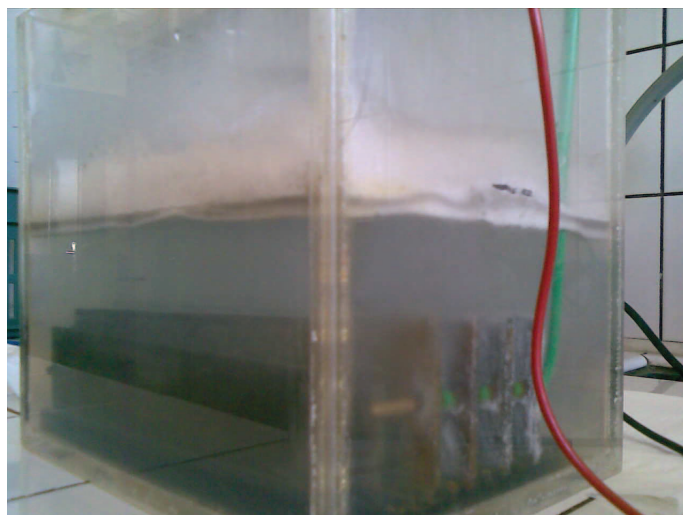


Figure 2.19: Floc layers during electrocoagulation of pilot firefighting water 2 at 2 A, after 30 min.

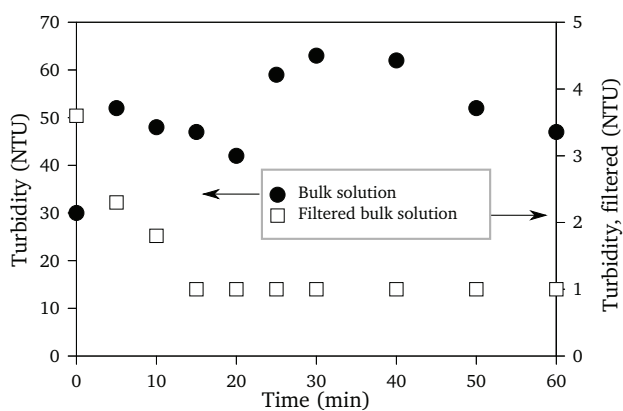


Figure 2.20: Turbidity during electrocoagulation at 2 A of pilot firefighting water 2 (PFW2). ●: in bulk solution; □: after 0.45 μm PVDF syringe filtration.

Fluorinated surfactant concentration during electrocoagulation decreased from 94 to 9 mg L^{-1} after 1 h, which represented nearly a 90% decrease (figure 2.21).

This made the electrocoagulation interesting for the screening of treatment processes.

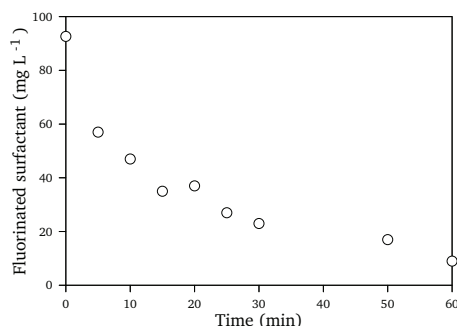


Figure 2.21: Fluorinated surfactant concentration during PFW2 electrocoagulation, 60 min, after 0.45 μm PVDF filtration

Conclusion on the screening of pretreatment processes

The turbidity after an efficient pretreatment process was expected to be 2 *NTU* or less. Decantation and centrifugation gave too high turbidities (17 *NTU* and 4.3 *NTU* respectively). Filtration experiments suffered from serious filter clogging because of inadequate pore dimensions considering the smaller particles contained in pilot firefighting waters. It could be noticed that surfactant solution with no particles also fouled filters, and microfiltration membranes. Ultrafiltration gave turbidities < 1 *NTU* and fluorinated surfactant micelles were retained. The retentate was concentrated and the permeate concentration in fluorinated surfactant was close to its cmc. However, the fouling with pilot firefighting water was very high: the permeability was ten times lower than the expected water permeability. The efficiencies of filtration processes alone were not satisfying, thus an additional physicochemical process was required.

Coagulating agents were tested under two forms: polymeric coagulants and flocculants, and aluminium hydroxide from electrocoagulation. The only coagulants and flocculants able to remove turbidity after filtration were cationic flocculants. These compounds had to be used at relatively high concentration and produced sticky and hardly handleable floc. Aluminium hydroxide from electrocoagulation seemed to be the only coagulant tested able to trap the suspended matter properly. This process also required a filtration step but seemed to produce a conventional floc.

2.3.4 Screening of treatment processes

Two main processes for the treatment of water containing fluorinated surfactants were identified during the bibliographic study, and could be tested at the laboratory: adsorption and membrane processes. Electrocoagulation was also tested as it was shown in the previous section to be able to reduce the fluorinated surfactant concentration in pilot firefighting water 1.

2.3.4.1 Adsorption

The adsorbents used during adsorption screening experiments were powder activated carbon: C301 from Chemviron Carbon, a mesoporous powder activated carbon; and an ion exchange resin: Lewatit VP OC 1064 from Lanxess, which is a macroporous adsorber made of a crosslinked polystyrene matrix without functional groups. Adsorption experiments were carried out with accurate volumes near 100 mL of surfactant solution in 300 mL erlenmeyer. The mixing device was a Julabo SW23 heated incubator. Initial fluorinated surfactant concentrations ranged from 140 to 2000 mg L⁻¹ and the solutions also contained proportional amounts of components from the foaming solution, in deionized water (Tab 2.15). Their closeness to actual firefighting water is illustrated in figure 2.22.

Resin was washed in milli-Q water before use. The mass was determined by weighing the involved amount recovered by paper filtration at the end of each experiment, after 105°C drying until constant mass. HPLC analysis were done with the supernatant, which did not require filtration. Activated carbon was more problematic as HPLC analysis required filtration. Paper filtration had to be done twice or more to get a clear solution, hence 0.45 µm polysulfone syringe filter were used, the recovery was 90%. With this filtration method, activated carbon could not be used hydrated: its accurate amount had to be weighed dry before each experiment. The mixtures were agitated overnight at 25°C and 180 rpm in the incubator.

Table 2.15: Composition of the model firefighting waters for adsorption experiments

Compounds	Weight ratio of active compound versus fluorinated surfactant
Dipropylene glycol methyl ether (Dowanol [®] DPM)	11.1
Sodium octyl sulfate (Disponil [®] 842)	3.5
Alkyl propionate (Tegotens [®] AM VSF)	1.3
Octyl glucoside (Simulsol [®] SL8)	1.3
Fluorinated surfactant	1.0

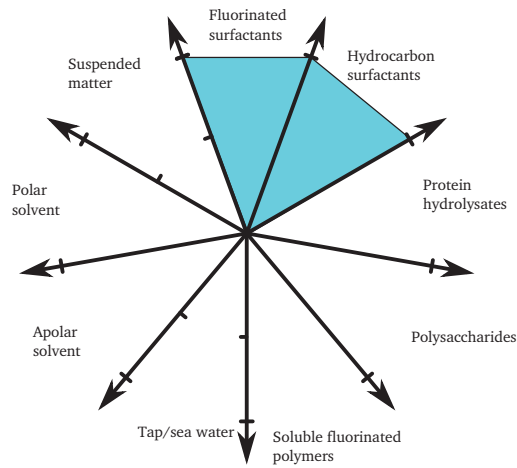


Figure 2.22: Sophistication of the solution for adsorption experiments

Adsorption isotherms were obtained by calculating adsorbents capacity q^* at different equilibrium concentrations:

$$q^* = \frac{m_{\text{adsorbed FS}}}{m_{\text{adsorbent}}} = \frac{(C_0 - C_{eq})V_{\text{solution}}}{m_{\text{adsorbent}}} \quad (2.6)$$

with q^* in mg g^{-1} , C_0 and C_{eq} the initial and the equilibrium fluorinated surfactant concentrations respectively in mg L^{-1} and V_{solution} the volume of surfactant solution in L for each experiment. Freundlich isotherms (section 1.2.1.3) were observed for both adsorbents for equilibrium fluorinated surfactant concentration below 500 mg L^{-1} (figure 2.23). Divergence from isotherms above this concentration could be due to the complex behavior of

concentrated surfactant mixtures.

The activated carbon and the resin with no functional group were apolar material. Therefore, polar interactions between these materials were not likely to occur and the adsorption could be expected to occur with the hydrophobic tails of surfactants towards the substrate. Fluorinated surfactants have a low cmc compared to hydrocarbon ones. Therefore, at high concentrations of the model solutions the free monomer concentration of the fluorinated surfactant was lower than the free monomer concentration of hydrocarbon ones. The fluorinated surfactant could be replaced at the surface of the adsorbents by the hydrocarbon monomers not involved in micelles, as a result of a hypothetical law of mass action.

Freundlich parameters reported in table 2.16 enabled the calculation of expected capacities between 30 and 40 $mg L^{-1}$, the fluorinated surfactant concentration after 30 *min* of electrocoagulation in section 2.3.3.4, which gave 82–87 and 152–178 $mg g^{-1}$ for activated carbon and resin respectively. Assuming a 50% yield, the treatment of 10,000 m^3 of firefighting water at 30–40 $mg g^{-1}$ of fluorinated surfactant (PFW1 after electrocoagulation and filtration) would require 7–9 and 4–4.5 ton of C301 powder activated carbon and Lewatitt VP OC 1064 respectively. Lewatitt resin's capacity was near twice C301 activated carbon's for the fluorinated surfactant concentrations in the range of PFW1 after 15–20 *min* of electrocoagulation (Section 2.3.3.4). In the context of a running adsorption process several issues could arise: the adsorbent consumption, its eventual replacement or recycling, its disposal and the still unknown leaking profile of adsorbent beds. However, at very low concentration for traces removal, if Freundlich isotherms were still verified at concentrations below 100 $\mu g L^{-1}$, activated carbon's capacity would be far higher than resin's (figure 2.23). In these conditions activated carbon would be more interesting for an eventual final treatment step.

Table 2.16: Freundlich parameters for the fluorinated surfactant isotherms obtained with C301 powder activated carbon and Lewatitt VP OC 1064

Adsorbent	K_F	$\frac{1}{n}$	R^2
C301 powder activated carbon	39.25	0.216	0.93
Lewatitt VP OC 1064	24.07	0.542	0.94

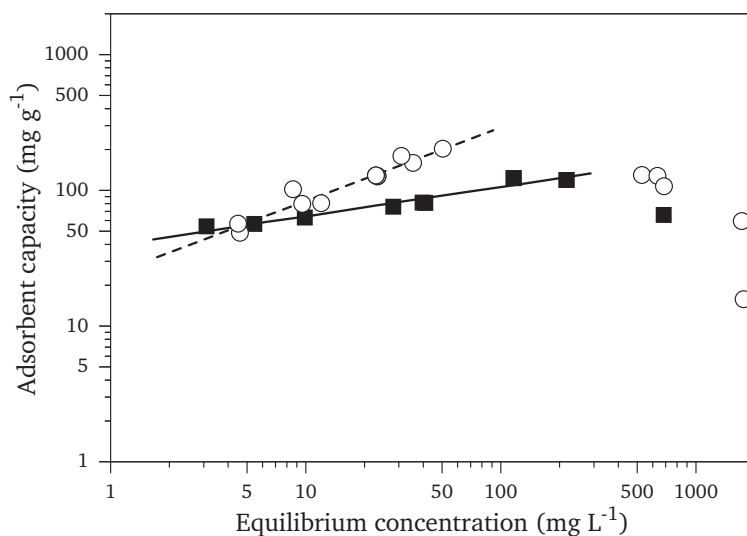


Figure 2.23: Fluorinated surfactant adsorption isotherms for ■: C301 powder activated carbon and ○: Lewatit VP OC 1064 ion exchange resin. Solid trend line: Freundlich isotherm for activated carbon, dashed trend line: Freundlich isotherm for the resin. Initial solutions compositions were proportional to foaming solution composition, from 140 to 1000 and 2000 mg L^{-1} of fluorinated surfactant for carbon and resin respectively.

2.3.4.2 Electrocoagulation

As seen in section 2.3.3.4, electrocoagulation was able to decrease the concentration of fluorinated surfactant in pilot firefighting waters. Therefore this process was tested as a treatment process to determine the maximum reachable fluorinated surfactant removal. In case of treatment process, electrocoagulation would also be used as a pretreatment process, performing both steps at a time. Therefore, for this experiment, a model solution, MFW2, was designed to match a foaming solution diluted to 90 mg L^{-1} of fluorinated surfactant, near the 94 mg L^{-1} found in PFW2. NaCl was added to enhance the conductivity of the solution (table 2.17, figure 2.24). The electrocoagulation experiment was done in the cell used in Section 2.3.3.4, with 3 L of model firefighting water, and the current was set to 2 A. The current density was 24.5 A m^{-2} . Electroflotation and mixing took place with help of bubbles convection. HPLC analysis of electrocoagulation samples were done after filtration on $0.45 \mu\text{m}$ PVDF syringe filters.

Table 2.17: Composition of model firefighting water 2 for electrocoagulation as a treatment process

Compound	Concentration ($mg\ L^{-1}$)
Dipropylene glycol methyl ether (Dowanol [®] DPM)	995
Sodium octyl sulfate (Disponil [®] 842)	318
Alkyl propionate (Tegotens [®] AM VSF)	119
Octyl glucoside (Simulsol [®] SL8)	119
Fluorinated surfactant	90
Sodium chloride ($NaCl$)	$11\ g\ L^{-1}$

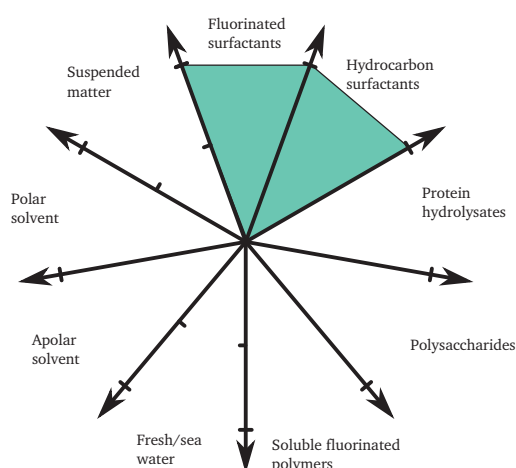


Figure 2.24: Complexity of the MFW2 solution used during electrocoagulation screening as a treatment process

For the assessment of electrocoagulation as a treatment process, electrocoagulation was done during 5 h on a MFW2. In this solution, conductivity was increased by adding $NaCl$ up to a 0.2 M concentration. Hence voltage was much lower, between 1.7 and 2.0 V. Bubbles and floc seemed much thinner than during $NaCl$ -free experiments, maybe due to the catalysis of the reaction by Cl^- [86]. Initial pH was 6 and quickly arose to a 9.6 plateau (figure 2.25). Turbidity was not measured during this experiment, as the interest was the fluorinated surfactant concentration. The initial concentration after 0.45 μm PVDF syringe filtration was $89\ mg\ L^{-1}$ and decreased to $29\ mg\ L^{-1}$ at 30 min (figure 2.26). After 1 h the concentration remained stable near $10\ mg\ L^{-1}$, a hundred times the target concentration. Despite the interesting removal of almost 90% of the initial fluorinated surfactant, electrocoagulation did

not match the expected efficiency as a treatment process.

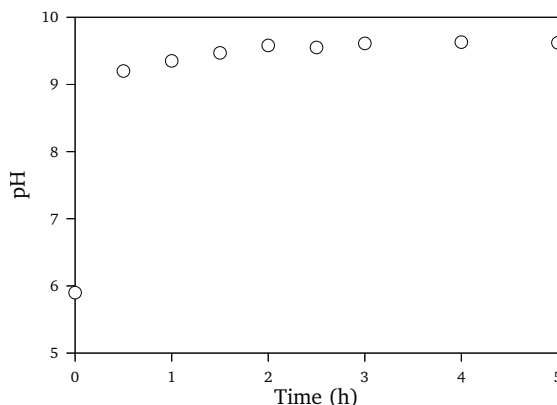


Figure 2.25: pH during electrocoagulation of the MFW2 (3 L), at a current density of 24.5 A m^{-2}

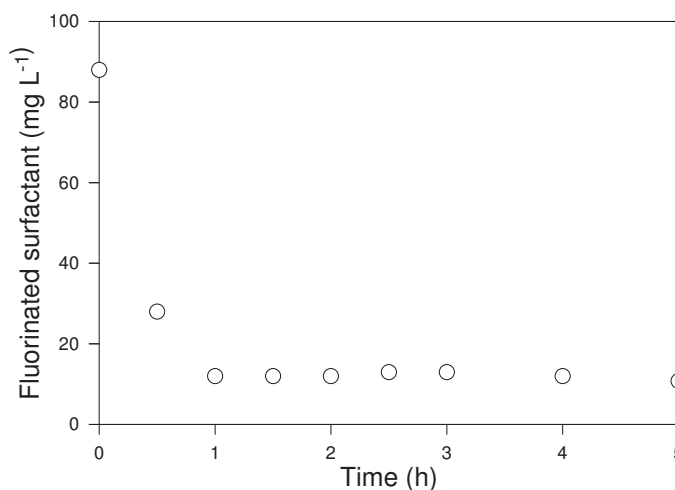


Figure 2.26: Fluorinated surfactant concentration during MFW2 electrocoagulation (3 L), at a current density of 24.5 A m^{-2}

2.3.4.3 Reverse osmosis

Reverse osmosis experiments were done on a Millipore ProScale nanofiltration and reverse osmosis pilot, with an Osmonics SG1821C-28D reverse osmosis membrane, with a thin film polyamide active phase. Pilot dead volume was 0.8 L, its pump rotation rate was set to 20 Hz and operating pressure was 20 bar. The pilot was used in full recycling mode (figure 2.4). Reverse osmosis was used on MFW3 which composition is listed in table 2.18. This model solution represented AFFF foaming solution diluted to reach a fluorinated surfactant concentration near 30 mg L^{-1} , the order of magnitude of the concentration found after 15 min

of electrocoagulation of 3 L of pilot firefighting water at 2 A (section 2.3.3.4). Its complexity is represented in figure 2.27.

Table 2.18: Model firefighting water 3 composition

Compound	Concentration ($mg L^{-1}$)
Dipropylene glycol methyl ether (Dowanol [®] DPM)	338
Sodium octyl sulfate (Disponil [®] 842)	100
Alkyl propionate (Tegotens [®] AM VSF)	43
Octyl glucoside (Simulsol [®] SL8)	37
Fluorinated surfactant from the fraction	29

Volume: 5 L, pH: 6.5

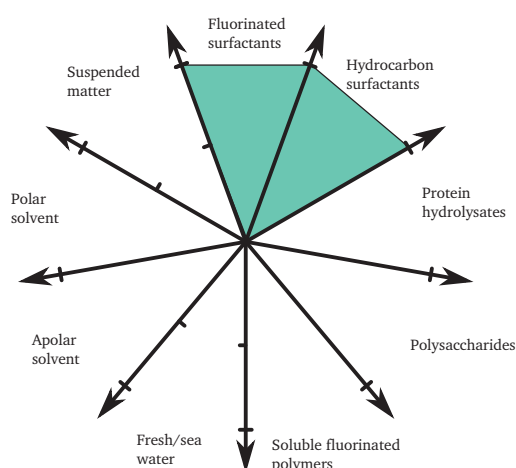


Figure 2.27: Sophistication of the solution used during reverse osmosis screening (MFW3)

This preliminary experiment was done to check what was the fluorinated surfactant retention rate. 5 L of MFW3 (table 2.18) were used in this experiment which lasted 4 hours. The permeability took 1 hour to stabilize around $1 L h^{-1} m^{-2} bar^{-1}$ (near 50% of the permeability for deionized water) and then remained barely constant during the rest of the experiment (figure 2.28). Permeates and retentates at 5 min and 3.6 hour were analyzed by HPLC, the results are presented in table 2.19. No surfactants were detected in both permeates and the fluorinated surfactant concentrations in both retentates were 22 and $21 mg L^{-1}$. Taking into account the dilution factor due to the dead volume, the expected concentration was

$25 \pm 5 \text{ mg L}^{-1}$. The difference between expected and measured fluorinated surfactant concentration in the retentate was below the measurements error. Reverse osmosis of MFW3 showed quick, stable and little fluorinated surfactant adsorption, and flux stabilization at 1 hour. Permeate concentrations were below the limit of detection of 1.4 mg L^{-1} . The initial membrane water permeability could be recovered after cleaning, so reverse osmosis was a promising process for the treatment step.

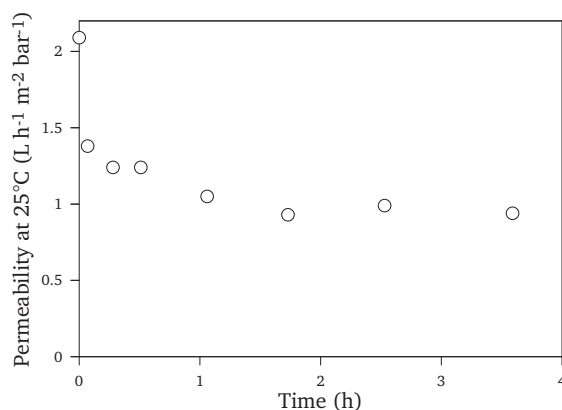


Figure 2.28: Permeability at 25°C during MFW3 full recycle reverse osmosis

Table 2.19: Fluorinated surfactant concentrations during MFW3 full recycle reverse osmosis

Time	Permeate Concentration (mg L^{-1})	Retentate concentration (mg L^{-1})	Expected fluorinated surfactant in the retentate (mg L^{-1})
5 min	< 1.4 (not detected)	22 ± 1	25 ± 5
3.6 h	< 1.4 (not detected)	21 ± 1	25 ± 5

Conclusion on the screening of treatment processes

During the screening of treatment processes, electrocoagulation showed too low performances in fluorinated surfactant removal, with remaining concentrations near 10 mg L^{-1} . Adsorption on activated carbon and unfunctionalized resin showed interesting results, but

these processes required consequent adsorbent supply. Therefore reverse osmosis was preferred because of its high efficiency and its autonomy in raw materials.

General conclusion

In this chapter, the processes identified and chosen after the bibliographic study were screened and compared. It is now known that the mobile unit will be composed of at least two steps: a pretreatment to remove the suspended matter from the firefighting water; and a treatment step to remove the fluorinated surfactant. The screening was done with pilot firefighting waters and model solutions (section 2.3.2). The processes were assessed on the basis of turbidity and fluorinated surfactant concentration measurements (section 2.3.1).

Only ultrafiltration and coagulation combined with filtration could provide turbidities reaching the expectations for the pretreatment step (table 2.20). Unfortunately, ultrafiltration of pilot firefighting water showed very high fouling. Coagulation methods required further floc segregation, by means of a physical treatment such as decantation or filtration. Electrocoagulation had the advantage of being compact and requiring only a metallic anode and electricity, minimizing raw material supply. Though the most appropriate process for the floc segregation was not determined, electrocoagulation was chosen as the main part of the pretreatment process.

Table 2.20: Comparison of turbidities obtained after pretreatment processes during the present screening. The aim was 2 NTU or lower.

Processes	Final turbidity (NTU)	Remarks
Decantation	17.0	Too high turbidity.
centrifugation	4.3	Too high turbidity.
Filtration	Clarification :11.0, 0.45 μm PVDF syringe filtration: 7.7	Too high turbidity, high fouling
Ultrafiltration	0.1–0.4	Acceptable turbidity, but high fouling.
Coagulation–floculation (cationic flocculants)	0.8–2, after 0.45 μm PVDF syringe filtration	Acceptable turbidity, sticky floc that required segregation, coagulant supply, dilution and mixing.
Electrocoagulation	1, after 0.45 μm PVDF syringe filtration	Acceptable turbidity, but required floc segregation, a metallic electrode and electricity.

Though able to decrease the fluorinated surfactant concentration during the pretreatment, electrocoagulation was not found efficient as a treatment process (table 2.21). Activated carbon and resin showed affinities with the fluorinated surfactant and interesting sorption capacities during adsorption experiments. However, for these processes substantial amounts are required, especially if the adsorbent is not recycled. Such a recycling would typically involve organic polar solvents and require the setting up of a whole purification process to recycle this solvent. On the contrary, membrane processes are compact, autonomous in raw materials and their output waste is nothing but the concentrated retentate. In addition, reverse osmosis showed high retention of fluorinated surfactant, as the surfactant was not detected in the permeate. Therefore membrane processes were chosen as treatment processes.

Table 2.21: Comparison of treatment processes on the basis of the present screening

Processes	Final fluorinated surfactant concentration ($mg\ L^{-1}$)	Remarks
Electrocoagulation	9–10	Too high concentration.
Adsorption with activated carbon and resin	not determined: required chromatography experiments.	Interesting sorption capacities, but unknown leaking curves. Required substantial amounts of adsorbent. Regeneration would require an additional recycling process involving polar solvents.
Reverse osmosis	< 1.4 (not detected)	High retention, but membrane fouling. Compact process, raw material autonomy, waste: concentrated retentate.

The composition of the pilot firefighting waters must be kept in mind. These waters were assumed to contain no protein hydrolysates, no polymers, no polar solvents and no sea water. Protein hydrolysates and polymers could interfere with the electrocoagulation process, and the presence of seawater with membrane processes, whereas the presence of polar solvents could interfere with both. These interferences will be considered in the corresponding following chapters.

To conclude, the screening for both pretreatment and treatment processes for firefighting water identified two processes as likely to fulfill the constraints of a mobile unit. Electrocoagulation–filtration as a pretreatment has the advantage over conventional coag-

ulation of being efficient on the suspended matter removal after filtration, being compact and making use of a solid soluble anode and electricity. This combination of process will be extensively studied in Chapter 3. Reverse osmosis with polyamide thin film membrane showed interesting retention rates and despite the investment cost for such processes, the compactness, the absence of reactants needed and the possibilities of automatization and continuous operation made this process the more likely to fulfill the constraints for a mobile unit. Reverse osmosis will be extensively studied in Chapter 4.

Chapter 3

Pretreatment of firefighting water by electrocoagulation

Introduction

During the screening done in the previous chapter, electrocoagulation was chosen for the removal of turbidity and suspended matter in pilot firefighting waters. This chapter will start with a bibliographic study on the electrocoagulation process, to clarify its principles, theory and applications. Then electrocoagulation of pilot firefighting water will be optimized at the laboratory scale and tested on an industrial pilot. Finally, the complexity of several phenomenon behind the electrocoagulation process will be observed during a study aiming at identifying a parameter influencing significantly the minimal electrocoagulation charge loading for the pretreatment of pilot firefighting waters.

3.1 Electrocoagulation theory and bibliography

In the course of the present thesis, preliminary filter experiments as pretreatment showed a dramatic fouling on various filters including membrane filters (microfiltration and ultra-filtration) by water used during fire extinguishment, pinpointing the need of a coagulation method to remove suspended matter from these waters. Electrocoagulation was chosen as a pretreatment process in the previous screening, as it seemed the most relevant process considering the constraints due to the mobility of the foreseen unit. In this section, the elec-

trocoagulation process will be described. An insight in the complex mechanisms , still not completely understood, will be given to help the conceptual preparation of the experimental part of this chapter.

3.1.1 Electrocoagulation principles

3.1.1.1 Description of the process

Electrocoagulation is a wastewater treatment process able to remove various suspended solids as well as organic or inorganic soluble compounds (section 3.1.1.3). This process is based on the introduction of coagulating metallic salts in the water by electrodisolution of a soluble metallic anode, usually made of iron or aluminium. These metallic salts have the effect of destabilizing colloidal suspensions and removing some dissolved compounds from water (section 3.1.2). The matter to remove is basically transferred from the water to the sludge produced during this process. Electrocoagulation adds some suspended matter to the solution, however, as this suspended matter is coagulant and adsorbent, the resulting sludge is coagulated. It may then be separated by conventional processes such as decantation, flotation or filtration, which might have been inefficient or unworkable before electrocoagulation (section 3.1.1.2). Electrocoagulation was reported to be highly efficient, compact, relatively low cost, completely automatizable and electrocoagulation reactors range from basic to very sophisticated design [85].

3.1.1.2 Processes for removal of the floc

The floc produced in solution during electrocoagulation is subject to settling and electroflotation. Electroflotation is a process in which electrolytic gas bubbles (here hydrogen produced at the cathode) lift particles to the surface of the solution [85] (figure 3.2d). Settling or electroflotation predominance depends on the current density of electrocoagulation. Physical separation of the floc can also be achieved by hydrocycloning, centrifuging, flotation, dissolved air flotation and filtration [87].

3.1.1.3 Electrocoagulation process applications

Electrocoagulation is able to remove a great variety of suspended matter and chemicals, which have been reviewed by Emamjomeh and Sivakumar [88]. This process has been used to treat water containing organic pollutants, such as dye and textile wastewaters [89, 90, 91, 92, 93, 94], industrial wastewaters [95, 96, 97, 98], restaurant wastewaters [99, 100], oil-in-water emulsions [101, 86, 102], or waters containing surfactants [103, 49, 51, 104]. Electrocoagulation is able to remove heavy metals from water such as chromium [105, 106], mercury [107], arsenic [108, 109], Ni^{2+} , Cu^{2+} and Zn^{2+} [110]. Water hardness [111], fluoride [112, 113], boron [114] or clay [115, 116, 117] can also be treated by electrocoagulation. The versatility of this process is due to the complex mechanisms taking place in the electrocoagulation reactor.

3.1.2 Electrocoagulation theory

Electrocoagulation is a process known since the end of the 18th century [118], however, the complex mechanisms behind this process are yet to be clearly understood. Multiple mechanisms such as electrochemical reactions, aluminium speciation, coagulation and flotation/sedimentation are involved and operate synergistically to remove pollutants from water [119]. The most frequently used electrode material is aluminium [87] and the electrocoagulation cell available in the laboratory also had electrodes made of this material. Therefore the mechanisms of electrocoagulation will be described in the following sections, with focus on aluminium electrodes.

3.1.2.1 Coagulation theory

Coagulation-flocculation is a classical pretreatment in wastewater treatment plants, removing various particles and dissolved organic matter. Coagulant can be aluminium or ferric salts (aluminium sulfate, ferric chloride, ferric sulfate, polyaluminium chloride), or polyelectrolytes. It is commonly admitted that coagulation occurs according to two mechanisms: charge neutralization and sweep flocculation (figure 3.1).

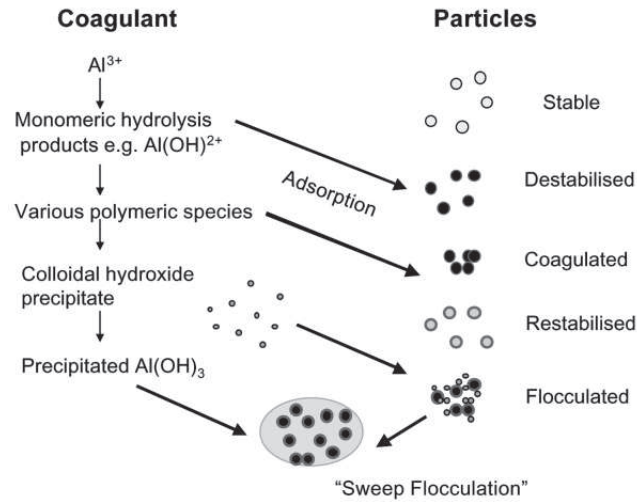


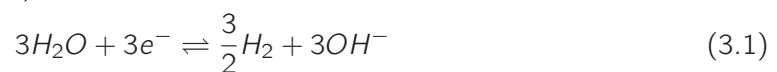
Figure 3.1: Interaction of aluminium species with initially negatively charged particles in water. The particles on the right hand side are initially stable and then become destabilized by charge neutralization. At higher coagulant dosages they can become restabilized by charge reversal and incorporated in a flocculant hydroxide precipitate ('sweep flocculation'). Image taken from [45].

Charge neutralization takes place when cationic coagulants lower the zeta potential of the solution and/or bind to oppositely charged pollutants, enabling aggregation of the matter that was previously stabilized by charge repulsion. Sweep flocculation is a process in which pollutants are "trapped" in a growing hydroxide precipitate [45]. Once coagulated, the removal of previously suspended matter becomes easier by settling or filtering. As mentioned earlier, the final unit we consider here has to be mobile so processes have to fit the constraints of compactness, material and chemical input minimization, automatization and continuous operation in addition to efficiency. In the previous screening chapter, electrocoagulation was preferred to conventional coagulation for these reasons.

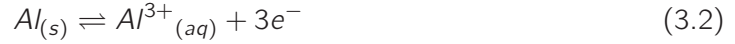
3.1.2.2 Electrocoagulation theory

Coagulants in electrocoagulation, *Fe* or *Al* salts generally, are electrochemically introduced by *in situ* dissolution of a metallic anode. When aluminium anode is used, the following reactions take place [120, 85]:

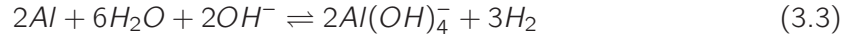
At the cathode (figure 3.2b):



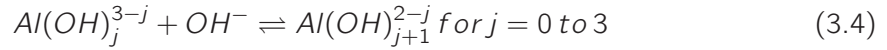
At the aluminium anode (figure 3.2a):



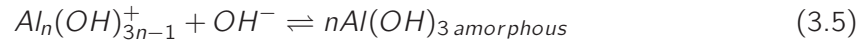
At high pH, in case of aluminium cathode, cathodic dissolution can occur [121]:



Al^{3+} can react with OH^{-} produced in equation 3.1 to form the following hydroxides [122, 45]:



In addition, formation of many polymeric aluminium salts such as $Al_2(OH)_2^{4+}$, $Al_6(OH)_{15}^{3+}$, $Al_7(OH)_{17}^{4+}$, $Al_8(OH)_{20}^{4+}$, $Al_{13}O_4(OH)_{24}^{7+}$, $Al_{13}(OH)_{34}^{5+}$ over a wide pH range has been proposed [123]. Aluminium hydroxide species finally precipitate according to complex kinetics to form amorphous $Al(OH)_3$ [91, 97] (figure 3.2a):



3.1.2.3 Active species in electrocoagulation

Charged hydroxo cationic complexes can effectively remove pollutants by charge neutralization, or adsorption and precipitation of amorphous aluminium hydroxide at their surface. As colloidal aluminium hydroxide particles are positively charged up to pH 8, these might also be effective charge-neutralizing agents [45]. Amorphous aluminium hydroxide precipitate is held responsible for soluble or colloid pollutant adsorption and sweep flocculation [45, 91, 97] (figure 3.2c).

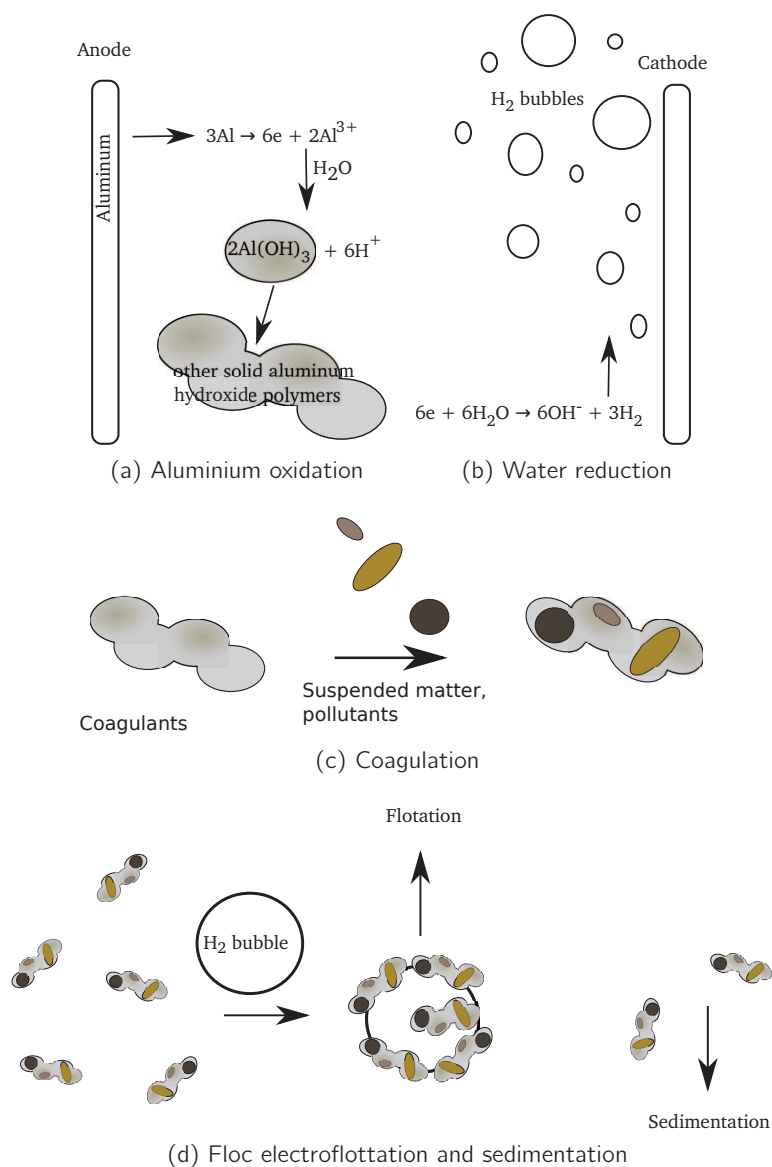


Figure 3.2: Removal mechanisms in electrocoagulation

Large networks of aluminium hydroxide have also been reported to chemically adsorb monoatomic species such as F^- by OH^- substitution [112, 113]. Electrocoagulation with aluminium electrodes was reported to show the best efficiency between pH 6 and 9 [49], which corresponds to the existence zone of amorphous $\text{Al}(\text{OH})_3$ which dissolves at pH higher than 9.5 (figure 3.3).

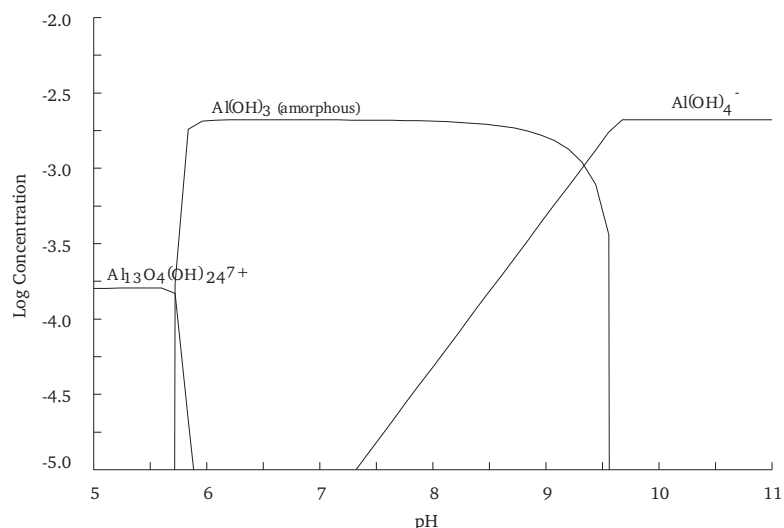


Figure 3.3: Aluminium speciation in aqueous solution, obtained by Hydra/Medusa software, for aqueous solution containing 2.1 mM of Al^{3+} , assuming amorphous aluminium hydroxide as the only possible solid species.

3.1.2.4 Parameters influencing the electrocoagulation process

In electrochemical processes, the most obvious key parameters are the potential and the current. In electrocoagulation, the quality of the water is directly related to the amount of cation produced. This amount is governed by the charge loading in the process, and for aluminium the electrochemical equivalent mass is $335.6 \text{ mg A}^{-1} \text{ h}^{-1}$ [85]. This is directly related to the current density: the current per area of electrode which determines the rate of the process. The quality of the water treated was found not to significantly increase above a critical charge loading value [99].

The current efficiency is the ratio of current consumed to produce a target product to that of total consumption. It depends on current density, pH, temperature and flow rate. With aluminium electrodes, a current efficiency of 120–140% is not unusual. It is attributed to pitting corrosion of the electrode (equation 3.3), and the reaction is catalysed by chlorine anions [121, 110].

The potential as well as the power consumption are strongly dependent on the conductivity of the solution. Therefore the use of a supporting electrolyte is of great interest to minimize the energy consumption of the process. *NaCl* has the advantage of increasing the

current efficiency, whereas other ions like HCO_3^- , SO_4^{2-} , Ca^{2+} or Mg^{2+} can lead to the formation of an insulating layer which would decrease the current efficiency and increase the potential [85, 110, 124].

Whereas pH influences the current efficiency only when the conductivity is low, it is crucial for the solubility of metal hydroxides. Electrocoagulation with aluminium was found to have better efficiency at neutral pH, where the amorphous $\text{Al}(\text{OH})_3$ floc is predominant (figure 3.3). During the process, the hydrogen evolution at the cathode (equation 3.1, figure 3.2b) is more or less compensated by the hydrolysis of the metallic cations (equation 3.4, figure 3.2a). However, the pH may evolve if some OH^- from the floc is exchanged by other anions such as F^- [113].

3.1.3 Electrocoagulation in the scope of firefighting water pretreatment

Firefighting waters contain various surfactants, may contain polymers, protein hydrolysates. Pilot firefighting waters from the present work were found to contain some suspended matter which was assumed to hydrophobic organic matter such as ash or soot, resulting from incomplete combustion of n-heptane. This suspended matter was sufficiently stable not to sediment spontaneously, and this stability was most probably due to the presence of surfactants. Though the exact nature of the suspended matter remained unknown, electrocoagulation (followed by floc segregation) was found during the screening to be an efficient treatment for its removal.

In the system of an electrocoagulation cell treating firefighting water, expected interactions would be electrostatic interactions, between polyaluminium complexes positively charged [123], aluminium hydroxide positively charged up to pH 8 [45] on the one hand, and anionic compounds, such as colloids or anionic surfactants on the other hand. Another kind of interactions are Lewis acid-base interactions (AB), as aluminium is a Lewis acid and could interact with electron-donor compounds. Hydrophobic interactions should also be considered as aluminium hydroxide is a hydrophobic colloid stabilized by Al^{3+} or OH^- ions, depending on the conditions [125].

Electrocoagulation with iron [51] and aluminium [49] electrodes was found to be efficient on anionic surfactants, with removals near 90%, which could be explained by electrostatic

interactions between cationic coagulants and anionic surfactants. The electrocoagulation with iron and aluminium electrodes of several nonylphenol ethoxylates solutions was also investigated [126]. In the studied NP n EO molecules, n the number of ethoxylate units was 4, 16 and 40. The higher n , number of ethoxylate units, the more hydrophilic the surfactant. For both electrodes, it was found that the lower n , the higher the affinity of the surfactant to the coagulant. These results were interpreted by the authors in terms of higher solution in water of more hydrophilic surfactants, but steric hindrance on the coagulants by voluminous polar heads could also be relevant. NPEO are nonionic surfactants, so electrostatic interactions could not occur. Therefore in that case, either AB interactions and/or LW interactions between the coagulants and the surfactant seemed to be significant.

Like the polar head of NPEO, most of natural organic matter (biopolymers and carbohydrates for instance) is strongly electron donor. This marked monopolarity is responsible for the solubility of such compounds which spontaneously repel one another in water [127]. Regardless of their electrostatic properties, compounds such as Al^{3+} and $Al(OH)_3$, which are Lewis acids, can “capture” the excess of electron donicity, cancelling the polar interaction of the compounds with water. This decrease of solubility can have a crucial impact on destabilization and coagulation of electron donor compounds, and the role of AB interactions is seen as underrated by Van Oss in processes involving the addition of plurivalent cations[6].

Conclusion

The scope of application of electrocoagulation is very wide, as it can remove a great variety of pollutants, and the design of electrocoagulators ranges from rustic to very sophisticated designs. However, this apparently simple process is driven by fairly complex underlying mechanisms. It involves an interplay between electrochemistry, coagulation and flotation/sedimentation. The coagulation part of the process is directly concerned by interparticle and intermolecular interaction. Though charge neutralization and sweep flocculation are commonly admitted to be the main phenomenon involved in coagulation and electrocoagulation processes, in solutions such as firefighting waters containing various surfactants the other kinds of interactions, namely Lifshitz-Van der Waals (LW) and Lewis acid base (AB) interactions should be kept in mind. Moreover, in firefighting water, surfactants and

suspended matter may compete in affinity with the coagulants. The aim of the next paragraph is the optimization of charge loading/aluminium dose and floc removal for the purpose of firefighting water pretreatment, as well as the study of the phenomenon taking place in such a system.

3.2 Material and methods

3.2.1 Electrocoagulation and filtration

Two different cells were used to carry out electrocoagulation experiments (figure 3.4). EC1 cell had a volume of 3 to 5 L, 815 cm² of aluminium anode and stainless steel cathode. EC2 cell had a volume from 0.5 to 2 L, reversible aluminium electrodes, and an anode surface of 350 cm². Suspended floc was removed by press filter dead-end filtration, achieved on a device with a filtration surface of 50 cm² supplied by Choquenot, using a Masterflex peristaltic pump (Cole Parmer Instruments). At the laboratory scale, the volume of electrocoagulated pilot firefighting water was not sufficient to enable the formation of a cake as a filtering media. Hence the filter was coated with 2.4 mm of CaCO₃ before each filtration experiment.



Figure 3.4: Electrocoagulation cells. Left: EC1 cell, right: EC2 cell

3.2.1.1 Turbidity measurements

Turbidity measurements in nephelometric turbidity units (NTU) were achieved the same way as in chapter 2, section 2.2.1.1., with a HACH 2100AN turbidimeter.

3.2.1.2 HPLC analysis

HPLC–ELSD analysis for fluorinated surfactant analysis were performed according to the method detailed in chapter 2, section 2.2.1.2. An improvement was brought to this method in order to perform separation and quantification of the non-volatile compounds contained in the pilot firefighting water. The isocratic pump was replaced by a Hitachi *L*–2130 gradient pump. The only volatile compound that could not be detected by ELSD was Dowanol[®] DPM, the cosolvent. The four surfactants, namely Disponil[®] SOS 842, Tegotens[®] AM VSF, Simulsol[®] SL8, and fluorinated surfactant, could be separated with the gradient given in table 3.1. A chromatogram is given in figure 3.5 to illustrate the separation of surfactants and the retention times. As the chemicals used in this study were industrial preparation, some of them contained impurities that were revealed by HPLC. Disponil[®] SOS 842, which is a mixture of sodium octyl and decyl sulfate, as well as Simulsol[®] SL8, which is a mixture of octyl and decyl alkylglucosides, both gave two peaks on the chromatograms. For these compounds, the calibrating curves and the analysis were based on the sum of the areas of their two peaks.

Table 3.1: Composition of the gradient given to the Hitachi *L* – 2130 gradient pump, for the simultaneous analysis of surfactants from pilot firefighting waters.

Time (min)	Methanol	Water	Ammonium acetate, 1 mol L^{-1}
0	60	39	1
11	99	0	1
14	99	0	1
16	60	39	1
18	60	39	1

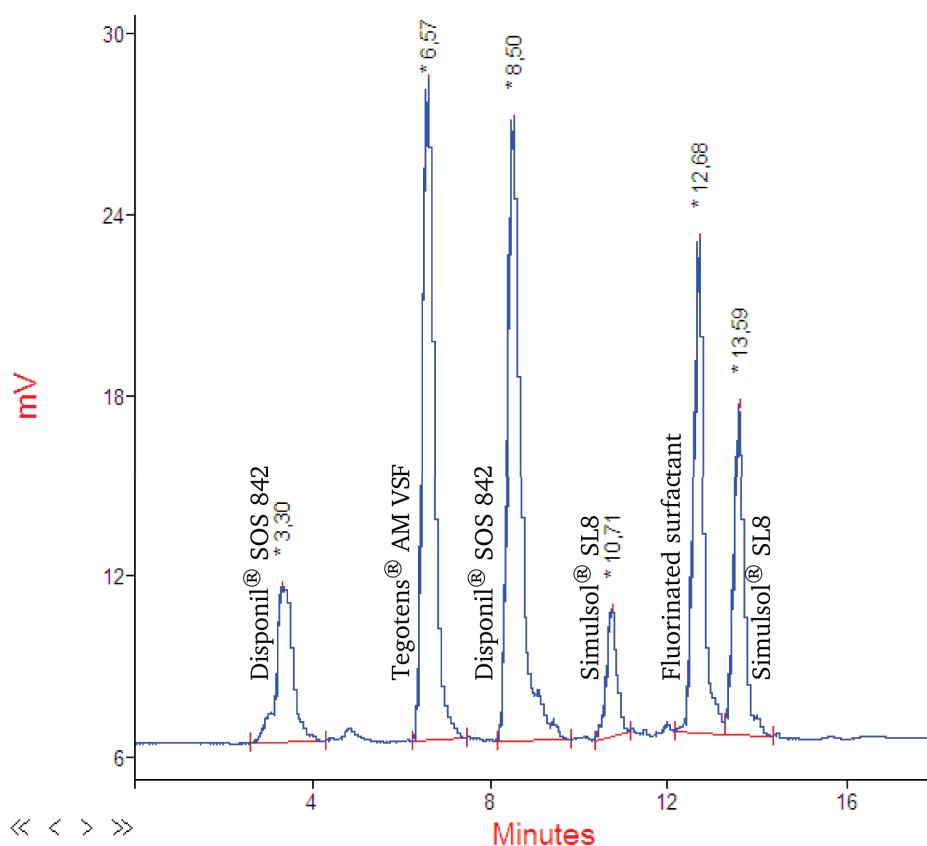


Figure 3.5: Chromatogram of a calibrating solution containing at 3.30 and 8.50min: Disponil® SOS 842; 6.57 min: Tegotens® AM VSF; 10.71 and 13.59 min: Simulsol® SL8 ; 12.68: fluorinated surfactant. The identification of the peaks were done by analysis of single surfactant solutions (not shown).

Calibration curves were established with solution containing 2 mg L^{-1} to 1000 mg L^{-1} for each surfactant. Above 1000 mg L^{-1} , the samples were too concentrated for the detector and the obtained areas did not fit the calibrating curves obtained with lower concentrations. Therefore, with this method, solutions containing concentrations of surfactants superior to this concentration had to be diluted to be analyzed. The limits of detection and quantification were not investigated at this point because all samples encountered during electrocoagulation experiments were concentrated enough to fit the calibration curves. Each sample from electrocoagulation experiments had to be filtered with $0.45 \mu\text{m}$ PVDF syringe filters to protect the column.

3.2.1.3 Aluminium atomic absorption spectrometry

Aluminium quantification was done by atomic absorption with a Varian SpectrAA 220 atomic absorption spectrometer, with a reducing flame of acetylene fuel and nitrous oxide support, data was gathered and processed on a computer by the SpectrAA 220 2.10 software. Wavelength was set to 232 nm and 2 g L^{-1} of potassium chloride were added to the sample in order to minimize aluminium ionization in the flame, samples were acidified with HNO_3 . Detection ranged from 0.5 to 250 mg L^{-1} , the error was below 5%.

3.2.1.4 Firefighting water used during the study of the pretreatment by electrocoagulation

For the experiment done in this chapter, four different pilot firefighting water were used (table 3.2). In addition electrocoagulation was tested on two real industrial firefighting waters and on model solutions. The details on these additional solutions will be given in the corresponding sections.

Table 3.2: Pilot firefighting waters used in this chapter

Denomination	Volume (L)	Turbidity (NTU)	Turbidity after $0.45\text{ }\mu\text{m}$ filtration* (NTU)	Fluorinated surfactant concentration* (mg L^{-1})
PFW1	20	30	7.7	82
PFW2	17	27	4.2	94
PFW3	50	52	—	133
PFW4	5	70	45	144

*: fluorinated surfactant concentrations measured after filtration.

3.3 Optimization of the electrocoagulation process applied to firefighting water

The main parameter in the electrocoagulation process is the charge loading, *i.e.* the electricity required to bring to the solution the necessary amount of coagulant. The object of this section is to investigate and assess the minimum charge loading for the electrocoagulation of firefighting water and then to remove the floc in order to obtain pretreated pilot firefighting

water. The aim for the final turbidity was previously chosen as $< 2 \text{ NTU}$, the turbidity due to the compounds from the foaming solution before application to a fire. Electrocoagulation will also be tested on several real industrial firefighting waters produced in uncontrolled conditions.

3.3.1 Electrocoagulation of the suspended matter and turbidity removal from pilot firefighting waters

3.3.1.1 Identification of an indicator for the end of suspended matter electrocoagulation

In this section, electrocoagulation experiments were done with pilot firefighting waters, which sophistications regarding real firefighting water are depicted in figure 3.6. During the pre-treatment screening, 3 L PFW2 was electrocoagulated in EC1 cell at 2 A (25 A m^{-2}). It was observed that at the end of the experiment the electroflotated floc presented three layers, with a dark one at the middle. Additional information that were out of the scope of the screening will be presented here. Pictures of the floc formation during this experiment are displayed in figure 3.7. The same successive steps occurred in every pilot firefighting water electrocoagulation experiments. At first a latency phase was observed, here during 5 min, during which the floc produced and electroflotated was white (figure 3.7a, here the white floc is merged with the foam). Then, near 5 min, the core solution became more turbid, and the electroflotated floc was dark gray (figure 3.7b). After that, near 15 min, the cloudiness of the core solution decreased and the electroflotated floc gradually shifted from dark gray to white (figure 3.7c, 3.7d). For the rest of the experiment, the floc remained white (figure 3.7e).

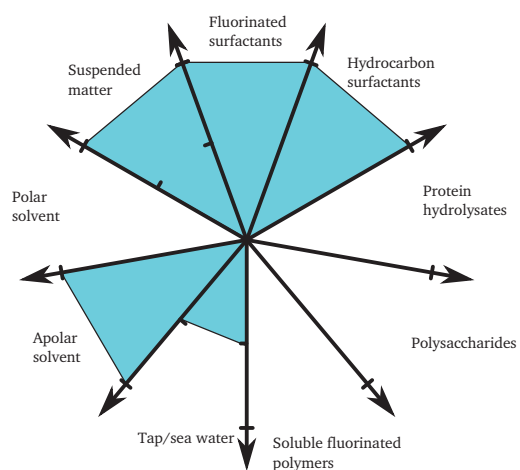


Figure 3.6: Sophistication of the pilot firefighting waters 1, 2, 3 and 4.

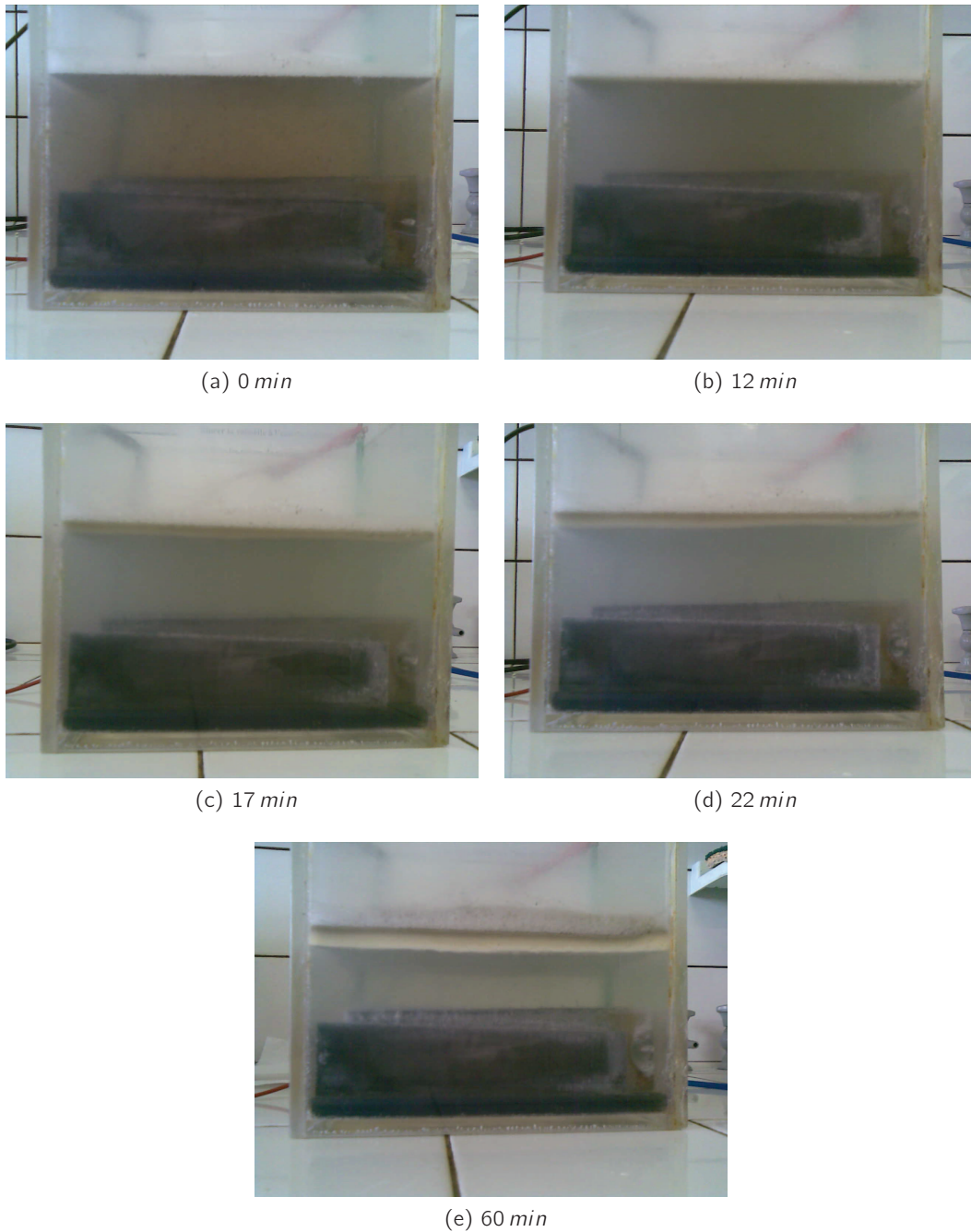


Figure 3.7: Floc formation during the electrocoagulation of pilot firefighting water 2, 3 L, in EC1 cell, 2 A.

It has been seen in chapter 2, section 2.3.3.4 that after 15 min, the turbidity after PVDF syringe filtration of the electrocoagulated PFW2 was near 1 NTU (figure 3.8). This duration of 15 min was the same as the time at which the dark floc gradually turned clearer. The suspended matter seemed to be responsible for the dark color of the floc. During the initial latency step the floc was clear, and so was it after 15 min. It could therefore be assumed

that in this experiment, the suspended matter electrocoagulation was performed between 5 and 15 min (active phase, figure 3.8). It can be noticed that during the latency phase, if nothing seemed to occur visually, the turbidity after filtration decreased. This could be explained by suspended matter coagulation since the latency phase, even if it did not seem to be electroflotated.

The gradual color shift of the electroflotated floc from dark to white was assumed to be due to some inertia in dark floc electroflotation, which progressively mixed with clear floc after all the suspended matter was electrocoagulated. Thus, the visual observation of the electroflotated floc turning clearer seemed to be a good indication of the end of the electrocoagulation pretreatment in terms of required charge loading and aluminium dose. 15 min at 2 A for 3 L of PFW2 corresponded to a charge loading of 600 C L^{-1} or 0.167 A h L^{-1} , and an aluminium dose of 55.9 mg L^{-1} assuming a unity current efficiency. These values had to be verified at different volumes and current density.

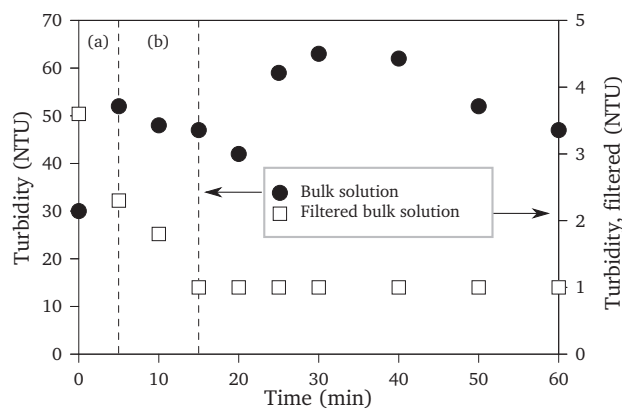


Figure 3.8: Turbidity during electrocoagulation at 2 A of pilot firefighting water 2 (PFW2). ●: in bulk solution; □: after $0.45 \mu\text{m}$ PVDF syringe filtration. (a): latency phase; (b): active phase.

3.3.1.2 Assessment of the minimum charge loading and aluminium dose

Electrocoagulation experiments with PFW3 were done at different current densities and different pilot firefighting water volume to estimate minimal pretreatment times and charge loading per volume visually (table 3.3). Minimal time seemed to depend on the volume of the solution and on the charge loading passing through it. However, the estimated minimal needed charge loadings per volume varied, with an average of 540 C L^{-1} , i.e. 0.150 A h L^{-1} and an aluminium dose of 50.3 mg L^{-1} . These differences could be related

to the difficulty to estimate precisely when the white floc came back, as it showed up in the bulk solution before complete electroflotation of the electrocoagulated suspended matter. In addition, EC2 electrodes were both made of aluminium, which could enable higher current efficiency via pitting corrosion at the cathode (equations 3.1 and 3.3). In that case shorter times and charge loadings would be needed for a given aluminium dose, which seems to be verified for current densities $> 0.9 \text{ mA cm}^{-2}$ in EC2 cell (table 3.3). After $0.45 \mu\text{m}$ PVDF syringe filtration all solution had a turbidity of less than 1 NTU , which confirmed the validity of considering the color shift of the floc as an indicator of the end of the electrocoagulation.

Table 3.3: Visual estimation of the minimal pretreatment time for PFW3. Experiments done in *a*: EC2 cell; *b*: EC1 cell.

j (mA cm^{-2})	0.9^a	1.2^b	1.4^a	1.4^a	1.9^a	2.5^b
i (mA)	330	1000	490	490	655	2000
Volume (mL)	500	3000	500	1000	500	3000
Visual minimal time (min)	15	30	8	15	7	15
Visual minimal charge loading (C L^{-1})	594	600	470	441	546	600

For the experiments done in the EC2 cell, the lower the current density, the higher the minimal charge loading per volume, which high limit seemed to approach 600 C L^{-1} , the minimal loading charge obtained with the stainless steel cathode of EC1 cell. This was consistent with a higher aluminium cathodic dissolution for higher current densities [121]. Aluminium dosing more than charge loading, and aluminium speciation were the key parameters in electrocoagulation of pilot firefighting waters.

The case of pilot firefighting water containing n-heptane-in-water emulsion. Electrocoagulation was reported to be efficient to treat water containing oil-in-water emulsion [102, 86, 101]. As the water used during fire extinguishment may contain such emulsions, an experiment was done with PFW4. This pilot firefighting water presented a turbidity of 70 NTU whereas the turbidity of emulsion-free firefighting waters 1 and 2 were near 30 NTU .

Hence this difference of turbidity could be attributed to the emulsion. 3 L PFW4 were electrocoagulated at 1 A in EC1 cell. Turbidity of the bulk solution was measured before and after 0.45 μm PVDF filter syringe filtration (figure 3.9). Initial turbidity increase seemed to be due to floc formation and its further decrease to floc sedimentation and electroflotation. At the beginning of the experiment, filtration only removed about 20 NTU but after 30 min, turbidity after syringe filtration was near 1 NTU. Hence a 600 C L^{-1} charge loading per volume in EC1 cell was sufficient to remove the turbidity due to heptane-in-water emulsion in addition to the one due to suspended matter.

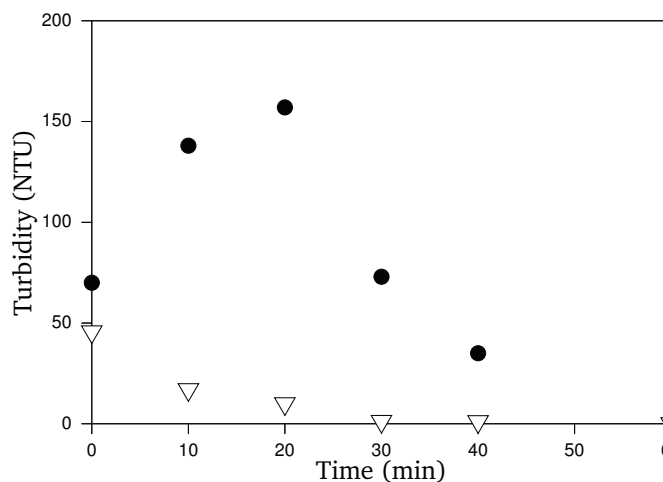


Figure 3.9: Turbidity during electrocoagulation of PFW4, 3 L, 1 A. ●: in bulk solution; ▽: after 0.45 μm PVDF syringe filtration.

The charge loading required for the removal of the turbidity from firefighting waters was identical with or without the presence of the n-heptane-in-water emulsion. This value did not seem to vary significantly with the volume of solution or the current density. Thus it was assumed that electrocoagulation of pilot firefighting water, the first step of the pretreatment, was achieved with a charge loading of 600 C L^{-1} in EC1 cell. The removal of the floc, the second step of the pretreatment could then be studied.

3.3.2 Pretreatment of firefighting waters by electrocoagulation and floc removal

3.3.2.1 Pilot firefighting water by electrocoagulation–press filtration in the laboratory

To produce electrocoagulated pilot firefighting waters, batches were done in EC1 cell. 4 L of pilot firefighting water 3 were electrocoagulated at 1 A during 40 min, the time needed for the identified necessary charge loading per volume. Centrifugation was tried for the removal of the floc from the obtained solutions. Centrifugation at 3,000 and 5,000 rpm were tried during 5, 10, and 15 min and the turbidity of each resulting solution was 21–27 NTU. Centrifugation was therefore considered not sufficient for the removal of the floc after electrocoagulation. The removal of the floc was done by filtration on a press filter. Preliminary experiments showed that turbidity after direct press filtration was not satisfying because at the laboratory scale, electrocoagulated pilot firefighting water bulk solution did not contain enough floc to form a filtering cake. Therefore filter press was coated with 2.4 mm of CaCO_3 to fasten the formation of the filtering media on the filter.

The filter press probe was then introduced in the cell below the layer of electroflotated floc, to pump only the bulk solution which contained 1.126 g L^{-1} of dry matter. The volume needed to form an efficient floc filtering media on the coated filter was 750 mL. Hence the first 750 mL were discarded, on the contrary to the following clear filtrate. Filtration showed a cake filtration profile (figure 3.10) with a corresponding floc specific resistance of $2.6 \cdot 10^{12} \text{ m kg}^{-1}$. Therefore, this solution presented a conventional behavior in filtration, on the contrary to pilot firefighting water (Section 2.3.3.1). The use of a filtration additive could facilitate the floc filtration if needed. The operation was done twice and both resulting filtrates were mixed to get 6 L of pretreated PFW3 at pH 6.9, showing a turbidity of 0.4 NTU, 0.837 g L^{-1} of dry matter and non-detected aluminium concentration. The use of filtration in conjunction of electrocoagulation enabled the production of a pretreated pilot firefighting water suitable for membrane processes.

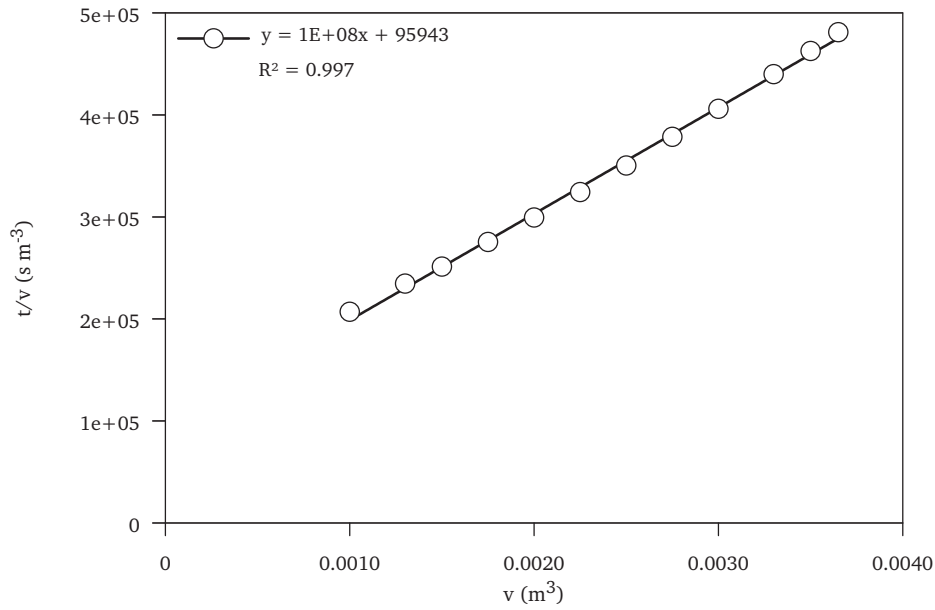


Figure 3.10: Ratio of time by filtered volume t/v , versus the volume v during filter press of pretreated pilot firefighting water bulk solution.

3.3.2.2 Pilot firefighting water electrocoagulation on an industrial pilot

The majority of pilot firefighting water electrocoagulation experiments were done at the laboratory scale in small electrocoagulation cells. In order to assess the validity on the previous findings, an external test was ordered at Serep, in an Solvin[®] electrocoagulator of patented design (figure 3.11). Serep ran an electrocoagulation test with pilot firefighting water 3 with aluminium anode, at 15 V, 20 A, and at a flow of 60 L h^{-1} .

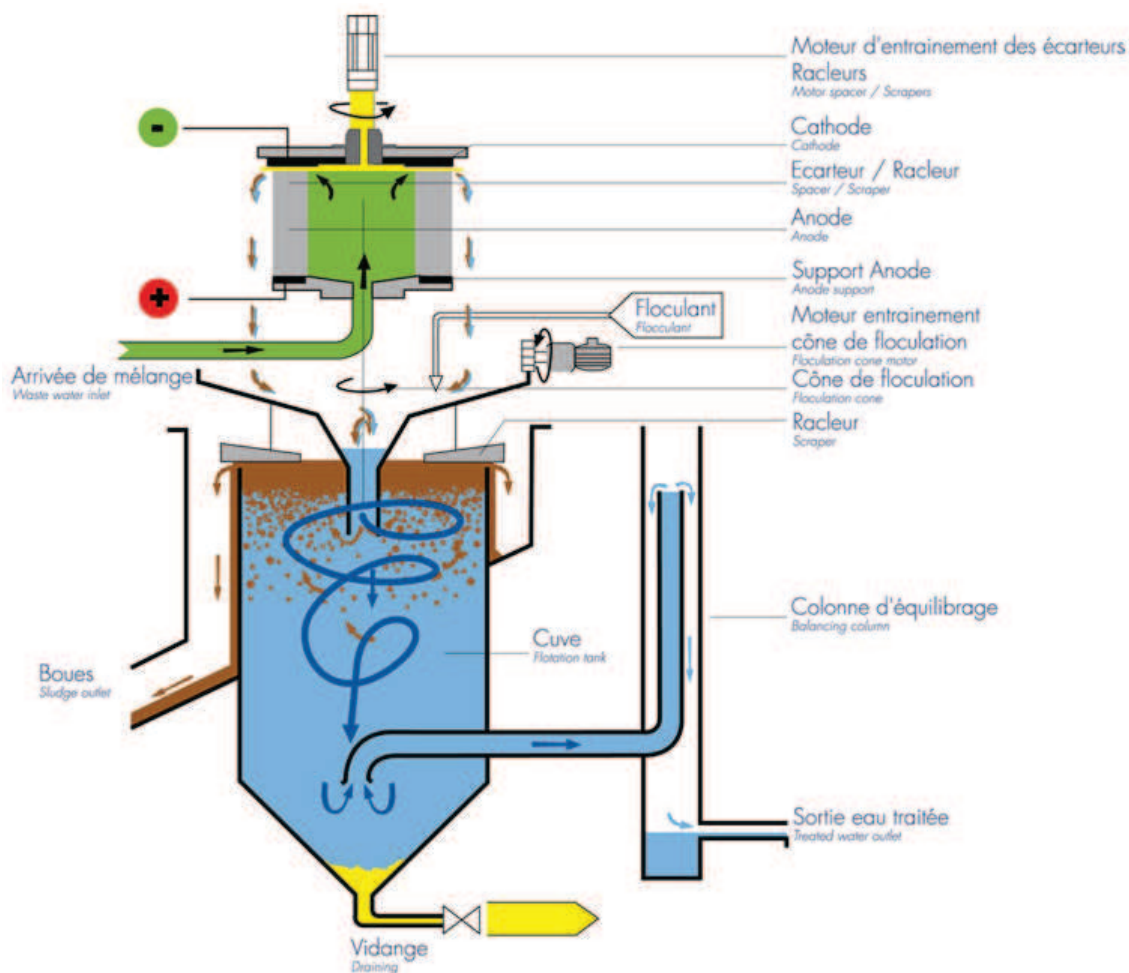


Figure 3.11: Schematics of the Serep's Solvin[®] electrocoagulator. Image: Serep.

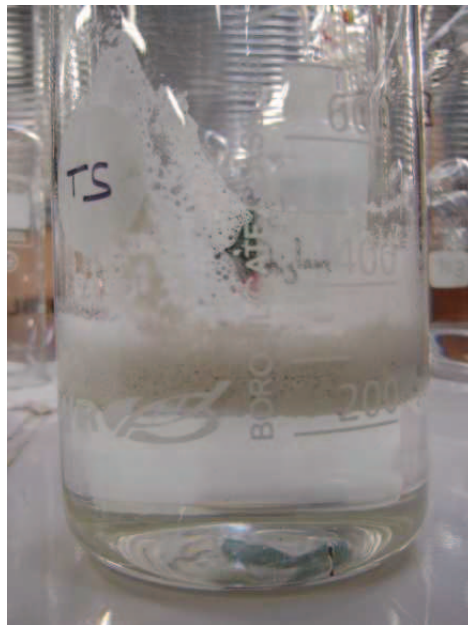
The charge loading was therefore $1,200 \text{ C L}^{-1}$ and the aluminium dose 112 mg L^{-1} , which was twice higher than the minimum previously identified. For this experiment, the conductivity of PFW3, which was initially $633 \mu\text{S cm}^{-2}$ was adjusted between $3\text{--}5 \text{ mS cm}^{-1}$ with NaCl . The conductivity requirements in this process is important for the minimization of energy consumption. The current is high so the potential has to be low. The floc separation was done by flocculation with addition of 5 mL^{-1} of Ferrocryl 8723 (figure 3.12). After electrocoagulation and flotation, the resulting pretreated firefighting water had a turbidity of 0.6 NTU . Though some work remained for the optimization of NaCl , aluminium and flocculant dose, these results confirmed the efficiency of electrocoagulation–flocculation–flotation as a pretreatment process for pilot firefighting water 3 at higher scale.



(a) Initial state



(b) After electrocoagulation



(c) After flocculation

Figure 3.12: Pilot firefighting water 3 electrocoagulation by Serep, at 16 A and 60 L h^{-1} , with aluminium anode.

3.3.2.3 The case of industrial firefighting waters

All the previous pretreatment experiments were done with pilot firefighting waters. The sophistication of the firefighting water will be increased in this section. Electrocoagulation was tried on industrial firefighting waters produced in uncontrolled conditions. Industrial firefighting water 1 (IFW1, figure 3.13), resulting from the extinction of apolar solvent with an alcohol resistant fluoroproteinic film forming foam (FFFP AR). Though the composition of the initial solution remained unknown, this firefighting water was expected to contain at least a fluorinated surfactant and protein hydrolysates. The initial turbidity was very high and the minimum charge loading found in EC1 cell at 1 A for 1.75 L of solution was 1200 C L⁻¹ to obtain a turbidity of 1 NTU (table 3.4). This was twice the charge loading required for pilot firefighting waters in the laboratory, but was the default charge loading in the industrial pilot.

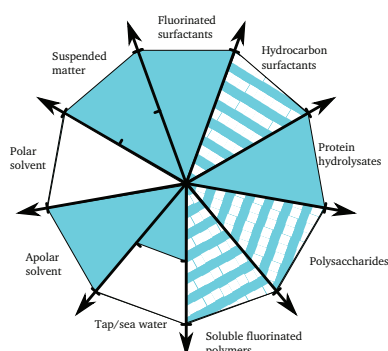


Figure 3.13: Sophistication of industrial firefighting water 1

Table 3.4: Turbidity during the electrocoagulation of industrial firefighting water 1, 1 A, 1.75 L in EC1 cell

Charge loading (C L ⁻¹)	Turbidity in core solution (NTU)	Turbidity after 0.45 μm PVDF syringe filtration (NTU)
0	221	3.6
309	267	2.7
857	392	2.7
1200	not measured	1

Industrial firefighting water 2 (IFW2, figure 3.14) resulted from the use of the same kind of firefighting foam, but on polar solvents. This firefighting water was very different from those resulting from fires of apolar solvents. Its color was orange, its turbidity was very low:

1.5 *NTU*, and 1.35 *NTU* after 0.45 μm PVDF syringe filtration. The electrocoagulation of 3 *L* of this solution at 1 *A* in EC1 cell showed that the decrease of this latter turbidity to 1 *NTU* would take a charge loading of 1200 C L^{-1} (table 3.5). The case of polar solvent was strongly different. The low turbidity could result from better combustion thanks to oxygen atoms present in the solvent molecules, resulting in little soot production. In addition, the presence of water soluble organic polar solvent is known to modify the polarity of water [127], as well as to have AB interaction with Lewis acids such as *Al*. These two facts could greatly disturb the electrocoagulation process observed with firefighting waters from apolar solvents either by modifying the solubility of the surfactants and partial desactivation of the coagulant. Industrial firefighting water 2 already had a satisfying turbidity and electrocoagulation seemed to be useless in that case, but the presence of polar solvents such as ethanol or acetone would be of great importance in the context of a further treatment with membrane processes.

Table 3.5: Turbidity during the electrocoagulation of industrial firefighting water 2, 1 *A*, 3 *L* in EC1 cell

Charge loading (C L^{-1})	Turbidity in core solution (<i>NTU</i>)	Turbidity after 0.45 μm PVDF syringe filtration (<i>NTU</i>)
0	1.5	1.3
160	61.1	1.5
300	150	1.2
600	223	1.1
900	227	1.1
1200	143	1

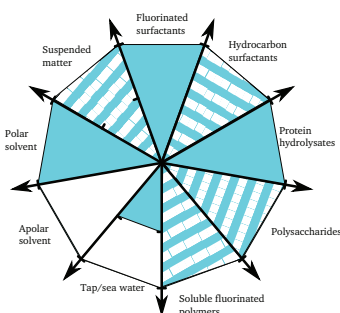


Figure 3.14: Sophistication of industrial firefighting water 2

Conclusion

The optimization of electrocoagulation applied to pilot firefighting water showed that an apparent minimal charge loading of 600 C L^{-1} was required for the pretreatment. This charge loading was also confirmed for a pilot firefighting water containing heptane-in-water emulsion. This corresponded to 0.167 A h L^{-1} , and to an aluminium dose of 55.9 mg L^{-1} assuming a unit current efficiency. The floc removal could be achieved by filtration on a coated press filter at the laboratory. The efficiency of electrocoagulation on pilot firefighting water was confirmed by an external experiment on an industrial electrocoagulator, in which floc removal was successfully achieved by flocculation. Real industrial firefighting waters containing protein hydrolysates were electrocoagulated. The industrial firefighting water resulting from the extinction of apolar solvent required twice the minimal charge loading for pilot firefighting waters and the industrial firefighting water containing polar solvents showed a turbidity of less than 2 NTU and therefore did not seem to require electrocoagulation to remove suspended matter.

3.4 Study of some phenomena occurring during electrocoagulation of firefighting water

Electrocoagulation was successfully used to remove the turbidity from pilot firefighting water down to 2 NTU or less, with floc removal achieved either by filtration and flocculation. In this section, the purpose will be the study of parameters such as charge loading, solution composition or current density as well as the identification of factors influencing the minimal charge loading required for the pretreatment of firefighting waters.

3.4.1 Influence of electrocoagulation on surfactant concentrations

The evolution of surfactant concentrations in 3 L of pilot firefighting water 3 was measured by HPLC during electrocoagulation at 0.5 A (figure 3.15). The surfactants the most significantly affected by electrocoagulation were Disponil[®] SOS 842 and the fluorinated surfactant. Disponil[®] SOS 842 is an anionic alkylsulfate surfactant which could have electrostatic interactions with the cationic coagulant, and/or replace OH^- groups in the floc (section 3.4.2.2).

The fluorinated surfactant is an amphoteric fluorinated surfactant and Tegotens[®] AM VSF is an amphoteric hydrocarbon surfactant which was not as much affected by electrocoagulation as the fluorinated surfactant. The concentration of Simulsol[®] SL8, an alkyl glucoside surfactant, showed little variation.

The fluorinated surfactant seemed to have a higher affinity with the floc than Tegotens[®] AM VSF and Simulsol[®] SL8 did. These three surfactants, on the contrary to Disponil[®] SOS 842, do not have a net charge at pH 7–8. Therefore electrostatic interactions could not occur between these compounds and the floc. The remaining possible interactions could be Lewis AB and/or LW interactions and for the amphoteric compounds ion–dipole interactions. The fact that Simulsol SL8 was the less affected suggested that ion–dipole interactions were preponderant. The stronger affinity of the floc to the fluorinated surfactant could be explained by higher hydrophobic interactions. It should be noted that the surfactant the most likely subject to electron acceptor interaction via hydrogen–heteroatom bounds, *i.e.* Simulsol[®] SL8, was also the one having the weakest interactions with the electron acceptor aluminium coagulant.

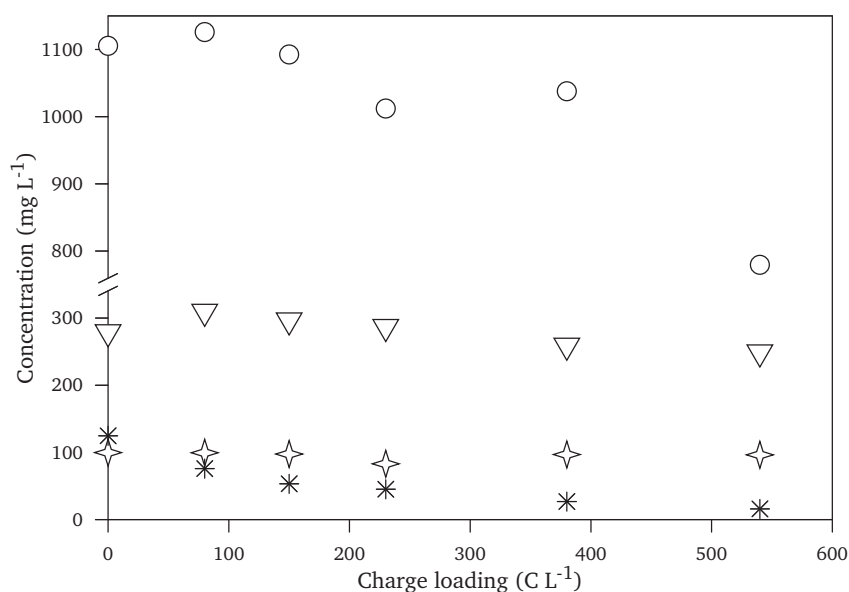


Figure 3.15: Surfactant concentrations versus charge loading during electrocoagulation of pilot firefighting water 4 at 0.5 A, in EC1 cell. ○: Disponil[®] SOS 842 (alkyl sulfate); ▽: Tegotens[®] AM VSF (alkyl propionate); ☆: Simulsol[®] SL8 (alkyl glucoside), *: fluorinated surfactant.

3.4.2 Influence of the current density and charge loading

3.4.2.1 Influence of the current density and charge loading on aluminium concentration

Electrocoagulation experiments of PFW3 in EC2 cell were done at various charge loading and current densities. Aluminium was quantified by atomic absorption in two types of $0.45\ \mu\text{m}$ PVDF syringe filtered samples: the bulk solution–dissolved aluminium, and the whole solution mixed with its floc acidified with HCl 37% to pH 1–total aluminium. The results are listed in table 3.6. Dissolved aluminium concentrations were estimated near $1\ \text{mg L}^{-1}$ independently of the charge loading as long as pH did not exceed 8. For high charge loadings, as pH were 8.2 and 10.3, dissolved aluminium concentrations were 2.6 (estimated value) and $29\ \text{mg L}^{-1}$ respectively. Aluminium current efficiencies were calculated on the basis of the following equation:

$$\eta_{CE} = \frac{3n_{Al}F}{it} \quad (3.6)$$

with n_{Al} the mole number of aluminium, η_{CE} the current efficiency, $F = 96,500\ \text{C mol}^{-1}$ the Faraday constant, i the current intensity in A and t the time of electrolysis in s . Aluminium current efficiencies all exceeded 100% in EC2 cell with both electrodes made of aluminium (table 3.3). This can be explained by the cathodic chemical dissolution of aluminium by OH^- (Eq. 3.3) produced by water reduction [121].

Table 3.6: Aluminium concentrations in bulk solution and whole acidified solutions after $0.45\ \mu\text{m}$ PVDF syringe filtration. *: Electrocoagulation of $1000\ \text{mL}$ of PFW3. Other experiments were done with $500\ \text{mL}$ of PFW1, ^e: estimated concentrations. Every experiments were done in EC2 cell.

Charge loading (C L^{-1})	j (mA cm^{-2})	Final pH	Dissolved aluminium (mg L^{-1})	Total aluminium (mg L^{-1})	Aluminium current efficiency
588	1.4	7.8	0.7^e	82	150%
588*	1.4	7.8	0.9^e	102	186%
1170	1.9	7	not detected	184	169%
1176	1.4	7.5	0.8^e	168	153%
1188	0.9	7.2	1.2^e	130	117%
2352	1.4	8.2	2.6^e	374	170%
3528	1.4	10.3	29	673	205%

3.4.2.2 Influence of the aluminium dose and pH on fluorinated surfactant concentration

Fluorinated surfactant concentrations of PFW3 solutions electrocoagulated in EC2 cells were measured by HPLC analysis after filtration on $0.45\ \mu\text{m}$ PVDF syringe filters (samples from table 3.6). Fluorinated surfactant removal seemed to be directly related to total charge loading as long as pH did not exceed 8 (figure 3.16). Above pH 9.5 the prominent species among total aluminium becomes $Al(OH)_4^-$ (figure 3.3), which is soluble and less efficient for electrocoagulation [125]. A too high pH seemed to be the reason why electrocoagulation was less efficient on fluorinated surfactant removal at $374\ \text{mg L}^{-1}$ of total aluminium than at $673\ \text{mg L}^{-1}$. The nearest value to the minimal charge loading of $600\ \text{C L}^{-1}$, was $588\ \text{C L}^{-1}$ for aluminium doses of 82 and $102\ \text{mg L}^{-1}$ gave fluorinated surfactant concentration near $40\ \text{mg L}^{-1}$.

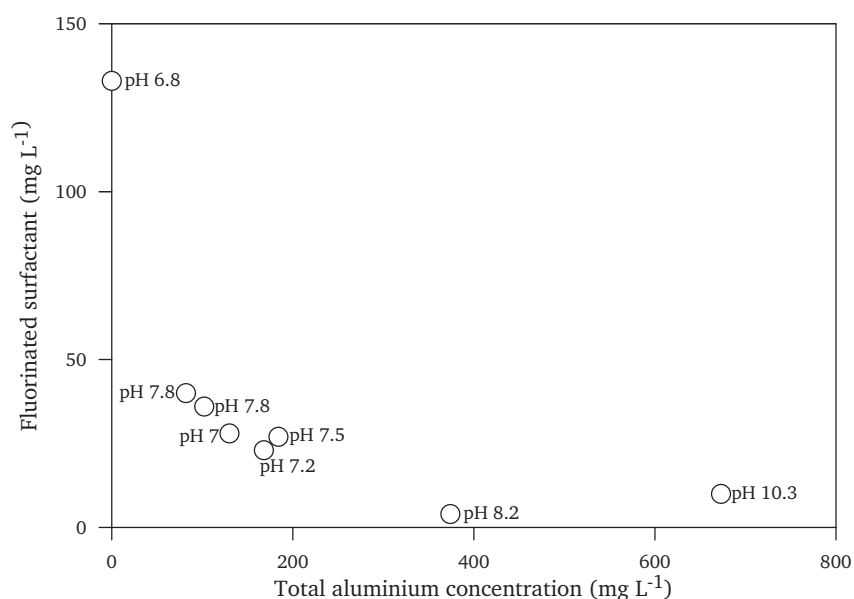


Figure 3.16: Fluorinated surfactant concentration and pH of the samples versus total aluminium concentration. Total aluminium concentrations were measured after acidic dissolution at pH 1 with acetic acid, 37%. Samples from electrocoagulation experiments of PFW3 in EC2 cell.

Fluoride ions have been reported to be removed in electrocoagulation by substitution with OH^- in the floc [112, 113]. In our case, pH increase (table 3.6) could be due to substitution of OH^- from the floc with anionic surfactant sodium octylsulfate (SOS). $3\ \text{L}$ of $1000\ \text{mg L}^{-1}$ sodium octylsulfate solution were electrocoagulated at $1\ \text{A}$ in EC1, pH was

measured and quantification of single SOS surfactant was possible by HPLC (figure 3.17). SOS concentration decreased quickly during the first 30 min whereas the bulk solution raised a plateau at pH 11 and after that, SOS concentration decreased far much slower. The pH increase seemed consistent with an increase in OH^- concentration in solution, due to its substitution in the floc by SOS. The pH plateau could be due to the $Al(OH)_3$ dissolution (Eq. 3.4, figure 3.3), acting as a buffer and reducing the concentration of available amorphous $Al(OH)_3$, leading to a decrease of SOS removal by electrocoagulation.

Deionized water could not be used directly for the blank experiment because its conductivity was too low to permit electrocoagulation. Instead 3 L of a $NaCl$ 0.5 g L^{-1} solution were used, and showed a pH peak at the beginning of the experiment, and then a plateau very near to the pH above which $Al(OH)_4^-$ becomes predominant (figure 3.3). The initial high pH could be due to substitution of OH^- in the floc by chloride anions and the pH plateau could result from the buffering effect of $Al(OH)_3$ dissolution. It could not be stated whether the pH increase in the blank experiment was due to chloride anions or was intrinsic to electrocoagulation. However, the anionic surfactant seemed responsible for the gap between the blank plateau near to pH 9.3 and the plateau of pH 11.5, meaning stronger substitution in the floc.

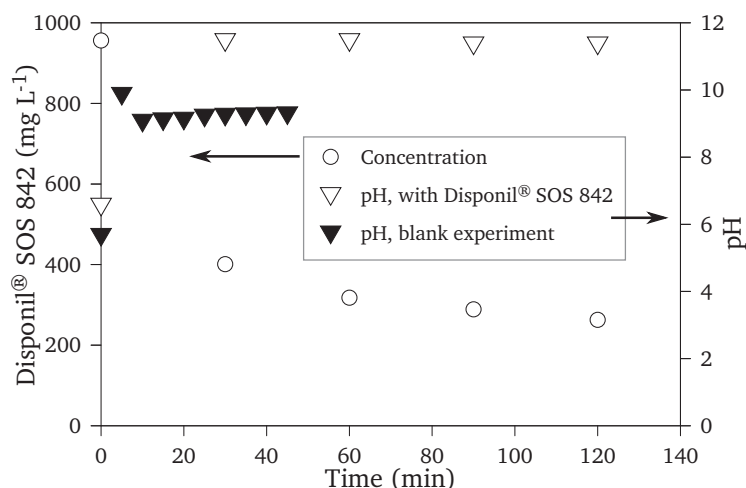


Figure 3.17: pH evolution during electrocoagulation of 3 L of: a Disponil® SOS 842 solution; a blank $NaCl$, 0.5 g L^{-1} solution, at 1 A in EC1 cell.

3.4.2.3 Influence of current density on fluorinated surfactant concentrations

It has been seen in section 3.3.1 that within the range of 0.9 to 2.5 mA cm^{-2} the current density did not seem to significantly affect the required charge loading for the pretreatment of firefighting waters. However, it was observed that in EC2 cell which both electrodes were made of aluminium, the current density within the previous range increased the current efficiency. The influence of the current density on the fluorinated surfactant concentrations in pilot firefighting waters was studied. Concentrations versus charge loading for different pilot firefighting waters and different intensities are plotted in figure 3.18. The concentration evolutions at 1 and 2 A were very close, even for pilot firefighting waters with different initial fluorinated surfactant concentrations. However, at 0.5 A , the decrease of concentration was markedly steeper for the same charge loading. At 20 A the residual fluorinated surfactant concentration was higher than every other concentrations observed during electrocoagulation of firefighting waters.

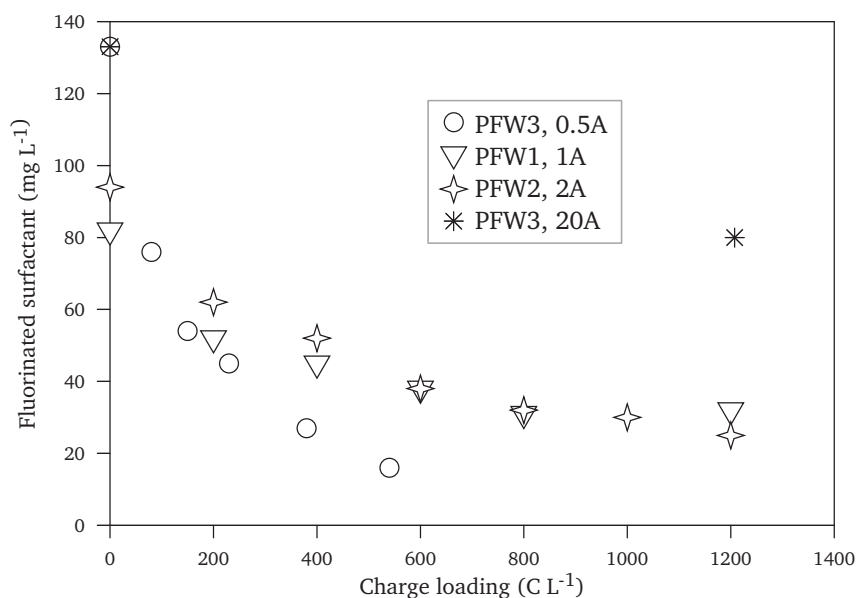


Figure 3.18: Fluorinated surfactant concentration in different pilot firefighting waters versus charge loading for different current densities during electrocoagulation experiments. ○: PFW3, 0.5 A; ▽: PFW1, 1 A; ☆: PFW2, 2 A; *: PFW3 20 A. Every experiments were done at the laboratory in EC1 cell, except * done by Serep.

The optimal charge loading for the pretreatment could not be investigated at Serep like it had been in the laboratory. The charge loading applied by Serep was twice the requirements identified in the laboratory on EC1 and EC2 cells, and successfully removed the unwanted

turbidity from pilot firefighting water 4. The high remaining concentration in fluorinated surfactant indicated that at high current densities, the removal of the fluorinated surfactant was decreased meanwhile the suspended matter was removed. Therefore, at high current densities, electrocoagulation might be less selective towards surfactants in pilot firefighting waters, and in Serep's Solvin[®] electrocoagulator the optimal charge loading for the removal of suspended matter could be improved.

3.4.3 Influence of the fluorinated surfactant concentration on the minimal charge loading

Experiments were done to compare the visual pretreatment time for model solutions containing different initial concentrations in fluorinated surfactant (table 3.7 and figure 3.19). These model solutions contained C401 activated carbon from Chemviron Carbon as a substitute to the suspended matter contained in pilot firefighting waters. Electrocoagulation experiments were done in EC1 cell, at 2 A, with 3 L of solution. Samples were taken for surfactant analysis at initial time and at the visual pretreatment time. The results are given in table 3.8.

Table 3.7: Composition in $mg\ L^{-1}$ of model solutions blank, A, B, C, D and E. Every solutions were prepared with tap water, except the blank which was prepared with deionized water containing $0.5\ g\ L^{-1}$ of NaCl.

Compounds	Blank	A	B	C	D	E
C401 activated carbon		700			500	100
Dowanol [®] DMP	0	3000			3012	3040
Disponil [®] SOS 842	0	580			970	962
Tegotens [®] AM VSF	0	220			368	373
Simulsol [®] SL8	0	180			238	241
Fluorinated surfactant	0	280	0	100	271	273

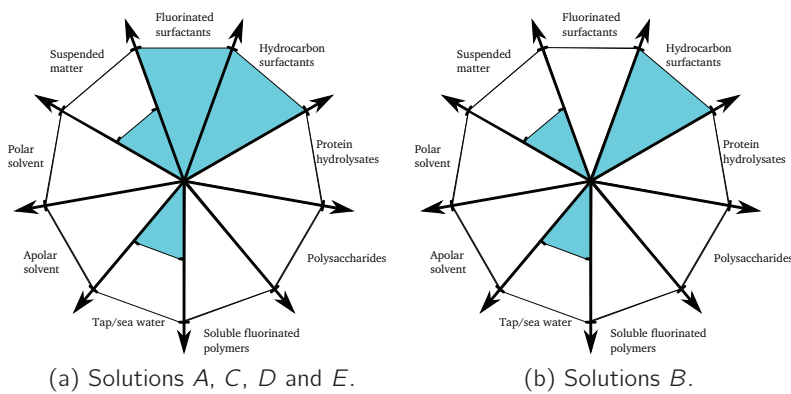


Figure 3.19: Sophistication of model solution A, B, C, D and E.

The necessary charge loading for activated carbon from the blank solution was higher than for solution A, but lower than for solutions B and C (table 3.8a). Regarding solutions A, B and C, the higher the fluorinated surfactant concentration, the lower the necessary charge loading. High fluorinated surfactant concentration of solution A seemed to favor electrocoagulation of activated carbon, whereas lower and especially zero concentrations seemed to hinder it. Moreover, the decrease of hydrocarbon surfactant concentration was by far higher during the electrocoagulation of solution B. This could be due to the longer time of electrocoagulation, but also to the absence of fluorinated surfactant. In these conditions of electrocoagulation, the affinity of the fluorinated surfactant with the floc seemed to be higher than the affinity of the floc with other surfactants. This was confirmed during the electrocoagulation of solutions D and E, where concentrations surfactants other than the fluorinated did not change that much (table 3.8b). It could be noticed that in solution B, the missing Disponil[®] SOS 842 was higher than for solutions A and C. It seemed that in absence of fluorinated surfactant, the adsorption of other surfactants on the activated carbon increased.

Table 3.8: Initial and final concentrations in $mg L^{-1}$ and visual pretreatment times during electrocoagulation of 3 L of model solutions in EC1 cell.

(a) Blank, solutions A, B and C at 2 A

	Blank	A		B		C	
Compounds	–	Initial	Final	Initial	Final	Initial	Final
C401 activated carbon	700	700	–	700	–	700	–
Disponil [®] SOS 842	0	536	488	478	133	522	501
Tegotens [®] AM VSF	0	215	210	224	28	198	177
Simulsol [®] SL8	0	131	89	111	28	92	85
Fluorinated surfactant	0	129	46	0	0	29	25
Visual pretreatment time	22 min	15 min		50 min		30 min	
Charge loading ($C L^{-1}$)	880	600		2,000		1,200	

(b) Solutions D and E at 1 A

	D		E	
Compounds	Initial	Final	Initial	Final
C401 activated carbon	500	–	100	–
Disponil [®] SOS 842	876	874	858	917
Tegotens [®] AM VSF	262	225	337	254
Simulsol [®] SL8	170	160	237	211
Fluorinated surfactant	180	66	248	73
Visual pretreatment time	30 min		49 min	
Charge loading ($C L^{-1}$)	600		980	

Model solutions D and E were electrocoagulated at 1 A in EC1 cell to measure the influence of the amount of artificial suspended matter. The results showed that the higher activated carbon content, the lower the necessary charge loading (table 3.8b). These results could be explained on the basis of initial fluorinated surfactant concentrations. In model solution D the initial concentration of free fluorinated surfactant after syringe filtration was $180 mg L^{-1}$, whereas it was $249 mg L^{-1}$ in solution E. The activated carbon played the role of adsorbent, decreasing the concentration of surfactants, including the fluorinated surfactant, in bulk solution. Here, the higher the free fluorinated surfactant concentration, the higher the necessary charge loading.

The initial concentration of free fluorinated surfactant seemed to play a crucial role for the electrocoagulation of activated carbon in all the previous model solutions. Initial concentrations of 0 and $29 mg L^{-1}$ required higher charge loading than for an initial concentration of $129 mg L^{-1}$, whereas for higher concentrations of free fluorinated surfactant the higher the initial concentration, the higher the necessary charge loading. The optimal initial fluorinated

surfactant concentration for a minimal pretreatment time and charge loading seemed to be somewhere between 30 and 130 mg L^{-1} , an interval in which one can find the cmc of this surfactant near 50 mg L^{-1} .

Fluorinated surfactants have much lower cmcs than hydrocarbon ones. Surface aggregation, when it occurs, begins at the critical aggregation concentration, which is lower than the cmc. Assuming that the fluorinated surfactant forms surface aggregates on activated carbon at concentration $> 30 \text{ mg L}^{-1}$ could provide an explanation to the previous observations. Considering the apolar nature of activated carbon, the polar heads are expected to be oriented towards water. The polar head of the fluorinated surfactant can interact with the floc *via* its electron donicity, and the density of aggregation of fluorinated surfactant on the floc should be higher than that of other surfactants given its cmc and possible cac.

The proposed mechanism occurring in the previous experiments is the following: at high concentration the fluorinated surfactant, under the form of free monomers, and more probably micelles, compete with the suspended matter for the removal by the floc. At high concentrations, the suspended matter is probably covered to the maximum by fluorinated surfactants aggregates, whereas at lower concentrations, this coverage could be partial. Moreover, at low fluorinated concentration, the adsorption of anionic surfactant was higher, which could result in electrostatic stabilization of the suspended matter.

Considering the blank experiment, the lower necessary charge loading for solution A could be due to higher affinity of the suspended matter covered by fluorinated surfactants aggregates versus: raw activated carbon (blank), partially covered suspended matter (C) and surfactant solution without fluorinated surfactant (B). The required charge loadings for these solutions were in the order: $A < \text{blank} < C < B$. For higher fluorinated surfactant concentrations, the higher required charge loading could be due to the competition between fluorinated surfactant micelles and fluorinated surfactant covered suspended matter. Therefore, considering the removal of hydrophobic suspended matter in these model firefighting waters, a minima of charge loading is expected for concentrations permitting maximum adsorption of the fluorinated surfactant on the suspended matter and minimal free fluorinated surfactant concentration in the bulk.

Conclusion

The study of some of the underlying phenomenon taking place during the electrocoagulation of pilot and model firefighting waters confirmed that the process is rather complex. The main parameter, the aluminium dose, is not only related to the charge loading, but also on the pH of the solution. The higher the pH, the higher the current efficiency. During pilot firefighting water electrocoagulation, the pH was shown to increase, and at too high pH, the efficiency of the coagulant decreases. This stressed the importance of pH in electrocoagulation.

The current density was shown to influence the resulting fluorinated surfactant concentration: the higher the current density, the higher the resulting fluorinated surfactant concentration. However, in electrocoagulation experiments in the laboratory, the current density did not seem to be related to the charge loading required for the pretreatment. On the contrary, initial free fluorinated surfactant had a direct influence on this charge loading. It seemed that the closer the free fluorinated surfactant concentration to the cmc, the minimal the charge loading required for an efficient electrocoagulation of the suspended matter. However, the higher resulting fluorinated surfactant concentration measured after the high current test in industrial pilot suggested that, at high current density, the affinity of the fluorinated surfactant for the floc decreased. This was probably due to the slow adsorption kinetics of the fluorinated surfactant, and should result higher selectivity of the floc for suspended matter. Thus high current densities should result in lower required charge loading for electrocoagulation of firefighting water, but also to a higher residual concentration of fluorinated surfactant.

Deeper study of the influence of the fluorinated surfactant concentration could not be done in the scope of this thesis. Further work on this subject ought to be done in consideration of floc–surfactant and floc–suspended matter interaction dynamics, as well as surface aggregates. Elements of explanations about the trends of the affinities of surfactants with the floc could be proposed on the basis of molecular interactions.

Conclusion on the pretreatment by electrocoagulation and floc removal

In this chapter, the electrocoagulation process was applied to pilot, model and industrial firefighting waters. Considering the design of the mobile unit, an optimal charge loading of 600 C L^{-1} , or an aluminium dose of at least 55.9 mg L^{-1} , was found for pilot firefighting water in the laboratory. This optimal charge could not be directly confirmed on an industrial electrocoagulator for practical reasons, however this process was found to remove efficiently the unwanted turbidity from pilot firefighting waters. After electrocoagulation, the floc could either be removed by filtration and flocculation. The application of electrocoagulation to real industrial firefighting waters containing protein hydrolysates was found to be efficient on the water from the extinction of an apolar solvent fire at the cost of a higher charge loading. For the water resulting from the extinction of polar solvent fire, electrocoagulation seemed useless because these firefighting waters showed little turbidity. However, the presence of polar solvent such as acetone is of great concern for a further treatment with organic membranes.

The study of the parameters influencing the pretreatment of pilot firefighting waters showed that surfactant concentrations, especially fluorinated surfactant concentration, were determinant for the minimal charge loading. A minimum excess of fluorinated surfactant, or maximal current density seemed to be necessary to enhance the suspended matter removal. But higher initial concentrations resulted in higher required charge loadings. The phenomenon behind these observations were too complex to be demonstrated in the scope of this thesis. The fluorinated surfactant seemed to help the electrocoagulation as long as its concentration was high enough to adsorb on, and saturate the suspended matter, and at the same time, as long as its excess concentration was as low as possible. From an industrial point of view, the fact that the current density was shown to influence the residual fluorinated surfactant concentration (the higher the current density, the lower the residual concentration) indicated that at industrial scale electrocoagulation should be done at high current density to minimize aluminium consumption.

Chapter 4

Treatment of pretreated firefighting water by reverse osmosis

Introduction

Membrane processes, which have been briefly introduced in Chapter 2, will be more extensively described here with a particular focus on reverse osmosis and nanofiltration. Before the experimental study of the reverse osmosis of real and model pretreated firefighting waters in different devices, the following bibliographic study will try to relate the rejection rates and flux decline to the membrane and solute properties. Then, the membrane–surfactant system will be described, as well as the expected phenomena able to take place during the reverse osmosis of real and model pretreated firefighting waters. Reverse osmosis of these firefighting waters will be experimentally studied in several steps with several reverse osmosis pilots of increasing membrane area. Thanks to the information brought by the two following sections, some interesting experimental phenomena will finally be discussed.

4.1 Description and theory of membrane processes

In this section, the differences between membrane processes will be recalled. Membrane properties will be presented to prepare description of rejection and flux decline in membrane processes.

4.1.1 Membrane processes properties

4.1.1.1 The different kinds of membrane processes

In membrane processes, specific selective membranes are used to perform separations under a driving force. The scope of this work is limited to membrane processes using the pressure gradient across the membrane (the transmembrane pressure) as a driving force. The differences between membrane processes come from the different natures of their corresponding membranes and the separation operations they permit.

The four pressure driven membrane processes are microfiltration (MF), ultrafiltration (UF), nanofiltration (NF) and reverse osmosis (RO). Their separation possibilities are illustrated in figure 4.1. Microfiltration retains particles by means of sieving. Microfiltration membranes have pore size ranging from 0.1 to 10 μm and the transmembrane pressure ranges from 0.1 to 2 bar . The permeability in microfiltration is generally high ($> 50 L h^{-1} m^{-2} bar^{-1}$) and this process is frequently used as a pretreatment step.

Ultrafiltration (UF) retains both particles and macromolecules by the same sieving mechanism as MF. UF membranes are characterized by their molecular weight cut-off (MWCO) more than by their pore size. Components with a molecular mass above the cut-off have a high retention, whereas components with a molecular mass below the cut-off are retained only partially. The cut-off for UF lies typically between a few 1,000 and 100,000 Da , which corresponds with pore sizes between a few nanometer and 0.1 μm . Permeabilities between 10 and 50 $L h^{-1} m^{-2} bar^{-1}$ are obtained with pressures between 1 and 5 bar .

Reverse osmosis (RO) is able to retain small organic molecules and ions from a solution. This process uses dense membranes which have a high hydrodynamic resistance, hence the obtained permeabilities are low ($0.05 - 1.4 L h^{-1} m^{-2} bar^{-1}$) and pressure gradients are high (10 – 100 bar). Instead of sieving, separation is obtained due to sorption and diffusion through the membrane.

Nanofiltration (NF) is situated between UF and RO. Nanofiltration membranes are basically modified RO membranes having high water fluxes. NF membranes require much lower pressures (5 – 20 bar) than RO, leading to significant energy savings. Moreover, NF combines a high permeability ($1.5 - 15 L h^{-1} m^{-2} bar^{-1}$) with a high retention of dissolved organic molecules with a molecular mass above 200 Da . The cut-off of NF is situated be-

tween 150 and 1,000 *Da*. Due to charge interactions with the membrane, multivalent ions are also well retained.

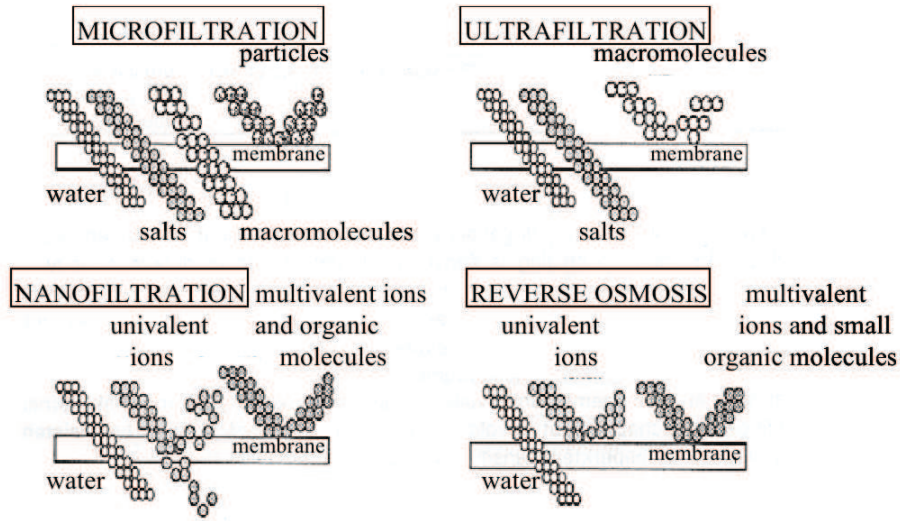


Figure 4.1: Schematic representation of membrane processes and of the kind of separation performed [128]

4.1.1.2 Description of filtration operations

Several parameters are used to describe filtration operations, which can be batch or continuous:

- The volume reduction ratio VRR and rejection rate R (introduced in Chapter 2):

$$VRR = \frac{V_0}{V_R} = \frac{Q_0}{Q_R} \quad (4.1)$$

$$R = 1 - \frac{C_P}{C_R} \quad (4.2)$$

with V_0 the initial feed volume and V_R the final retentate volume for batch operations, or Q_0 the feed flow and Q_R the retentate flow for continuous operations for VRR ; with C_P and C_R the permeate and retentate concentrations respectively for R .

- The concentration factor CF :

$$CF = \frac{C_R}{C_0} \quad (4.3)$$

with C_R the retentate concentration and C_0 the initial feed concentration.

- The extraction factor EF :

$$EF = \frac{V_P}{V_0} = \frac{Q_P}{Q_0} \quad (4.4)$$

with V_0 the initial feed volume and V_P the permeate volume for batch operations, or Q_0 the feed flow and Q_P the permeate flow for continuous operations.

Batchwise filtration Assuming volume conservation:

$$V_0 = V_R + V_P \quad (4.5)$$

$$-dV_R = dV_P \quad (4.6)$$

the mass balance of the operation is:

$$V_0 C_0 = V_R C_R + V_P \overline{C_P} \quad (4.7)$$

During the time dt , a permeate fraction dV_P is extracted and its concentration remains almost constant, but this results in a variation in volume and concentration for the retentate side.

$$C_P dV_P = -d(C_R V_R) \quad (4.8)$$

The concentration factor CF can be determined as function of the volume reduction ratio VRR . After the previous equations we have:

$$C_P dV_P = -C_R dV_R - V_R dC_R \quad (4.9)$$

$$-C_P dV_R = -C_R dV_R - V_R dC_R \quad (4.10)$$

$$\frac{1}{V_R} dV_R = -\frac{1}{R C_R} dC_R \quad (4.11)$$

Integrating this equation between initial ($V_R = V_0$, $C_R = C_0$) and final (V_R , C_R) states yields:

$$\int_{V_0}^{V_R} \frac{1}{V_R} dV_R = \int_{C_0}^{C_R} -\frac{1}{R C_R} dC_R \quad (4.12)$$

$$\ln \frac{V_R}{V_0} = \frac{1}{R} \ln \frac{C_0}{C_R} \quad (4.13)$$

$$CF = \frac{C_R}{C_0} = FRV^R \quad (4.14)$$

The filtration time necessary to reach a given VRR on an installation of known membrane area can be calculated, as well as the membrane area required to reach a given VRR in a given filtration time. The filtered volume during the time dt on a membrane of area A is:

$$dV_P = -dV_R = J A dt \quad (4.15)$$

The permeate flux depends on the increasing retentate concentration, therefore on the VRR . If the variation of the flux with VRR is known:

$$dt = \frac{-dV_R}{J A} = \frac{V_0}{J A VRR^2} dVRR \quad (4.16)$$

$$t = \int_{VRR=1}^{VRR} \frac{V_0}{J A VRR^2} dVRR \quad (4.17)$$

which also gives:

$$A = \frac{1}{t} \int_{FRV=1}^{FRV} \frac{V_0}{J VRR^2} dVRR \quad (4.18)$$

Continuous filtration In continuous mode, flows and concentrations are constants, conservations of volumes and masses give:

$$Q_0 = Q_R + Q_P \quad (4.19)$$

$$Q_0 C_0 = Q_R C_R + Q_P C_P \quad (4.20)$$

The permeate concentration C_P can be linked to the retentate and feed concentration on the basis of the previous equations, and the definitions of R and EF (equations 4.2 and 4.4):

$$C_R = \frac{Q_0 C_0 - Q_P C_P}{Q_R} = \frac{Q_0 C_0 - Q_P C_R(1 - R)}{Q_R} \quad (4.21)$$

$$C_R \left(1 + \frac{Q_P}{Q_R} (1 - R) \right) = \frac{Q_0 C_0}{Q_R} \quad (4.22)$$

$$C_R = C_0 \frac{Q_0}{Q_R + Q_P (1 - R)} = C_0 \frac{Q_0}{Q_0 - R Q_P} \quad (4.23)$$

$$C_R = \frac{C_0}{1 - EF R} \quad (4.24)$$

$$C_P = \frac{(1 - R) C_0}{1 - EF R} \quad (4.25)$$

The area can be calculated on the basis of the desired permeate flow the measured at the corresponding C_R concentration:

$$A = \frac{Q_P}{J C_R} \quad (4.26)$$

4.1.2 Membrane properties

Considering the nature of the membrane material there are two kinds of membranes: inorganic and organic membranes. Inorganic membranes are more expensive, the contrary to organic membranes they have a higher tolerance to heat and chemicals. Membranes can be symmetric, asymmetric or composite. Symmetric and asymmetric membranes are made of the same material whereas composite membranes are combination of different layers of different materials. The permeability of the membrane depends on the membrane thickness. For higher permeabilities, thinner membranes are preferred, therefore membranes for

nanofiltration and reverse osmosis show asymmetric structures.

On the contrary to symmetric membranes, the porosity of asymmetric membranes varies along the membrane thickness. The top layer is very thin ($thickness \leq 1 \mu m$) compared to the rest of the membrane, it has the lowest porosity and performs the separation. The porous layer, the larger part of the membrane ($50\text{--}150 \mu m$), supports the top layer and does not influence the selectivity or the permeability. The two main materials for the preparation of asymmetric membranes are cellulose esters or aromatic polyamide [129]. In composite or thin film composite (TFC) membranes, the layers are made of different materials. The active layer ($0.1\text{--}0.2 \mu m$) is made of aromatic polyamide, the support layer ($\approx 50 \mu m$) is made of polysulfone and physical resistance is brought by the base fabric layer (figure 4.2).

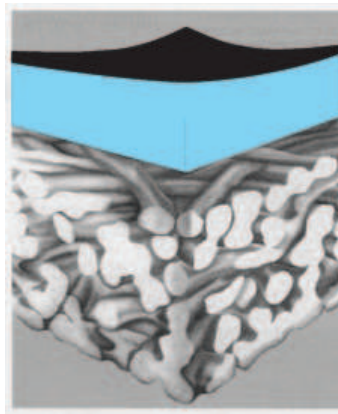


Figure 4.2: Schematic representation of a composite membrane [130]

Membranes are packed in membrane modules of different geometries: plate-and-frame module, spiral-wound module, tubular module and hollow fiber module. Separation occurs in membrane processes according to the membrane properties. The most obvious property is probably the pore size of the membrane, from which results the sieving effect of membranes. For UF and NF membranes, the rejection characteristics can be illustrated by the molecular weight cut-off in $g\ mol^{-1}$ or Da , which is the molecular mass of a solute with 90 % retention. MWCO is generally assessed by rejection measurements of polyethylene glycols of molar weight from 150 to 100,000 $g\ mol^{-1}$. This concept is based on the observation that molecules get larger as their mass increases. If the molecule is larger, then steric hindrance and sieving increase, and the molecule will be more rejected than a smaller one. However, MWCO is not an absolute parameter as it depends strongly on the kind of molecule observed

and on the experimental conditions. In addition, for NF membranes, MWCO can be poorly related to rejection [131], it is a rough estimate of the sieving effect.

For NF and RO membrane, a better indicator of the rejection properties of the membrane is the desalting degree, or the salt rejection (for $NaCl$, $MgSO_4$ or Na_2SO_4 , 500–2,000 $mg\ L^{-1}$, depending on the membrane). The desalting degree was found to be directly related to the retention of alcohols, polysaccharides and pesticides [131]. The porosity, or pore density of the membrane also gives an interesting insight on the rejection properties, as well as the membrane roughness. Roughness is quantified by the vertical deviations from an ideal planar surface. Roughness measurements are strongly dependent on the device used to obtain the data and how this data is processed to obtain the amplitude parameters. Two common amplitude parameters are R_a (Eq. 4.27), the arithmetic average of the absolute values, and R_{RMS} (Eq. 4.28) the root mean squared average of the absolute values.

$$R_a = \frac{1}{n} \sum_{i=1}^n |y_i| \quad (4.27)$$

$$R_{RMS} = \sqrt{\frac{1}{n} \sum_{i=1}^n y_i^2} \quad (4.28)$$

Roughness was found related to the water permeability, with a roughness increase increasing permeability [132], which could be due to the increase of specific membrane area. Hydrodynamics and colloidal fouling were found to depend on membrane morphology, which is somehow related to the environment of the membrane. For instance, evolution of roughness was observed during membrane soaking in water [133]. Membrane roughness can be measured by atomic force microscopy (AFM), an imagery technique in which a surface is probed by the measurement of the repulsive or attractive forces applied to a cantilever approaching the interface.

According to their chemistry, nanofiltration and reverse osmosis membranes can acquire electric charges due to dissociation of functional groups or adsorption of anions when in contact with a solution. Isoelectric point and membrane charge, as function of the pH , can be determined by means of streaming potential measurements [129]. Membranes can show different hydrophilicity depending on the contact angles measured with water, which gives

a rough indication of the affinity of the membrane material with water. More sophisticated contact angle measurements can be performed with probe liquids [134, 135].

4.1.3 Separation mechanisms

Separation mechanisms in membrane processes result from the interactions of the membrane with solution containing a solvent and solutes. Based on both membrane and molecular properties, Bellona extensively reviewed the factors governing the rejection of organic molecules by nanofiltration and reverse osmosis membranes, with a focus on organic micropollutants [131]. Sieving appears to be one of the main factors behind solute rejection, however the smaller pore size does not necessarily mean highest rejection of low molecular weight uncharged organic solutes. Another important factor is electrostatic repulsion between membranes and solutes of the same charge. If charges are opposite, a solute can as well be retained via the retention of its counter ion for reasons of electroneutrality in the solution.

The most complex rejection factors depend on molecular interaction between the solute and the membrane surface, which are also dependent on the membrane morphology. High pressure membranes are considered hydrophobic and can therefore interact with apolar molecules. Indication on the apolar character of a molecule can be given by its octanol/water partition coefficient (K_{ow}). Highly apolar molecules can adsorb on the membrane, giving high apparent retention rates. However, the membrane may reach saturation and the solute may leak, leading to lower equilibrium retention rates. Retention rates may also decrease with increasing concentration in the retentate. There, the increased concentration gradient results in higher diffusion of the solute through the membrane.

The polarity of the solute also plays a significant role. For instance, hydrogen bonding and acidity properties in the solutes decrease retention rates. Hydrogen bonding is involved in permeation of water through the membrane material, and this kind of compounds may compete with water and not be well retained. Moreover, the solution matrix may as well interact with the membrane and modify the retention rates obtained for the same solutes in deionized water. Rejection mechanisms and properties involved in the solute and the membrane are summed up in table 4.1. Rejection can result in a combination of these mechanisms, as the different solute and membrane properties may be simultaneously involved.

Table 4.1: Summary of the rejection mechanisms for reverse osmosis and nanofiltration, and their origin in solute and membrane properties [131]

Rejection mechanisms	Solute properties	Membrane properties
Sieving effect	Molecular weight, size and geometry	Membrane cut-off, pore size, porosity
Electrostatic repulsion	Solute charge (as function of pK_a and pH)	Membrane charge (as function of pK_a and pH)
Diffusion, partition and sorption hindering	Partition coefficient (K_{ow}) and diffusion coefficient (D) in the membrane material, solute polarity	Hydrophilicity, surface morphology, membrane material and chemical functions

4.1.4 Flux decline and membrane fouling

The design of membrane processes units is strongly dependent on the expected permeate flow. Therefore the flux of water passing through the membrane is a parameter that should be maximized to reduce the investment cost. Unfortunately, one of the main drawback of membrane processes is flux decline, which is mainly due to concentration polarization and fouling [129]. Concentration polarization is the increase in concentration occurring in tangential filtration due to rejection of solute (figure 4.3a). In reverse osmosis, nanofiltration and ultrafiltration, this increase of concentration results in an increase in osmotic pressure and therefore in a decrease of effective transmembrane pressure, which leads to flux decline. The flux can also decrease because of concentration polarization when the concentration at the membrane reaches the gel concentration, which enables the formation of a gel layer (figure 4.3b).

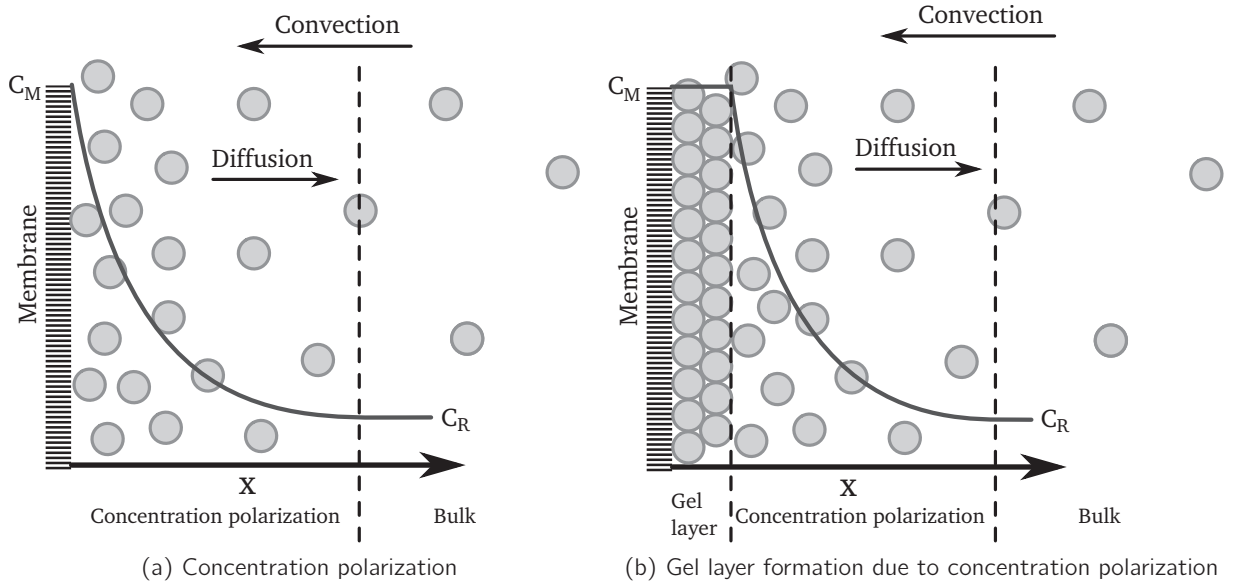


Figure 4.3: Concentration polarization in membrane processes. C_R : concentration of the solute in the retentate, C_M : concentration at the membrane.

The resistance-in-series model Fouling can result from several mechanisms such as pore blocking, adsorption, cake or gel layer formation. Flux decline is strongly dependent on the feed solution and on the membranes. The resistance-in-series model is commonly employed to describe flux decline [129]. In this model the flux J is function of the driving force ΔP , the viscosity η and the total resistance R_{tot} :

or

$$J = \frac{\Delta P}{\eta R_{tot}} \quad (4.29)$$

R_{tot} includes the intrinsic resistance of the membrane to pure water, R_m and every additional resistances: R_{cp} for concentration polarization, R_a for adsorption, R_g for a gel layer, R_c for a cake and R_p for pore blocking. Details about these resistances and their causes are summed-up in table 4.2. R_{tot} is the sum of all resistances:

$$R_{tot} = R_m + R_{cp} + R_a + R_g + R_c + R_p \quad (4.30)$$

Table 4.2: Various resistances to mass transfer and their causes in membrane processes

Resistance	Cause
R_m	Intrinsic membrane resistance to water, resulting from resistance to mass transfer across the membrane
R_{cp}	Concentration polarization
R_a	Adsorption of solute in the membrane pores, resulting in decrease of pore size and/or surface modification due to adsorption on the membrane surface
R_g	Formation of a gel layer when the solute reaches its gel formation concentration consequently to concentration polarization
R_c	Formation of a cake of particles or colloids retained by the membrane and accumulating at its surface
R_p	Pore blocking by particles or compounds of similar size to the pores, preventing further permeation through blocked pores

As flux decline strongly depends on interaction between the compounds in feed solution and the membrane, fouling may be minimized by appropriate pretreatment, and choice of membrane material having minimal or repulsive interactions with the solutes of interest. Concentration polarization and deposit formation at the membrane surface can be decreased by applying turbulent *via* high cross-flow velocity. Flux decline can as well be reduced thanks to appropriate periodic cleaning.

The convection–diffusion model In the bulk solution, the solute concentration is C_R . The concentration polarization occurs in the concentration polarization layer, or diffusion layer. At the membrane, the solute concentration is C_M . The concentration gradient taking place in the diffusion layer gives rise to a diffusive flux of the compound from the membrane to the bulk, which oppose to the convective flux towards the membrane. On the permeate side, the solute concentration is C_P , and the mass balance for this rejected solute between the membrane and the distance x in the diffusion layer towards the bulk gives:

$$-J C_x + D \frac{dC_x}{dx} = -J C_P \quad (4.31)$$

with J , the flux of solution through the membrane in $m^3 s^{-1} m^{-2}$, C_x the concentration of the solute at the distance x of the membrane in the retentate side in $mol m^{-3}$, C_P the concentration of the solute in the permeate in $mol m^{-3}$ and D the diffusion coefficient of the solute in the concentration polarization layer in $m^2 s^{-1}$. Equation 4.31 gives:

$$Jdx = D \frac{dC_x}{C_x - C_P} \quad (4.32)$$

By integration over the width δ , in m , of the diffusion layer we obtain:

$$J \int_0^\delta dx = D \int_{C_M}^{C_0} \frac{dC_x}{C_x - C_P} \quad (4.33)$$

$$J = \frac{D}{\delta} \ln \frac{C_M - C_P}{C_R - C_P} \quad (4.34)$$

If the membrane is perfectly selective, the rejection is 100% and $C_P = 0$, then:

$$J = \frac{D}{\delta} \ln \frac{C_M}{C_R} \quad (4.35)$$

The permeate flux through the membrane depends on the rejected compound *via* its diffusion coefficient and concentration at the membrane. It also depends on hydrodynamic conditions, because an increase in cross-flow velocity results in a decrease of the thickness δ of the diffusion layer. Finally, C_M is dependent on the pressure. The resistance-in-series model was found more suitable in the course of this work.

4.2 Description of the membrane–surfactant system

The parameters influencing rejection and flux decline summed-up in the previous section will here be applied to the membrane–surfactant system. These notion will help to give an *a priori* insight of what can be expected during the reverse osmosis of pretreated firefighting waters.

4.2.1 Membrane processes and surfactants

Surfactants are amphiphilic molecules presenting an apolar tail and a hydrophilic head. Considering intermolecular forces in water, surfactants can interact *via*:

- Hydrophobic interactions, with apolar tails being excluded from water by apolar Lifshitz–Van der Waals (LW) interactions and lack of polar interaction;

- Electrostatic interactions, with charged entities in case of ionic surfactants;
- Polar Lewis acid–base interactions (AB), if the molecule contains electron donor and/or electro acceptor groups as well as acidic protons or basic groups;

Most of reverse osmosis or nanofiltration membranes have active layers made of aromatic thin film polyamide or cellulose esters. The intermolecular forces able to arise are basically of the same kind as for surfactants:

- Hydrophobic LW interactions, with apolar regions of the polymer;
- Electrostatic interactions, with charged entities if the membrane is charged;
- Polar Lewis acid–base interactions (AB);

Zeta potential of various thin film polyacetate and cellulose reverse osmosis and nanofiltration membranes were measured by means of streaming potential by Elimelech *et al* [136]. Membranes were shown to be amphoteric, positively charged at low *pH* and negatively charged at high *pH*. The isoelectric points of every membranes in *NaCl* $0.01 \text{ mol } L^{-1}$ was comprised between *pH* 3 and *pH* ≈ 5 , meaning that most of nanofiltration and reverse osmosis membranes are virtually negatively charged at *pH* > 5 –6. However, the resulting membrane charge also depends strongly on the solution chemistry and the adsorption of charged compounds that can modify the membrane surface charge [136].

Regardless of the surface chemistry of membranes, a rough insight of non-electrostatic membrane properties can be obtained from contact angle measurements. Solid surface tensions of polyamide [135, 137] and cellulose acetate membranes [134, 138] have been measured, showing an apolar surface tension γ^{LW} near to 32 – $45 \text{ mN } m^{-1}$ for both membranes. The polar components of the solid surface tension were different, but the electron donor component, γ^- , seemed predominant for most of membranes (table 4.3). However, contact angle measurements on dried polar solids having a strong γ_S^- component often results in low observed γ_S^+ because the electron acceptor component is “neutralized” by the excess of electron donor component [127]. Therefore these results indicate that substantial apolar interactions can be expected from these kind of membranes, as well as polar interactions preferably with electron acceptor molecules, but not exclusively. The expected interactions between surfactants and membranes are listed in table 4.4.

Table 4.3: Solid surface tension of several polyamide and cellulose membranes, in $mN m^{-1}$, determined by contact angle measurements

Membrane material	γ_S^{LW}	γ_S^+	γ_S^-	Reference
Aromatic polyamide (XLE)	35	≈ 1	10–20	[135]
Cellulose acetate	39.4	1.17	20.48	[134]
Piperazine (HL)	44.7	1	26.5	[137]
Piperazine (NF270)	43.3	2.4	26	[137]
m-phenylene diamine (NF 90)	36.6	0.7	9.3	[137]
m-phenylene diamine (ESPA 4)	35.3	3.7	2.3	[137]
Thin film composite polyamide (FT-30)	32.2	1.82	28.68	[138]
Cellulose acetate (CD)	38.1	0.01	37.43	[138]
Cellulose acetate (CE)	37.5	1.69	28.51	[138]

Table 4.4: Expected interactions of various kind of surfactants with nanofiltration and reverse osmosis membranes in water at neutral pH . Each surfactant is expected to show hydrophobic interactions, either *via* apolar (LW) interactions between the membrane polymer and the hydrophobic tail, and *via* the exclusion of hydrophobic entities due to polar (AB) cohesion of water.

Surfactants	Electrostatic interactions	Polar AB interactions
Anionic surfac-tants	Repulsive electrostatic interaction due to like-charged polar head and membrane	Possible interactions with eventual acidic hydrogen on the membrane
Cationic surfac-tants	Attractive electrostatic interaction due to oppositely charged polar head and membrane	
Non ionic surfac-tants		Electron acceptor polar heads: interactions with electron donor groups of the membrane, electron donor polar heads: interactions with acidic hydrogens, in a lesser extend due to the electron donor character of the membranes
Zwitterionic surfac-tants	According to the charge of the polar head depending on pH , ion–dipole interaction	According to the electron donor and/or electron acceptor characters of the polar head
Fluorinated surfac-tants	According to the polar head	According to the polar head

After sections 4.1.3 and 4.1.4, one can conclude that maximal surfactant rejection and minimal flux decline can both be achieved by minimizing the interactions between the surfactants and the membranes. The minimization of surfactant–membrane interaction was found to be related to the membrane’s hydrophobicity for anionic [139] and non ionic POE surfactants [140]. Negative membrane charges increase anionic surfactant rejection [139].

Boussu described the filtration of anionic, cationic and non ionic surfactants with various nanofiltration membranes [128]. The main factor governing flux decline was adsorption of surfactants and pore blocking when the adequateness between pore size and surfactant size permitted it. The non ionic surfactant was best retained and caused least fouling with the most hydrophilic membranes with lowest cut-off. For the anionic surfactant, electrostatic repulsion increased the rejection and lowered the flux decline for each membrane compared to the non ionic surfactant. The cationic surfactant showed poor retention compared to the other surfactants with membranes of too high cut-off. Fouling by cationic surfactant was due to hydrophobic and attractive electrostatic interactions. No membrane–surfactant studies taking into account solid surface tension components and related surfactant properties were found in literature during this thesis, despite this approach was found relevant during the study of biofouling [137] or membrane fouling by colloids [138].

4.2.2 A priori description of the membrane/pretreated firefighting water system

As seen in the previous section, one can expect from most of reverse osmosis and nanofiltration membranes electrostatic interaction due to the membrane surface charge. Considering the surfactant mixture contained in pilot firefighting waters (see figure 1.21 and table 1.11), the expected electrostatic interactions with the membrane in water are the following: electrostatic repulsion of the anionic surfactant; ion–dipole interaction with the amphoteric surfactants (hydrocarbon and fluorinated).

Given that membranes appeared to be strongly electron donor, they may interact with surfactants having electron acceptor polar heads, *i.e.* every compounds except the anionic surfactant. Membranes also showed an electron acceptor character, and therefore may virtually interact with each compound of the pilot firefighting water. However, polar (AB) in-

teraction may be repulsive in water, especially in case of two strongly monopolar compounds of the same character, *i.e.* electron donor–electron donor or electron acceptor–electron acceptor [127]. The pronounced electron donor character of the membranes may allow such a repulsion in water with other strongly electron donor compounds.

The hydrophobic character of membranes can give rise to apolar (LW) interactions. However, in water, the interactions between the hydrophobic parts of the membrane and of the surfactants will be mainly driven by the polar (AB) cohesion of water. Hydrophobic adsorption is very likely to occur. Will hydrophobic interactions be stronger with the fluorinated surfactants? The cohesion energy between two bodies 1 and 2 immersed in a liquid 3 is [6]:

$$\begin{aligned}\Delta G_{132} = & -2[\sqrt{\gamma_1^{LW}\gamma_3^{LW}} + \sqrt{\gamma_2^{LW} + \gamma_3^{LW}} - \sqrt{\gamma_1^{LW}\gamma_2^{LW}} - \gamma_3^{LW} \\ & + \sqrt{\gamma_3^+}(\sqrt{\gamma_1^-} + \sqrt{\gamma_2^-} + \sqrt{\gamma_3^-}) + \sqrt{\gamma_3^-}(\sqrt{\gamma_1^+} + \sqrt{\gamma_2^+} + \sqrt{\gamma_3^+}) \\ & - \sqrt{\gamma_1^+\gamma_2^-} - \sqrt{\gamma_1^-\gamma_2^+}] \quad (4.36)\end{aligned}$$

which gives, if water is the only polar compound in the system:

$$\Delta G_{132} = -2[\sqrt{\gamma_1^{LW}\gamma_3^{LW}} + \sqrt{\gamma_2^{LW} + \gamma_3^{LW}} - \sqrt{\gamma_1^{LW}\gamma_2^{LW}} - \gamma_3^{LW} + 2\sqrt{\gamma_3^+\gamma_3^-}] \quad (4.37)$$

After calculations with the values given in table 4.5, we obtain:

$$\Delta G_{\text{octane water polyethylene}} = -101.95 \text{ mJ m}^{-2}$$

$$\Delta G_{\text{octane water Teflon}^\text{®}} = -102.02 \text{ mJ m}^{-2}$$

Table 4.5: Surface tensions of octane, polyethylene, Teflon[®] and water [127]

Compound	γ^{LW}	γ^+	γ^-
Octane	21.6	0	0
Polyethylene	33.0	0	0
Teflon [®]	17.9	0	0
Water	21.8	25.5	25.5

Both energies are negative, implying spontaneous attraction. This attraction appears to be slightly higher for octane and Teflon[®] in water, but the difference between that of octane and polyethylene in water is very small. Therefore, differences between hydrocarbon–hydrocarbon and hydrocarbon–fluorinated hydrophobic interactions in water are expected to be minimal. The difference of membrane affinity between hydrocarbon and fluorinated surfactant is expected to depend mainly on the difference of polar heads.

A quick description of the potential interactions that may occur between the surfactants from pilot firefighting waters and reverse osmosis/nanofiltration membrane has been given. However, these interactions may also strongly depend on the feed solution. For instance, the ionic strength may hinder electrostatic interactions, and the concentration of each surfactant, in combination to their cmc might also play a great role.

4.3 Material and methods

The experimental study of the reverse osmosis was done in three steps, with increasing volume and duration between each step. First, available membrane materials were screened in an flat sheet Osmonics Sepa CFII reverse osmosis and nanofiltration cell. Then real and model pretreated pilot firefighting waters were tested in a Millipore pilot with a laboratory scale spiral-wound module, and the observed properties were checked during longer experiments in a semi-industrial Polymem pilot.

4.3.1 Solutions used for membrane processes experiments and surfactants analysis

For the work on the treatment step of the mobile unit, the pretreatment was assumed granted and most of the solutions used were synthetic mixtures of the surfactants used in pilot firefighting waters. However, some actual electrocoagulation-pretreated pilot firefighting water was also used as a control. Industrially, reverse osmosis is expected to reject the fluorinated surfactant from pretreated firefighting waters, in order to provide a permeate containing as little fluorinated surfactant concentration as possible. Given the membrane processes principles, this cannot be achieved without the production of a concentrated retentate, as the water passes through the membrane. The more concentrated the retentate,

the lower its volume: the amount of concentrated retentate to incinerate will be minimal with maximal concentration factor (CF , equation 4.3).

To study the reverse osmosis at high concentration factor, and thus high volume reduction, most of the solutions used were near 20 times the concentration measured after electrocoagulation at the laboratory, at 0.5 A and 540 C L^{-1} , *i.e.* $CF = 20$ (table 4.6). In the absence of information about its concentration, Dowanol[®] DPM was assumed unaffected by the pretreatment. These highly concentrated solutions were used for the membrane screening in the Osmonics cell, as well as in the semi-industrial Polymem Pilot.

Table 4.6: Composition of the $CF20$ model solution

Name of commercial product	Active compound concentration (mg L^{-1})
Dowanol [®] DPM	54000
Disponil [®] SOS 842	16000
Tegotens [®] AM VSF	4000
Simulsol [®] SL8	2000
Fluorinated surfactant	800

The reverse osmosis of 5 L of actual pilot firefighting water 3, pretreated by electrocoagulation and filtration in the laboratory as described in Chapter 3, was done to check the behavior of the membrane with real pretreated pilot firefighting water. The measurement of flux decline as function of concentration was done with a model solution which concentration was increased by successive addings. The composition of this solution is given in table 4.7. Another experiment was done with a model solution with the same proportions as the previous model solution, but on the basis of a fluorinated surfactant concentration of 470 mg L^{-1} . The compositions of $CF20$ solutions used during the long experiments are given in table 4.8.

Table 4.7: Artificially concentrated model pretreated pilot firefighting water composition after additions

Adding	0	1	2	3	4
Total volume (L)	3.8	4.3	4.8	5.3	5.8
Dowanol [®] DPM ($mg\ L^{-1}$)	270	562	1122	2258	4561
Disponil [®] SOS 842 ($mg\ L^{-1}$)	87	175	357	734	1476
Tegotens [®] AM VSF ($mg\ L^{-1}$)	20	43	85	127	220
Simulsol [®] SL8 ($mg\ L^{-1}$)	20	43	90	185	355
Fluorinated surfactant ($mg\ L^{-1}$)	23	46	100	205	417

Table 4.8: Compositions in $mg\ L^{-1}$ of CF20 solutions for tests 1 and 2 in the Polymem pilot. The volumes were 40 L, including the dead volume.

Name of commercial product	Test 1	Test 2
Dowanol [®] DPM	51650	43551
Disponil [®] SOS 842	16000	14777
Tegotens [®] AM VSF	4001	2289
Simulsol [®] SL8	2008	1868
Fluorinated surfactant	804	745

Surfactant quantification was done by the HPLC method described in Chapter 3. To detect surfactant low concentration ($< 2\ mg\ L^{-1}$) a sample concentration method was set up. This method consisted of 1–volume reduction by evaporation, 2–surfactants redissolution by a 70% methanol recovery solution containing $30\ mg\ L^{-1}$ of *NaCl*. Accurate volumes near 60 mL of dilute solutions were evaporated to dry at 90°C in glass vials. After cooling at room temperature 3 mL of recovery solution were added to the vials before vortex agitation. The resulting solutions contained concentrated surfactants that allowed analysis down to $0.2\ mg\ L^{-1}$, with an average recovery rate of 90%. Samples of lower concentration were analyzed by solid phase extraction (SPE) and liquid chromatography coupled with mass spectrometry (LC-MS) by the Norwegian Institute for Air Research (NILU). NILU's laboratories are accredited according to NS-EN ISO/IEC 17025.

The concentration in free monomers of surfactants contained in CF20 solution was estimated by surfactant quantification in an ultrafiltration permeate, as ultrafiltration is known to retain surfactant micelles [63, 64]. 2 L of CF20 solution were ultrafiltered on a Rayflow

X100 ultrafiltration pilot with a Watson Marlow 624U peristaltic pump, a LAUDA RM6 thermocryostat, and 200 cm^2 5 kD polyethersulfone membranes from Novasep at 2 bar . According to appearing rejections (table 4.9), Disponil[®] SOS 842 was mainly under the form of monomer, whereas the fluorinated surfactant was mostly involved in micelles. Tegotens[®] AM VSF and Simulsol[®] SL8 distributions were intermediate. Disponil[®] SOS 842 had the highest concentration in $CF20$ solutions (table 4.8) and also seemed to have the highest monomer content in these concentrated solutions. The eventuality of mixed micellization and synergies between surfactants in $CF20$ solutions unfortunately remained out of the scope of this work.

Table 4.9: Monomer content in $CF20$ solutions, estimated on the basis of ultrafiltration permeate concentration (given) and retentate concentration after equilibrium (not given)

Surfactant	Concentration ($mg L^{-1}$)	Appearing rejection
Disponil [®] SOS 842	10135	13%
Tegotens [®] AM VSF	2000	41%
Simulsol [®] SL8	643	67%
Fluorinated surfactant	66	92%

4.3.2 Devices used for reverse osmosis experiments

4.3.2.1 Osmonics Sepa CFII cell

The screening of different available membrane materials was done with a Sepa CFII cell from Osmonics. The cell accepts flat sheet membranes, with an effective area of 140 cm^2 . The Osmonics polyamide and cellulose acetate nanofiltration and reverse osmosis membranes retained for the screening are listed in table 4.10. The setup comprised a high pressure pump, a by-pass, a pressure valve and a tank (see figure 4.4). Pressure and flow were adjusted by the interplay of the two valves and superficial velocities were 0.1 and 0.5 $m s^{-1}$. Every experiments were done with a 31 mil spacer (0.7874 mm), in recycle mode, at 30°C, at the pressures recommended by the supplier for each membrane (table 4.10). Prior to use, membranes were washed 20 min with water, then with $NaOH$, pH 10–10.5, 30 min , and then with water again until neutral pH . Salt rejections were measured except for the CK membrane, and the dead volume of the setup was 150 mL . Salts concentrations were determined by ionic chromatography.

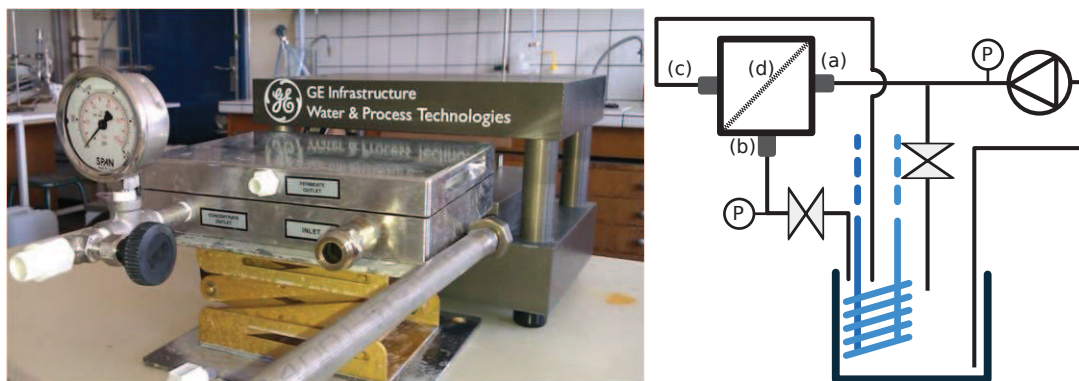


Figure 4.4: Osmonics setup for membrane screening. (a): feed, (b): retentate, (c): permeate, (d): membrane

Table 4.10: Membranes used in the Sepa CFII cell for the screening

Membranes	SG	AD	CE	CK	DK
Type and material	RO, thin film polyamide	RO, polyamide	RO, cellulose acetate	NF, cellulose acetate	NF, thin film polyamide
Recommended pressure (<i>Bar</i>)	15.5	55	30	15	7
Salt rejection (given by the supplier)	98.2%, <i>NaCl</i> 2 g L^{-1}	99.5%, <i>NaCl</i> 2 g L^{-1}	97.0%, <i>NaCl</i> 2 g L^{-1}	92.0%, <i>Na₂So₄</i> 2 g L^{-1}	98.0%, <i>MgSO₄</i> 2 g L^{-1}
Measured salt rejection	98.7%	88.4%	94.9%	—	99.1%

4.3.2.2 Millipore ProScale pilot

A Millipore nanofiltration and reverse osmosis pilot (figure 4.5) was used with a SG1812C-28D reverse osmosis spiral membrane supplied by Osmonics, with a thin film polyamide active phase of 0.37 m^2 surface area and feed spacers of 28 mil (0.7112 mm). Pilot had a dead volume of 0.8 L , superficial velocity was $84.10^{-3}\text{ m s}^{-1}$ and operating pressure was 20 bar , all permeability measurements were scaled to 25°C .

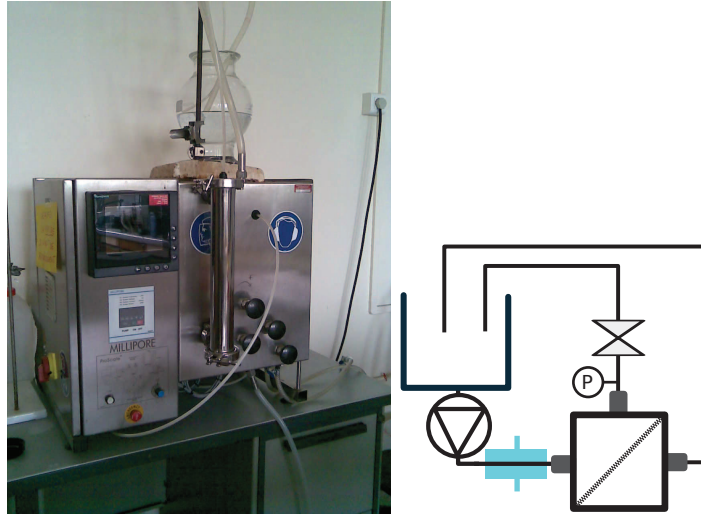


Figure 4.5: Millipore pilot

4.3.2.3 Polymem pilot

Longer experiments were performed with a reverse osmosis pilot from Polymem (figure 4.6). The pilot had a 100 L tank, a dead volume of 9.9 L, a high pressure pump, a recirculation loop and was equipped with a thin film polyamide CSM RE2540-FE reverse osmosis membrane with an area of 2.5 m^2 . The recirculation rate was set to 50%, the pressure to 30 bar and the superficial velocity to 0.09 m s^{-1} and the temperature inside the loop was maintained at 30°C by an external thermocryostat.

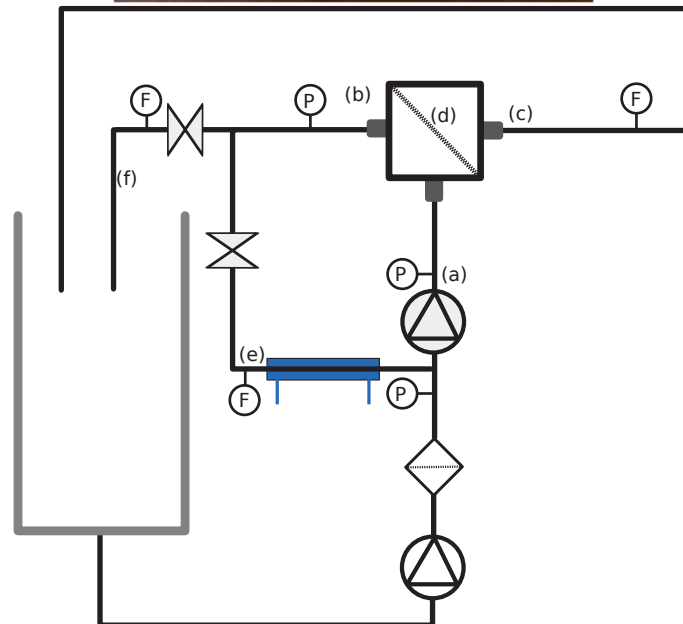


Figure 4.6: Polymem reverse osmosis pilot. (a): feed, (b): retentate, (c): permeate, (d): membrane, (e): recirculation, (f): reject

Table 4.11: Summary of the reverse osmosis and nanofiltration pilots properties

Naming	Osmonics	Millipore	Polymem
Tank volume	5 L	5 L	100 L
Dead volume	150 ml	800 mL	9.9 L
membrane nature	Set of flat sheet polyamide and cellulose acetate reverse osmosis and nanofiltration membranes (see table 4.10)	Spiral-wound smooth fouling resistant thin film polyamide SG1812-28D reverse osmosis membrane	Spiral-wound fouling resistant thin film polyamide CSM RE2540-FE reverse osmosis membrane
Membrane area	140 cm ²	0.37 m ²	2.5 m ²
Feed spacer thickness	31 mil (0.7874 mm)	28 mil (0.7112 mm)	31 mil (0.7874 mm)
Water permeability (L h ⁻¹ m ⁻² bar ⁻¹ at 25°C)	See figure 4.7	2	2.4
Salt rejection		98.5%, NaCL 2g L ⁻¹	99.7%, NaCL 2g L ⁻¹
Operating pressure during the experiments	5–55 bar	20 bar	30 bar
Cross-flow velocity	0.1 and 0.5 m s ⁻¹	0.084 m s ⁻¹	0.071, 0.095 and 0.120 m s ⁻¹

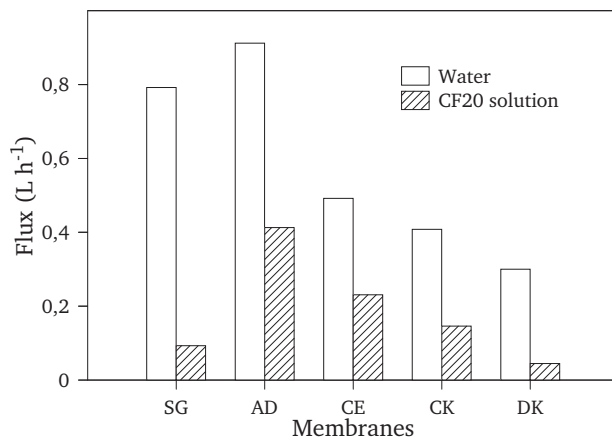
4.4 Experimental part

4.4.1 Screening of flat reverse osmosis and nanofiltration membranes in the Osmonics cell

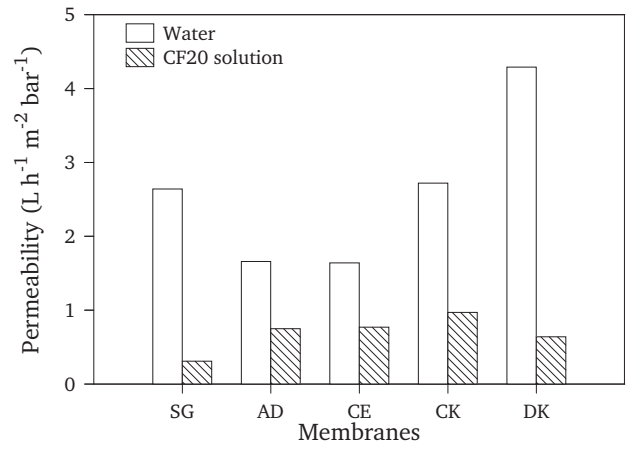
The screening of different membrane materials aimed at identifying the most appropriate membrane material for pretreated firefighting water, considering retention properties and flux decline. For this purpose, polyamide and cellulose acetate reverse osmosis and nanofiltration membranes were tested in the Osmonics cell. Experiments were done with 4–5 L of CF20 solutions, at 30°C and usual pressures for each cleaned membrane, except for the SG membrane which was used at 30 bar. The cross-flow velocity was set to 0.1 m s⁻¹ for two hours. Samples of permeate and retentate were taken and then the velocity was

set to 0.5 m s^{-1} for two hours before a second sampling. Surfactant concentrations were determined after evaporation–redissolution for the permeates, and after dilution by 20 for retentates.

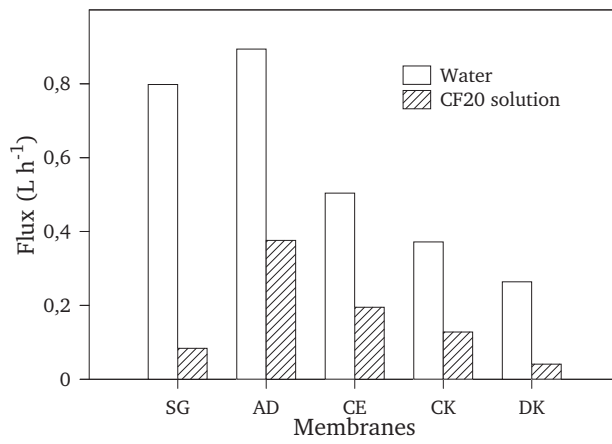
The fluxes and permeabilities were very near for both velocities (figure 4.7). The slight differences may have come from a difference in pressure drop due to different velocities. Each membrane showed severe flux decline. The highest flux was obtained with the AD membrane and the lowest with the DK membrane. However, to compare each membrane, the permeability is a better indicator because the flux depends on the pressure at which the membrane was used. The highest permeability was obtained with the CK membrane and the lowest with the SG membrane. Considering the ratio between the available flux with the CF20 solution to the initial water flux (table 4.12), we can see that the membrane showing the highest fouling were the thin film polyamide SG (reverse osmosis) and DK (nanofiltration) membranes.



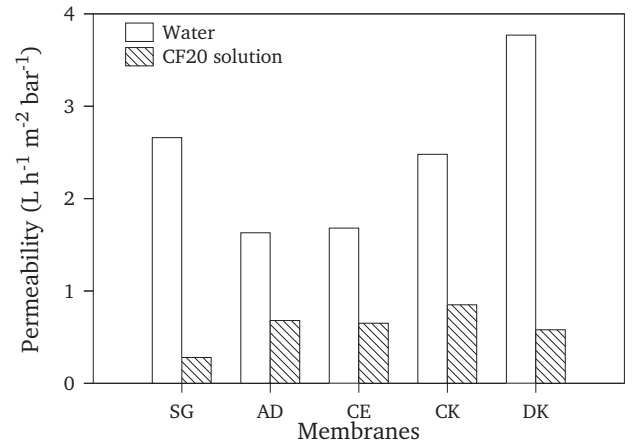
(a) Flux, 0.1 m s^{-1}



(b) Permeability, 0.1 m s^{-1}



(c) Flux, 0.5 m s^{-1}



(d) Permeability, 0.5 m s^{-1}

Figure 4.7: Flux and permeabilities at 25°C during membrane screening

Table 4.12: Flows, permeabilities and flux decline during membrane screening with *CF20* model solution in the Osmonics cell for cross-flow velocities of 0.1 and 0.5 $m s^{-1}$.

(a) Cross-flow velocity: 0.1 $m s^{-1}$

Membrane	Pressure (bar)	Water flow ($L h^{-1}$)	Water permeability ($L h^{-1} m^{-2} bar^{-1}$)	<i>CF20</i> flow ($L h^{-1}$)	<i>CF20</i> permeability ($L h^{-1} m^{-2} bar^{-1}$)	Available water flux with the <i>CF20</i> solution
SG	30	0.792	2.64	0.093	0.31	12%
AD	55	0.912	1.66	0.413	0.75	45%
CE	30	0.492	1.64	0.231	0.77	48%
CK	15	0.408	2.72	0.146	0.97	36%
DK	7	0.300	4.29	0.045	0.64	15%

(b) Cross-flow velocity: 0.5 $m s^{-1}$

Membrane	Pressure (bar)	Water flow ($L h^{-1}$)	Water permeability ($L h^{-1} m^{-2} bar^{-1}$)	<i>CF20</i> flow ($L h^{-1}$)	<i>CF20</i> permeability ($L h^{-1} m^{-2} bar^{-1}$)	Available water flux with the <i>CF20</i> solution
SG	30	0.798	2.66	0.084	0.28	10%
AD	55	0.894	1.63	0.376	0.68	42%
CE	30	0.504	1.68	0.195	0.65	39%
CK	15	0.372	2.48	0.128	0.85	34%
DK	7	0.264	3.77	0.041	0.58	15%

However, the choice of the appropriate membrane is also a matter of retention to perform the separation efficiently, especially the retention rate of the fluorinated surfactant. In figure 4.8 these retention rates are depicted for each membrane and both velocities. The membrane achieving the highest retention rate for the fluorinated surfactant is the SG membrane, with 99.38% and 99.43% for velocities of 0.1 and 0.5 $m s^{-1}$ respectively (table 4.13). This membrane is unfortunately the one that has the lowest rate of pure water flux available with the *CF20* solution. However, even with this high retention rates, the fluorinated surfactant concentrations in permeate were 4.8 and 4.1 $mg L^{-1}$ for velocities of 0.1 and 0.5 $m s^{-1}$ respectively (table 4.13). These concentrations were high considering the expected fluorinated surfactant concentration in the permeate ($< 0.1 mg L^{-1}$). This pointed out that the higher the concentration factor, the higher the concentration in retentate and thus the higher the concentration in the permeate. Therefore retention was preferred instead of flux and the SG membrane was chosen.

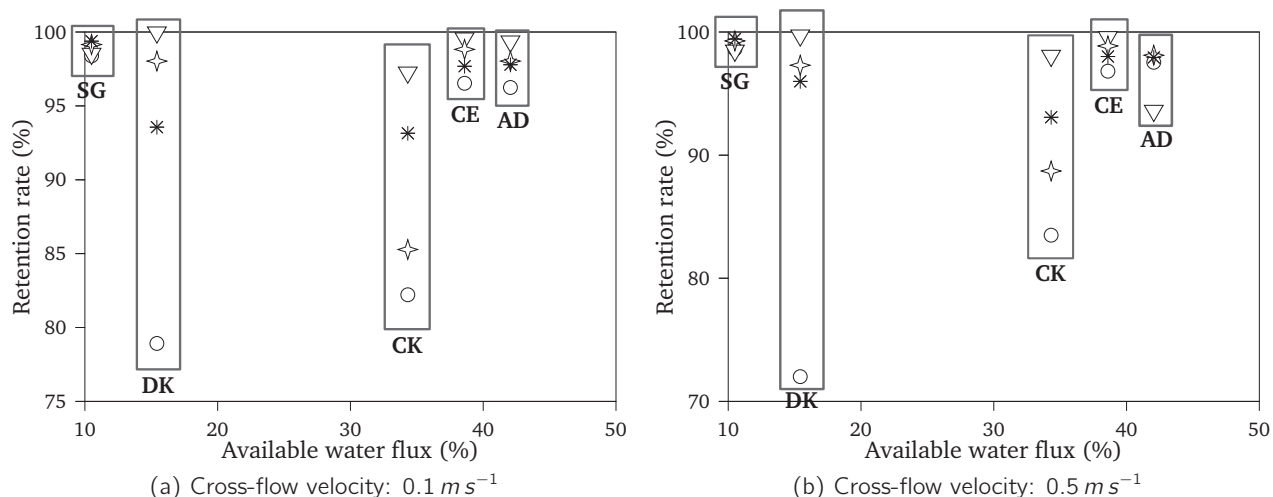


Figure 4.8: Surfactant retention rates for every tested membranes as function of the percentage of available water permeability in the Osmonics cell. ○: Disponil® SOS 842; ▽: Tegotens® AM VSF; ✧: Simulsol® SL8, *: fluorinated surfactant. From left to right: SG, DK, CK, CE and AD membranes. Operating pressures are given in table 4.10.

Table 4.13: Concentration in permeates and rejections of the fluorinated surfactant during membrane screening

Membrane	0.1 m s^{-1}		0.5 m s^{-1}	
	$C_P(\text{mg L}^{-1})$	R	$C_P(\text{mg L}^{-1})$	R
SG	4.8	99.4%	4.1	99.5%
AD	17.7	97.8%	13.8	98.1%
CE	13.7	97, 7%	10.1	98.4%
CK	44.1	93.2%	43.7	93.0%
DK	40.2	93.6%	8.0	98.4%

4.4.2 Reverse osmosis of model and pilot pretreated firefighting waters with a spiral-wound SG module

4.4.2.1 Reverse osmosis of pretreated pilot firefighting water

Reverse osmosis was used to treat 5 L of pretreated pilot firefighting water in the Millipore pilot. The experiment consisted of successively 15 min of full recycle, extraction of 2 L of permeate, 20 min of full recycle and extraction of 1.7 L of permeate. Results are presented in table 4.14. No surfactants were detected with the HPLC analytic system, and according to additional analysis performed by the Norwegian Institute for Air Research, fluorinated surfactant concentration in whole extracted volumes of permeate were 10.47 and

$16.39 \mu\text{g L}^{-1}$, giving apparent retention rates of 99.97% and 99.96% for the first and second permeates respectively. These retentate concentration did match the aimed concentration of $< 0.1 \text{ mg L}^{-1}$, however these experiments were done with low VRRs of 1.5 and 2.8. Mass balance showed some missing fluorinated surfactant in the retentate, assumed to be adsorbed on the membrane with an adsorption density between 73 and 162 mg m^{-2} .

Table 4.14: Fluorinated surfactant concentration and membrane permeability during pre-treated pilot firefighting water 3 reverse osmosis, 20 bar. ^a: additional results from the Norwegian Institute for Air Research (NILU).

Step	Permeability at 25°C ($\text{L h}^{-1} \text{ m}^{-2} \text{ bar}^{-1}$)	Retentate volume (L)	VRR	Expected retentate concentration (mg L^{-1})	Measured retentate concentration (mg L^{-1})	Mean permeate concentration ($\mu\text{g L}^{-1}$)	Fluorinated surfactant mass balance (mg)
Full recycle	1.033	5.8	1	27 ± 5	20 ± 1	–	-40 ± 10
Concentration	0.914	–	–	–	–	10.47^a	–
Full recycle	0.921	3.8	1.5	41 ± 11	34 ± 2	–	-27 ± 10
Concentration	0.779	–	–	–	–	16.39^a	–
Full recycle	0.760	2.1	2.8	74 ± 33	46 ± 2	–	-60 ± 38

4.4.2.2 Reverse osmosis of synthetic pretreated firefighting water

Reverse osmosis was done on a pretreated pilot firefighting water until a volume reduction ratio of 2.8 but the study of reverse osmosis at high volume reduction ratios would have required more than the whole available pilot firefighting water. Hence the study of pretreated pilot firefighting water concentration with reverse osmosis was done by artificial concentration of the model pretreated firefighting water by successive additions (table 4.7), in full recycle mode.

After each adding, flasks were rinsed three times with permeates and measurements were done 1 h later. During the experiment, membrane permeability decreased with increasing concentrations (figure 4.9). Though permeability decrease was strong, higher concentrations lead to small permeability reductions. Considering the fluorinated surfactant concentrations, permeabilities were the same magnitude as previous experiments, near results from Tang *et al* [66] obtained with PFOS solutions and thin film composite polyamide ESPA RO membrane from Hydronautics, and to the data obtained with the flat sheet SG membrane during the

screening despite the different composition of the feed solution.

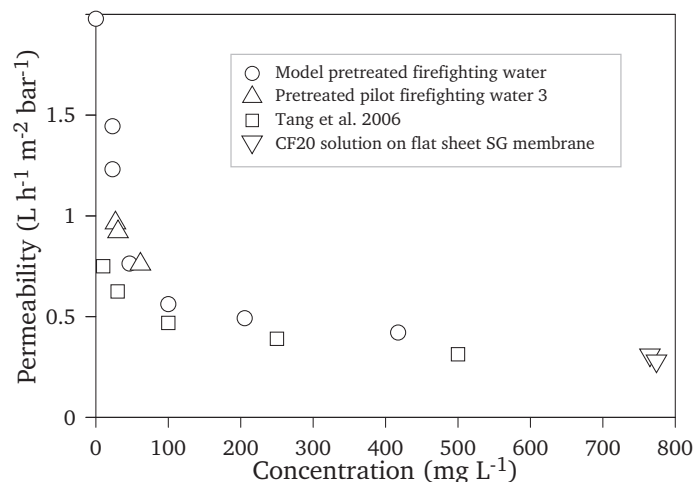


Figure 4.9: Permeability versus total fluorinated surfactant concentration in the system during reverse osmosis of model pretreated pilot firefighting water in the Millipore pilot with a spiral-wound SG membrane at 20 *bar*. The membrane used by Tang et al. was an ESPA membrane, the pressure was 13.8 *bar* and the fluorinated surfactant was PFOS. The data from flat sheet SG membrane is from section 4.4.1.

No surfactants were detected in every permeates with the conventional HPLC method. The difference between expected and measured fluorinated surfactant concentrations in retentates showed that rather little amount of adsorbed fluorinated surfactant for low concentrations and was smaller than the measurements error for every higher concentrations (table 4.15). Relative adsorption of the fluorinated surfactant seemed to be limited at high concentrations. An additional reverse osmosis experiment with a model pretreated firefighting water, containing 470 mg L^{-1} of fluorinated surfactant, was done to quantify fluorinated surfactant concentration in permeate with the evaporation method. After two hours of equilibrium, permeate concentration was 0.271 mg L^{-1} , corresponding to a 99.94% retention rate, near to the results obtained in section 4.4.1.

The SG membrane in spiral-wound module showed high retention rates, even higher than those measured with flat sheet SG membrane in the Osmonics cell. These differences could result from direct manipulation of the flat sheet membrane when mounting and pressurizing the cell whereas membranes in spiral-wound modules are already mounted. Therefore, retention rates of CE and AD membranes that were not selected after the screening should be checked in spiral-wound modules. In case of interesting retention rates, these membranes could increase the permeability of the unit and reduce operating costs but this work could

Table 4.15: Fluorinated surfactant concentrations during artificially concentrated model pilot firefighting water 2 reverse osmosis, 20 bar, full recycle, 1h equilibrium after adding

Adding	Expected fluorinated surfactant in retentate ($mg\ L^{-1}$)	Measured fluorinated surfactant ($mg\ L^{-1}$)	Difference (mg)
0	23±4	18±1	19±5
1	46±7	46±3	–
2	100±15	99±5	–
3	205±30	218±11	–
4	417±52	401±20	–

not be done during the thesis.

The SG membrane fouling with increasing concentration showed that most of the flux decline occurred at relatively low concentration, between 0 and 200 $mg\ L^{-1}$ of fluorinated surfactant, meaning that the flux decline between a concentration of 400 $mg\ L^{-1}$ and 800 $mg\ L^{-1}$ for instance should be small (figure 4.9). The adsorption of fluorinated surfactant also seemed to reach a limit at high concentration. However, these tests were done over short periods and the stability of the membrane's behavior regarding flux decline and retention has to be examined over longer periods. In the literature, some fluorinated surfactants have shown high initial rejection, and progressive leaking over time during nanofiltration experiments [68]. This eventual undesired leaking had to be checked in the case of firefighting water reverse osmosis. In addition, the concentrations of the other surfactants were not measured yet and could provide useful information.

4.4.3 Study of the reverse osmosis on longer periods in an industrial pilot

According to the manufacturer, SG membrane is a smooth fouling resistant thin film polyamide membrane for brackish water. The membrane used in the polymem pilot for long experiments was not an SG membrane, but a CSM RE2540-FE membrane, which was also a fouling resistant thin film polyamide reverse osmosis membrane. Two experiments were done with this membrane and 40 L of CF20 solution: the first during 8 h and the second during 10 days.

During both tests, the flux decline was strong (figure 4.10), the available ratio of initial permeability was 20–25%. However, in both cases, the flux declined very quickly, within the first minutes, and no transition between pure water flux and CF20 flux could be observed.

Yet quick, the flux declined seemed to stabilize over long periods during test 2, near a permeability of $0.5 \text{ L h}^{-1} \text{ m}^{-2} \text{ bar}^{-1}$. The concentration difference between the two solutions employed explained the slight difference in permeability between the two tests. Between the two tests, the membrane was washed with a water solution containing 5% v:v ethanol and $0.5 \text{ g L}^{-1} \text{ NaCl}$. This cleaning did not seem to be sufficient to recover the initial water permeability, but the remaining fouling did not cause more flux decline in the second experiment. The flux decline caused by the surfactant solution, though high, appeared to be fast, stable and largely reversible.

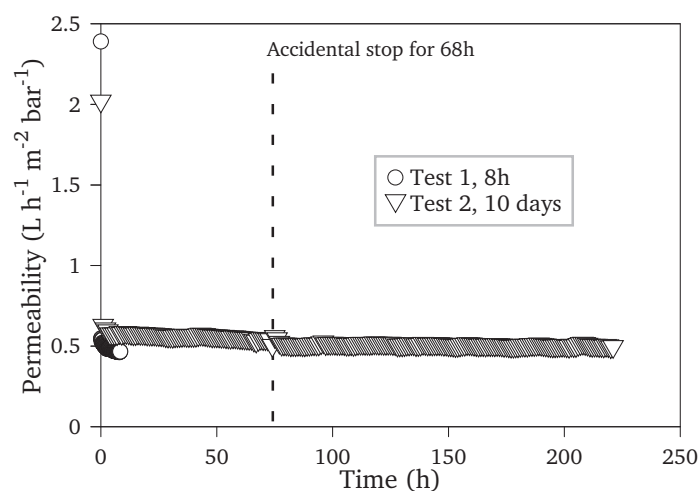


Figure 4.10: Permeability at 25°C during reverse osmosis in the Polymem pilot of 40 L of CF20 solution, at 30 bar , and cross-flow velocity of 0.095 m s^{-1} . The initial points were the water permeabilities before the experiments.

All retention rates were very high, *i.e.* $> 99.75\%$ for every surfactants (figure 4.11). The values for each surfactant seemed to correlate between both experiments, especially for the increasing initial retention of Disponil[®] SOS 842. The anionic surfactant had the lowest retention rate in spite of the electrostatic repulsion and the retention rates of the other surfactants were $> 99.9\%$ but no rejection tendency according to the chemistry of surfactants could be extracted from experimental data. The rejection of the fluorinated surfactant was very high, $> 99.95\%$ except for the last measurement.

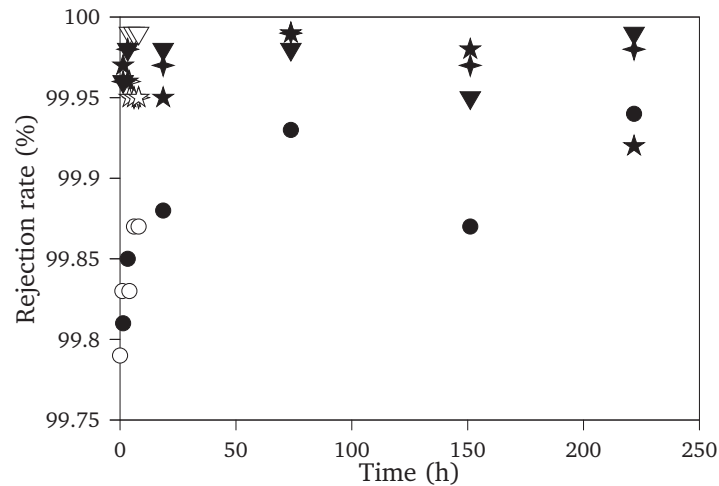


Figure 4.11: Retention rates during reverse osmosis in the Polymem pilot of 40 L of CF20 solution, at 30 bar, and cross-flow velocity of 0.095 m s^{-1} .

Test 1: ○: Disponil® SOS 842; ▽: Tegotens® AM VSF; ☆: Simulsol® SL8, ☆: fluorinated surfactant.

Test 2: ●: Disponil® SOS 842; ▼: Tegotens® AM VSF; ★: Simulsol® SL8, ★: fluorinated surfactant.

At the end of the second test, the cross-flow velocity was varied, according to the possibilities of the pilot, to investigate eventual changes in permeability and retention. Results are given in table 4.16 and the superficial velocity did not have any clear effect on permeability nor on surfactant rejection. Considering the average of every measured rejection rates in the Polymem pilot (table 4.17), the order of rejection seemed to be Disponil® SOS 842 < fluorinated surfactant \simeq Simulsol® SL8 < Tegotens® AM VSF. The average fluorinated surfactant rejection rate was 99.95%, very near to the values measured with the spiral-wound SG module.

Table 4.16: Permeability at 25°C and retention rates as function of the superficial velocity during reverse osmosis in the Polymem pilot of 40 L of CF20 solution at 30 bar.

Cross-flow velocity (m s^{-1})	Time since the beginning of Test 2	Duration before the measurement	Average permeability ($\text{L h}^{-1} \text{ m}^{-2} \text{ bar}^{-1}$)	Disponil® SOS 842 rejection	Tegotens® AM VSF rejection	Simulsol® SL8 rejection	fluorinated surfactant rejection
0.071	238 h	16 h	0.491	99.82%	99.96%	99.96%	99.94%
0.095	222 h	18 h	0.506	99.94%	99.99%	99.98%	99.92%
0.120	362 h	17 h	0.519	99.94%	99.99%	99.97%	99.96%

Table 4.17: Average rejection rates

Surfactants	Rejection
Disponil [®] SOS 842	99.86%
Tegotens [®] AM VSF	99.98%
Simulsol [®] SL8	99.96%
Fluorinated surfactant	99.95%

The mass balance was estimated for each surfactant, based on initial composition of the solutions, on retentate concentration and on an estimation of the loop volume of 5 L. Adsorption densities depicted in figure 4.12 assumed the membrane was the only interface where significant adsorption took place. The surfactant that adsorbed the most (more than ten times the others) was the Disponil[®] SOS 842, in spite of its negative charge and the membrane's negative charge. This unexpected result will be discussed in section 4.5.2. This surfactant was also the one that had the highest concentration. Therefore, assuming that the fouling was due to adsorption of surfactants, it could be mainly attributed in the mixture to the adsorption of anionic surfactant. This hypothesis could be verified by the filtration of Disponil[®] SOS 842 alone but for material reasons this could not be done in the course of this thesis.

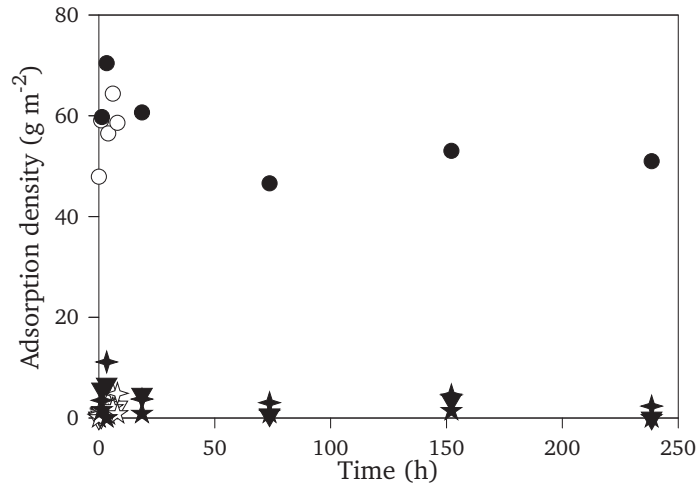


Figure 4.12: Surfactants adsorption density during reverse osmosis in the Polymem pilot of 40 L of CF20 solution, at 30 bar, and cross-flow velocity of 0.095 m s^{-1} .

Test 1: ○: Disponil® SOS 842; ▽: Tegotens® AM VSF; ☆: Simulsol® SL8, ☆: fluorinated surfactant.

Test 2: ●: Disponil® SOS 842; ▼: Tegotens® AM VSF; ★: Simulsol® SL8, ★: fluorinated surfactant.

Table 4.18: Summary of the experimental results obtained during reverse osmosis experiments. The only surfactant considered is the fluorinated surfactant.

Devices	Osmonics cell	Millipore pilot	Polymem pilot
Membranes	SG, flat sheet	SG, spiral-wound	RE2540-FE, spiral-wound
$C_R \text{ (mg L}^{-1}\text{)}$	765–774	23–417	804
C_P	4.8–4.1 (mg L^{-1})	$\simeq 10\text{--}271 \text{ }\mu\text{g L}^{-1}$	110–665 $\mu\text{g L}^{-1}$
R	99.38–99.48%	99.94–99.97%	99.95–99.99%
Flow (L h^{-1})	1.54–1.40	3–11	37.5
Permeability ($\text{L h}^{-1} \text{ m}^{-2} \text{ bar}^{-1}$)	0.31–0.28	0.4–1.5	0.5
Available water permeability	12–10%	20%	21%

4.5 Discussion

Reverse osmosis was found efficient for the removal of surfactants from firefighting water. The results obtained in the previous section will be processed here to study the flux decline, the adsorption and the rejection of surfactants in order to propose explanations for these phenomena.

4.5.1 Study of the flux decline with the spiral-wound SG membrane

In this section, the retentate concentration of the fluorinated surfactant will be taken as a reference, even though it did not directly account for the concentrations of the other surfactant also present in proportional concentrations. It has to be kept in mind that these compounds might also participate to the flux decline. From the results of section 4.4.2.2, the permeability was plotted against $\ln(1/C_R)$, with C_R the concentration of fluorinated surfactant in the retentate in mg L^{-1} (figure 4.13). This plot was done in order to check how the diffusion model (equation 4.35) described the flux decline in this experiment, neglecting the permeate concentration and assuming constant concentration at the membrane. The linear correlation was loose, the diffusion model was not a good candidate.

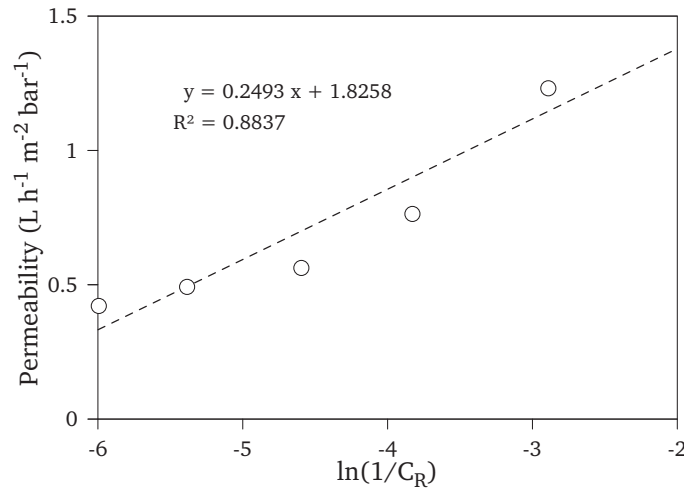


Figure 4.13: Permeability as function of logarithm of the inverse of fluorinated surfactant concentration in the retentate during model pretreated firefighting water reverse osmosis with a spiral-wound SG membrane. The concentration of the fluorinated surfactant is an indicator of the global concentration of other surfactants also present.

After the experiments in sections 4.4.2 and 4.4.3, we know that surfactant adsorption on the membrane occurred. Therefore, an adsorption-based instead of a diffusion-based model should be considered. If we describe the flux decline on the basis of the resistance-in-series model, after equation 4.29 the permeability is L :

$$L = \frac{1}{\eta R_{tot}} \quad (4.38)$$

Assuming that only adsorption is responsible for the flux decline, the total resistance is:

$$R_{tot} = R_m + R_a \quad (4.39)$$

R_m , the intrinsic membrane resistance can be obtained on the basis of equation 4.38 and the membrane water permeability when $C_R = 0$:

$$R_m = \frac{1}{L_{water} \eta} = 1.82 \cdot 10^{14} \text{ m}^{-1} \quad (4.40)$$

Therefore, with equations 4.38, 4.39 and 4.40 we find:

$$R_a = \frac{1}{\eta L} - R_m \quad (4.41)$$

On the basis of experimental data, the plot of R_a versus C_R interestingly recalled the shape of a Langmuir isotherm (figure 4.14). Though the amount of the surfactants adsorbed on the membrane was not determined, it was assumed that R_a could be described by the following equation, analogue to Langmuir:

$$R_a = R_a^{max} \frac{K C_R}{1 + K C_R} \quad (4.42)$$

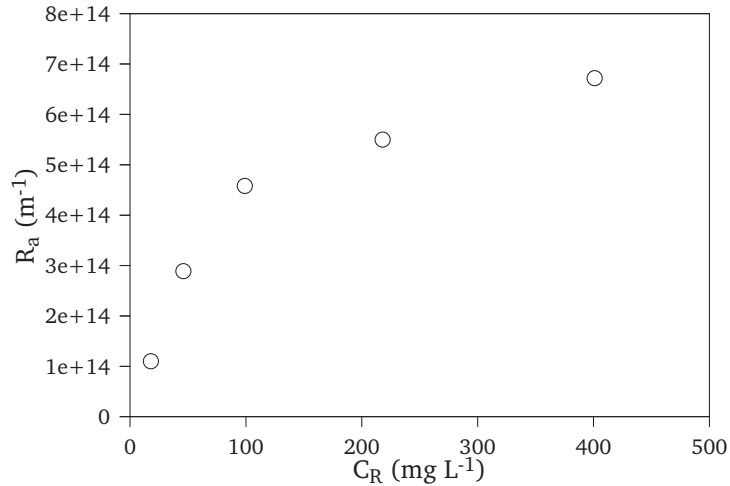


Figure 4.14: R_a , the resistance to mass transfer due to adsorption, versus C_R the retentate concentration of the fluorinated surfactant, during reverse osmosis of model pretreated firefighting water in the Millipore pilot, at 20 bar, with a spiral-wound SG membrane. The concentration of the fluorinated surfactant is an indicator of the global concentration of other surfactants also present.

The plot of $1/R_a$ versus $1/C_R$ was almost linear (figure 4.15). The linear regression (excluding the point corresponding to the lowest concentration) enabled a calculation of R_a^{max} and K :

$$R_a^{max} = \frac{1}{\text{intercept}} = 7.7 \cdot 10^{14} \text{ m}^{-1} \quad (4.43)$$

$$K = \frac{\text{intercept}}{\text{slope}} = 13.1 \text{ mg m}^{-2} \quad (4.44)$$

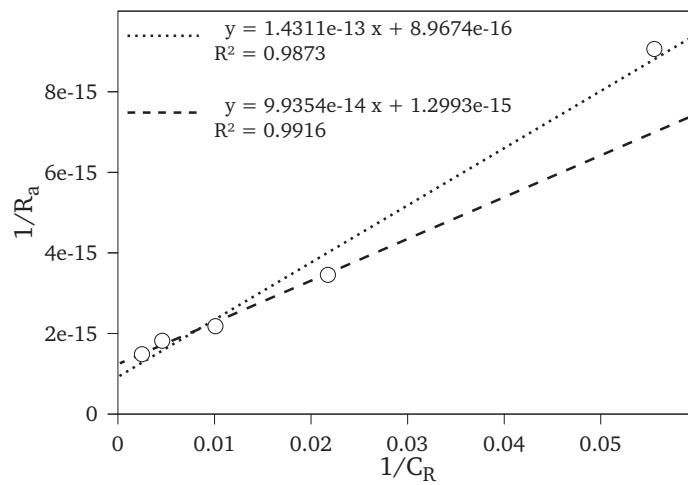


Figure 4.15: $1/R_a$ (m) versus $1/C_R$ ($L \text{ mg}^{-1}$) during reverse osmosis of model pretreated firefighting water in the Millipore pilot, at 20 bar, with a spiral-wound SG membrane. C_R , the retentate concentration of the fluorinated surfactant is an indicator of the global concentration of other surfactants also present.

The permeability L as function of C_R could be modeled by equation 4.45 and this model was confronted to experimental data in figure 4.16.

$$L = \frac{1}{\eta(R_m + R_a^{max} \frac{K C_R}{1 + K C_R})} \quad (4.45)$$

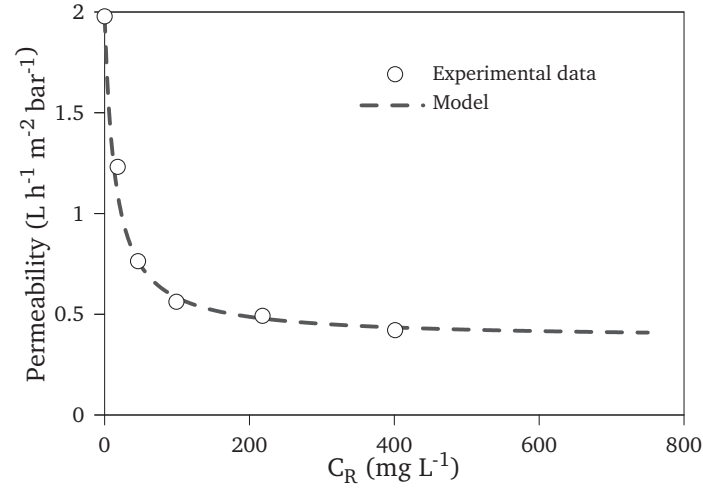


Figure 4.16: Model and experimental data for the permeability versus retentate concentration of the fluorinated surfactant, during reverse osmosis of model pretreated firefighting water in the Millipore pilot, at 20 bar, with a spiral-wound SG membrane. The concentration of the fluorinated surfactant is an indicator of the global concentration of other surfactants also present.

It could not be checked whether or not the surfactants in the mixture adsorbed on the membrane according to a Langmuir adsorption. However, on the basis of the fluorinated surfactant concentration, the model described very well the experimental data. The resistance due to adsorption seemed to be directly related to the retentate concentration, in the same way as the adsorption density is related to the equilibrium concentration in Langmuir isotherms. Several assumptions were made for this model: the equilibrium permeability was assumed reached for each concentration, the bulk concentration of the fluorinated surfactant was taken as a reference for the global retentate concentrations in surfactant mixture, R_a was assumed to depend on a Langmuir-type expression (equation 4.42) .

Though no adsorption isotherm were obtained experimentally, according to our model of flux decline, the adsorption of the surfactant mixture could follow a Langmuir-type adsorption isotherm, which appeared to directly impact the flux decline. In this hypothesis, the limit in flux decline would be reached at saturation of the membrane, and there would still remain a minimum permeability. After the value obtained for R_a^{max} (equation 4.43), the permeability after maximum adsorption would be $L_{min} = 0.378 \text{ L h}^{-1} \text{ m}^{-2} \text{ bar}^{-1}$. Therefore, from an industrial point of view, with a SG membrane the volume of pretreated pilot firefighting water could be highly reduced, without additional high fouling due to the surfactant mixture. Some additional work would be required to improve the model by considering the concentration of

each surfactant, higher concentrations and permeabilities over long periods. The assessment of its validity on other reverse osmosis membranes would also be interesting.

4.5.2 Adsorption of surfactants at the RE2540-FE membrane

The stability of the permeability and rejection was confirmed during longer reverse osmosis experiments in the Polymem pilot. The flux decline was high and quick, and was mostly attributed to the adsorption of the anionic surfactant, in concentrated solutions such as CF20 solutions. At the first sight, this compound was expected to show repulsive electrostatic interactions. But considering its high adsorption density (figure 4.12), the anionic surfactant seemed to adsorb *via* its hydrophobic tail, interacting with hydrophobic parts of the membrane, hiding them from water, regardless electrostatic interactions. Rather than a surface having a uniform surface charge, the membrane could be a patchwork of anionic sites on a hydrophobic support. This would be conform to both polar and apolar character of reverse osmosis membranes (table 4.3), and would account for the observed adsorption of the anionic surfactant. The other surfactants also showed some adsorption density, which opened the question of mixed adsorption of surfactants at the membrane surface. This field is very broad and the data collected was not sufficient to discuss this point.

However, the higher adsorption density of the anionic surfactant compared with other surfactants could be related to its higher monomer content (table 4.9, section 4.3.1). In CF20 solutions, adsorption seemed to be mostly due to the free anionic surfactant while other surfactants were significantly involved in micelles, thus less available for adsorption. This phenomenon was already observed in Section 2.2.4.1 during the screening of activated carbon and resin as substrates for the adsorption process. The decrease in fluorinated surfactant adsorption density with increasing model solution concentration, observed for both materials, could be due to the free anionic surfactant “replacing” other surfactants with limited monomer concentrations on the surface to form micelles. There, the adsorption seemed rather to be due to the hiding of hydrophobic parts of the membrane and of the surfactants from water, either in surface aggregates or in micelles if possible, than to any polar interactions.

The anionic surfactant was the main compound involved in adsorption of the membrane and thus presumably in flux decline. As an anionic compound, it could be selectively re-

moved by processes taking advantage of its charge. However, the other surfactants also adsorbed on the membrane. As the adsorption density of the fluorinated surfactant was higher at low surfactant mixture concentrations, at least on the spiral-wound SG membrane (section 4.4.2.1), the adsorption density of the other surfactants in absence of anionic surfactant could be higher on the membrane material. This could not be checked during this work, but fouling minimization by selective anionic surfactant removal, if desired, should be carefully studied with particular attention to the behavior of the other surfactants, and the eventual changes in their adsorption and rejection.

4.5.3 Diffusion of surfactants in the membrane

During the first test with the Polymem pilot, the membrane was free of any surfactants. A time lag was observed for the permeation of the surfactants at the beginning of the experiment. This time lag can be related to the diffusion coefficients of the compounds in the membrane [129]. The amount of penetrant Q_t was calculated for each sample as following:

$$Q_{t+1} = Q_t + \overline{C_{P,t,t+1}} \overline{V_{P,t,t+1}} \quad (4.46)$$

Q_t as function of time for the steady state is given by [129]:

$$Q_t = \frac{D c_i}{l} \left(t - \frac{l^2}{6D} \right) \quad (4.47)$$

with D , the diffusion coefficient, l the membrane thickness, and c_i the feed concentration of the considered compound. By extrapolating the linear plot of $Q_t/(l c_i)$, the intercept θ with the time axis is:

$$\theta = \frac{l^2}{6D} \quad (4.48)$$

Even if the membrane thickness is not known, the diffusion coefficients of different compounds in the membrane can be compared:

$$\frac{D}{l^2} = \frac{1}{6\theta} \quad (4.49)$$

Applied to the data of the first reverse osmosis test of *CF*20 solution with the Polymem pilot (figure 4.17), diffusion coefficient of the surfactants in the membrane could be estimated (figure 4.19). The most diffusive compound seemed to be the Disponil[®] SOS 842, and diffusion coefficient were in the inverse order to average retention rates (table 4.17), except for the fluorinated surfactant and Simulsol[®] SL8 which had very close retention rates. The diffusion coefficients were not in the same order as elution in HPLC analysis with the C8 column (Section 3.2.1.3), especially for Tegotens[®] AM VSF, which was the second peak and had the lowest estimated diffusion coefficient. Assuming that mainly “hydrophobic” interactions took place between the surfactants and the stationary phase in HPLC elution, the different order of permeation through the membrane could indicate that additional phenomena could be present. The diffusion properties of surfactants in the membrane seemed to have a role in their rejection, especially for the Disponil[®] SOS 842, which was the most diffusive, the most adsorbed and the less rejected.

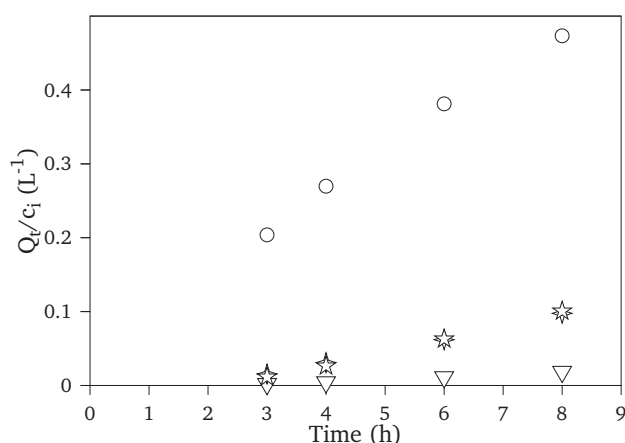


Figure 4.17: Time lag for surfactant permeation during the first test with the Polymem pilot (Section 4.4.3). ○: Disponil[®] SOS 842; ▽: Tegotens[®] AM VSF; ☆: Simulsol[®] SL8, ★: fluorinated surfactant.

Table 4.19: Linear regressions of data from figure 4.17 and diffusion coefficients estimation

	Disponil [®] SOS 842	Tegotens [®] AM VSF	Simulsol [®] SL8	Fluorinated surfactant
Slope	0.053	0.003	0.016	0.018
Intercept	−0.05	−0.008	−0.034	−0.044
R^2	0.995	0.996	0.998	0.998
θ (h)	0.9	2.7	2.1	2.4
D/l^2 (s^{-1})	$5 \cdot 10^{-5}$	$2 \cdot 10^{-5}$	$2 \cdot 10^{-5}$	$2 \cdot 10^{-5}$

Conclusion

Current knowledge about the separation mechanisms of small organic molecules in reverse osmosis has been reviewed, and rejection as well as flux decline were related to membrane, solution and solute properties. Polyamide and cellulose acetate membrane materials were screened in a flat sheet cell. The most appropriate membrane considering rejection was a smooth anti foulant thin film polyamide SG membrane, designed for brackish water. However, because of membrane fouling, there was a trade-off between high rejection and low flux decline. The SG membrane showed even better rejection properties in spiral-wound module with both real and model pretreated firefighting waters. Though the flux decline was high, it seemed to tend to an asymptote with the increasing concentration. The stabilities of rejection and flux decline were confirmed during longer tests on an industrial pilot with another fouling resistant thin film polyamide membrane for brackish water, a RE2540-FE membrane.

The flux declined caused by the surfactant mixtures was found linked to adsorption in two ways. The flux decline seemed mainly due to the adsorption of the anionic surfactant which showed the highest adsorption density in concentrated solutions. This surfactant also showed lowest rejection and highest diffusion properties. However, selective removal of this compound for purpose of flux enhancement, if desired, should be carefully studied. Indeed, with little or no anionic surfactant in the solutions, there would be more “free room” for the hydrophobic adsorption of the other surfactants on the membrane, which could decrease their rejections. The second link was *via* a model proposed to describe the flux decline as function of the fluorinated surfactant concentration, somehow representing the global surfactant concentration.

This model combined the resistance-in-series model to a Langmuir adsorption model by expressing the adsorption resistance as function of the retentate concentration. Though this model would require to be tuned on the basis of extended experimental data, it adequately described the flux decline with retentate concentration of the model pretreated firefighting water. Further work could be done on the subject *via* membrane surface characterization, and study of mixed adsorption as well as mixed micellization of surfactant mixtures.

In this chapter, solid data was gathered, such as the average rejection of the fluorinated surfactant in the industrial pilot which was 99.95%, and the permeability of the membrane

of $0.5 \text{ L h m}^{-2} \text{ bar}^{-1}$ with model solution representing pretreated firefighting water concentrated by a factor 20. This could allow the calculation of the area required for the mobile unit in a last chapter.

Chapter 5

Answers to the scientific and industrial purposes

Introduction

In chapter 1, two purposes were proposed. The industrial purpose was to find the most appropriate combination of processes to extract fluorinated surfactants from the firefighting water after a large scale fire event. The final mobile unit was expected to treat 4,000–10,000 m^3 in 3-6 months, leading to a waste containing concentrated fluorinated surfactant (FS) and to purified water containing less than $100 \mu g L^{-1}$ of FS. The chosen processes had to be compact, as autonomous as possible in raw materials and chemicals and easily automatable. The target firefighting water (FFW) chosen resulted from the extinguishment of apolar solvent with AFFF. The scientific purpose of this work was the study of the behavior of surfactants at interfaces in the context of two water treatment processes, namely electrocoagulation and reverse osmosis. In this chapter, the most important results on surfactants behavior during the tested processes are summed up and the design of the most important steps of the mobile unit is proposed.

5.1 Scientific purpose

In chapter 1, a helpful theoretical framework for this context was found in Van Oss theory decomposing the surface tension into its components: γ^{LW} the Lifshitz van der Waals

apolar surface tension component, and the Lewis acid-base (AB) polar components of the surface tension: γ^+ the electron acceptor and γ^- the electron donor components [127]. In condensed matter, LW interaction are always possible, even if both compounds are polar. AB interactions can occur only between compounds of opposite polarity able to share electron, *i.e.* between electron donor and electron acceptor compounds (figure 5.1).

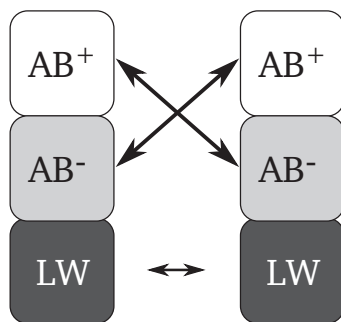


Figure 5.1: Apolar (LW) and polar (AB) interactions between two compounds. Self-interaction of water can be depicted this way.

5.1.1 Experimental context

The surface tension of water is especially high because of the dual polar character of this molecule (figure 5.1). This water cohesion leads to exclusion of compounds unable to participate its hydrogen bonding network. These compounds are “hydrophobic” because of their lack of polar AB character. However, this does not mean they do not interact with water: LW interactions persist in condensed phase. Hydrophilic compounds, on the contrary, can be monopolar, *e.g.* strictly electron donor or electron acceptor, or bipolar. Hydrophilic compounds have stronger AB interaction with water than with themselves, which leads to their aqueous solubilization.

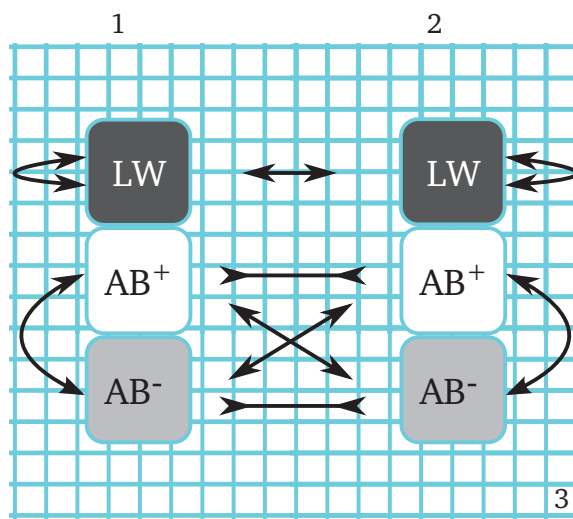


Figure 5.2: Interactions between compounds 1 and 2 immersed in a liquid 3. Interaction of 3 with 1 and 2, as well as 3–3 interactions are not depicted, but can be represented by the figure 5.1.

A representation of the different characters of the compounds encountered during this work is given in figure 5.3. Surfactant molecules are constituted of an apolar tail and a polar head. Surfactants present both apolar and polar characters but these are not evenly distributed in the molecules, instead they are strongly localized. Polar heads will always interact with water, but the distortion of the hydrogen bonding network due to their hydrophobic tail causes their exclusion from the bulk *via* adsorption at air–water or solid–water interfaces, and micellization when the CMC is reached. The adsorption at air–water interface loosens the water cohesion of this interface and results in the famous decrease of surface tension due to surfactants, which helps wetting. The adsorption of surfactants on solid surfaces and their ability to interact with oils or fats results in their cleaning properties.

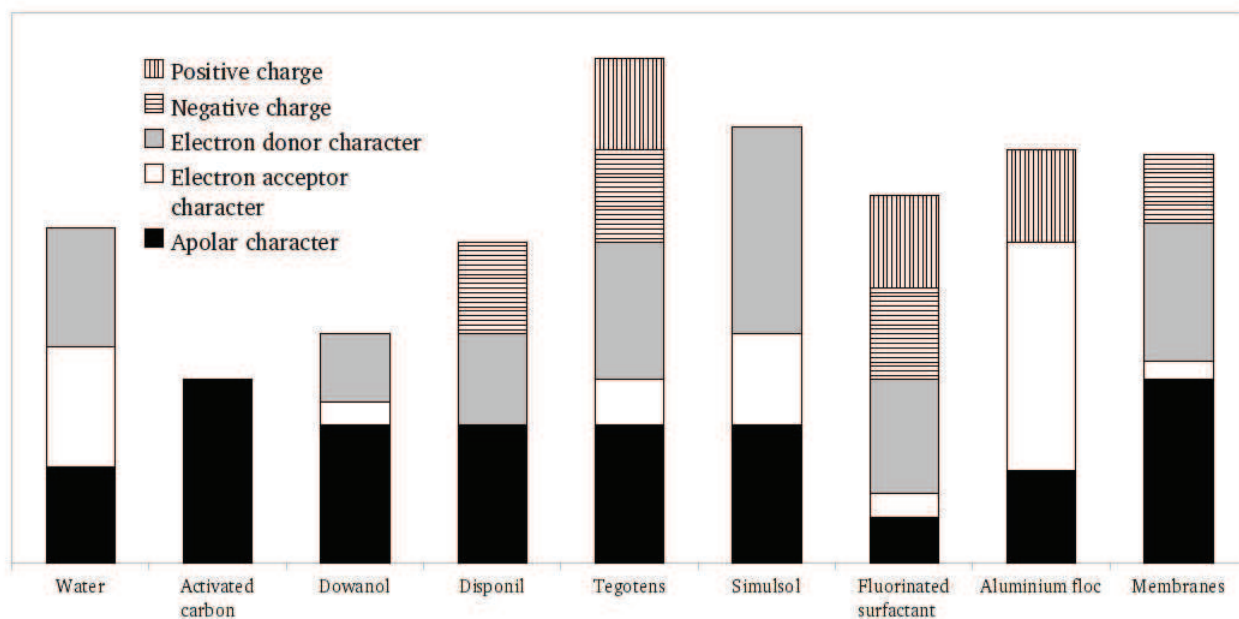


Figure 5.3: Schematic representation of the electrostatic, polar and apolar characters of the compound encountered during this work

Firefighting waters are aqueous mixtures of various surfactants. They may contain suspended matter, proteins and polymers. In this system, surfactants can be under the form of free monomers in water, involved in micelles if their concentration is higher than the CMC, adsorbed at the air–water interface or at the suspended matter–water interface.

5.1.2 The case of adsorption

In the context of pilot firefighting water, the suspended solids resulting from solvent combustion seemed to be apolar. The adsorption of surfactants was therefore expected to be the polar head towards water. The fluorinated surfactant was present at a concentration higher than its CMC, and a fraction of it was therefore involved in micelles. The tricky question of mixed micellization could not be deeply investigated in the course of this work. However, considering the driving forces resulting in micellization, micelles of fluorinated surfactants could also host some other hydrocarbon surfactants as they represent a hydrophobic medium. This could also be enhanced in case of favorable AB interactions between the polar heads of these surfactants. The same reflexion could also apply to mixed adsorption on hydrophobic solid surfaces. Indeed, adsorption isotherms of the fluorinated surfactant from model firefighting water solutions on activated carbon and ion non-functionalized ion exchange resin showed a

decrease of the adsorption density for high concentrations.

This was believed to result from replacement of the fluorinated surfactant, which has a low free monomer concentration – and therefore low activity – because of its low cmc, by other hydrocarbon surfactants having a higher activity because of their higher cmcs. The free monomer concentrations from ultrafiltration permeate of concentrated model fire-fighting water solution showed that the free monomer concentrations were of the order Disponil[®] SOS 842 >> Tegotens[®] AM VSF > Simulsol[®] SL8 >> fluorinated surfactant. The fluorinated surfactant therefore could be assumed to have the lowest activity for adsorption on hydrophobic solids and could be held back in micelles. Not only the fluorinated surfactant has low LW interaction ability because of its fluorinated tail, its polar head is also bipolar which could account for its higher self affinity under the form of micelles in water.

5.1.3 The case of electrocoagulation

Aluminium hydroxide floc from electrocoagulation is a Lewis acid and it is positively charged up to *pH* 9. It is therefore expected to have interactions with negatively charged components (which was observed with the anionic surfactant), but also with electron donor components. Electrocoagulation of activated carbon in water required more charge loading than in model firefighting water. The absence of fluorinated surfactant in the surfactants from the mixture seemed to stabilize the activated carbon. When the fluorinated surfactant concentration was lower than the CMC, the lower the concentration, the higher the required charge loading. When the fluorinated surfactant concentration was higher than the CMC, the higher the concentration, the higher the charge loading.

The activated carbon seemed to have a higher affinity with the floc when saturated by the fluorinated surfactant, but the excess of fluorinated surfactant micelles seemed to compete with the activated carbon for interactions with the floc. It seemed that either micellar or surface aggregates of fluorinated surfactant (surfactant aggregates could be mixed) had higher affinity with the floc than raw activated carbon. This could be explained by favorable AB interactions between the floc and the polar head of the surfactants, which density was higher in these aggregates.

5.1.4 The case of reverse osmosis

The most common nanofiltration and reverse osmosis membrane have a negative surface charge above their isoelectric point (pH 5–6), a strong electron donor character, a weak electron acceptor character and a stronger apolar character. According to the high adsorption density of the anionic surfactant during reverse osmosis experiments, the membrane–surfactants interactions seemed to occur mainly *via* hydrophobic interactions. The surfactant adsorption at the membrane surface appeared to be mixed, and the adsorption density seemed to be governed by the free monomer concentrations. The flux decline observed during reverse osmosis was, predictably, governed by the adsorption of surfactants. The fouling due to adsorption of the surfactant mixture was successfully described by a combination of the resistance-in-series and Langmuir adsorption models. For further membrane optimization, reverse osmosis membrane materials with γ^+ and γ^{LW} components as low as possible, and probably high surface charge as well as high electron donor character should be tested. Nevertheless, the data gathered during this thesis enabled the following scale-up.

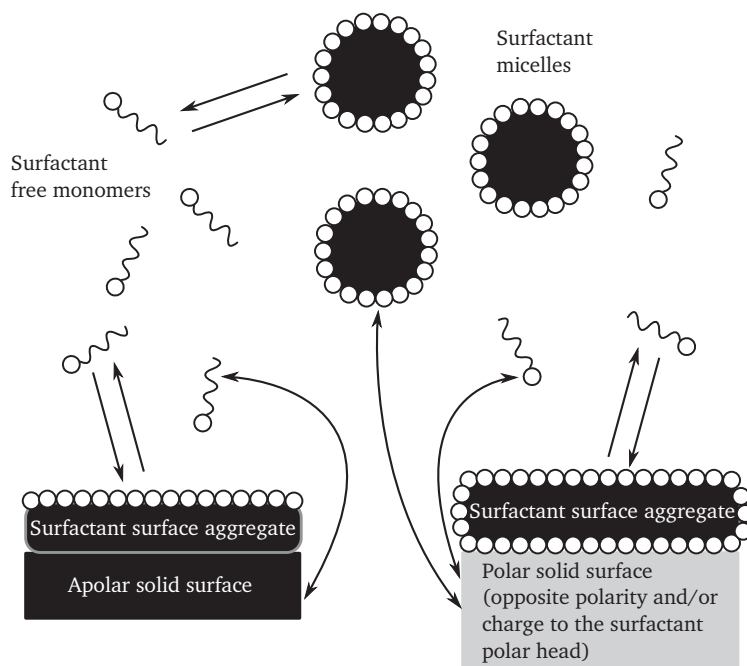


Figure 5.4: Interactions of surfactants with solid surfaces in aqueous media. At microscopic scales, some real solid surface such as reverse osmosis membranes could be a patchwork of polar and apolar zones. The possible mixed micellization and surface aggregation in surfactant mixtures is not represented.

5.2 Industrial scale-up

5.2.1 Industrial purpose

The typical firefighting water to treat has the composition described in table 5.1. In this design the objective was to treat $10,000\text{ m}^3$ in 5 months, representing a flow of $3,000\text{ L h}^{-1}$ 24/7. Cleaning and maintenance steps were ignored for this first design. After screening (chapter 2) and deeper study of selected processes (chapter 3 and 4), the first design of the mobile unit can be described in figure 5.5. The continuous mode is necessary for all steps. Optimal charge for electrocoagulation (EC) is 600 C L^{-1} corresponding to the consumption of 56 mg L^{-1} of metallic aluminium assuming a unity current efficiency. The optimal parameters for EC in Serep's Solvin[®] electrocoagulator are 15 A and 3 V .

Filtration is one possibility for floc segregation and could be done in continuous mode but could also be replaced by centrifugation or flotation depending on efficiency, compactness and cost (this part was out of the scope here). Reverse osmosis tested in conditions of Polymem pilot presented FS retention rate (R) and permeability respectively equal to 99.95 and $0.5\text{ L h}^{-1}\text{ m}^{-2}\text{ bar}^{-1}$, with a volume reduction ratio of 20 and a transmembrane pressure of 30 bar . Only one membrane was tested at pilot scale and new membranes with better permeability could be found. But these results can be used for the first design.

Table 5.1: Typical firefighting water composition

Compound	Concentration (mg L^{-1})
Dipropylene glycol methyl ether (Dowanol [®] DPM)	3,000
Sodium octyl sulfate (Disponil [®] 842)	1,000
Sodium caprylamphopropionate (Tegotens [®] AM VSF)	300
Octyl glucoside (Simulsol [®] SL8)	100
Fluorinated surfactant	80–140

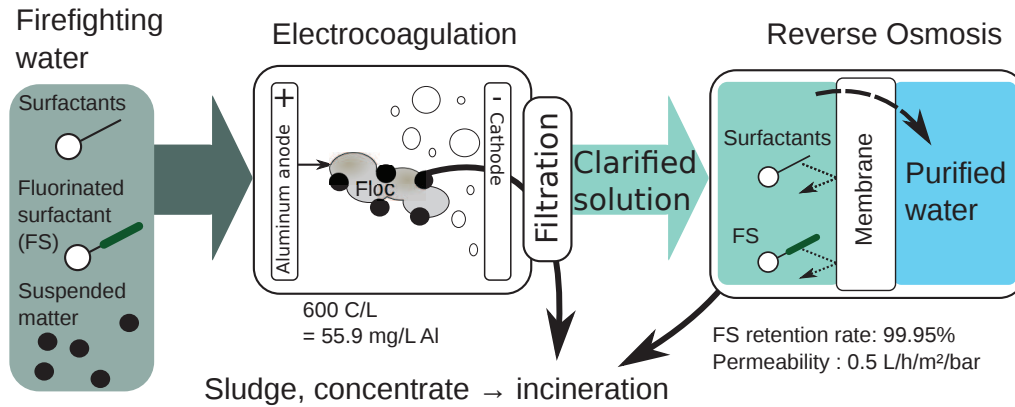


Figure 5.5: First design of the mobile unit

5.2.2 Results

The objective of this design is to calculate the mass of aluminium and the membrane area needed, and the retentate and permeate flow rates, the FS concentration in permeates, the mass of solid and liquid wastes. The flow sheet in figure 5.6 is considered. The loss of water in EC-floc segregation is neglected. FS concentration was assume to reduce to 80 mg L^{-1} during EC, as observed during Serep's test. This was the least favorable case of fluorinated surfactant concentration, as at the laboratory scale it was twice less. The final concentration in purified water must be $\leq 0.1 \text{ mg L}^{-1}$. Three options for the reverse osmosis are considered: the direct membrane filtration (option 1) or a two steps membrane filtration (option 2) to reach the target concentration in permeate, and the possibility of retentate recycling in EC (option 3). Permeate and retentate flow rates and retentate concentration depend on retention rate and chosen extraction factor (EF) according to equations described in section 4.1.1.2.

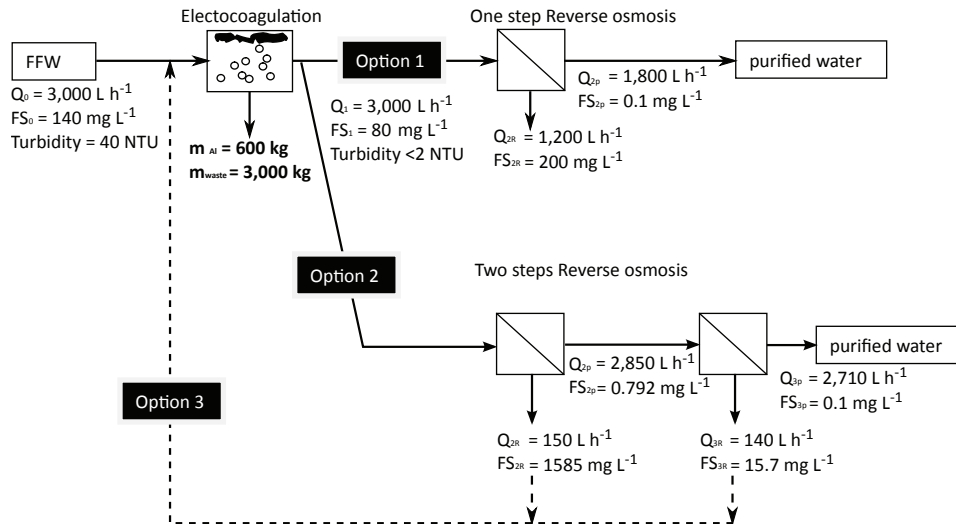


Figure 5.6: Flow sheet

5.2.2.1 Electrocoagulation

According to results described in chapter 3, 56 mg L^{-1} of metallic aluminium are needed. So to treat $10,000 \text{ m}^3$ an average mass of 600 kg Al will be necessary. Considering that the floc contains mostly $Al(OH)_3$, and that particles to remove have a negligible mass compared to the mass of aluminium hydroxide, the mass of dried solid waste will be equal to 1733 kg . The waste will not be dried after filtration and it will contain water. With a dried extract of 60% (mass of solid/mass total of waste), the real mass of waste would represent 2890 kg .

5.2.2.2 Membrane processes

To reach 0.1 mg L^{-1} in one step with R equal to 0.9995, the maximum extraction factor can be calculated with equation 5.1 for option 1 and equation 5.2 for option 2. Maximum EF for option 1 and for option 2 are respectively equal to 0.6 and 0.986. The first option is experimentally reachable but the second one would lead to a very high concentration in first retentate and viscosity could rise in dramatic manner. That is why a lower EF equal to 19/20 was selected for calculations in option 2. But further optimization of EF could be realized. Design results are presented in table 5.2 and the two options are represented in figure 5.6.

Option 1:

$$EF = \frac{1}{R} \left(1 - (1 - R) \frac{FS_1}{FS_{2p}} \right) \quad (5.1)$$

Option 2:

$$EF = \frac{1}{R} \left(1 - (1 - R) \sqrt{\frac{FS_1}{FS_{2p}}} \right) \quad (5.2)$$

Table 5.2: Design results for membrane processes with one step of reverse osmosis (option 1) or two steps (option 2)

Option 1		Option 2			
Step 1		Step 1		Step 2	
EF	0.6	EF	0.95	EF	0.95
FS_{2p}	0.1 mg L^{-1}	FS_{2p}	0.792 mg L^{-1}	FS_{3p}	0.008 mg L^{-1}
FS_{2R}	200 mg L^{-1}	FS_{2R}	1585 mg L^{-1}	FS_{3R}	15.7 mg L^{-1}
Q_{2p}	$1.80 \text{ m}^3 \text{ h}^{-1}$	Q_{2p}	$2.85 \text{ m}^3 \text{ h}^{-1}$	Q_{3p}	$2.71 \text{ m}^3 \text{ h}^{-1}$
Q_{2R}	$1.20 \text{ m}^3 \text{ h}^{-1}$	Q_{2R}	$0.15 \text{ m}^3 \text{ h}^{-1}$	Q_{3R}	$0.14 \text{ m}^3 \text{ h}^{-1}$
A	120 m^2	A_2	190 m^2	A_2	180 m^2

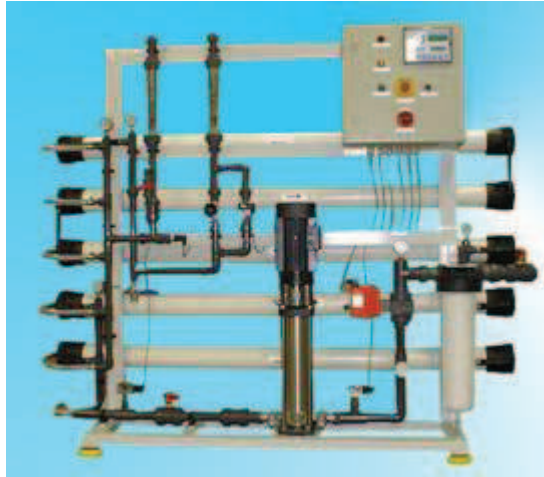
5.2.3 Discussion

Option 1 permits to reach the limit with 40% of the water rejected and sent to incineration. Necessary area is 120 m^2 . Option 2 permits to reach a lower concentration than the decided limit and to incinerate only 1/10 of the fire fighting water. But a membrane area of 370 m^2 is needed. The recycling of retentate Q_{3R} into the feed of the first RO step could still minimize the volume to incinerate to approximately 1/20. The high concentration of FS_{2R} was not tested experimentally and could result in a higher viscosity as well as lower permeability. Some work for industrial optimization remains to be done, as FS_{2R} depends on several factors such as the concentration at the output of electrocoagulation or the chosen extraction factor.

Option 3 could be interesting because it would lead to only one outlet of FS in EC solid waste; but according to chapter 3 results, if the FS is too important, the aluminium consumption becomes more important. An economic study should be realized to make an objective choice but with the actual knowledge, this option will not be proposed. A combination of option 1 at a higher EF , combined with adsorption could also be considered.

However, due to the current lack of knowledge about adsorption on columns as well as supply in adsorbent, this potential solution will not be proposed either.

According to membrane suppliers, with classical industrial modules of 80×4 inches (2 *m* length, 10 *cm* of diameter), option 1 would require 4 modules and option 2 10 modules. This still represents a compact process, small enough to enter a container. Examples of medium reverse osmosis plant for up to 3.5 $m^3 h^{-1}$, are presented by several suppliers. For example, Polymem and Lenntech propose plant containerization.



(a) Medium reverse osmosis plant for up to 3.5 m³ h⁻¹, Lenntech, Size: 2.7m length, 0.8m large, 1.8m high. 4 KW. Source: <http://www.lenntech.com>



(b) Containerizable reverse osmosis plant. Source: <http://www.lenntech.com>



(c) Containerizable reverse osmosis plant. Source: <http://www.polymem.fr>

Figure 5.7: Examples of compact containerizable membrane processes plants. a) and b): Lenntech, c) Polymem

The actual cost for incineration is 1 € kg⁻¹. Prices for wastes incineration with and

without treatment are summed up in table 5.3. The economy realized for incineration will have to be compared to investment and operation costs (energy and material consumption, cleaning operations, human costs) of the treatment unit. More detailed information should be asked to process suppliers.

Table 5.3: Costs of incineration

	Raw firefighting water	Option 1	Option 2
Mass of liquid (T)	10,000	4,000	500
Mass of solid (T)	0	3	3
Price (k€)	10,000	4,000	503

Conclusion

The theoretical framework of this thesis was summed-up. The decomposition of surface tension into its polar and apolar components provided useful information to describe the phenomena observed during adsorption, electrocoagulation and reverse osmosis of surfactant-containing firefighting waters. An industrial scale-up was proposed on the basis of the results collected during this work. The mobile unit should be constituted of an electrocoagulator and two successive steps of reverse osmosis. The answers proposed to the scientific issues encountered should be useful for industrial optimization of the unit.

General conclusion

The use of firefighting foams during large scale industrial fires of liquid hydrocarbon implies a treatment of the resulting firefighting waters. At the moment of this work, these waters are treated by incineration in halogen-resistant incinerators, which is expensive not only because of the process itself, but also because of the shipping of large amounts of water – up to $20,000\text{ m}^3$ – to adequate incinerators. Firefighting foams are made of water, air, additives and mixtures of surfactants which may contain various hydrocarbon and fluorinated surfactants. These foams are specially formulated to spread over the surface of burning liquids and fluorinated surfactants, which are able to highly reduce the water surface tension, play a key role in the efficiency of firefighting foams. The need for specific firefighting water treatment is due to presence of surfactants, and to the high chemical and thermal resistance of fluorinated surfactant resulting from the particular chemistry of these chemicals. The industrial aim of this work was to propose an alternative process for the firefighting waters, which requirements were not only efficiency in minimization of the amounts of matter to incinerate, but also compactness and material sobriety to enable its mobility.

Because of their intrinsic surface properties and chemical purpose, the study of water treatment processes in the context of surfactant solutions could not be done without a proper understanding of the behavior of these chemicals with interfaces. In chapter 1, the notions of interfacial tension, intermolecular interactions and adsorption have been introduced. These interactions can be electrostatic, apolar in the Lifshitz-van der Waals sense (LW) or polar in the Lewis acid-base sense (AB). The behavior of two compounds immersed in water not only depends of the interaction between these two compounds, but also on their interactions with water, as well on the interaction of water with itself. As all these kinds of interaction can occur simultaneously, the assimilation of hydrophobic compound to apolarity and hydrophilic

compounds to ionic or polar components was not always satisfying to describe the behavior of surfactants in water treatment processes, and for this purpose, the decomposition of surface tension into its apolar and polar components was of great help.

Due to the great variety of actual firefighting waters, the experimental work was mainly done with model and pilot solution. These solutions were standardized experimental approximations of water resulting from the extinguishment of n-heptane fires with an aqueous film forming foam (AFFF). In chapter 2, relevant processes identified in a bibliographic study were screened. After this screening, pilot firefighting waters appeared to require a pretreatment step for the removal of suspended matter, and a treatment step for water purification. Given the industrial constraints for the mobile unit, electrocoagulation and reverse osmosis were chosen for the pretreatment and treatment steps respectively.

Electrocoagulation was deepened in chapter 3. An optimal charge loading of 600 C L^{-1} , or an aluminium dose of at least 55.9 mg L^{-1} , was found for pilot firefighting water. This process was found to remove efficiently the unwanted suspended matter from pilot firefighting waters. Reverse osmosis was deepened in chapter 4. The most appropriate membranes for fluorinated surfactant rejection were fouling resistant thin film polyamide membranes, with rejection rates near 99.95%. The permeability for model solutions with a concentration factor of 20 was near $0.5\text{ L h}^{-1}\text{ m}^{-2}\text{ bar}^{-1}$.

The data collected in chapters 3 and 4 enabled to propose answers to the industrial and scientific purposes. A scale-up of a mobile unit constituted of an electrocoagulation step and two successive reverse osmosis steps was established. For the treatment of $10,000\text{ m}^3$ of firefighting water at a rate of $3\text{ m}^3\text{ h}^{-1}$, this unit would consume 600 kg of aluminium and require a total area of 370 m^2 . The resulting matter to incinerate was estimated to $3,000\text{ kg}$ of solid and 500 m^3 of liquid. In addition, mechanisms could be proposed for the observed phenomenon that occurred during both of these processes. After these results, further work could be done in both industrial and scientific fields. The proposed mechanisms could help the industrial optimization of the unit, and reverse osmosis could be studied with a higher focus on the membrane surface modifications.

References

List of publications

7th World Surfactants Congress (CESIO 2008), Paris: E. Couallier, M. Rakib, C. Baudequin, R. Severac, M. Pabon, Separation of fluorinated surfactants from firefighting water by membrane processes (oral presentation)

International Congress of Membranes (ICOM 2011), Amsterdam : C. Baudequin, E. Couallier, M. Rakib, I. Deguerry, R. Severac, M. Pabon, Fouling of RO membrane by hydrocarbonated and fluorinated surfactants contained in firefighting water: measure and characterisation (oral presentation)

C. Baudequin, E. Couallier, M. Rakib, I. Deguerry, R. Severac and Martial Pabon, Purification of firefighting water containing a fluorinated surfactant by reverse osmosis coupled to electrocoagulation-filtration, Separation and Purification Technology (2011), pp. 275 - 282

Bibliography

- [1] H. HSE, S. Executive, Buncefield Incident 11 December 2005: The Final Report of the Major Incident Investigation Board, HSE Books, 2008.
- [2] M. Pabon, J. M. Corpart, Fluorinated surfactants: synthesis, properties, effluent treatment, *Journal of Fluorine Chemistry* 114 (2) (2002) 149 – 156.
- [3] P.-G. de Gennes, F. Brochard-Wyart, D. Quéré, *Gouttes, bulles, perles et ondes*, Belin, 2002.
- [4] D. F. Evans, H. Wennerström, *The Colloidal Domain: Where Physics, Chemistry, Biology, and Technology Meet*, 2nd Edition, Wiley-VCH Verlag GmbH, 1999.
- [5] M. J. Rosen, *Surfactants and Interfacial Phenomena*, Third Edition, John Wiley and Sons, Inc., 2004.
- [6] C. J. van Oss, Development and applications of the interfacial tension between water and organic or biological surfaces, *Colloids and Surfaces B: Biointerfaces* 54 (1) (2007) 2 – 9.
- [7] C. Sheindorf, M. Rebhun, M. Sheintuch, A freundlich-type multicomponent isotherm, *Journal of Colloid and Interface Science* 79 (1) (1981) 136 – 142.
- [8] J. N. Israelachvili, *Intermolecular and Surfaces Forces*, Elsevier Science, 1991.
- [9] R. Nagarajan, E. Ruckenstein, Theory of surfactant self-assembly: a predictive molecular thermodynamic approach, *Langmuir* 7 (12) (1991) 2934–2969.

- [10] R. A. Johnson, R. Nagarajan, Modeling self-assembly of surfactants at solid/liquid interfaces. i. hydrophobic surfaces, *Colloids and Surfaces A: Physicochemical and Engineering Aspects* 167 (1-2) (2000) 31 – 46.
- [11] R. Zhang, P. Somasundaran, Advances in adsorption of surfactants and their mixtures at solid-solution interfaces, *Advances in Colloid and Interface Science* 123-126 (SPEC ISS) (2006) 213 – 229.
- [12] F. Tiberg, J. Brinck, L. Grant, Adsorption and surface-induced self-assembly of surfactants at the solid-aqueous interface, *Current Opinion in Colloid & Interface Science* 4 (6) (1999) 411 – 419.
- [13] C. A. Moody, J. A. Field, Perfluorinated surfactants and the environmental implications of their use in fire-fighting foams, *Environmental Science & Technology* 34 (18) (2000) 3864–3870.
- [14] R. Ma, K. Shih, Perfluorochemicals in wastewater treatment plants and sediments in hong kong, *Environmental Pollution* 158 (5) (2010) 1354 – 1362.
- [15] H.-J. Lehmler, Synthesis of environmentally relevant fluorinated surfactants—a review, *Chemosphere* 58 (11) (2005) 1471 – 1496.
- [16] J. P. Giesy, K. Kannan, Perfluorochemical surfactants in the environment, *Environmental Science & Technology* 36 (7) (2002) 146A–152A, PMID: 11999053.
- [17] D. R. Lide, *Hanbook of Chemistry an Physics*, 76th, CRC Press, 1995.
- [18] W. R. Dolbier, Structure, reactivity, and chemistry of fluoroalkyl radicals, *Chemical Reviews* 96 (5) (1996) 1557–1584.
- [19] J. H. Clint, Micellization of mixed nonionic surface active agents, *J. Chem. Soc., Faraday Trans. 1* 71 (1975) 1327–1334.
- [20] D. Rubingh, *Solution Chemistry of Surfactants*, Springer, 1979.
- [21] P. M. Holland, D. N. Rubingh, *Mixed Surfactant Systems*, American Chemical Society, 1992.

- [22] G. Sugihara, S. Nagadome, S.-W. Oh, J.-S. Ko, A review of recent studies on aqueous binary mixed surfactant systems, *Journal of Oleo Science* 57 (2) (2008) 61–92.
- [23] H. Akbas, M. Iscan, T. Sidim, Composition of mixed anionic/nonionic surfactant micelles, *Journal of Surfactants and Detergents* 3 (1) (2000) 77–80.
- [24] T. P. Goloub, R. J. Pugh, B. V. Zhmud, Micellar interactions in nonionic/ionic mixed surfactant systems, *Journal of Colloid and Interface Science* 229 (1) (2000) 72–81.
- [25] K. Danov, S. Kralchevska, P. Kralchevsky, K. Ananthapadmanabhan, A. Lips, Mixed solutions of anionic and zwitterionic surfactant (betaine): Surface-tension isotherms, adsorption, and relaxation kinetics, *Langmuir* 20 (13) (2004) 5445 – 5453.
- [26] P. Mukerjee, A. Y. S. Yang, Nonideality of mixing of micelles of fluorocarbon and hydrocarbon surfactants and evidence of partial miscibility from differential conductance data, *Journal of Physical Chemistry* 80 (12) (1976) 1388–1390.
- [27] L. Nordstierna, I. Furo, P. Stilbs, Mixed micelles of fluorinated and hydrogenated surfactants, *Journal of the American Chemical Society* 128 (20) (2006) 6704–6712.
- [28] L. Nordstierna, I. Furo, P. Stilbs, Mixed adsorption of fluorinated and hydrogenated surfactants, *Langmuir* 22 (19) (2006) 7969–7974.
- [29] M. Amato, E. Caponetti, D. Martino, L. Pedone, 1h and 19f nmr investigation on mixed hydrocarbon-fluorocarbon micelles, *Journal of Physical Chemistry B* 107 (37) (2003) 10048–10056.
- [30] P. Barthelemy, V. Tomao, J. Selb, Y. Chaudier, B. Pucci, Fluorocarbon-hydrocarbon nonionic surfactants mixtures: A study of their miscibility, *Langmuir* 18 (7) (2002) 2557–2563.
- [31] J. Szymanowski, J. Blaszcak, A. Sobczynska, B. Twardochleb, E. Meissner, Surface activity of surfactant mixtures containing fluorinated amphiphiles, *Tenside, Surfactants, Detergents* 38 (6) (2001) 368 – 372.

- [32] D. Varade, C. Rodriguez-Abreu, L. Shrestha, K. Aramaki, Wormlike micelles in mixed surfactant systems: Effect of cosolvents, *Journal of Physical Chemistry B* 111 (35) (2007) 10438–10447.
- [33] R. G. Shrestha, L. K. Shrestha, K. Aramaki, Formation of wormlike micelle in a mixed amino-acid based anionic surfactant and cationic surfactant systems, *Journal of Colloid and Interface Science* 311 (1) (2007) 276–284.
- [34] R. G. Shrestha, L. K. Shrestha, K. Aramaki, Wormlike micelles in mixed amino acid-based anionic/nonionic surfactant systems, *Journal of Colloid and Interface Science* 322 (2) (2008) 596–604.
- [35] E. Blanco, J. M. Ruso, G. Prieto, F. Sarmiento, On relationships between surfactant type and globular proteins interactions in solution, *Journal of Colloid and Interface Science* 316 (1) (2007) 37 – 42.
- [36] R.-C. Lu, A.-N. Cao, L.-H. Lai, J.-X. Xiao, Protein-surfactant interaction: Differences between fluorinated and hydrogenated surfactants, *Colloids and Surfaces B: Biointerfaces* 64 (1) (2008) 98 – 103.
- [37] M. G. Semenova, L. E. Belyakova, Y. N. Polikarpov, I. Stankovic, A. S. Antipova, M. S. Anokhina, Analysis of light scattering data on the sodium caseinate assembly as a response to the interactions with likely charged anionic surfactant, *Food Hydrocolloids* 21 (5-6) (2007) 704–715.
- [38] M. Tsianou, P. Alexandridis, Surfactant–Polymer interactions, in *Mixed Surfactant Systems*, Marcel Dekker (New York), 2005 2nd Ed., Rev. and Expanded, Ch. 18, p. 657.
- [39] E. Kissa, *Fluorinated Surfactants: Synthesis, Properties, Applications*, Vol. 50, Surfactant Science Series, 1994.
- [40] M. M. Schultz, C. P. Higgins, C. A. Huset, R. G. Luthy, D. F. Barofsky, J. A. Field, Fluorochemical mass flows in a municipal wastewater treatment facility, *Environmental Science & Technology* 40 (23) (2006) 7350–7357.

- [41] C. Kunacheva, S. Tanaka, S. Fujii, S. K. Boontanon, C. Musirat, T. Wongwattana, B. R. Shivakoti, Mass flows of perfluorinated compounds (pfcs) in central wastewater treatment plants of industrial zones in thailand, *Chemosphere* 83 (6) (2011) 737 – 744.
- [42] J. Thompson, G. Eaglesham, J. Reungoat, Y. Poussade, M. Bartkow, M. Lawrence, J. F. Mueller, Removal of pfos, pfoa and other perfluoroalkyl acids at water reclamation plants in south east queensland australia, *Chemosphere* 82 (1) (2011) 9 – 17.
- [43] J. Hermia, Constant pressure blocking filtration laws - application to power-law non-newtonian fluids, *Transactions of the American Institute of Chemical Engineers* 60 (1982) 183–187.
- [44] G. T. F. B. Metcalf & Eddy, Inc, *Wastewater Engineering Treatment Disposal Reuse*, McGraw-Hill Inc.,US, 1990.
- [45] J. Duan, J. Gregory, Coagulation by hydrolysing metal salts, *Advances in Colloid and Interface Science* 100-102 (2003) 475–502.
- [46] P. Moussas, A. Zouboulis, A study on the properties and coagulation behaviour of modified inorganic polymeric coagulant–polyferric silicate sulphate (pfsis), *Separation and Purification Technology* 63 (2) (2008) 475 – 483.
- [47] S. Haydar, J. A. Aziz, Coagulation-flocculation studies of tannery wastewater using combination of alum with cationic and anionic polymers, *Journal of Hazardous Materials* 168 (2-3) (2009) 1035 – 1040.
- [48] T. Chatterjee, S. Chatterjee, D. S. Lee, M. W. Lee, S. H. Woo, Coagulation of soil suspensions containing nonionic or anionic surfactants using chitosan, polyacrylamide, and polyaluminium chloride, *Chemosphere* 75 (10) (2009) 1307 – 1314.
- [49] J. Ge, J. Qu, P. Lei, H. Liu, New bipolar electrocoagulation-electroflotation process for the treatment of laundry wastewater, *Separation and Purification Technology* 36 (1) (2004) 33 – 39.

- [50] E. Yüksel, I. A. Sengil, M. Özacar, The removal of sodium dodecyl sulfate in synthetic wastewater by peroxi-electrocoagulation method, *Chemical Engineering Journal* 152 (2009) 347 – 353.
- [51] E. Onder, A. S. Koparal, U. B. Ogutveren, An alternative method for the removal of surfactants from water: Electrochemical coagulation, *Separation and Purification Technology* 52 (3) (2007) 527 – 532.
- [52] Q. Zhang, S. Deng, G. Yu, J. Huang, Removal of perfluorooctane sulfonate from aqueous solution by crosslinked chitosan beads: Sorption kinetics and uptake mechanism, *Bioresource Technology* 102 (3) (2011) 2265 – 2271.
- [53] C. Cachet, M. Keddam, V. Mariotte, R. Wiart, Adsorption of perfluorinated surfactants on gold electrodes-ii. behaviour of ionic compounds, *Electrochimica Acta*, 35 (15) (1993) 2203 – 2208.
- [54] V. Ochoa-Herrera, R. Sierra-Alvarez, Removal of perfluorinated surfactants by sorption onto granular activated carbon, zeolite and sludge, *Chemosphere* 72 (10) (2008) 1588 – 1593.
- [55] S. Deng, Q. Zhou, G. Yu, J. Huang, Q. Fan, Removal of perfluorooctanoate from surface water by polyaluminium chloride coagulation, *Water Research* 45 (4) (2011) 1774 – 1780.
- [56] Q. Yu, S. Deng, G. Yu, Selective removal of perfluorooctane sulfonate from aqueous solution using chitosan-based molecularly imprinted polymer adsorbents, *Water Research* 42 (12) (2008) 3089 – 3097.
- [57] Q. Yu, R. Zhang, S. Deng, J. Huang, G. Yu, Sorption of perfluorooctane sulfonate and perfluorooctanoate on activated carbons and resin: Kinetic and isotherm study, *Water Research* 43 (4) (2009) 1150 – 1158.
- [58] D. J. Lampert, M. A. Frisch, G. E. Speitel Jr., Removal of perfluorooctanoic acid and perfluorooctane sulfonate from wastewater by ion exchange, *Practice Periodical of Hazardous, Toxic, and Radioactive Waste Management* 11 (1) (2007) 60 – 68.

- [59] Y. Qu, C. Zhang, F. Li, X. Bo, G. Liu, Q. Zhou, Equilibrium and kinetics study on the adsorption of perfluorooctanoic acid from aqueous solution onto powdered activated carbon, *Journal of Hazardous Materials* 169 (1-3) (2009) 146 – 152.
- [60] S. Senevirathna, S. Tanaka, S. Fujii, C. Kunacheva, H. Harada, B. Ariyadasa, B. Shivakoti, Adsorption of perfluorooctane sulfonate (n-pfos) onto non ion-exchange polymers and granular activated carbon: Batch and column test, *Desalination* 260 (1-3) (2010) 29 – 33.
- [61] S. Senevirathna, S. Tanaka, S. Fujii, C. Kunacheva, H. Harada, B. Shivakoti, R. Okamoto, A comparative study of adsorption of perfluorooctane sulfonate (pfos) onto granular activated carbon, ion-exchange polymers and non-ion-exchange polymers, *Chemosphere* 80 (6) (2010) 647 – 651.
- [62] P. Aimar, Filtration membranaire (oi, nf uf), mise en œuvre et performance, Tech. Rep. J2793, *Techniques de l'Ingénieur* (2006).
- [63] R. Urbanski, E. Goralska, H.-J. Bart, J. Szymanowski, Ultrafiltration of surfactant solutions, *Journal of Colloid and Interface Science* 253 (2) (2002) 419 – 426.
- [64] I. Escudero, M. Ruiz, J. Benito, J. Cabezas, D. Dominguez, J. Coca, Recovery of [alpha]-phenylglycine by micellar extractive ultrafiltration, *Chemical Engineering Research and Design* 84 (7) (2006) 610–616.
- [65] Y. Kaya, C. Aydiner, H. Barlas, B. Keskinler, Nanofiltration of single and mixture solutions containing anionics and nonionic surfactants below their critical micelle concentrations (cmcs), *Journal of Membrane Science* 282 (1-2) (2006) 401 – 412.
- [66] C. Tang, Q. Fu, A. Robertson, C. Criddle, J. Leckie, Use of reverse osmosis membranes to remove perfluorooctane sulfonate (pfos) from semiconductor wastewater, *Environmental Science & Technology* 40 (23) (2006) 7343–7349.
- [67] C. Tang, Q. Fu, C. Criddle, J. Leckie, Effect of flux (transmembrane pressure) and membrane properties on fouling and rejection of reverse osmosis and nanofiltration membranes treating perfluorooctane sulfonate containing wastewater, *Environmental Science & Technology* 41 (6) (2007) 2008–2014.

- [68] E. Steinle-Darling, M. Reinhard, Nanofiltration for trace organic contaminant removal: Structure, solution, and membrane fouling effects on the rejection of perfluorochemicals, *Environmental Science & Technology* 42 (14) (2008) 5292–5297.
- [69] H. F. Schröder, R. J. Meesters, Stability of fluorinated surfactants in advanced oxidation processes—a follow up of degradation products using flow injection-mass spectrometry, liquid chromatography-mass spectrometry and liquid chromatography-multiple stage mass spectrometry, *Journal of Chromatography A* 1082 (1) (2005) 110–119.
- [70] S. C. Panchangam, A. Y.-C. Lin, K. L. Shaik, C.-F. Lin, Decomposition of perfluorocarboxylic acids (pfcas) by heterogeneous photocatalysis in acidic aqueous medium, *Chemosphere* 77 (2) (2009) 242 – 248.
- [71] H. Hori, E. Hayakawa, K. Koike, H. Einaga, T. Ibusuki, Decomposition of nonafluoropentanoic acid by heteropolyacid photocatalyst $\text{H}_3\text{PW}_{12}\text{O}_{40}$ in aqueous solution, *Journal of Molecular Catalysis A: Chemical* 211 (1-2) (2004) 35 – 41.
- [72] H. Hori, A. Yamamoto, K. Koike, S. Kutsuna, I. Osaka, R. Arakawa, Photochemical decomposition of environmentally persistent short-chain perfluorocarboxylic acids in water mediated by iron(ii)/(iii) redox reactions, *Chemosphere* 68 (3) (2007) 572 – 578.
- [73] C. D. Vecitis, H. Park, J. Cheng, B. T. Mader, M. R. Hoffmann, Kinetics and mechanism of the sonolytic conversion of the aqueous perfluorinated surfactants, perfluorooctanoate (pfoa), and perfluorooctane sulfonate (pfos) into inorganic products, *Journal of Physical Chemistry A* 112 (18) (2008) 4261 – 4270.
- [74] S. C. Panchangam, A. Y.-C. Lin, J.-H. Tsai, C.-F. Lin, Sonication-assisted photocatalytic decomposition of perfluorooctanoic acid, *Chemosphere* 75 (5) (2009) 654 – 660.
- [75] P. Théron, P. Pichat, C. Guillard, C. Pétrier, T. Chopin, Degradation of phenyltrifluoromethylketone in water by separate or simultaneous use of TiO_2 photocatalysis and 30 or 515 khz ultrasound, *Phys. Chem. Chem. Phys.* 1 (19) (1999) 4663–4668.

- [76] R. Dillert, D. Bahnemann, H. Hidaka, Light-induced degradation of perfluorocarboxylic acids in the presence of titanium dioxide, *Chemosphere* 67 (4) (2007) 785 – 792.
- [77] J. Eastoe, A. Dupont, D. C. Steytler, Fluorinated surfactants in supercritical co₂, *Current Opinion in Colloid & Interface Science* 8 (3) (2003) 267 – 273.
- [78] E. Goetheer, M. Vorstman, J. Keurentjes, Opportunities for process intensification using reverse micelles in liquid and supercritical carbon dioxide, *Chemical Engineering Science* 54 (10) (1999) 1589 – 1596.
- [79] N. U. Soriano Jr., R. Venditti, C. D. Saquing, D. Bushey, D. S. Argyropoulos, Solubilizing amino acids and polypeptides in supercritical co₂ via reverse micelle formation, *Colloids and Surfaces A: Physicochemical and Engineering Aspects* 315 (1-3) (2008) 110–116.
- [80] B. G. Lipták, *Instrument Engineers' Handbook: Process measurement and analysis*, CRC Press, 2003.
- [81] X. Liu, C. A. Pohl, J. Weiss, New polar-embedded stationary phase for surfactant analysis, *Journal of Chromatography A* 1118 (1) (2006) 29 – 34, 18th Annual International Ion Chromatography Symposium.
- [82] H. S. Park, H. R. Ryu, C. K. Rhee, Simultaneous separation of nine surfactants of various types by hplc with evaporative light scattering detection, *Talanta* 70 (3) (2006) 481 – 484.
- [83] S. H. Im, Y. H. Jeong, J. J. Ryoo, Simultaneous analysis of anionic, amphoteric, non-ionic and cationic surfactant mixtures in shampoo and hair conditioner by rp-hplc/elsd and lc/ms, *Analytica Chimica Acta* 619 (1) (2008) 129 – 136, papers presented at the 9th Asian Conference on Analytical Chemistry (Asianalysis IX) - 9th Asianalysis 2007.
- [84] S. Heron, M.-G. Maloumbi, M. Dreux, E. Verette, A. Tchaplal, Method development for a quantitative analysis performed without any standard using an evaporative light-scattering detector, *Journal of Chromatography A* 1161 (1-2) (2007) 152 – 156, 26th International Symposium on the Separation of Proteins, Peptides and Polynucleotides,

26th International Symposium on the Separation of Proteins, Peptides and Polynucleotides.

- [85] G. Chen, Electrochemical technologies in wastewater treatment, *Separation and Purification Technology* 38 (1) (2004) 11 – 41.
- [86] M. Carmona, M. Khemis, J.-P. Leclerc, F. Lapique, A simple model to predict the removal of oil suspensions from water using the electrocoagulation technique, *Chemical Engineering Science* 61 (4) (2006) 1237 – 1246.
- [87] P. K. Holt, Electrocoagulation: Unravelling and synthesising the mechanisms behind a water treatment process, Ph.D. thesis, University of Sydney. *Chemical Engineering* (2003).
- [88] M. M. Emamjomeh, M. Sivakumar, Review of pollutants removed by electrocoagulation and electrocoagulation/flotation processes, *Journal Of Environmental Management* 90 (5) (2009) 1663–1679.
- [89] A. Aouni, C. Fersi, M. B. S. Ali, M. Dhahbi, Treatment of textile wastewater by a hybrid electrocoagulation/nanofiltration process, *Journal of Hazardous Materials* 168 (2-3) (2009) 868 – 874.
- [90] O. Can, M. Kobya, E. Demirbas, M. Bayramoglu, Treatment of the textile wastewater by combined electrocoagulation, *Chemosphere* 62 (2) (2006) 181 – 187.
- [91] M. Kobya, O. T. Can, M. Bayramoglu, Treatment of textile wastewaters by electrocoagulation using iron and aluminum electrodes, *Journal Of Hazardous Materials* 100 (1-3) (2003) 163–178.
- [92] A. Essadki, M. Bennajah, B. Gourich, C. Vial, M. Azzi, H. Delmas, Electrocoagulation/electroflotation in an external-loop airlift reactor–application to the decolorization of textile dye wastewater: A case study, *Chemical Engineering and Processing: Process Intensification* 47 (8) (2008) 1211 – 1223.
- [93] A. Gürses, M. Yalçın, C. Dogar, Electrocoagulation of some reactive dyes: a statistical investigation of some electrochemical variables, *Waste Management* 22 (5) (2002) 491–499.

- [94] N. Daneshvar, A. Oladegaragoze, N. Djafarzadeh, Decolorization of basic dye solutions by electrocoagulation: An investigation of the effect of operational parameters, *Journal of Hazardous Materials* 129 (1-3) (2006) 116–122.
- [95] I. Linares-Hernandez, C. Barrera-Diaz, G. Roa-Morales, B. Bilyeu, F. Urena-Nunez, A combined electrocoagulation-sorption process applied to mixed industrial wastewater, *Journal of Hazardous Materials* 144 (1-2) (2007) 240 – 248.
- [96] M. Khemis, J.-P. Leclerc, G. Tanguy, G. Valentin, F. Lapique, Treatment of industrial liquid wastes by electrocoagulation: Experimental investigations and an overall interpretation model, *Chemical Engineering Science* 61 (11) (2006) 3602 – 3609.
- [97] M. Zaied, N. Bellakhal, Electrocoagulation treatment of black liquor from paper industry, *Journal of Hazardous Materials* 163 (2-3) (2009) 995–1000.
- [98] A. M. Deshpande, S. Satyanarayan, S. Ramakant, Electrochemical pretreatment of wastewater from bulk drug manufacturing industry, *Journal of Environmental Engineering* 135 (8) (2009) 716–719.
- [99] X. Chen, G. Chen, P. L. Yue, Separation of pollutants from restaurant wastewater by electrocoagulation, *Separation and Purification Technology* 19 (1-2) (2000) 65 – 76.
- [100] Z. Murthy, C. Nancy, A. Kant, Separation of pollutants from restaurant wastewater by electrocoagulation, *Separation Science and Technology* 42 (4) (2007) 819 – 833.
- [101] P. Canizares, F. Martinez, J. Lobato, M. A. Rodrigo, Break-up of oil-in-water emulsions by electrochemical techniques, *Journal of Hazardous Materials* 145 (1-2) (2007) 233 – 240.
- [102] M. Khemis, G. Tanguy, J. Leclerc, G. Valentin, F. Lapique, Electrocoagulation for the treatment of oil suspensions : Relation between the rates of electrode reactions and the efficiency of waste removal, *Process Safety and Environmental Protection* 83 (1 B) (2005) 50 – 57.
- [103] S. P. Novikova, T. L. Shkorbatova, E. Y. Sokol, Purification of effluent from the production of synthetic detergents by electrocoagulation, *Soviet Journal of Water*

Chemistry and Technology (English Translation of Khimiya i Tekhnologiya Vo 4 (4) (1982) 82 – 87.

- [104] F. Aloui, S. Kchaou, S. Sayadi, Physicochemical treatments of anionic surfactants wastewater: Effect on aerobic biodegradability, *Journal of Hazardous Materials* 164 (1) (2009) 353 – 359.
- [105] G. Mouedhen, M. Feki, M. De Petris-Wery, H. Ayedi, Electrochemical removal of cr(vi) from aqueous media using iron and aluminum as electrode materials: Towards a better understanding of the involved phenomena, *Journal of Hazardous Materials* 168 (2-3) (2009) 983–991.
- [106] I. Zongo, J.-P. Leclerc, H. A. Maïzœga, J. Wižœthižœ, F. Lapique, Removal of hexavalent chromium from industrial wastewater by electrocoagulation: A comprehensive comparison of aluminium and iron electrodes, *Separation and Purification Technology* 66 (1) (2009) 159–166.
- [107] C. P. Nanseu-Njiki, S. R. Tchamango, P. C. Ngom, A. Darchen, E. Ngameni, Mercury(ii) removal from water by electrocoagulation using aluminium and iron electrodes, *Journal of Hazardous Materials* 168 (2-3) (2009) 1430–1436.
- [108] P. Kumar, S. Chaudhari, K. Khilar, S. Mahajan, Removal of arsenic from water by electrocoagulation, *Chemosphere* 55 (9) (2004) 1245–1252.
- [109] W. H. Kuan, C. Y. Hu, M. C. Chiang, Treatment of as(v) and as(iii) by electrocoagulation using al and fe electrode, *Water Science And Technology* 60 (5) (2009) 1341–1346.
- [110] G. Mouedhen, M. Feki, M. D. P. Wery, H. Ayedi, Behavior of aluminum electrodes in electrocoagulation process, *Journal of Hazardous Materials* 150 (1) (2008) 124 – 135.
- [111] M. Malakootian, N. Yousefi, The efficiency of electrocoagulation process using aluminum electrodes in removal of hardness from water, *Iranian Journal Of Environmental Health Science & Engineering* 6 (2) (2009) 131–136.

- [112] N. Mameri, A. Yeddou, H. Lounici, D. Belhocine, H. Grib, B. Bariou, Defluoridation of septentrional sahara water of north africa by electrocoagulation process using bipolar aluminium electrodes, *Water Research* 32 (5) (1998) 1604 – 1612.
- [113] F. Shen, X. Chen, P. Gao, G. Chen, Electrochemical removal of fluoride ions from industrial wastewater, *Chemical Engineering Science* 58 (3-6) (2003) 987 – 993.
- [114] Y. Xu, J. Q. Jiang, K. Quill, J. Simon, K. Shettle, Electrocoagulation: a new approach for the removal of boron containing wastes, *Desalination And Water Treatment-Science And Engineering* 2 (1-3) (2009) 131–138.
- [115] P. Canizares, F. Martinez, M. Carmona, J. Lobato, M. Rodrigo, Continuous electrocoagulation of synthetic colloid-polluted wastes, *Industrial and Engineering Chemistry Research* 44 (22) (2005) 8171 – 8177.
- [116] M. J. Matteson, R. L. Dobson, R. W. Glenn, N. S. Kukunoor, W. H. Waits, E. J. Clayfield, Electrocoagulation and separation of aqueous suspensions of ultrafine particles, *Colloids And Surfaces A-Physicochemical And Engineering Aspects* 104 (1) (1995) 101–109.
- [117] M. H. Al-Malack, A. A. Bukhari, N. S. Abuzaid, Crossflow microfiltration of electrocoagulated kaolin suspension: fouling mechanism, *Journal Of Membrane Science* 243 (1-2) (2004) 143–153.
- [118] E. Vik, D. Carlson, A. Eikum, E. Gjessing, Electrocoagulation of potable water, *Water Research* 18 (11) (1984) 1355–1360.
- [119] H. A. Moreno-Casillas, D. L. Cocke, J. A. Gomes, P. Morkovsky, J. Parga, E. Peterson, Electrocoagulation mechanism for cod removal, *Separation and Purification Technology* 56 (2) (2007) 204 – 211.
- [120] M. Y. A. Mollah, R. Schennach, J. R. Parga, D. L. Cocke, Electrocoagulation (ec) - science and applications, *Journal of Hazardous Materials* 84 (1) (2001) 29 – 41.
- [121] T. Picard, G. Cathalifaud-Feuillade, M. Mazet, C. Vandensteendam, Cathodic dissolution in the electrocoagulation process using aluminium electrodes., *J Environ Monit* 2 (1) (2000) 77–80.

- [122] P. K. Holt, G. W. Barton, M. Wark, C. A. Mitchell, A quantitative comparison between chemical dosing and electrocoagulation, *Colloids and Surfaces A: Physicochemical and Engineering Aspects* 211 (2-3) (2002) 233 – 248.
- [123] M. Y. Mollah, P. Morkovsky, J. A. Gomes, M. Kesmez, J. Parga, D. L. Cocke, Fundamentals, present and future perspectives of electrocoagulation, *Journal of Hazardous Materials* 114 (1-3) (2004) 199 – 210.
- [124] J. Trompette, H. Vergnes, On the crucial influence of some supporting electrolytes during electrocoagulation in the presence of aluminum electrodes, *Journal of Hazardous Materials* 163 (2-3) (2009) 1282–1288.
- [125] M. Bennajah, Traitement des rejets industriels liquide par électrocoagulation/électroflotation en réacteur airlift, Ph.D. thesis, Institut National Polytechnique de Toulouse (2007).
- [126] G. Ciorba, C. Radovan, I. Vlaicu, S. Masu, Removal of nonylphenol ethoxylates by electrochemically-generated coagulants, *Journal of Applied Electrochemistry* 32 (5) (2002) 561–567.
- [127] C. van Oss, *Interfacial forces in aqueous media*, Taylor & Francis, 2006.
- [128] K. Boussu, Influence of membrane characteristics on flux decline and retention in nanofiltration, Ph.D. thesis, Katholieke Universiteit Leuven (2007).
- [129] M. Mulder, *Basic Principles of Membrane Technology*, 2nd edition, Springer-Verlag New York, LLC, 1996.
- [130] J.-C. Remigy, S. Desclaux, Filtration membranaire (oi, nf uf), présentation des membranes et modules, Tech. Rep. J2791, Techniques de l'Ingénieur (2007).
- [131] C. Bellona, J. E. Drewes, P. Xu, G. Amy, Factors affecting the rejection of organic solutes during nf/ro treatment—a literature review, *Water Research* 38 (12) (2004) 2795 – 2809.

- [132] S.-Y. Kwak, S. G. Jung, S. H. Kim, Structure-motion-performance relationship of flux-enhanced reverse osmosis (ro) membranes composed of aromatic polyamide thin films, *Environmental Science & Technology* 35 (21) (2001) 4334–4340.
- [133] S. Al-Jeshi, A. Neville, An investigation into the relationship between flux and roughness on ro membranes using scanning probe microscopy, *Desalination* 189 (1-3) (2006) 221 – 228, selected paper from the 10th Aachen Membrane Colloquium.
- [134] T. Bialopiotrowicz, B. Janczuk, The wettability of a cellulose acetate membrane in the presence of bovine serum albumin, *Applied Surface Science* 201 (1-4) (2002) 146 – 153.
- [135] G. Hurwitz, G. R. Guillen, E. M. Hoek, Probing polyamide membrane surface charge, zeta potential, wettability, and hydrophilicity with contact angle measurements, *Journal of Membrane Science* 349 (1-2) (2010) 349 – 357.
- [136] M. Elimelech, W. H. Chen, J. J. Waypa, Measuring the zeta (electrokinetic) potential of reverse osmosis membranes by a streaming potential analyzer, *Desalination* 95 (3) (1994) 269 – 286.
- [137] A. Subramani, E. M. Hoek, Direct observation of initial microbial deposition onto reverse osmosis and nanofiltration membranes, *Journal of Membrane Science* 319 (1-2) (2008) 111 – 125.
- [138] J. A. Brant, A. E. Childress, Assessing short-range membrane-colloid interactions using surface energetics, *Journal of Membrane Science* 203 (1-2) (2002) 257 – 273.
- [139] C. K. Yeom, S. H. Lee, J. M. Lee, Effect of the ionic characteristics of charged membranes on the permeation of anionic solutes in reverse osmosis, *Journal of Membrane Science* 169 (2) (2000) 237 – 247.
- [140] G. Cornelis, K. Boussu, B. Van der Bruggen, I. Devreese, C. Vandecasteele, Nanofiltration of nonionic surfactants - effect of the molecular weight cutoff and contact angle on flux behavior, *Industrial & Engineering Chemistry Research* 44 (20) (2005) 7652–7658.

List of Figures

1.1	Fire triangle	4
1.2	Typical system of foam generation, <i>i.e.</i> nozzle	5
1.3	Film formation and spreading as a result of a positive spreading coefficient	6
1.4	Influence of the AFFF components on the spreading coefficient of a water drop on a hydrocarbon liquid.	6
1.5	Photographs from the Buncefield incident (credits: Chiltern Air Support)	10
1.6	Stabilizing interaction differences of bulk and interface molecule in a pure liquid	13
1.7	Contact angles between a liquid L and a solid surface S in case of partial wetting and absence of wetting	14
1.8	Work of adhesion, or free energy of interaction between a surface S and a liquid L	15
1.9	Work of cohesion for a liquid L	16
1.10	Simplified representation of a surfactant molecule	23
1.11	Summary of molecular interactions between a polar solvent and surfactant molecules. A , B , C , D and E refer to equation 1.26.	26
1.12	Surfactant monomers and micelle formation in water	27
1.13	Packing parameter illustration	27
1.14	Adsorption of surfactants on hydrophobic surface. a: surfactant monomers, b: surfactant micelle, c: isolated adsorbed surfactant monomer, d: surface aggregates	30
1.15	Adsorption of surfactants on hydrophilic surface. a: surfactant monomers, b: surfactant micelle, c: isolated adsorbed surfactant monomer, d: surface aggregates	32

1.16	(n+1):m fluorotelomer hydrophobic tail	32
1.17	The three main families of perfluorinated surfactants regarding their polar heads, after [14]	33
1.18	Molecular orbitals and polarity of the C–F bond. Source: http://www.math.jussieu.fr	34
1.19	Thermogravimetric analysis of a fluorinated surfactant (with courtesy of DuPont)	34
1.20	Volume of (a): perhydrogenated and (b):perfluorinated homologous molecules	35
1.21	Formula of the compounds contained in the pilot firefighting waters	40
2.1	Fluorinated surfactants mostly found in the water treatment literature	45
2.2	Chemical structure of the fluorinated surfactant considered in this work	46
2.3	Membrane process	54
2.4	The two main setups for membrane pilots	55
2.5	Ultrafiltration of a micellar surfactant solution. a: surfactant monomer, b: surfactant micelle. Dynamic equilibrium between surfactant monomers and micelles, as well as surfactant adsorption not pictured.	56
2.6	Evaporative light scattering detector schematics. Source: http://www.spectrotech.com	64
2.7	n-heptane fire for pilot firefighting water production (0.25 m^2).	66
2.8	Molecules contained in the pilot firefighting waters	68
2.9	Assessment chart for the representativity firefighting waters relative to actual firefighting waters. Dashed area: possible, yet unknown presence of the considered compound.	71
2.10	Sophistication of pilot firefighting waters 1 and 2	72
2.11	Pilot firefighting water Durieux filter clarification	73
2.12	Pilot firefighting water $0.7\mu\text{m}$ paper filter microfiltration	73
2.13	Flow evolution during model firefighting water 1 (MFW1) and pilot firefight- ing water 1 (PFW1) filtrations on $0.7\mu\text{m}$ paper filter, under vacuum, with a glass frit support.	74
2.14	Fouling profiles during model firefighting water 1 (MFW1) and pilot firefight- ing water 1 (PFW1) filtrations on $0.7\mu\text{m}$ paper filter, under vacuum, with a glass frit support.	75

2.15	Evolution of permeabilities during model firefighting water 1 (MFW1) and clarified pilot firefighting water 2 (PFW2, after Durieux filter clarification) filtrations on $0.3\ \mu\text{m}$ PVDF Osmonics microfiltration membrane	76
2.16	Membrane permeabilities during ultrafiltration with polyethersulfone membranes of the pilot firefighting water 1 (PFW1). Membrane cutoffs: \circ : $10\ \text{kDa}$; ∇ : $30\ \text{kDa}$; \star : $100\ \text{kDa}$	78
2.17	Schema of the electrocoagulation cell	83
2.18	pH during electrocoagulation of pilot firefighting water 2 (PFW2, $3\ \text{L}$), 60min, at $2\ \text{A}$ (current density of $24.5\ \text{A m}^{-2}$)	83
2.19	Floc layers during electrocoagulation of pilot firefighting water 2 at $2\ \text{A}$, after $30\ \text{min}$	84
2.20	Turbidity during electrocoagulation at $2\ \text{A}$ of pilot firefighting water 2 (PFW2). \bullet : in bulk solution; \square : after $0.45\ \mu\text{m}$ PVDF syringe filtration.	84
2.21	Fluorinated surfactant concentration during PFW2 electrocoagulation, 60 min, after $0.45\ \mu\text{m}$ PVDF filtration	85
2.22	Sophistication of the solution for adsorption experiments	87
2.23	Fluorinated surfactant adsorption isotherms for \blacksquare : C301 powder activated carbon and \circ : Lewatit VP OC 1064 ion exchange resin. Solid trend line: Freundlich isotherm for activated carbon, dashed trend line: Freundlich isotherm for the resin. Initial solutions compositions were proportional to foaming solution composition, from 140 to 1000 and $2000\ \text{mg L}^{-1}$ of fluorinated surfactant for carbon and resin respectively.	89
2.24	Complexity of the MFW2 solution used during electrocoagulation screening as a treatment process	90
2.25	pH during electrocoagulation of the MFW2 ($3\ \text{L}$), at a current density of $24.5\ \text{A m}^{-2}$	91
2.26	Fluorinated surfactant concentration during MFW2 electrocoagulation ($3\ \text{L}$), at a current density of $24.5\ \text{A m}^{-2}$	91
2.27	Sophistication of the solution used during reverse osmosis screening (MFW3)	92
2.28	Permeability at 25°C during MFW3 full recycle reverse osmosis	93

3.1	Interaction of aluminium species with initially negatively charged particles in water. The particles on the right hand side are initially stable and then become destabilized by charge neutralization. At higher coagulant dosages they can become restabilized by charge reversal and incorporated in a flocculant hydroxide precipitate ('sweep flocculation'). Image taken from [45].	100
3.2	Removal mechanisms in electrocoagulation	102
3.3	Aluminium speciation in aqueous solution, obtained by Hydra/Medusa software, for aqueous solution containing 2.1 mM of Al^{3+} , assuming amorphous aluminium hydroxide as the only possible solid species.	103
3.4	Electrocoagulation cells. Left: EC1 cell, right: EC2 cell	106
3.5	Chromatogram of a calibrating solution containing at 3.30 and 8.50min: Disponil [®] SOS 842; 6.57 min: Tegotens [®] AM VSF; 10.71 and 13.59 min: Simulsol [®] SL8 ; 12.68: fluorinated surfactant. The identification of the peaks were done by analysis of single surfactant solutions (not shown). . . .	108
3.6	Sophistication of the pilot firefighting waters 1, 2, 3 and 4.	111
3.7	Floc formation during the electrocoagulation of pilot firefighting water 2, 3 L, in EC1 cell, 2 A.	112
3.8	Turbidity during electrocoagulation at 2 A of pilot firefighting water 2 (PFW2). ●: in bulk solution; □: after 0.45 m PVDF syringe filtration. (a): latency phase; (b): active phase.	113
3.9	Turbidity during electrocoagulation of PFW4, 3 L, 1 A. ●: in bulk solution; ▽: after 0.45 m PVDF syringe filtration.	115
3.10	Ratio of time by filtered volume t/v , versus the volume v during filter press of pretreated pilot firefighting water bulk solution.	117
3.11	Schematics of the Serep's Solvin [®] electrocoagulator. Image: Serep.	118
3.12	Pilot firefighting water 3 electrocoagulation by Serep, at 16 A and 60 L h^{-1} , with aluminium anode.	119
3.13	Sophistication of industrial firefighting water 1	120
3.14	Sophistication of industrial firefighting water 2	121

3.15	Surfactant concentrations versus charge loading during electrocoagulation of pilot firefighting water 4 at 0.5 A, in EC1 cell. ○: Disponil [®] SOS 842 (alkyl sulfate); ▽: Tegotens [®] AM VSF (alkyl propionate); ☆: Simulsol [®] SL8 (alkyl glucoside), ✱: fluorinated surfactant.	123
3.16	Fluorinated surfactant concentration and pH of the samples versus total aluminium concentration. Total aluminium concentrations were measured after acidic dissolution at pH 1 with acetic acid, 37%. Samples from electrocoagulation experiments of PFW3 in EC2 cell.	125
3.17	pH evolution during electrocoagulation of 3 L of: a Disponil [®] SOS 842 solution; a blank NaCl, 0.5 g L ⁻¹ solution, at 1 A in EC1 cell.	126
3.18	Fluorinated surfactant concentration in different pilot firefighting waters versus charge loading for different current densities during electrocoagulation experiments. ○: PFW3, 0.5 A; ▽: PFW1, 1 A; ☆: PFW2, 2 A; ✱: PFW3 20 A. Every experiments were done at the laboratory in EC1 cell, except ✱ done by Serep.	127
3.19	Sophistication of model solution A, B, C, D and E.	129
4.1	Schematic representation of membrane processes and of the kind of separation performed [128]	136
4.2	Schematic representation of a composite membrane [130]	140
4.3	Concentration polarization in membrane processes. C_R : concentration of the solute in the retentate, C_M : concentration at the membrane.	144
4.4	Osmonics setup for membrane screening. (a): feed, (b): retentate, (c): permeate, (d): membrane	155
4.5	Millipore pilot	156
4.6	Polymem reverse osmosis pilot. (a): feed, (b): retentate, (c): permeate, (d): membrane, (e): recirculation, (f): reject	157
4.7	Flux and permeabilities at 25°C during membrane screening	160

4.8	Surfactant retention rates for every tested membranes as function of the percentage of available water permeability in the Osmonics cell. ○: Disponil [®] SOS 842; ▽: Tegotens [®] AM VSF; ☆: Simulsol [®] SL8, ✱: fluorinated surfactant. From left to right: SG, DK, CK, CE and AD membranes. Operating pressures are given in table 4.10.	162
4.9	Permeability versus total fluorinated surfactant concentration in the system during reverse osmosis of model pretreated pilot firefighting water in the Millipore pilot with a spiral-wound SG membrane at 20 bar. The membrane used by Tang et al. was an ESPA membrane, the pressure was 13.8 bar and the fluorinated surfactant was PFOS. The data from flat sheet SG membrane is from section 4.4.1.	164
4.10	Permeability at 25°C during reverse osmosis in the Polymem pilot of 40 L of CF20 solution, at 30 bar, and cross-flow velocity of 0.095 m s ⁻¹ . The initial points were the water permeabilites before the experiments.	166
4.11	Retention rates during reverse osmosis in the Polymem pilot of 40 L of CF20 solution, at 30 bar, and cross-flow velocity of 0.095 m s ⁻¹ . Test 1: ○: Disponil [®] SOS 842; ▽: Tegotens [®] AM VSF; ☆: Simulsol [®] SL8, ✱: fluorinated surfactant. Test 2: ●: Disponil [®] SOS 842; ▼: Tegotens [®] AM VSF; ✦: Simulsol [®] SL8, ★: fluorinated surfactant.	167
4.12	Surfactants adsorption density during reverse osmosis in the Polymem pilot of 40 L of CF20 solution, at 30 bar, and cross-flow velocity of 0.095 m s ⁻¹ . Test 1: ○: Disponil [®] SOS 842; ▽: Tegotens [®] AM VSF; ☆: Simulsol [®] SL8, ✱: fluorinated surfactant. Test 2: ●: Disponil [®] SOS 842; ▼: Tegotens [®] AM VSF; ✦: Simulsol [®] SL8, ★: fluorinated surfactant.	169
4.13	Permeability as function of logarithm of the inverse of fluorinated surfactant concentration in the retentate during model pretreated firefighting water reverse osmosis with a spiral-wound SG membrane. The concentration of the fluorinated surfactant is an indicator of the global concentration of other surfactants also present.	170

4.14	R_a , the resistance to mass transfer due to adsorption, versus C_R the retentate concentration of the fluorinated surfactant, during reverse osmosis of model pretreated firefighting water in the Millipore pilot, at 20 bar, with a spiral-wound SG membrane. The concentration of the fluorinated surfactant is an indicator of the global concentration of other surfactants also present.	171
4.15	$1/R_a$ (m) versus $1/C_R$ ($L\ mg^{-1}$) during reverse osmosis of model pretreated firefighting water in the Millipore pilot, at 20 bar, with a spiral-wound SG membrane. C_R , the retentate concentration of the fluorinated surfactant is an indicator of the global concentration of other surfactants also present.	172
4.16	Model and experimental data for the permeability versus retentate concentration of the fluorinated surfactant, during reverse osmosis of model pretreated firefighting water in the Millipore pilot, at 20 bar, with a spiral-wound SG membrane. The concentration of the fluorinated surfactant is an indicator of the global concentration of other surfactants also present.	173
4.17	Time lag for surfactant permeation during the first test with the Polymem pilot (Section 4.4.3). ○: Disponil [®] SOS 842; ▽: Tegotens [®] AM VSF; ☆: Simulsol [®] SL8, ☆: fluorinated surfactant.	176
5.1	Apolar (LW) and polar (AB) interactions between two compounds. Self-interaction of water can be depicted this way.	180
5.2	Interactions between compounds 1 and 2 immersed in a liquid 3. Interaction of 3 with 1 and 2, as well as 3–3 interactions are not depicted, but can be represented by the figure 5.1.	181
5.3	Schematic representation of the electrostatic, polar and apolar characters of the compound encountered during this work	182
5.4	Interactions of surfactants with solid surfaces in aqueous media. At microscopic scales, some real solid surface such as reverse osmosis membranes could be a patchwork of polar and apolar zones. The possible mixed micellization and surface aggregation in surfactant mixtures is not represented.	184
5.5	First design of the mobile unit	186
5.6	Flow sheet	187

5.7	Examples of compact containerizable membrane processes plants. a) and b):	
	Lenntech, c) Polymem	190

List of Tables

1.1	Foam types according to their expansion rate	4
1.2	Firefighting foams	8
1.3	Some common flammable hydrocarbons in industrial environment	8
1.4	Firefighting water complexity summary	11
1.5	Types of surfactants according to their polar heads [5]	24
1.6	Differences in interfacial tension in $mN\ m^{-1}$ of n-octane and n-octanol with water, on microscopic and macroscopic scales.	25
1.7	Micellar structure according to the packing parameter	27
1.8	Interactions driving the adsorption of surfactants in aqueous phase, according to the nature of the interface	29
1.9	Bond energies in $kcal\ mol^{-1}$ for various heteroatoms with hydrogen and methyl group [17]	33
1.10	Surface tensions for ideal solid surfaces [18]	35
1.11	Properties of pilot firefighting water components polar heads and their potential polar interactions	41
2.1	Adsorption processes applied to fluorinated surfactants	50
2.3	Membrane processes and relative order of magnitude of membrane properties [62]	56
2.4	Comparison of the processes identified in the bibliographic study	60
2.5	Components of the 3% foaming base used to generate pilot firefighting waters. Deionized water represented 72.6% wt, diethanolamine was added to reach $pH\ 7.5$	66

2.6	Foaming solution composition after dilution of the foaming base to 3% v:v in tap water	67
2.7	Pilot firefighting waters properties	72
2.8	MFW1 composition	74
2.9	Evolution of the fluorinated surfactant concentrations during microfiltration experiments with a 0.3 <i>m</i> PVDF Osmonics membrane	77
2.10	Summary of permeability properties of the different membranes used for ultrafiltration of firefighting water 1	79
2.11	Turbidity in permeate and retentate during ultrafiltration of MFW1 with different membranes	79
2.12	Fluorinated surfactant concentrations in permeate and retentate during ultrafiltration of MFW1 with different membranes	79
2.13	Retention rates of the fluorinated surfactant during ultrafiltration of pilot firefighting water 1 with polyethersulfone membranes	80
2.14	Cationic flocculants preliminary experiments results	82
2.15	Composition of the model firefighting waters for adsorption experiments . . .	87
2.16	Freundlich parameters for the fluorinated surfactant isotherms obtained with C301 powder activated carbon and Lewatitt VP OC 1064	88
2.17	Composition of model firefighting water 2 for electrocoagulation as a treatment process	90
2.18	Model firefighting water 3 composition	92
2.19	Fluorinated surfactant concentrations during MFW3 full recycle reverse osmosis	93
2.20	Comparison of turbidities obtained after pretreatment processes during the present screening. The aim was 2 <i>NTU</i> or lower.	94
2.21	Comparison of treatment processes on the basis of the present screening . .	95
3.1	Composition of the gradient given to the Hitachi <i>L</i> – 2130 gradient pump, for the simultaneous analysis of surfactants from pilot firefighting waters. . .	107
3.2	Pilot firefighting waters used in this chapter	109
3.3	Visual estimation of the minimal pretreatment time for PFW3. Experiments done in <i>a</i> : EC2 cell; <i>b</i> : EC1 cell.	114

3.4	Turbidity during the electrocoagulation of industrial firefighting water 1, 1 A, 1.75 L in EC1 cell	120
3.5	Turbidity during the electrocoagulation of industrial firefighting water 2, 1 A, 3 L in EC1 cell	121
3.6	Aluminium concentrations in bulk solution and whole acidified solutions after 0.45 m PVDF syringe filtration. *: Electrocoagulation of 1000 mL of PFW3. Other experiments were done with 500 mL of PFW1, ^e : estimated concentrations. Every experiments were done in EC2 cell.	124
3.7	Composition in $mg\ L^{-1}$ of model solutions blank, A, B, C, D and E. Every solutions were prepared with tap water, except the blank which was prepared with deionized water containing $0.5\ g\ L^{-1}$ of NaCl.	128
3.8	Initial and final concentrations in $mg\ L^{-1}$ and visual pretreatment times during electrocoagulation of 3 L of model solutions in EC1 cell.	130
4.1	Summary of the rejection mechanisms for reverse osmosis and nanofiltration, and their origin in solute and membrane properties [131]	143
4.2	Various resistances to mass transfer and their causes in membrane processes	145
4.3	Solid surface tension of several polyamide and cellulose membranes, in $mN\ m^{-1}$, determined by contact angle measurements	148
4.4	Expected interactions of various kind of surfactants with nanofiltration and reverse osmosis membranes in water at neutral pH. Each surfactant is expected to show hydrophobic interactions, either via apolar (LW) interactions between the membrane polymer and the hydrophobic tail, and via the exclusion of hydrophobic entities due to polar (AB) cohesion of water.	148
4.5	Surface tensions of octane, polyethylene, Teflon [®] and water [127]	150
4.6	Composition of the CF20 model solution	152
4.7	Artificially concentrated model pretreated pilot firefighting water composition after addings	153
4.8	Compositions in $mg\ L^{-1}$ of CF20 solutions for tests 1 and 2 in the Polymem pilot. The volumes were 40 L, including the dead volume.	153

4.9	Monomer content in <i>CF</i> 20 solutions, estimated on the basis of ultrafiltration permeate concentration (given) and retentate concentration after equilibrium (not given)	154
4.10	Membranes used in the Sepa CFII cell for the screening	155
4.11	Summary of the reverse osmosis and nanofiltration pilots properties	158
4.12	Flows, permeabilities and flux decline during membrane screening with <i>CF</i> 20 model solution in the Osmonics cell for cross-flow velocities of 0.1 and 0.5 $m s^{-1}$	161
4.13	Concentration in permeates and rejections of the fluorinated surfactant during membrane screening	162
4.14	Fluorinated surfactant concentration and membrane permeability during pre-treated pilot firefighting water 3 reverse osmosis, 20 bar. ^a : additional results from the Norwegian Institute for Air Research (NILU).	163
4.15	Fluorinated surfactant concentrations during artificially concentrated model pilot firefighting water 2 reverse osmosis, 20 bar, full recycle, 1h equilibrium after adding	165
4.16	Permeability at 25°C and retention rates as function of the superficial velocity during reverse osmosis in the Polymem pilot of 40 L of <i>CF</i> 20 solution at 30 bar. 167	
4.17	Average rejection rates	168
4.18	Summary of the experimental results obtained during reverse osmosis experiments. The only surfactant considered is the fluorinated surfactant.	169
4.19	Linear regressions of data from figure 4.17 and diffusion coefficients estimation 176	
5.1	Typical firefighting water composition	185
5.2	Design results for membrane processes with one step of reverse osmosis (option 1) or two steps (option 2)	188
5.3	Costs of incineration	191

Conception d'une unité mobile pour le post-traitement d'eau utilisée pendant l'extinction d'incendie

Mots Clés : Traitement d'eau, électrocoagulation, procédé membranaire, osmose inverse, tensioactifs, tensioactifs fluorés, extinction d'incendie

Résumé en français :

L'extinction de feux de liquides inflammables sur des installations industrielles telles que les dépôts de carburant ou les raffineries entraîne l'utilisation de milliers de mètres cubes d'eau, composé majeur des mousses anti-incendie. Ces dernières contiennent généralement des tensioactifs hydrocarbonés ainsi que des tensioactifs fluorés qui se retrouvent dans les eaux d'extinction, ainsi que les suies et les restes de solvants. Les tensioactifs fluorés jouent un rôle clé dans l'efficacité des mousses anti-incendie en raison de leur nature chimique particulière. En raison de la présence des tensioactifs fluorés, le traitement actuel de l'eau d'extinction d'incendie est l'incinération dans des incinérateurs haute température et résistant aux halogènes. Les tensioactifs sont des composés amphiphiles qui ont comme propriétés d'abaisser la tension superficielle de l'eau et de former des agrégats en solution : les micelles. Les tensioactifs peuvent également s'adsorber aux interfaces ainsi qu'aux surfaces solides, et éventuellement y former des agrégats de surface, analogues aux micelles en solution. L'objectif industriel de la présente thèse est de proposer une unité mobile de traitement de ces eaux afin de concentrer les composés fluorés et limiter les volumes à incinérer. Les critères de sélection des procédés que nous avons retenus sont les suivants : compacité, peu ou pas de produits chimiques ou solides nécessaires. L'objectif scientifique de ce travail est de mieux comprendre le comportement de ces composés au cours des procédés d'électrocoagulation/filtration et d'osmose inverse.

Des essais préliminaires ont été réalisés et ont permis de choisir les procédés suivant : l'électrocoagulation couplée à la filtration comme prétraitement pour séparer les particules en suspension et les traces d'émulsions éventuelles de la phase aqueuse et l'osmose inverse comme traitement pour concentrer les tensioactifs fluorés.

A l'échelle du laboratoire, l'électrocoagulation, permettant le retrait de la matière en suspension, a été optimisée pour des eaux d'extinction d'incendie pilotes et un mécanisme a été proposé. L'efficacité de ce procédé a ensuite été vérifiée sur un pilote industriel.

L'osmose inverse d'eaux d'extinction d'incendie pilotes pré-traitées par électrocoagulation/filtration a montré de forts taux de rétention du tensioactif fluoré. Une comparaison de différents matériaux membranaires a été réalisée sur un module d'osmose inverse plan avec des solutions modèles. Des essais de filtration de longue durée, à l'échelle pilote, ont permis de suivre l'évolution de la rétention des tensioactifs et du flux de perméat. Ces données ont été utilisées pour réaliser le dimensionnement d'une unité mobile de post traitement d'eau d'extinction d'incendie.

Les perspectives de ce travail sont les suivantes : La prise en charge de la réalisation d'une unité mobile devrait être menée par un partenaire de DuPont de Nemours qu'il reste à identifier. L'étude sur la modification de l'état de surface des membranes est poursuivie dans le cadre d'une nouvelle thèse et permettra à terme de mieux choisir les conditions opératoires de filtration et de nettoyage au cours des procédés membranaires et ainsi d'améliorer les performances du procédé.

Design of a mobile post-treatment unit for the water used during fire extinguishment

Key words: water treatment, electrocoagulation, membrane processes, reverse osmosis, surfactants, fluorinated surfactants, firefighting

Summary

Extinguishment of large solvent fire leads to the production of fire fighting water, which are collected thanks to the design of industrial infrastructures. Depending on the nature of the firefighting foam used, the resulting water may require the removal of fluorinated surfactants potentially present. After decantation of the organic phase, fire fighting waters essentially contain surfactants. Surfactants are amphiphilic chemicals having the ability to lower both interfacial and surface tensions by adsorbing in an oriented fashion at interface. Surfactant can form micellar aggregates in solution and on interfaces under certain conditions, and have a pronounced influence on interfacial phenomena. Hence, before considering any water treatment process, interfacial science and surfactant were introduced. This work has a dual purpose. The industrial purpose is to provide an economically viable alternative to water incineration. The foreseen unit will have to be mobile and able to extract fluorinated surfactants from water at a rate of $1\text{--}4.5\text{ m}^3\text{h}^{-1}$ ($20,000\text{ m}^3$ in 4-6 months). The scientific purpose of this work is the study of the behavior of surfactants in the context of water treatment processes.

The state of the art of relevant water treatment processes and an experimental screening with real firefighting water permitted to identify two steps as likely to fit the constraints of a mobile unit: electrocoagulation-filtration coupled with reverse osmosis.

The electrocoagulation process followed by filtration was applied to pilot, model and industrial firefighting waters. This process was found to remove efficiently the unwanted turbidity from pilot firefighting waters.

Current knowledge about the separation mechanisms of small organic molecules in reverse osmosis has been reviewed, and rejection as well as flux decline were related to membrane, solution, and solute properties. Polyamide and cellulose acetate membrane materials were screened in a flat sheet cell. The stabilities of rejection and flux decline were confirmed during longer tests (several days) on an industrial pilot with the most appropriate membrane.

A final design study confirmed the possibility to combine electrocoagulation-filtration and reverse osmosis to treat firefighting waters.